Using Kolmogorov Equations to Investigate Hedging Errors

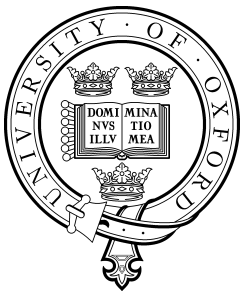

Alan Whitley

St Anne's College

University of Oxford

A thesis submitted for the degree of

Doctor of Philosophy

Trinity 2015

Abstract

This thesis presents a study of hedging errors caused by model mis-specification, making use of a Kolmogorov forward equation with δ-function initial conditions. The method is used to calculate the probability distribution of hedging errors at maturity for a number of realistic examples. An analysis of numerical schemes used to solve the Kolmogorov forward equation is presented, making particular use of Fourier transform techniques. Much of the analysis applies to a 'toy' model which captures the main features of the hedging problem. Detailed analysis of a semi-discrete Fourier numerical method for solving the toy model problem leads to a complete description of the accuracy and stability behaviour of the scheme. The thesis also includes a novel time-change method which solves the heat equation with δ-function initial conditions, using the Crank-Nicolson method, and which demonstrates improved convergence of the scheme. The numerical analysis included in the thesis explores further aspects of Fourier transform methods applied to the analysis of Partial Differential Equations with Dirac data and variable coefficients.

Acknowledgements

I would first of all like to recognise the support I have received from the Mathematical Institute of the University of Oxford and thank all the staff for their help while I have studied there. In addition, I want to thank St. Anne's College for welcoming me into their membership and for providing me with many enjoyable teaching opportunities. I would also like to thank all the staff of the College who have given me so much support in so many different ways.

I am overwhelmingly grateful for the support provided to me by my supervisor Christoph Reisinger while studying with him. He has shown tremendous understanding towards me and has given me so much encouragement, support, advice and time. It has been a great pleasure to work with him.

I would also like to thank various members of the Institute, especially Mike Giles, Michael Monoyios, Endre Süli and Greg Gyurko.

Thanks go to my family and friends, especially my daughter Anne, my son William and my brothers Peter and John, for all their support during my period of study.

Finally, it is very hard to properly express in words the fantastic support given to me by my wife, Carol. She has shown great understanding with my aspirations and has made a very significant contribution to the success of my studies.

Contents

List of Figures

Chapter 1

Introduction

1.1 Motivation for the thesis

In recent years there has been tremendous growth in the markets for financial derivatives which are sophisticated financial instruments constructed with reference to underlying tradeable financial securities (or other assets) such as bonds, shares, barrels of oil, etc. These underlyings all have their own risk profiles (e.g. share prices can go up or down, bonds might default, etc.) and the sellers of derivatives are essentially re-packaging these risks to make them of interest to buyers of the derivatives. As a result of this re-packaging, the sellers of derivatives themselves have exposure to a complicated collection of risks. However, they do not have to passively accept these risks but can actively manage their portfolios to tailor the risk in their portfolios to their own requirements. This activity is called risk management .

One of the simplest examples of a financial derivative is the European call option where the seller (or writer) of the call receives a payment (the premium) from the buyer (holder) and, in exchange, guarantees to make available for sale to the buyer one unit of the underlying (one share, say) at a price specified in advance (the strike price) at a time also specified in advance (the maturity of the option). The buyer of the call option is not obliged to exercise the option at maturity but will clearly do so if the price of the underlying is above the strike price at maturity.

In this case, as the future share price is uncertain, the option holder faces some risk but this is limited, on the downside, to the premium that has to be paid. On the other hand, the option holder faces unlimited upside exposure which, of course, will be welcomed. However, the risks to which the option writer is exposed are exactly

the opposite and include exposure to unlimited downside risk.

The writer of a call option does not have to passively accept this risk profile but can implement a trading strategy to mitigate the risks – i.e. he can set up a portfolio which can then be actively managed up to maturity so that the obligations to the option buyer can always be met at that time. For example, the seller could simply buy one share and hold it to maturity.

The cost of that particular strategy (as reflected in the premium that must be paid to buy it) is not optimal and the trader will still be exposed to risk. In certain circumstances, a better trading strategy is available that can eliminate all risk for the trader while still ensuring that he meets his obligations to the buyer. In the classic setting of the Black-Scholes model, it is well known that the seller of the option can eliminate all the risk from his portfolio if he follows a specific trading strategy, delta-hedging, maintaining a dynamically adjusted portfolio made up of assets and bonds which is guaranteed to exactly meet his obligations when the option matures.

This particular aspect of risk management is called hedging, and in the idealised case just discussed, the delta-hedging strategy will provide, in theory, complete insurance against the risks taken on by the seller of the option.

In practice, however, the option writer will face a number of obstacles to achieving a perfect hedge. These range from uncertainty about the 'true' behaviour of the underlying, to operational issues that hinder implementation of a particular hedging strategy. Examples of the latter are frictions due to trading costs, the need to hedge at discrete time intervals, restrictions on short-selling, liquidity issues, etc.

Although modern mathematical finance provides a number of sophisticated tools that derivative sellers can use to understand the risks they have taken on and use to devise effective hedging strategies, no such mathematical framework will be perfect. In practice, there is always the possibility that hedging errors will occur, by which we mean that the hedging strategy employed fails to provide the expected protection against the risks in the portfolio.

Model uncertainty (see, for example, [16]), i.e. the lack of complete knowledge of the law governing the stochastic behaviour of the underlyings, can lead to hedging errors

for a variety of reasons. In some cases, the trader may believe he knows the true model when he does not and certain kinds of hedging errors will arise from hedging with a mis-specified model. In other cases, the uncertainty in the model structure or parameters may be recognised by the trader and a robust hedging strategy might have to be employed.

Clearly, there is a need for methods of analysing errors that can or do occur as a result of model mis-specification and these methods can also be used to guide the selection of hedging strategies. In order to quantify the range of hedging errors that might occur, an understanding of the probability distribution of the errors would be valuable. This probability distribution will be a function of both the hedging strategy employed and the actual behaviour of the underlyings.

In this thesis we review some of the literature on hedging errors and present a novel method of estimating probability distributions for hedging errors. This new approach has been based on the use of a Kolmogorov forward equation (KFE).

Other papers in the literature consider ways in which information on the hedging error distribution might be used to diagnose model mis-specification errors, such as in [4]. In these studies, the hedging error distributions are found by Monte Carlo simulation (though not always by direct simulation of the hedging process). Our new approach provides an alternative to the Monte Carlo method.

In order to assess this new approach we wanted to explore the novel features of the KFEs we used and, in particular, the theoretical behaviour of numerical schemes used to solve them. The difficulty comes from a combination of Dirac data, degeneracy, and variable coefficients.

Our paper ([36]) co-authored with Christoph Reisinger, and published in 2013, reported on a novel time-change method applied to solving the heat equation with δ-function initial conditions, using the Crank-Nicolson method. Apart from demonstrating improved convergence for that scheme, the paper also highlighted the usefulness of Fourier transform techniques for these types of problems. These methods then proved to be useful for our subsequent KFE studies.

As it was not possible to perform detailed numerical analysis on our real-life KFE examples, due to their complexity, we instead concentrated on the study of a 'toy' model KFE which captures the main features of our KFE examples.

Apart from the direct relevance to the KFE problem, the toy model Partial Differential Equation (PDE) (for which Kolmogorov gives an early reference in [25]) is significant in its own right and has a long history. More recently, the equation has been studied in a paper by Porretta and Zuazua [34] (where further references can be found) in which they investigate both discrete and semi-discrete numerical schemes for the solution of the PDE. Their main interest is in the late-time behaviour and decay rates of the solution.

We stress, however, that these references in the literature to the Kolmogorov PDE do not address the case of δ-function initial conditions, which we have analysed in this thesis.

Our motivation for the numerical analysis we performed was to explore further aspects of Fourier transform methods for the KFE, which has variable coefficients, and to obtain information on the convergence behaviour of the numerical schemes we developed for the KFE. We were able to establish a complete description of the convergence behaviour for one of the schemes (the semi-discrete Fourier method) and made some progress with the others.

1.2 Applications and contributions

This thesis has contributed to the study of hedging errors under model mis-specification.

Given a knowledge of both the correct asset model and the erroneous hedging strategy employed (which may be based on an incorrect asset model), we can study how the resulting hedging errors evolve over the lifetime of the instrument.

- We have developed a new method of calculating hedging error distributions using PDE techniques based on the Kolmogorov forward equation. This offers an alternative to calculating hedging error distributions by using Monte Carlo simulation.

- We presented a number of realistic examples of the extended Kolmogorov forward equation which can be used to calculate hedging error distributions in the presence of model mis-specification.

- The KFEs used have δ-function initial conditions and studies included in this thesis have contributed to further understanding of the numerical solution of PDEs with these initial conditions, building on the work of [5].

- In the last part of the thesis, while seeking to analyse the behaviour of the numerical schemes used to solve the KFE, we provide further insight into the use of Fourier transform methods to investigate stability and accuracy for certain types of variable-coefficient PDEs, again with δ-function initial conditions. We hope that this analysis, apart from supporting our specific studies, will encourage further use of Fourier transform methods for these kinds of problems.

1.3 Outline

This thesis describes work carried out to develop a new method of calculating the distribution of hedging errors in the presence of model mis-specification.

A major theme running through the thesis is the necessity to use and understand the solution of PDEs with δ-function initial conditions. The use of Fourier transform methods is key to this analysis and the thesis builds on and extends existing literature. This work lead to the publication of a paper co-authored by Christoph Reisinger.

We give a brief outline of the thesis in the following few paragraphs.

In Chapter 2 we present a natural time-change for the heat equation with a δ-function initial condition which, when applied to the Crank-Nicolson numerical scheme, restores convergence of the scheme. The chapter makes extensive use of Fourier transform techniques which are a main tool used throughout the thesis.

In Chapter 3 we introduce hedging and describe the behaviour of hedging errors in the presence of model mis-specification and develop the mathematical framework for

our further analysis. We find the expected form for the dynamics of hedging errors and move to on to derive an extended Kolmogorov forward equation which can be solved to find the hedging error distribution at maturity. We present a number of examples of the KFE, for various types of model mis-specification. The numerical results obtained by solving these KFEs are presented in Chapter 6.

As we are not able to find analytical solutions to the KFEs we develop, we resorted to numerical solution methods and in Chapter 4 we describe and discuss the numerical methods and schemes we used.

In Chapter 5, we return to our continuing theme of Fourier analysis, and analyse the stability and accuracy for a 'toy' model that captures the essential features of the KFE and apply Fourier transform techniques to the analysis of the various numerical schemes used for this model.

In Chapter 6 we present the numerical results of our application of the KFE to various examples of model mis-specification.

Finally, in Chapter 7 we summarise the main results of the thesis, interpret the findings and suggest further lines of enquiry that might be investigated.

Chapter 2

Fourier analysis applied to a locally refined Crank-Nicolson scheme for the heat equation with Dirac data

In this chapter we present the material from a paper written with my supervisor, Christoph Reisinger ([36]), which was published in 2013.

We investigated the stability of the popular Crank-Nicolson scheme as applied to the heat equation when solved with δ-function initial conditions. It is known that under those circumstances the Crank-Nicolson scheme fails to converge as the grid is refined in a very natural way. This behaviour was analysed in [5], making use of Fourier transform techniques. This chapter presents a simple and natural 'time-change' of the heat equation (a transformation of time variable) which leads to a Crank-Nicolson scheme that always converges.

Fourier transform techniques were again used in this chapter, reinforcing the usefulness of this approach to analysing stability in the presence of δ-function (non-smooth) initial conditions. We will use similar techniques later in the thesis when we study the hedging error problem.

2.1 Background

The Crank-Nicolson scheme is a popular time-stepping scheme for the numerical approximation of diffusion equations and is particularly heavily used for applications in computational finance.

This is due to a combination of favourable properties: its simplicity and ease of implementation (especially in one dimension); second order accuracy in the timestep for sufficiently regular data; and unconditional stability in an L_2 sense.

However, there are well-documented problems which arise from the fact that the scheme is at the cusp of stability in the sense that it is *A-stable* [see 38] but does not dampen so-called stiff components effectively (i.e., is not *strongly A-stable*).

Specifically, a straightforward Fourier analysis of the scheme applied to a standard finite difference discretisation of the heat equation shows that high wave number components are reflected in every time step but asymptotically do not diminish over time.

This gives rise to problems for applications with non-smooth data, where the behaviour of these components over time plays a crucial role in the smoothing of solutions.

Examples where this is relevant include Dirac initial data, as they appear naturally for adjoint equations [see 15], and piecewise linear and step function payoff data in the computation of option prices [see 46]. There, the situation is exacerbated if sensitivities of the solution to its input data (so-called 'Greeks') are needed; see [37] for an early discussion of issues with time-stepping schemes in this context.

There is a sizeable body of literature concerned with schemes with better stability properties, in particular *L-stable* schemes [see 38] which share with the underlying continuous equation the property that high wave number components decay increasingly fast in time.

Examples for schemes with this property include sub-diagonal Padé schemes based on rational approximations of the exponential function.

In [35], the author proposes to replace the first 2μ steps of a higher-order Padé scheme of order (μ, μ) (e.g., the Crank-Nicolson scheme for $\mu = 1$) by a lower-order sub-diagonal Padé scheme with order $(\mu - 1, \mu)$ (e.g., backward Euler for $\mu = 1$), and shows that this restores optimal convergence order for diffusion equations; the case $\mu = 1$ is already analysed in [26]. We will refer to this latter scheme specifically as

the *Rannacher scheme*.

It is demonstrated in [33] how this procedure can be used to obtain stable and accurate approximations to option values and their sensitivities for various non-smooth payoff functions.

This has been widely adopted in financial engineering practice. [24] extend this to more general Padé schemes and demonstrate numerically the stability and accuracy in practice for options with exotic payoffs.

Further adaptations are possible, for instance, [45] give an application to discretely sampled barrier options, where discontinuities are introduced at certain points in time and a new 'start-up' is needed (see already [35] for the provision of such restarts in an abstract context).

[5] analyse the behaviour of the Crank-Nicolson numerical scheme when used to solve a convection-diffusion equation with constant coefficients and Dirac delta function initial conditions. The numerical solution obtained by this method diverges as the time step goes to zero with the ratio $\lambda = k/h$ of the time step, k, to the space step, h, held constant.

Their analysis in the frequency domain shows that there are errors associated with high wave numbers which behave as $O(h^{-1})$ and which will eventually overwhelm the $O(h^2)$ errors associated with low wave numbers as the time step goes to zero, thus explaining why the errors in this scheme will eventually increase as the time step is reduced.

Keeping the ratio λ constant is desirable because the Crank-Nicolson central difference scheme is second order consistent in both space and time and the numerical scheme is more efficient if this property is exploited.

The authors extended their analysis to show why the incorporation of a small number of initial fully implicit time steps (i.e., the Rannacher scheme, [26, 35]) eliminates this divergence.

2.2 Overview

In this chapter, an alternative method of avoiding the divergence is proposed and analysed. The idea is to introduce a time change into the partial differential equation (PDE), $u_t = \frac{1}{2} u_{xx}$, by transforming the original time variable, t, to

$$\tilde{t} = \sqrt{t}$$

and solving the equation numerically using the Crank-Nicolson scheme in the new variables.

The time change applies to the heat equation (2.1) on $\mathbb{R} \times [0, T]$ and can be considered natural as the heat equation with suitable initial data admits similarity solutions which depend on $x/\sqrt{t}$. From a probabilistic angle, the heat equation is the Kolmogorov forward equation for the transition density of Brownian motion whose standard deviation at time t is $\sqrt{t}$.

After the time change, the numerical scheme has a uniform space step, h, in the x direction, and a uniform step in the $\tilde{t}$ direction, k, so that $\tilde{t}_n = nk$, for $n = 0, ..., N$ and there are N time steps.

The main result of the chapter is given by the following Theorem.

Theorem 2.2.1 *The Crank-Nicolson central difference scheme with uniform time steps exhibits second order convergence (in the maximum norm) for the time-changed heat equation, with Dirac initial data, as the time step k tends to zero with $\lambda = k/h$ held fixed, provided that $\lambda \leq 1/\sqrt{2}$. For $\lambda \geq 1/\sqrt{2}$ the scheme is still convergent with order $1/\lambda^2$.*

The proof of the Theorem is developed in Sections 2.3, 2.4, and 2.5 and concludes with the proof in 2.5.

The peculiar dependence of the convergence rate on the mesh ratio is in fact seen to be sharp up to a logarithmic factor.

It also follows from the analysis of the heat equation that the computational complexity under an optimal choice of the mesh ratio is lower than for the Rannacher scheme in its optimal refinement regime.

As an added benefit, we obtain experimental second order convergence for the value, delta and gamma of European and American options.

[12] observe that at-the-money prices of European and American options computed by a Crank-Nicolson finite difference scheme exhibit a reduced convergence order of 1 in the time step k, which improves to 2 for Rannacher start-up in the case of European options, but only to 3/2 for American options.

This last observation is rationalised by the square-root behaviour of the value and exercise boundary for short time-to-expiry. A heuristic adaptive time-stepping scheme based on this observation is shown there to restore second order convergence.

It is further demonstrated numerically in [41] that a non-uniform scheme with time points $t_n = (kn)^2$ for $n = 0, ..., \sqrt{T}/k = N$, provides a similar remedy. The step size hence increases in proportion to $2\sqrt{t}$ and the smallest (the first) step is of size T/N^2.

This is almost equivalent to the time-changed scheme, introduced above, with constant steps of size $\sqrt{T}/N$.

The only difference between the schemes is in the treatment of the time-dependent coefficients of the central difference terms in the x-direction after the time change has been applied. If the time change method is applied in this alternative fashion, it still leads to the same convergence behaviour

We extend the numerical investigation from [41] to show that in addition to second order convergence of the values, we also obtain second order for the Delta, and for the Gamma the order predicted by the analysis of the heat equation with Dirac data, and that even without Rannacher start-up.

The remainder of this chapter is organised as follows.

In Section 2.3, we apply the time change transformation to the heat equation, describe the transformed numerical scheme, and calculate the discrete Fourier transform of the numerical solution.

Then, in Section 2.4, we perform asymptotic analysis of the error between the transform and the transform of the true solution, identifying four wave number regimes which will then be used in the later analysis.

In Section 2.5, we use the results of the asymptotic analysis to determine the asymptotic behaviour of the errors between the numerical solution and the true solution, from which we deduce the convergence behaviour of the transformed scheme and hence Theorem 2.2.1.

Section 2.6 contains numerical results illustrating these findings and compares the computational complexity to the Rannacher scheme.

In Section 2.7 we introduce two variants of the basic time change scheme, one where the initial conditions are smoothed and one where the time change scheme is combined with Rannacher time-stepping.

In Section 2.8, the time change transformation is applied to the Black-Scholes equation and the solution method is used to calculate the gamma of a European call option. The behaviour of the resulting errors is described and explained in terms of the values of the strike and volatility.

Finally, in Section 2.9, the time change transformation is applied to a penalty method used to calculate the price of an American put, as described in [12]. Section 2.10 concludes.

2.3 The Crank-Nicolson scheme applied to the transformed heat equation and its behaviour in the Fourier domain

To simplify the analysis, we restrict attention to the heat equation (i.e., we do not consider any convection terms)

$$u_t = \tfrac{1}{2}\, u_{xx}, \tag{2.1}$$

for $t \in [0, T]$, $x \in \mathbb{R}$, where the solution, u, satisfies $u(x, 0) = \delta(x)$, where δ is the Dirac delta function and which, after the change of time variable, becomes

$$u_{\tilde{t}} = \tilde{t}\, u_{xx},$$

where $\tilde{t} = \sqrt{t}$.

The transformed equation is then discretised using the Crank-Nicolson method, leading to the following numerical scheme

$$\frac{U_j^{n+1} - U_j^n}{k} = \frac{1}{2}\,\tilde{t}_n\,\frac{U_{j+1}^n - 2U_j^n + U_{j-1}^n}{h^2} + \frac{1}{2}\,\tilde{t}_{n+1}\,\frac{U_{j+1}^{n+1} - 2U_j^{n+1} + U_{j-1}^{n+1}}{h^2}, \tag{2.2}$$

where U_j^n is the numerical solution at the spatial grid node j at the 'time' step n, and where the space grid, in principle, extends from $-\infty$ to $+\infty$, with $x_j = jh$ for $j \in \mathbb{Z}$. In the transformed 'time' direction, we have $\tilde{t}_n = nk$, for $1 \leq n \leq N$, where N is the number of timesteps.

We can simplify this to

$$(1 + (n+1)\lambda^2)U_j^{n+1} - \frac{1}{2}(n+1)\lambda^2 U_{j+1}^{n+1} - \frac{1}{2}(n+1)\lambda^2 U_{j-1}^{n+1}$$

$$= (1 - n\lambda^2)U_j^n + \frac{1}{2}n\lambda^2 U_{j+1}^n + \frac{1}{2}n\lambda^2 U_{j-1}^n,$$

where $\lambda = k/h$.

To study the behaviour of this scheme in the Fourier domain we apply the discrete Fourier transform to this equation (e.g., see [5] and [39]). Multiplying equation (2.2) by e^{isx_j}, summing over j and simplifying, we obtain the following recurrence for the Fourier transform

$$\widehat{U}^n(s) = h \sum_{j=-\infty}^{j=+\infty} U_j^n e^{isx_j}$$

at successive time steps,

$$\left(1 + 2(n+1)\lambda^2 \sin^2(sh/2)\right) \widehat{U}^{n+1}(s) = \left(1 - 2n\lambda^2 \sin^2(sh/2)\right) \widehat{U}^n(s).$$

The variable, s, appearing in the Fourier transform above, is called the (s-)wave number.

We use the discrete approximation

$$U_j^0 = \frac{\delta_{j,0}}{h} = \begin{cases} 1/h & j = 0, \\ 0 & j \neq 0, \end{cases}$$

to the Dirac delta and note that $\widehat{U}^0(s) \equiv 1$, so we have

$$\widehat{U}^N(s) = \frac{1(1-\xi)(1-2\xi)\dots(1-(N-1)\xi)}{(1+\xi)(1+2\xi)\dots(1+N\xi)}, \tag{2.3}$$

where $\xi = 2\lambda^2 \sin^2(sh/2)$ and we want to study the behaviour of $\widehat{U}^N(s)$ as $N \to \infty$ with $\tilde{T} := \sqrt{T} = kN$ and $\lambda = k/h$ held fixed.

In the subsequent analysis, it is often simpler to describe a condition on s, by stating the related condition on ξ, but it should be noted that the relationship between s and ξ depends on h.

In what follows, and to simplify the notation, we will fix $T = 1$, so that

$$N = \frac{1}{k} = \frac{1}{h\lambda}.$$

We note that the exact solution of the PDE is given by

$$u(x,t) = \frac{1}{\sqrt{2\pi t}} \exp\left(-\frac{x^2}{2t}\right) \tag{2.4}$$

and its Fourier transform is given by $\widehat{u}(s,t) = \exp(-s^2 t/2)$. So, for $t = \tilde{t} = 1$, we have $\widehat{u}(s,1) = \exp(-s^2/2)$.

As in [5] we can estimate the errors in the numerical solution (at time $t = \tilde{t} = 1$), i.e., the differences between the values of U_j^N and $u(x_j, 1)$, by applying the inverse Fourier transform to $\widehat{U}^N(s) - \widehat{u}(s,1)$.

2.4 Asymptotic analysis of the Fourier transform

In this section we identify four wave number regimes for the Fourier transform and obtain useful asymptotic estimates for $\widehat{U}^N(s)$, in each of these regimes.

Initially, we start by identifying three regimes, the low, intermediate and high wave number regimes (as in [5]), but then find it useful to subdivide the high wave number regime into two further regimes.

In essence, the wave number regimes are determined by the locations of the real zeros of the equation

$$\widehat{U}^N(s) = 0,$$

which are at s_m, for $m = m^*, \ldots, N-1$, for some integer $m^* \geq 1$, which depends only on λ, where

$$2\lambda^2 \sin^2(s_m h/2) = \frac{1}{m}.$$

and we note that $m^* \geq \frac{1}{2\lambda^2}$. Note that each s_m is a function of h and $s_m \to \infty$ as $h \to 0$, so these wave number boundaries increase in absolute terms while always being less than or equal to π/h.

The low wave number regime (which we will refer to as regime I) is, in part, defined by the requirement that all the terms in the numerator of the expression for $\widehat{U}^N(s)$ in equation (2.3) should be positive.

This requires that $\xi < 1/(N-1)$. If we assume the stronger condition that $\xi < 1/N$, we can write a truncated Taylor expansion for

$$\log(\widehat{U}^N(s)) = \sum_{m=1}^{N-1} \log(1 - m\xi) - \sum_{m=1}^{N} \log(1 + m\xi)$$

from which we can later derive an asymptotic estimate for $\widehat{U}^N(s)$.

As in [5], the low wave number regime is further restricted by the condition that $s < h^{-r}$, for a value r such that $r < \frac{1}{3}$, which ensures that the remainder terms in the Taylor expansion go to zero as $h \to 0$, so that we can derive a useful approximation for $\widehat{U}^N(s) - \widehat{u}(s, 1)$. As this condition also ensures that $\xi < 1/N$ asymptotically, this condition alone is sufficient to define the low wave number regime.

Next, there exists an intermediate wave number regime (regime II) defined by the range of wave numbers for which $\xi < 1/N$ but which are not in regime I (cf. [5]).

The high wave number regime is defined by the requirement that $\xi \geq 1/N$. If this condition on ξ is satisfied then some of the terms in the numerator of the expression for $\widehat{U}^N(s)$ in equation (2.3) will be negative. There will be an integer $m > 0$ such that $\xi \in [1/(m+1), 1/m]$ and the number of positive terms will remain fixed as N increases while the number of negative terms will increase with N. A particular negative factor $(1 - r\xi)$ can be rewritten as $-r\xi(1 - 1/r\xi)$, with $1/r\xi < 1$, and we can then write a truncated Taylor expansion for $\widehat{U}^N(s)$ in terms of $1/\xi$ which will then lead to an asymptotic value for $\widehat{U}^N(s)$.

At first sight, it might seem necessary to treat separately all the ξ-intervals of the form $[1/(m+1), 1/m]$, giving rise to an ever-growing set of wave number regimes but, in fact, it suffices for the results we wish to prove, to treat the last of these intervals, $[1/m^*, 2\lambda^2]$, separately and combine all the other intervals into a single regime.

So we define wave number regime III to correspond to the interval $[1/N, 1/m^*]$ and wave number regime IV to correspond to the interval $[1/m^*, 2\lambda^2]$. These ranges are equivalent to $s_N \leq s \leq s_{m^*}$ and $s_{m^*} < s \leq \pi/h$ respectively. We will obtain a uniform bound on the magnitude of $\widehat{U}^N(s)$ for $\xi \in [1/(m+1), 1/m]$ in regime III and an asymptotic value for the magnitude of $\widehat{U}^N(s)$ in the regime IV.

Table 2.1 summarises the wave number regimes giving their boundaries in terms of both ξ and s. (Only the regimes for positive wave numbers are shown. By symmetry, the regimes for the negative wave numbers are just the negatives of these intervals). The results of carrying out asymptotic expansions in the four wave number regimes are summarised in the following Lemma which gives the behaviour of the error between the two transforms, $\widehat{E}(s) = \widehat{U}^N(s) - \widehat{u}(s, 1)$.

Lemma 2.4.1 *The following formulae give the errors in the Fourier transform in each wave number regime (see Table 2.1).*

1. *In wave number regime I,*

$$\widehat{E}(s) = \widehat{u}(s,1)\left(\frac{1}{24}s^4 - \frac{1}{48}\lambda^2 s^6 + \frac{1}{8}\lambda^2 s^4\right) h^2(1 + o(1)).$$

Wave number regimes				
Regime	ξ_{min}	ξ_{max}	s_{min}	s_{max}
I	0	ξ_r	0	h^{-r}
II	ξ_r	$\frac{1}{N}$	h^{-r}	s_N
III	$\frac{1}{N}$	$\frac{1}{m^*}$	s_N	s_{m^*}
IV	$\frac{1}{m^*}$	$2\lambda^2$	s_{m^*}	$\frac{\pi}{h}$

Table 2.1: Limits of wave number regimes in terms of ξ and s. Here, $r < 1/3$, $\xi_r = 2\lambda^2 \sin^2(h^{1-r}/2)$, s_n are defined by $1/n = 2\lambda^2 \sin^2(s_n h/2)$ for $n = N$ and $n = m^*$, and $m^* \geq 1$ is the smallest n for which there exists such s_n

2. *In wave number regime II,*

$$\widehat{E}(s) = o(h^q)$$

for any $q > 0$.

3. *In wave number regime III,*

$$|\widehat{E}(s)| \leq \frac{((m+1)!)^2(N-m-1)!}{(2m+2)(N+m)!}$$

whenever $\xi = 2\lambda^2 \sin^2(sh/2) \in [1/(m+1), 1/m]$ *and, everywhere in this regime,*

$$\widehat{E}(s) = O(h^{2m^*+1})$$

for some $m^* \geq 1$.

4. *Finally, in wave number regime IV, there exists a positive, continuous, and hence bounded, function* $S(\cdot, m^*)$ *on* $[1/m^*, 2\lambda^2]$, *such that*

$$|\widehat{E}(s)| = S(\xi, m^*)h^{(1+\frac{2}{\xi})}(1 + O(h))).$$

Proof We first consider wave number regime I. Inspection of equation (2.3) shows that all the terms in the numerator are positive if $\xi \leq 1/N < 1/(N-1)$. We can then write $\log(U^N(s))$ as

$$\log(\widehat{U}^N(s)) = \sum_{j=1}^{N-1} (\log(1 - j\xi) - \log(1 + j\xi)) - \log(1 + N\xi) \tag{2.5}$$

and expand the component terms, $\log(1 \pm j\xi)$, by first expanding ξ in powers of h.

The calculations are very similar to those in [5] and we begin by first expanding $\xi = 2\lambda^2 \sin^2(sh/2)$ in powers of h to obtain

$$1 - j\xi = 1 - \frac{j\lambda^2 s^2}{2!}h^2 + \frac{j\lambda^2 s^4}{4!}h^4 - \frac{j\lambda^2 s^6}{6!}h^6 + \frac{j\lambda^2 s^8}{8!}h^8\theta_j \equiv \sum_{i=0}^{3} A_i h^{2i} \; + \; A_4 h^8,$$

where $|\theta_j| \leq 1$. Setting $\delta = h^2$, we define

$$\begin{aligned} g(\delta) &= 1 - j\xi = \sum_{i=0}^{3} A_i \delta^i \; + \; A_4 \delta^4, \\ f(\delta) &= \log(1 - j\xi) = \log\left(g(\delta)\right), \end{aligned}$$

and we can then expand $f(\delta)$ in terms of δ to obtain

$$\begin{aligned} \log(1 - j\xi) = &- \frac{j\lambda^2}{2!}s^2\delta + \frac{1}{2!}\left(\frac{2j\lambda^2}{4!} - \frac{j^2\lambda^4}{(2!)^2}\right)s^4\delta^2 \\ &+ \frac{1}{3!}\left(-\frac{6j\lambda^2}{6!} - \frac{2j^3\lambda^6}{(2!)^3} + \frac{6j^2\lambda^4}{2!4!}\right)s^6\delta^3 + Z_j s^8 \delta^4 \end{aligned}$$

and we have to ensure that the remainder Z_k is well-behaved. We do this by analysing the behaviour of

$$f^{(4)}(\delta) = \frac{p(\delta)}{g(\delta)^4},$$

where

$$p(\delta) = g(\delta)^3 g^{(4)}(\delta) + 2(g(\delta))^2 g'(\delta) g^{(3)}(\delta) + 6(g'(\delta))^2 g(\delta) g''(\delta) - 3(g''(\delta))^2 (g(\delta))^2 - 6(g'(\delta))^4.$$

Then $g(\delta) \to 1$ as $h \to 0$ if we ensure that $s < h^{-m}$, where $m < \frac{1}{2}$, because, for example,

$$|A_1\delta| = \frac{j\lambda^2 s^2 h^2}{2} < \frac{N\lambda^2 s^2 h^2}{2} = \frac{\lambda s^2 h}{2} \to 0.$$

Then h can be chosen small enough (or N large enough) so that

$$|1 + A_1\delta + A_2\delta^2 + A_3\delta^3 + A_4\delta^4| > \frac{1}{2}$$

so the denominator of $f^{(4)}(\delta)$ is bounded away from zero. Next we can show that

$$|g^{(i)}(\delta)| < \alpha_i |A_i|$$

for some constants, α_i for $i = 0, 1, 2, 3$ and 4, because of the constraint on s. We can finally conclude that

$$|f^{(4)}(\psi\delta)|\delta^4 < (2\alpha_4|A_4| + 4\alpha_1\alpha_3|A_1||A_3| + 48\alpha_1^2\alpha_2|A_1|^2|A_2| + 12\alpha_2^2|A_2|^2 + 96\alpha_1^4|A_1|^4)h^8.$$

and it follows that we can estimate asymptotically the remainder by just retaining the term proportional to $|A_1|^4h^8$ which is, in turn, proportional to $j^4\lambda^8s^8h^8$.

By changing the sign of j, we can obtain a similar expression for $\log(1 + j\xi)$ hence find that

$$\begin{aligned}&\log(1 - j\xi) - \log(1 + j\xi)\\ &= -j\lambda^2s^2h^2 + \frac{1}{12}j\lambda^2s^4h^4 - \frac{1}{360}j\lambda^2s^6h^6 - \frac{1}{12}j^3\lambda^6s^6h^6 + W_jj^4\lambda^8s^8h^8,\end{aligned}$$

where $|W_j| < K$ for some constant, K, and so

$$\begin{aligned}\log(\widehat{U}^N(s)) = &\left(-\lambda^2s^2h^2 + \frac{1}{12}\lambda^2s^4h^4 - \frac{1}{360}\lambda^2s^6h^6\right)\left(\sum_{j=1}^{N-1} j\right) - \frac{1}{12}\lambda^6s^6h^6\left(\sum_{j=1}^{N-1} j^3\right)\\ &+ \left(-\frac{\lambda^2s^2h^2}{2} + \frac{1}{24}\lambda^2s^4h^4 - \frac{1}{720}\lambda^2s^6h^6\right)N + \frac{1}{8}\lambda^4s^4h^4N^2 - \frac{1}{48}\lambda^4s^6h^6N^2\\ &- \frac{1}{24}\lambda^6s^6h^6N^3 + O(s^8h^3),\end{aligned}$$

because $(\sum_{j=1}^{j=N} j^4)\lambda^8s^8h^8 = O(N^5\lambda^8s^8h^8) = O(\lambda^3s^8h^3)$. So

$$\begin{aligned}\log(\widehat{U}^N(s)) = &\left(-\lambda^2s^2h^2 + \frac{1}{12}\lambda^2s^4h^4 - \frac{1}{360}\lambda^2s^6h^6\right)\left(\frac{1}{2}(N-1)N + \frac{N}{2}\right)\\ &- \frac{1}{12}\lambda^6s^6h^6\left(\left(\frac{1}{2}(N-1)N\right)^2 + \frac{N^3}{2}\right) + O(s^8h^3)\end{aligned}$$

as the remaining terms are dominated by $O(s^8h^3)$. Substituting $N = \frac{1}{h\lambda}$ we get

$$\begin{aligned}\log(\widehat{U}^N(s)) = &-\frac{1}{2}s^2 + \left(\frac{1}{24}s^4 - \frac{1}{48}\lambda^2s^6 + \frac{1}{8}\lambda^2s^4\right)h^2\\ &- \left(\frac{1}{720}s^6 + \frac{1}{48}\lambda^2s^6 + \frac{1}{48}\lambda^4s^6\right)h^4 + O(s^8h^3)\end{aligned}$$

and so we find that

$$\log(\widehat{U}^N(s)) = -\frac{1}{2}s^2 + \left(\frac{1}{24}s^4 - \frac{1}{48}\lambda^2 s^6 + \frac{1}{8}\lambda^2 s^4\right) h^2 + O(s^8 h^3) \tag{2.6}$$

because the s^6h^4 term of the expansion is dominated by the term $O(s^8h^3)$.

We require that the second term converges to zero as $h \to 0$ and the last term is asymptotically dominated by the second term. These conditions are satisfied by requiring that $s < h^{-r}$ with $r < \frac{1}{3}$ and this condition on s defines the upper limit of the wave number regime I.

We then have, with $\widehat{u}(s,1) = \exp(-s^2/2)$,

$$\widehat{U}^N(s) - \widehat{u}(s,1) = \widehat{u}(s,1)\left(\frac{1}{24}s^4 - \frac{1}{48}\lambda^2 s^6 + \frac{1}{8}\lambda^2 s^4\right) h^2(1 + o(1))$$

as we set out to prove.

We now consider wave number regime II.

The analysis is again similar to that in [5]. The lower limit of wave number regime II is $O(h^{-r})$ with $r < \frac{1}{3}$ (which corresponds to the upper limit of wave number regime I) and the upper limit of the regime corresponds to the first zero of $\widehat{U}^N(s)$, i.e., $s = (2/h)\sin^{-1}\sqrt{(1/2\lambda^2(N-1))}$, which is $O(h^{-\frac{1}{2}})$. In this regime each of the factors $(1 - m\xi)/(1 + (m+1)\xi)$ in $\widehat{U}^N(s)$ is positive and decreasing as s increases.

Consequently, the value of $\widehat{U}^N(s)$ will be less than or equal to its value at $s = h^{-r}$ for $0 < r < 1/3$. However, at $s = h^{-r}$ we have, for any $q > 0$,

$$\frac{\widehat{U}^N(s)}{h^q} = \frac{e^{-\frac{1}{2}h^{-2r}}}{h^q} \exp\left(h^{2(1-2r)}\left(\frac{1}{24} + \frac{\lambda^2}{8}\right) - h^{2(1-3r)}\frac{1}{48}\lambda^2 + o(1)\right) \to 0$$

as $h \to 0$, so $\widehat{U}^N(s) = o(h^q)$ at $s = h^{-\frac{1}{3}}$ and so we have $\widehat{U}^N(s) = o(h^q)$ throughout this regime.

Next we consider the high wave number regime which is split into two parts.

It is in wave number regimes III and IV that our analysis differs significantly from that in [5] where there are repeated factors in the corresponding expression for $\widehat{U}^N(s)$,

which results in a simpler expansion in terms of $1/\xi$.

In our case, $\widehat{U}^N(s)$ is a product of many different factors, so the analysis and expansion is more complicated. However, we can obtain our key results by breaking the high wave number regime into two parts and we will find that we only need to perform an expansion in regime IV.

For wave number regime III, which extends from $s_N = (2/h)\sin^{-1}\sqrt{(1/2\lambda^2 N)}$ to s_{m^*}, corresponding to ξ running from $1/N$ to $1/m^*$, with $m^* \geq 1$, we investigate the behaviour of $\widehat{U}^N(s)$ for values of s corresponding to values of ξ in the intervals $[1/(m+1), 1/m]$, where $m^* \leq m \leq N-1$. We write $\widehat{U}^N(s)$ as

$$\widehat{U}^N(s) = \left\{ \frac{1(1-\xi)(1-2\xi)..(1-m\xi)}{(1+\xi)(1+2\xi)..(1+(m+1)\xi)} \right\} \left\{ \frac{(1-(m+1)\xi)..(1-(N-1)\xi)}{(1+(m+2)\xi)..(1+N\xi)} \right\} \quad (2.7)$$

For the range of values of $\xi \in [1/(m+1), 1/m]$ being considered, the expression in the first set of curly brackets on the right hand side of the equation, is a product of non-negative factors, $(1-\nu\xi)/(1+(\nu+1)\xi)$, for $\nu = 0, ..., m$, each of which is decreasing in ξ, and so is bounded by its value evaluated at $\xi = 1/(m+1)$, i.e., $((m+1)!)^2/(2m+2)!$

Similarly, the expression in the second set of curly brackets is a product of factors $(1-\nu\xi)/(1+(\nu+1)\xi)$, for $\nu = m+1, ..., N-1$, which are all negative and whose magnitude is increasing with ξ. So the magnitude of this expression is bounded by the magnitude of the expression evaluated at $\xi = 1/m$, i.e., $(N-m-1)!(2m+1)!/(N+m)!$

Therefore, the magnitude of $\widehat{U}^N(s)$ for $1/(m+1) \leq \xi \leq 1/m$ is bounded by

$$W_{N,m} = \frac{((m+1)!)^2(N-m-1)!}{(2m+2)(N+m)!}, \quad (2.8)$$

and we consider the behaviour of this expression as m decreases from $N-1$ to m^*.

We have

$$\frac{W_{N,m-1}}{W_{N,m}} = \frac{N^2-m^2}{m(m+1)},$$

and this expression is less than one for

$$N^2 - m^2 < m(m+1),$$

which corresponds approximately to $m > N/\sqrt{2}$. This implies that, as m decreases from $N-1$, $W_{N,m}$ first decreases, reaching a minimum in the vicinity of $N/\sqrt{2}$ and then increases. So the maximum of $|\widehat{U}^N(s)|$ will occur either at $m = N-1$ or at $m = m^*$.

We now compare the values of $W_{N,m}$ at these values of m, by calculating the ratio

$$\frac{W_{N,m^*}}{W_{N,N-1}} = \frac{((m^*+1)!))^2}{(2m^*+2)} \frac{(N-m^*-1)!}{(N+m^*)!} \frac{(2N)!}{(N!)^2}.$$

By Stirling's formula, we have the approximation

$$\frac{(2N)!}{(N!)^2} \sim \frac{(2N)^{2N+\frac{1}{2}}e^{-2N}}{((N)^{N+\frac{1}{2}}e^{-N})^2} \sim \frac{2^{2N+\frac{1}{2}}}{N^{\frac{1}{2}}}$$

and we see that the exponential term dominates the other powers of N and $W_{N,m^*}/W_{N,N-1} \to \infty$ as $N \to \infty$. So, for large enough N, $W_{N,m}$ is maximised at $m = m^*$ and it then follows that the expression

$$\frac{((m^*+1)!)^2}{(2m^*+2)} \frac{(N-m^*-1)!}{(N+m^*)!} = O(N^{-2m^*-1}) = O(h^{2m^*+1})$$

gives a uniform bound on $|\widehat{U}^N(s)|$ in wave number regime III.

Finally, we consider wave number regime IV.

In this regime, we will find that we must perform an expansion of $\widehat{U}^N(s)$ from (2.7) and we write

$$\left|\widehat{U}^N(s)\right| = M(\xi, m^*) \left| \frac{(1-(m^*+1)\xi)\dots(1-(N-1)\xi)}{(1+(m^*+1)\xi)\dots(1+(N-1)\xi)} \right| (1+N\xi)^{-1},$$

where

$$M(\xi, m^*) = \left| \frac{(1-\xi)(1-2\xi)\dots(1-m^*\xi)}{(1+\xi)(1+2\xi)\dots(1+m^*\xi)} \right|,$$

so

$$\log\left(\left|\widehat{U}^N(s)\right|\right) = \log(M(\xi, m^*)) + \log\left\{ \frac{(1-\frac{1}{\xi(m^*+1)})\dots(1-\frac{1}{\xi(N-1)})}{(1+\frac{1}{\xi(m^*+1)})\dots(1+\frac{1}{\xi(N-1)})} \right\} + \log((1+N\xi)^{-1}), \tag{2.9}$$

and we seek an expansion of the right-hand side of this equation in terms of $1/\xi$, as follows.

We write

$$\log \frac{(1-\frac{1}{\xi(m^*+1)})\dots(1-\frac{1}{\xi(N-1)})}{(1+\frac{1}{\xi(m^*+1)})\dots(1+\frac{1}{\xi(N-1)})} = \sum_{j=m^*+1}^{j=N-1} \left(\log\left(1-\frac{1}{j\xi}\right) - \log\left(1+\frac{1}{j\xi}\right) \right).$$

We can expand the logarithmic terms for $\xi \in [1/m^*, 2\lambda^2]$ to get

$$\begin{aligned} \sum_{j=m^*+1}^{j=N-1} \left(\log(1-\frac{1}{j\xi}) - \log(1+\frac{1}{j\xi}) \right) &= \sum_{j=m^*+1}^{j=N-1} \left(\sum_{l=1}^{\infty} \frac{(-1)}{l(j\xi)^l} - \sum_{l=1}^{\infty} \frac{(-1)^{l+1}}{j(j\xi)^l} \right) \\ &= -\sum_{l=0}^{\infty} \frac{2}{(2l+1)\xi^{2l+1}} \left(\sum_{j=m^*+1}^{j=N-1} \frac{1}{j^{2l+1}} \right) \end{aligned}$$

and, for any N, this series converges absolutely in $1/\xi$ as we have just rearranged a finite sum of absolutely convergent series. We can write this as

$$\begin{aligned} &\sum_{j=m^*+1}^{j=N-1} \left(\log(1-\frac{1}{j\xi}) - \log(1+\frac{1}{j\xi}) \right) \\ &\quad = -\frac{2}{\xi} \left(\sum_{j=m^*+1}^{j=N-1} \frac{1}{j} \right) - \sum_{l=1}^{\infty} \frac{2}{(2l+1)\xi^{2l+1}} \left(\sum_{j=m^*+1}^{j=N-1} \frac{1}{j^{2l+1}} \right) \\ &\quad = -\frac{2}{\xi} \left(\sum_{j=m^*+1}^{j=N-1} \frac{1}{j} \right) + A(\xi, m^*) + B(\xi, N), \end{aligned} \tag{2.10}$$

where

$$\begin{aligned} A(\xi, m^*) &= -\sum_{l=1}^{\infty} \frac{2}{(2l+1)\xi^{2l+1}} \left(\sum_{j=m^*+1}^{\infty} \frac{1}{j^{2l+1}} \right), \\ B(\xi, N) &= \sum_{l=1}^{\infty} \frac{2}{(2l+1)\xi^{2l+1}} \left(\sum_{j=N}^{\infty} \frac{1}{j^{2l+1}} \right), \end{aligned}$$

and we must establish the convergence and size of the functions $A(\xi, m^*)$ and $B(\xi, N)$ (see below).

We also have

$$-\log(1+N\xi) = -\log N\xi - \log\left(1+1/N\xi\right) = -\log N\xi - \sum_{l=1}^{\infty} \frac{(-1)^{l+1}}{l(N\xi)^l}$$
$$= -\log N\xi - \frac{1}{N\xi} + C(\xi, N),$$

where

$$C(\xi, N) = -\sum_{l=2}^{\infty} \frac{(-1)^{l+1}}{l(N\xi)^l}$$

so that

$$\begin{aligned}
&\log\left(\left|\widehat{U}^N(s)\right|\right) \\
&= \log(M(\xi, m^*)) - \frac{2}{\xi}\left(\sum_{j=m^*+1}^{j=N-1} \frac{1}{j}\right) + A(\xi, m^*) + B(\xi, N) - \log N\xi - \frac{1}{N\xi} + C(\xi, N) \qquad (2.11) \\
&= \log(M(\xi, m^*)) - \frac{2}{\xi}\left(\sum_{j=m^*+1}^{j=N} \frac{1}{j}\right) + A(\xi, m^*) + B(\xi, N) - \log N\xi + \frac{1}{N\xi} + C(\xi, N) \\
&= P(\xi, m^*) - \frac{2}{\xi}\left(\sum_{j=1}^{j=N} \frac{1}{j}\right) + D(\xi, N) - \log N + O(N^{-1}),
\end{aligned}$$

where

$$P(\xi, m^*) = \log(M(\xi, m^*)) - \frac{2}{\xi}\left(\sum_{j=1}^{j=m^*} \frac{1}{j}\right) + A(\xi, m^*) - \log\xi$$

and

$$D(\xi, N) = B(\xi, N) + C(\xi, N).$$

Then we can write

$$\begin{aligned}
\log\left(\left|\widehat{U}^N(s)\right|\right) &= P(\xi, m^*) - \frac{2}{\xi}\left(\log N + \gamma + O(N^{-1})\right) + D(\xi, N) - \log N + O(N^{-1}) \\
&= Q(\xi, m^*) - \left(\frac{2}{\xi} + 1\right)\log N + O(N^{-1}) + D(\xi, N),
\end{aligned}$$

where γ is the Euler-Macheroni constant [see 43], and where

$$Q(\xi, m^*) = P(\xi, m^*) - \frac{2}{\xi}\gamma.$$

Then using $N = 1/(h\lambda)$ and assuming for now $D(\xi, N) = O(N^{-1})$, which we will show later, we get

$$\log\left(\left|\widehat{U}^N(s)\right|\right) = R(\xi, m^*) + \left(\frac{2}{\xi} + 1\right)\log h + O(h),$$

where

$$R(\xi, m^*) = Q(\xi, m^*) + \left(\frac{2}{\xi} + 1\right)\log\lambda.$$

Then we finally have

$$\left|\widehat{U}^N(s))\right| = S(\xi, m^*)h^{\left(\frac{2}{\xi}+1\right)}(1 + O(h))$$

as we were required to prove. We note that, written out in full, we have

$$S(\xi, m^*) = M(\xi, m^*)\lambda^{(\frac{2}{\xi}+1)}\exp\left(-\frac{2}{\xi}\left(\gamma + \sum_{j=1}^{j=m^*}\frac{1}{j}\right)\right)e^{A(\xi,m^*)}$$

and we note that $S(\cdot, m^*)$ is continuous and hence bounded on $[1/m^*, 2\lambda^2]$.

We still need to prove that $A(\xi, m^*) + B(\xi, N)$ is a valid rearrangement and proceed by proving that $A(\xi, m^*)$ is convergent. It will then follow that $B(\xi, N)$ is also convergent. In addition we will show that $D(\xi, N) = B(\xi, N) + C(\xi, N) = O(N^{-2})$.

Using Proposition 1 of [40], the following result is proved and stated in the abstract that paper.

For $r \geq 1$, we have

$$\sum_{j=m^*+1}^{j=\infty}\frac{1}{j^{2r+1}} = \frac{1}{2r(m^* + \theta_{m^*})^{2r}}$$

for some $\theta_{m^*} \geq \frac{1}{2}$.

Therefore,

$$\begin{aligned} |A(\xi, m^*)| &< \sum_{l=1}^{\infty} \frac{2}{(2l+1)} \frac{1}{\xi^{2l+1}} \frac{1}{2l(m^* + \frac{1}{2})^{2l}} \\ &= \left(m^* + \frac{1}{2}\right) \sum_{l=1}^{\infty} \frac{1}{l(2l+1)} \frac{1}{(\xi(m^* + \frac{1}{2}))^{2l+1}} \\ &< \frac{1}{3}\left(m^* + \frac{1}{2}\right) \eta^3 \sum_{l=0}^{\infty} \eta^{2l}, \end{aligned}$$

where $\eta = 1/(\xi(m^* + \frac{1}{2})) < 1$ and so $A(\xi, m^*)$ is convergent. It follows that $B(\xi, N)$ is convergent because $A(\xi, m^*) + B(\xi, N)$ is convergent.

Next we find out how $B(\xi, N)$ depends on N. We have

$$\begin{aligned} |B(\xi, N)| &< 2\sum_{l=1}^{\infty} \frac{1}{(2l+1)} \frac{1}{\xi^{2l+1}} \frac{1}{2l(N - 1 + \frac{1}{2})^{2l}} \\ &= 2N \sum_{l=1}^{\infty} \frac{1}{(2l+1)} \frac{1}{(N\xi)^{2l+1}} \frac{N^{2l}}{2l(N - \frac{1}{2})^{2l}}, \end{aligned}$$

and as $N/(N - \frac{1}{2}) \leq 2$, we have

$$|B(\xi, N)| < 2N \sum_{l=1}^{\infty} \frac{1}{(2l+1)} \frac{1}{(N\xi)^{2l+1}} \frac{2^{2l+1}}{4l} < \frac{1}{12} N \sum_{l=1}^{\infty} \left(\frac{2}{N\xi}\right)^{2l+1}.$$

Then because we have $2/\xi \leq 2m^*$, we find that for sufficiently large N, we have $2/N\xi < c < 1$ for a constant c and the geometric series converges and we find that

$$|B(\xi, N)| < \frac{1}{6} N \left(\frac{2}{N\xi}\right)^3 \frac{1}{\left(1 - \frac{2}{N\xi}\right)} = O(N^{-2})$$

and similarly for C. It then follows that $D(\xi, N) = O(N^{-2})$.

So then we have

$$\left|\widehat{U}^N(s)\right| = S(\xi, m^*) h^{(2/\xi+1)}(1 + O(h)), \tag{2.12}$$

where S is a function of ξ and m^*, which is positive and continuous on $[1/m^*, 2\lambda^2]$, as we wanted to show.

2.5 Error contributions from the various wave number regimes

The error in the numerical scheme at x_j is found by using the inverse Fourier transform

$$E_j = \frac{1}{2\pi} \int_{-\frac{\pi}{h}}^{\frac{\pi}{h}} \widehat{E}(s) \exp(-isx_j) \, \mathrm{d}s,$$

where $\widehat{E}(s)$ is the error in the Fourier transform.

So decomposing the error, applying the inverse Fourier transform and using symmetry, we can write

$$E_j = \sum_{i=1}^{4} E_j^i,$$

where

$$E_j^i = \frac{1}{\pi} \int_{I_i} \widehat{E}(s) \cos(sx_j) \, \mathrm{d}s, \tag{2.13}$$

where I_i is the wave number region for $i \in \{I, II, III, IV\}$. We then have the following Lemma which makes use of the results from Lemma 2.4.1.

Lemma 2.5.1 *With $E^i = (E_j^i)_{j\in\mathbb{Z}}$ defined in (2.13), the contribution to the error of the numerical scheme from the four wave number regimes is given by*

$$\begin{array}{lcll} E^I & = & O(h^2), & \\ E^{II} & = & o(h^q) & \text{for any } q > 0, \\ E^{III} & = & O(h^{2m^*}) & \text{for some } m^* \geq 1, \\ E^{IV} & = & O\left(h^{\frac{1}{\lambda^2}} / |\log h|^{\frac{1}{2}}\right). & \end{array}$$

Proof In wave number regime I, the analysis is similar to that in [5]. The key observation is that the term $\widehat{u}(s,1)(\frac{1}{24}s^4 - \frac{1}{48}\lambda^2 s^6 + \frac{1}{8}\lambda^2 s^4)$ has a readily identifiable inverse Fourier transform, and we deduce that the error contribution is $O(h^2)$.

In wave number regime II, we again follow the analysis in [5] to conclude that the error contribution from this regime will be dominated by h^q for any $q > 0$.
In wave number regime III, we can write

$$\int_{s_{N-1}}^{s_{m^*}} \left|\widehat{U}^N(s) \cos(sx_j)\right| \, \mathrm{d}s \leq \int_0^{\pi/h} \left|\widehat{U}^N(s)\right| \, \mathrm{d}s, \tag{2.14}$$

which is $\pi/h \cdot O(h^{2m^*+1})$, i.e., $O(h^{2m^*})$.

Finally, we consider the error contribution from wave number regime IV, i.e., where $s_{m^*} \leq s \leq \pi/h$.

We need to determine the behaviour, as $h \to 0$, of

$$\int_{s_{m^*}}^{\frac{\pi}{h}} S(\xi, m^*) h^{(1+\frac{2}{\xi})} \cos(s x_j)\, \mathrm{d}s,$$

the magnitude of which is maximised at $j = 0$ (this is because S is positive in this wave number regime). So we only need to consider the value of the maximum error, $F(h)$, given by

$$F(h) = \int_{s_{m^*}}^{\frac{\pi}{h}} S(\xi, m^*) h^{(1+\frac{2}{\xi})}\, \mathrm{d}s.$$

From $\xi = 2\lambda^2 \sin^2(sh/2)$, we find that

$$F(h) = \int_{\xi_{m^*}}^{2\lambda^2} \frac{S(\xi, m^*) h^{\frac{2}{\xi}}}{\sqrt{\xi}\sqrt{2\lambda^2 - \xi}}\, \mathrm{d}\xi.$$

As the lowest (i.e., dominant) order in h from $h^{\frac{2}{\xi}}$ occurs when $\xi = 2\lambda^2$ we expect that this integral will be close to $O(h^{\frac{1}{\lambda^2}})$.

We want to show that

$$I|\log h|^{\frac{1}{2}} = |\log h|^{\frac{1}{2}} \int_{\xi_{m^*}}^{2\lambda^2} \frac{S(\xi, m^*) h^{(\frac{2}{\xi} - \frac{1}{\lambda^2})}}{\sqrt{\xi}\sqrt{2\lambda^2 - \xi}} \mathrm{d}\xi = \frac{|\log h|^{\frac{1}{2}} F(h)}{h^{\frac{1}{\lambda^2}}} = O(1)$$

where $S(\cdot, m^*)$ is continuous and non-negative, so that

$$F(h) = \frac{h^{\frac{1}{\lambda^2}}}{|\log h|^{\frac{1}{2}}} O(1).$$

We make the substitution $\eta^2 = |\log h|(1 - \xi/2\lambda^2)$ to obtain

$$I = |\log h|^{-\frac{1}{2}} \int_0^{\eta^*} S^*(\eta, m^*) \exp\left(- \frac{\frac{\eta^2}{\lambda^2}}{1 - \frac{\eta^2}{|\log h|}} \right) \mathrm{d}\eta,$$

where $S^*(\eta, m^*) = 2S(2\lambda^2(1 - \frac{\eta^2}{|\log h|}), m^*)/\sqrt{(1 - \frac{\eta^2}{|\log h|})}$ is a continuous function for which $\exists\ S^*_{max}$ such that $|S^*(\eta, m^*)| < S^*_{max}$ for all $\eta \in [0, \eta^*]$, and where $\eta^{*2} =$

$|\log h|(1-\frac{\xi_{m^*}}{2\lambda^2}) = \alpha^2|\log h|$ with $\alpha = \sqrt{(1-\frac{\xi_{m^*}}{2\lambda^2})}$.

We split the integral into two parts, written as

$$I = I_1 + I_2,$$

where

$$I_1 = |\log h|^{-\frac{1}{2}} \int_0^{\overline{\eta}} S^*(\eta, m^*) \exp\left(-\frac{\frac{\eta^2}{\lambda^2}}{1-\frac{\eta^2}{|\log h|}}\right) \mathrm{d}\eta$$

and

$$I_2 = |\log h|^{-\frac{1}{2}} \int_{\overline{\eta}}^{\eta^*} S^*(\eta, m^*) \exp\left(-\frac{\frac{\eta^2}{\lambda^2}}{1-\frac{\eta^2}{|\log h|}}\right) \mathrm{d}\eta$$

with $\overline{\eta}$ chosen so that, asymptotically, I_1 dominates I_2, and we can take $\overline{\eta} = \alpha|\log h|^{\frac{1}{4}}$. Firstly, we consider I_2. For $h < 1$, the second factor of the integrand is decreasing in η, so

$$\begin{aligned}|I_2| <& |\log h|^{-\frac{1}{2}} S^*_{max} \exp\left(-\frac{\frac{\alpha^2|\log h|^{\frac{1}{2}}}{\lambda^2}}{1-\alpha^2|\log h|^{-\frac{1}{2}}}\right)(\alpha|\log h|^{\frac{1}{2}} - \alpha|\log h|^{\frac{1}{4}}) \\ <& \alpha S^*_{max} \exp\left(-\frac{\alpha^2|\log h|^{\frac{1}{2}}}{\lambda^2}\right)\end{aligned}$$

where S^*_{max} is a bound for S^* on $[\xi_{m^*}, 2\lambda^2]$.

We also find that

$$\lim_{h\to 0} I_1|\log h|^{\frac{1}{2}} = \lim_{h\to 0} \int_0^{\overline{\eta}} \frac{2S(2\lambda^2(1-\frac{\eta^2}{|\log h|}), m^*)}{\sqrt{(1-\frac{\eta^2}{|\log h|}}} \exp\left(-\frac{\frac{\eta^2}{\lambda^2}}{1-\frac{\eta^2}{|\log h|}}\right)\mathrm{d}\eta,$$

and after noting that $\frac{\overline{\eta}^2}{|\log h|} = \alpha|\log h|^{-\frac{1}{2}} \to 0$ and $\overline{\eta} \to \infty$ as $h \to 0$, we have

$$\lim_{h\to 0} I_1|\log h|^{\frac{1}{2}} = \int_0^{\infty} 2S(2\lambda^2, m^*) \exp\left(-\frac{\eta^2}{\lambda^2}\right)\mathrm{d}\eta = O(1),$$

so that

$$\lim_{h\to 0}\left|\frac{I_2}{I_1}\right| = \lim_{h\to 0} \alpha S^*_{max}|\log h|^{\frac{1}{2}} \exp\left(-\frac{\alpha^2|\log h|^{\frac{1}{2}}}{\lambda^2}\right) = 0$$

and we conclude that $I|\log h|^{\frac{1}{2}} = O(1)$.

It now follows that the error contribution in regime IV is $O\left(h^{\frac{1}{\lambda^2}}|\log h|^{-\frac{1}{2}}\right)$.

We now give the proof of Theorem 2.2.1, as follows.

Proof of Theorem 2.2.1

From Lemma 2.5.1 we have the following:

- For $\lambda \leq \frac{1}{\sqrt{2}}$ we have $m^* \geq 1$, so the convergence behaviour of the uniform time change scheme, with Dirac initial data, is eventually dominated by wave number regime I and the errors (in the maximum norm) will be $O(h^2)$.
- For $\lambda > 1/\sqrt{2}$, we have $m^* = 1$, so the numerical error of the scheme is dominated by wave number regime IV. The scheme still converges but the errors will now be $O\left(h^{\frac{1}{\lambda^2}}|\log h|^{-\frac{1}{2}}\right)$. The logarithmic factor in this expression is slow growing and the error will be close to $O(h^{1/\lambda^2})$ which is worse than $O(h^2)$.

So for $\lambda \leq \frac{1}{\sqrt{2}}$, the uniform time change scheme, with Dirac initial data, exhibits quadratic convergence (in the maximum norm) as $h \to 0$, with λ fixed. For $\lambda \geq \frac{1}{\sqrt{2}}$ the scheme is still convergent but with reduced order, $\frac{1}{\lambda^2}$, which is what was to be proved in Theorem 2.2.1 ∎.

For any value of λ, we get convergence in the transformed numerical scheme whereas, without the time change, the errors eventually increase as $h \to 0$, with λ controlling how small h has to be for the divergence to manifest itself in practice (see [5]).

2.6 Numerical results and complexity considerations

Numerical experiments have been performed to investigate the behaviour of the time-changed scheme used to solve the heat equation (2.1) with delta-function initial conditions. The analysis used $T = 1$ and the space domain was truncated at $x = \pm 10$. The numerical scheme was run with a largest value of $k = 0.01$, i.e., with 100 time steps in the transformed coordinates. The grid was repeatedly refined by dividing both h and k by 2.

The error (in the maximum norm) of the scheme was analysed by comparing the numerical results with the exact solution given by (2.4).

Figure 2.1: Error plots for the time-changed scheme

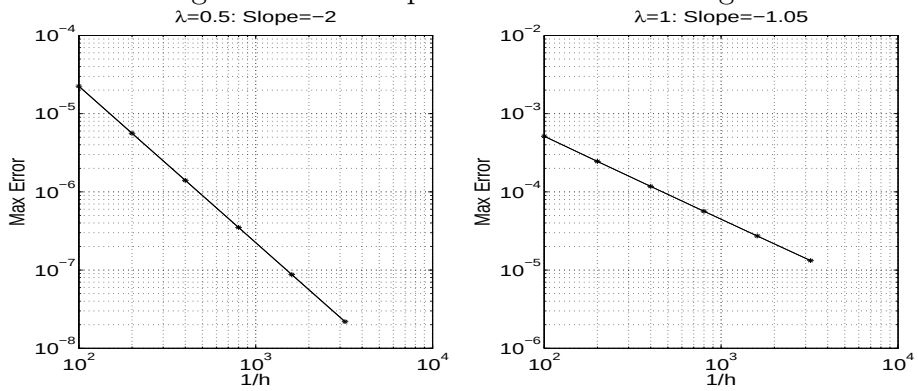

Figure 2.1 shows the log-log plots of the errors versus h for the cases $\lambda = 0.5$ and $\lambda = 1.0$, either side of $1/\sqrt{2}$. The estimated convergence orders of 2 and 1.05, respectively, are in line with Theorem 2.2.1.

The slope of the log-log plot was then plotted against the value of λ in Figure 2.2, along with the h exponent for the error derived from the analysis above, where we ignore the effect of the $|\log h|^{\frac{1}{2}}$ term on the behaviour of the error in wave number regime IV and just use the expression $\min(2, 1/\lambda^2)$.

Figure 2.2: Convergence order for the time-changed scheme as a function of λ

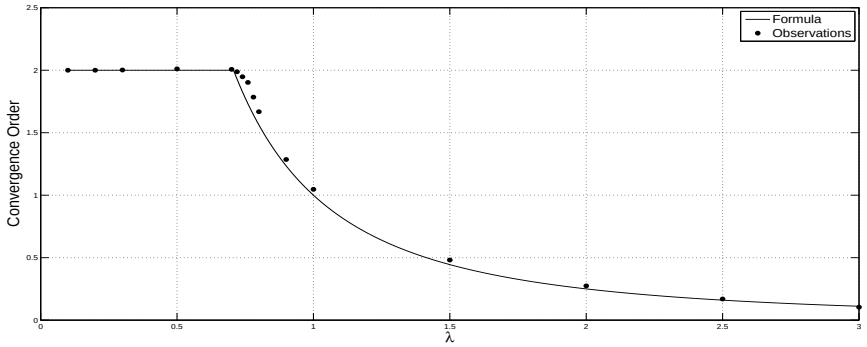

We see a good match between theory and experiment with the larger divergences being seen where λ is closest to the critical value of $1/\sqrt{2}$.

It is not possible to determine experimentally the h exponent with complete accuracy for two reasons.

Firstly, as $h \to 0$, the time required for each solution increases rapidly so, for comparison purposes, all the calculations were terminated when the number of time steps reached 3200.

As the overall error of the scheme is a mixture of errors with different h exponents, the behaviour of the scheme will not be entirely defined by the asymptotically dominating h exponent because the calculations terminate early. In particular, for λ slightly above $1/\sqrt{2}$, smaller values of h need to be reached before the error from wavenumber IV clearly dominates the other errors. Note that our analysis does not identify the weighting factors for the errors of different order in h.

Secondly, the additional term, $|\log h|^{-\frac{1}{2}}$, in the error behaviour in wave number regime IV will distort the error plot and tend to increase the apparent h exponent to some extent.

For values of λ above the critical value, we expect the asymptotic behaviour of wavenumber IV to dominate the error, $E(h)$, for small mesh size h. So, asymptotically, we expect to have $\mathrm{E(h)}/h^{\frac{1}{2\lambda^2}} \sim |\log h|^{-\frac{1}{2}}$, and a log-log plot between these two expressions would be expected to reveal a slope of -0.5 for sufficiently small h. Figure 2.3 shows this behaviour as $h \to 0$ and the numerical results support the asymptotic behaviour of the $|\log h|^{-\frac{1}{2}}$ term although the convergence is slow for values of λ near the critical value.

Figure 2.3: Time Change Scheme: Slope from plot of $\log(\mathrm{E(h)}/h^{\frac{1}{2\lambda^2}})$ against $\log|\log h|$ as a function of λ

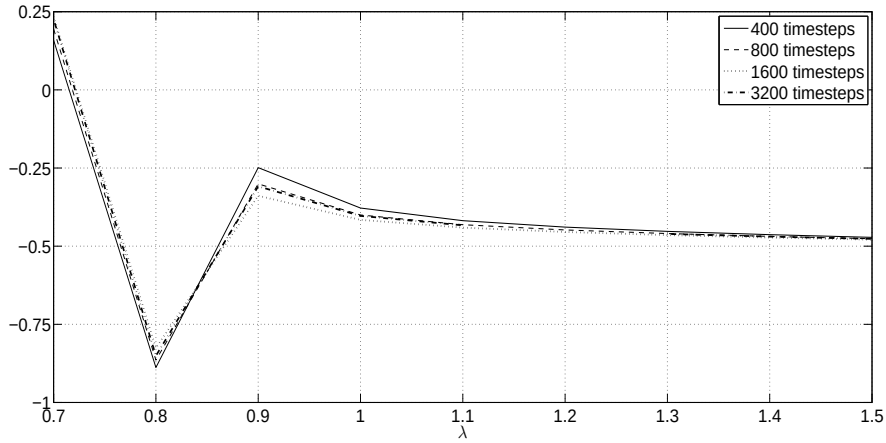

We have also carried out a comparison of the error performance between the time change scheme and the Rannacher scheme. For $\lambda \leq 1/\sqrt{2}$, both schemes will show quadratic convergence and, for small values of h, we can write (as in [5])

$$\widehat{U}_R^N(s) - \widehat{u}(s,1) = \widehat{u}(s,1)\left(\frac{1}{24}s^4 + \frac{1}{8}\lambda^2 s^4 - \frac{1}{96}\lambda^2 s^6\right) h^2(1+o(1))$$

and

$$\widehat{U}_{TC}^N(s) - \widehat{u}(s,1) = \widehat{u}(s,1)\left(\frac{1}{24}s^4 + \frac{1}{8}\lambda^2 s^4 - \frac{1}{48}\lambda^2 s^6\right) h^2(1+o(1)),$$

where $\widehat{U}_R^N(s)$ and $\widehat{U}_{TC}^N(s)$ are the Fourier transforms for the Rannacher and time-changed scheme in wave number regime I.
For $m \geq 1$, the m^{th} derivative of the cumulative Normal distribution, $N(x)$, has the Fourier transform given by

$$\widehat{N^{(m)}}(s) = (is)^{(m-1)} e^{-s^2/2}$$

so that the Fourier inverse of $(is)^{(m-1)}e^{-s^2/2}$ is $(1/\sqrt{2\pi})\ N^{(m)}(x)$. We can then estimate the ratio of the errors of the two schemes (at $x = 0$) as

$$\frac{E_{TC}}{E_R} = \frac{3\left(\frac{1}{24} + \frac{1}{8}\lambda^2\right) - 15\frac{1}{48}\lambda^2}{3\left(\frac{1}{24} + \frac{1}{8}\lambda^2\right) - 15\frac{1}{96}\lambda^2} = \frac{\frac{1}{8} + \frac{\lambda^2}{16}}{\frac{1}{8} + \frac{7\lambda^2}{32}}$$

by evaluating $N^{(5)}(0) = 3$ and $N^{(7)}(0) = -15$ from

$$
\begin{aligned}
N^{(5)}(x) &= \frac{1}{\sqrt{2\pi}}(x^4 - 6x^2 + 3)e^{-x^2/2} \\
N^{(7)}(x) &= \frac{1}{\sqrt{2\pi}}(-x^6 - 15x^4 + 45x^2 - 15)e^{-x^2/2}
\end{aligned}
$$

The ratio E_{TC}/E_R has been plotted as a function of λ in Figure 2.4 and the results compared to the empirical observations. There is a very good fit to the data and, for values of λ less than the critical value, there is a modest reduction in the error of the numerical scheme due to the time change method.

Figure 2.4: Ratio of the Time Change and Rannacher errors in the maximum norm (for up to 3200 timesteps)

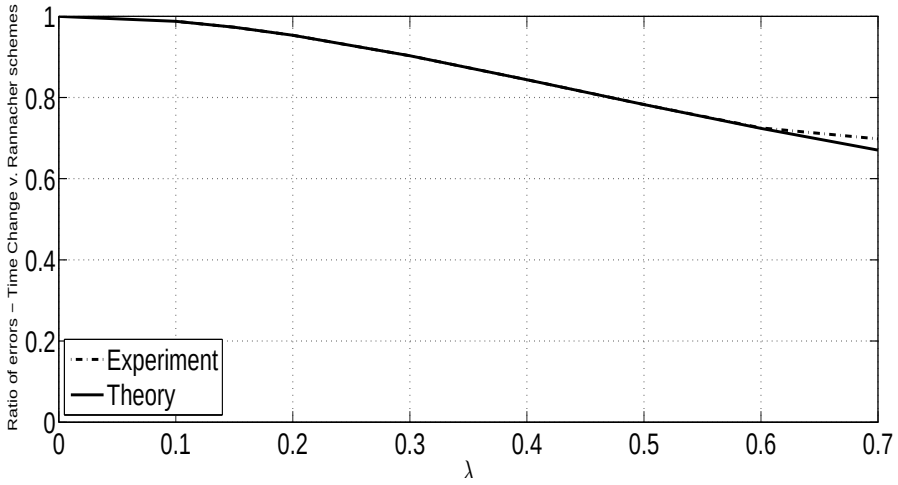

We are also interested in the computational efficiency of the schemes, so we have investigated the relative performance of the two schemes when both are subject to a constraint on the computational cost, C. We can write $C \sim c(1/k)(1/h)$ for some constant cost parameter c and we then can approximate the errors as

$$
\begin{aligned}
E_R &= ((1/8) + (7/32)\lambda^2)h^2 \\
&= (c/C)((1/8)(1/\lambda) + (7/32)\lambda)
\end{aligned}
$$

and similarly

$$
\begin{aligned}
E_{TC} &= ((1/8) + (1/16)\lambda^2)h^2 \\
&= (c/C)((1/8)(1/\lambda) + (1/16)\lambda).
\end{aligned}
$$

Here we assume that we use a direct solver for the PDE and do not take advantage of any special features such as the presence of time-independent coefficients. So for our analysis we assume that the same cost factor, c, applies to both schemes.

The errors E_R and E_{TC} will be separately minimised as functions of λ at

$$\lambda_R^* = \sqrt{(1/8)(32/7)} \sim 0.76$$

and

$$\lambda_{TC}^* = \sqrt{(1/8)(16/1)} \sim 1.41$$

Figure 2.5: Plot of ratio of Rannacher to time change optimal error at the same cost

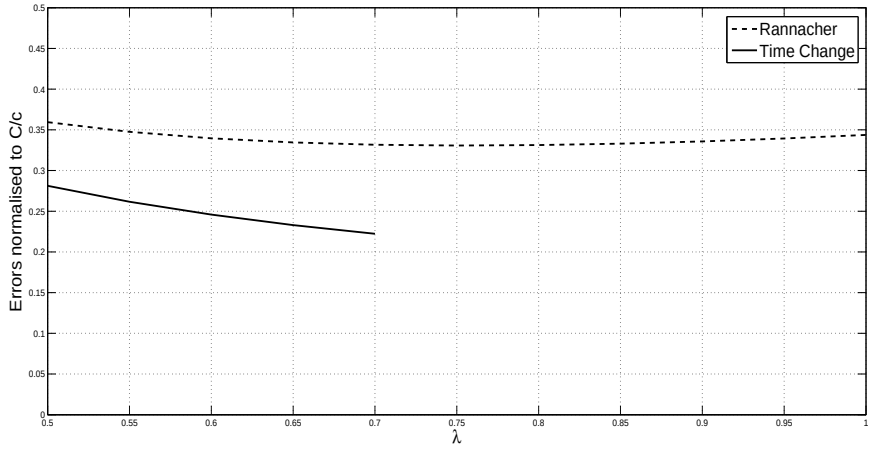

Note that for the time change the analysis is only valid for $\lambda \leq 1/\sqrt{2}$, after which lower order convergence is observed, so the minimum occurs at $1/\sqrt{2}$.

The plot (Figure 2.5) of the errors for $\lambda \leq 1/\sqrt{2}$, with the fixed computational cost, shows that the time change scheme has the lowest achievable error for the value of $\lambda = 1/\sqrt{2}$ and this error is, in turn, better than the error of the Rannacher scheme at the value λ_R^*.

2.7 Further variations of the time change approach

In this section we have investigated two further variants of the time change scheme.

Smoothed 'approximations' of the Dirac data

The first suggestion proposes the use of alternative, 'smoothed', approximations to the Dirac delta function which might be used as the initial condition for the scheme, e.g.,

$$\widetilde{U}_j^0 = \int_{-\infty}^{\infty} \Phi_h^{(k)}(x_j - x)\delta(x)\ \mathrm{d}x,$$

where $\Phi_h^{(k)}$ is a linear spline centred at 0 and with support $(-kh, kh)$, precisely,

$$\Phi_h^{(k)}(x) = \begin{cases} 0 & x \notin [-kh, kh], \\ \frac{1}{k^2h^2}\ (kh + x) & x \in [-kh, 0], \\ \frac{1}{k^2h^2}\ (kh - x) & x \in [0, kh]. \end{cases}$$

For $k = 1$, this reduces to the previous choice of initial condition whereas, for $k = 2$,

$$\widetilde{U}_j^0 = \begin{cases} 0 & j \notin \{-1, 0, 1\}, \\ \frac{1}{4h} & j \in \{-1, 1\}, \\ \frac{1}{2h} & j = 0. \end{cases} \tag{2.15}$$

The discrete delta is a triangular ramp function with increasing support, and is illustrated in Figure 2.6, where the vertical axis is normalised to $1/h$ and the horizontal axis is normalised to h.

Figure 2.6: Smoothed discrete delta functions

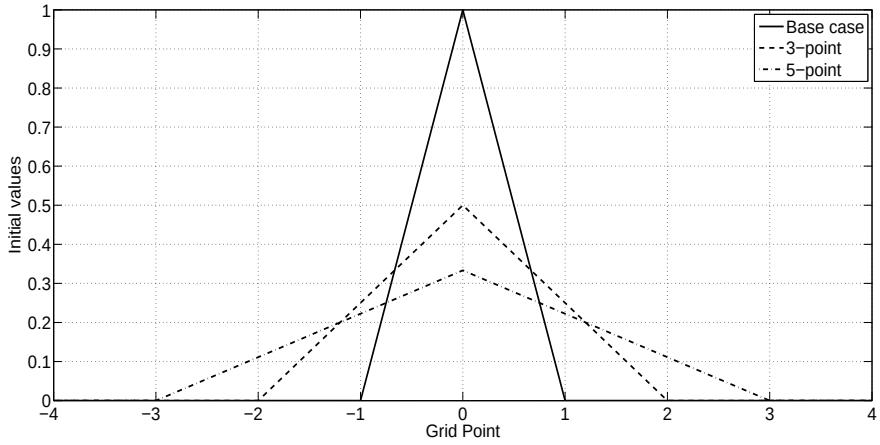

The time change scheme was run using the modified initial condition to investigate whether an improvement in accuracy might result.

We refer to the '3-point scheme' (where the initial condition has non-zero entries at only 3 grid points) and to the '5-point scheme' (where the initial condition has non-zero entries at only 5 grid points).

However, we first present a brief theoretical analysis of the expected performance based on modifying the Fourier analysis from Sections 2.4 and 2.5.

The Fourier transform of the initial condition (where $k > 1$) can be written as

$$\widehat{\widetilde{U}}^0(s) = h \sum_{j=-\infty}^{j=\infty} e^{isx_j} \widetilde{U}_j^0 = \frac{h}{k^2 h^2} \left(\sum_{m=1}^{k-1} h(k-m) e^{isx_{-m}} + kh + \sum_{m=1}^{k-1} h(k-m) e^{isx_m} \right)$$

$$= \frac{1}{k^2} \left(k + 2 \sum_{m=1}^{k-1} (k-m) \cos(msh) \right)$$

so that, for $k = 2$, we have

$$\widehat{\widetilde{U}}^0(s) = (2 + 4\cos(sh))/4 = \cos^2(sh/2)$$

and for $k = 3$, we have

$$\widehat{\widetilde{U}}^0(s) = (3 + 4\cos(sh) + 2\cos(2sh))/9 = (1 - 8\cos^2(sh/2) + 16\cos^4(sh/2))/9.$$

We can write the Fourier transform of the resulting scheme at T as

$$\widehat{\widetilde{U}}^N(s) = \widehat{U}^N(s) \widehat{\widetilde{U}}^0(s)$$

where $\widehat{U}^N(s)$ is the Fourier transform for the original problem, i.e., with the original initial conditions.

For the low wavenumber regime, we can expand the two terms separately to obtain

$$\widehat{\widetilde{U}}_k^N(s) \sim \left(\tilde{u}(s,1) + \tilde{u}(s,1) \left(\frac{1}{24} s^4 - \frac{1}{48} \lambda^2 s^6 + \frac{1}{8} \lambda^2 s^4 \right) h^2 \right) \widehat{\widetilde{U}}^0(s)$$

so for $k = 2$ we have

$$\widehat{\widetilde{U}}_2^N(s) \sim \left(\tilde{u}(s,1) + \tilde{u}(s,1) \left(\frac{1}{24} s^4 - \frac{1}{48} \lambda^2 s^6 + \frac{1}{8} \lambda^2 s^4 \right) h^2 \right) \left(1 - \frac{s^2 h^2}{4} \right)$$

and

$$\widehat{\widetilde{U}}_2^N(s) - \tilde{u}(s,1) \sim \tilde{u}(s,1) \left(\frac{1}{24} s^4 - \frac{1}{48} \lambda^2 s^6 + \frac{1}{8} \lambda^2 s^4 - \frac{s^2}{4} \right) h^2.$$

Applying the inverse transform to estimate the errors (noting that the Fourier transform for $s^2 e^{-\frac{s^2}{2}}$ at $x = 0$ is given by $N^{(3)}(0) = -1/\sqrt{2\pi}$) we find that the low

wavenumber error, E_2, of the scheme with the modified initial condition is approximately

$$E_2 \sim \left(\frac{\lambda^2}{16} - \frac{1}{8}\right) h^2$$

and so, recalling the low wavenumber error, E, of the original time change scheme, we have the error ratio

$$\frac{E_2}{E} \sim \frac{\frac{\lambda^2}{16} - \frac{1}{8}}{\frac{\lambda^2}{16} + \frac{1}{8}}.$$

From this we see that for λ near zero, the two schemes have almost identical errors, differing only by their sign, while for larger values of λ, below the critical value, we have $|E_2/E| < 1$, and near to the critical value of λ, the ratio of the errors is approximately 0.6.

The empirical behaviour compared with the theoretical behaviour is shown in Figure 2.7 and the scheme with $k = 2$ does indeed provide some improvement in the error.

Figure 2.7: Ratio of the Time Change and 3-point or 5-point errors in the maximum norm (for up to 3200 timesteps)

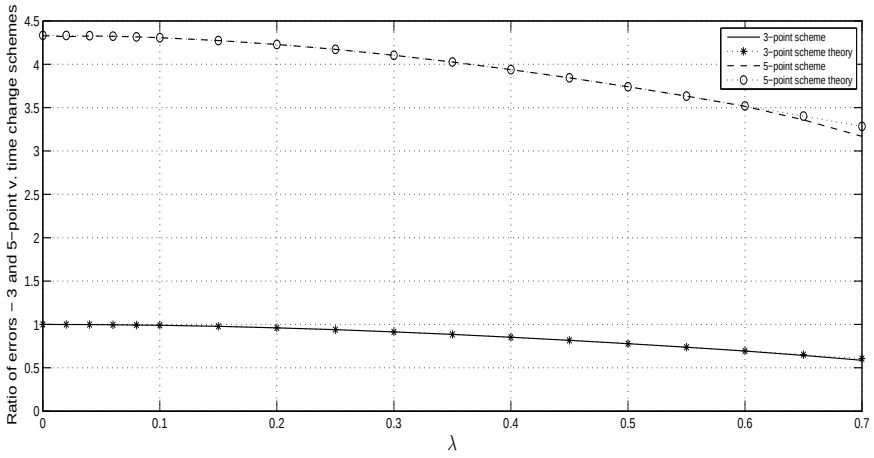

However, repeating the analysis for $k = 3$, we find that the smoothed scheme is now worse than the original scheme. In this case, the expansion of $\widehat{\widetilde{U}}^0(s)$ has the form

$$\widehat{\widetilde{U}}^0(s) \sim \left(1 - 2s^2h^2/3\ldots\right)$$

and the low wavenumber error, E_3, of the scheme takes the form of

$$E_3 \sim \left(\frac{\lambda^2}{16} - \frac{13}{24}\right) h^2$$

so that

$$\frac{E_3}{E} \sim \frac{\frac{\lambda^2}{16} - \frac{13}{24}}{\frac{\lambda^2}{16} + \frac{1}{8}}$$

and for λ near zero, the error ratio is approximately 4.33 and the empirical behaviour is also shown in Figure 2.7.

Turning to wavenumber regime IV, relevant for λ larger than the critical value, we consider only the case where $k = 2$. We assume $2\lambda^2 > 1$, and study the behaviour of the integral

$$I = \frac{F(h)}{h^{\frac{1}{\lambda^2}}} = \int_1^{2\lambda^2} \frac{S(\xi, 1)\cos^2(sh/2)h^{(\frac{2}{\xi} - \frac{1}{\lambda^2})}}{\sqrt{\xi}\sqrt{2\lambda^2 - \xi}}\, \mathrm{d}\xi,$$

where we note that $\cos^2(sh/2) = 1 - \xi/2\lambda^2$, and $S(\xi, 1)$ is continuous and non-negative on $\xi \in [1, 2\lambda^2]$ and we can show that $I = O(1/|\log h|^{\frac{3}{2}})$ so that $F(h) = h^{\frac{1}{\lambda^2}} O(1/|\log h|^{\frac{3}{2}})$, as follows.

Using the same substitution as above we obtain

$$I = |\log h|^{-\frac{3}{2}} \int_0^{\eta^*} S^*(\eta, 1) \left(\eta^2 \exp\left(-\frac{\frac{\eta^2}{\lambda^2}}{1 - \frac{\eta^2}{|\log h|}}\right)\right) \mathrm{d}\eta,$$

where $\eta^{*2} = |\log h|(1 - \frac{1}{2\lambda^2}) = \alpha^2 |\log h|$, with $\alpha = \sqrt{(1 - \frac{1}{2\lambda^2})}$.

Again by splitting range of the integration into two parts, we write

$$I = I_1 + I_2,$$

where I_1 is the integral from 0 to $\overline{\eta}$ (where we take $\overline{\eta} = \alpha |\log h|^{\frac{1}{4}}$) and I_2 is the integral from $\overline{\eta}$ to η^*.

We find that for sufficiently small h,

$$|I_2| < |\log h|^{-\frac{3}{2}} S^*_{max}(\alpha^2 |\log h|^{\frac{1}{2}}) \exp\left(-\frac{\frac{\alpha^2 |\log h|^{\frac{1}{2}}}{\lambda^2}}{1 - \alpha^2 |\log h|^{-\frac{1}{2}}}\right)(\alpha |\log h|^{\frac{1}{2}} - \alpha |\log h|^{\frac{1}{4}})$$

and so

$$|I_2| < \alpha^3 S^*_{max} |\log h|^{-\frac{1}{2}} \exp\left(-\frac{\alpha^2 |\log h|^{\frac{1}{2}}}{\lambda^2}\right)$$

where S^*_{max} is a bound for S^* on $[1, 2\lambda^2]$.

Again noting that $\frac{\eta^{*2}}{|\log h|} = \alpha |\log h|^{-\frac{1}{2}} \to 0$ as $h \to 0$, we also find that

$$\lim_{h\to 0} I_1 |\log h|^{\frac{3}{2}} = \int_0^\infty 2S(2\lambda^2, m^*)\eta^2 \exp\left(-\frac{\eta^2}{\lambda^2}\right) \mathrm{d}\eta,$$

and

$$\lim_{h\to 0} \left|\frac{I_2}{I_1}\right| = \lim_{h\to 0} |\log h| \exp\left(-\frac{\alpha^2 |\log h|^{\frac{1}{2}}}{\lambda^2}\right) = 0$$

so we have $I |\log h|^{\frac{3}{2}} = O(1)$ as required.

So for $2\lambda^2 > 1$, we find that the modified scheme still has the same order of convergence given by $1/\lambda^2$, with a different but still slowly varying logarithmic factor.

Once again, for values of λ above the critical value, we expect the asymptotic behaviour of wavenumber IV to dominate the error, $E(h)$, for small mesh size h. So, asymptotically, we expect to have $\mathrm{E(h)}/h^{\frac{1}{2\lambda^2}} \sim |\log h|^{-\frac{3}{2}}$, and a log-log plot between these two expressions would be expected to reveal a slope of -1.5 for sufficiently small h.

Numerical results shown in Figure 2.8 illustrate the asymptotic behaviour for large λ and we see that the convergence to the theoretical -1.5 slope is less good than for the basic time change (which approaches quite closely to the theoretical value if -0.5, as seen in Figure 2.3), presumably as rather more (and smaller) time steps are needed in this case.

In addition, Figure 2.9 compares the errors of the 3-point scheme to those of the basic time change scheme which shows a consistent improvement in the errors for large λ.

The 3-point scheme is seen to be beneficial, with error reduction in both the low and high wavenumber regimes.

Figure 2.8: 3-Point Scheme: Slope from plot of $\log(\mathrm{E(h)}/h^{\frac{1}{2\lambda^2}})$ against $\log|\log h|$ as a function of λ

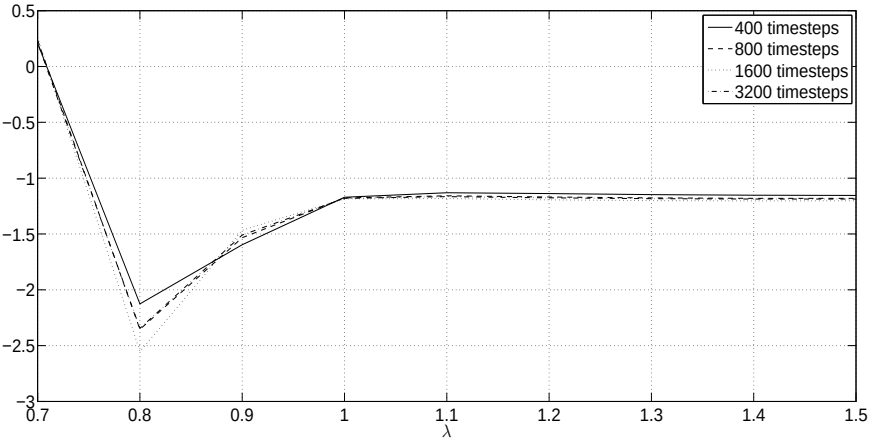

Figure 2.9: Comparison of errors of the basic Time Change scheme and the 3-point scheme

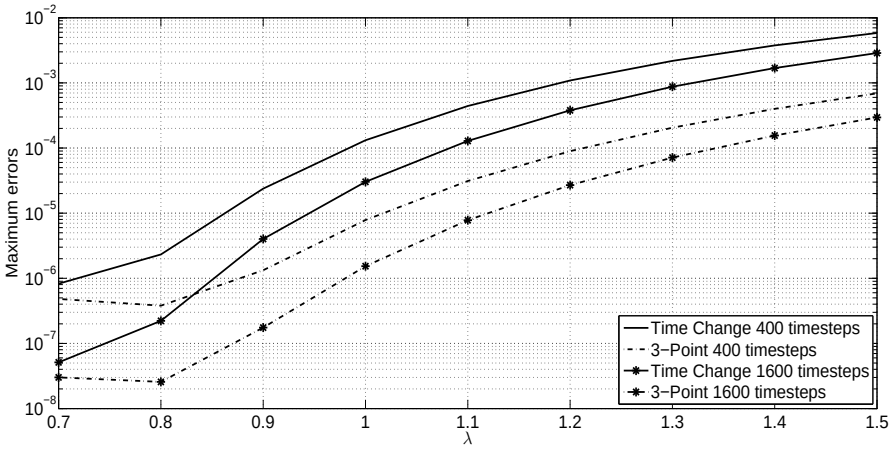

'Mixed' Time Change/Rannacher scheme

We also investigate the potential benefits of combining the time change scheme with Rannacher start-up.

The impact of the 'mixed' (Time Change/Rannacher) scheme was analysed by modifying the Fourier transform to replace the first two Crank-Nicolson steps with four appropriate Rannacher steps (taking account of the time change mechanism).

Then the Fourier transform for the mixed scheme is given by

$$\widehat{\widetilde{U}}^N = \left(\frac{1}{(1+\xi)(1+2\xi)(1+3\xi)(1+4\xi)}\right)\left(\frac{(1-2\xi)(1-3\xi)\dots}{(1+3\xi)(1+4\xi)\dots}\right)$$

where the first factor represents the Rannacher steps and the second factor represents the remaining Crank-Nicolson steps.

This can be written in the form

$$\widehat{\widetilde{U}}^N = \left(\frac{1}{(1-\xi)(1+3\xi)(1+4\xi)}\right)\widehat{U}^N,$$

where $\widehat{U}^N$ is the Fourier transform for the original time change scheme.

For the low wavenumber regime we can again make use of the asymptotic expansion for $\widehat{U}^N$ and expand the first factor to get an additional contribution to the leading term of $\log \widehat{\widetilde{U}}^N$ from

$$-\log(1-\xi) - \log(1+3\xi) - \log(1+4\xi) \sim 3\lambda^2 s^2 h^2.$$

Incorporating the extra term and applying the inverse Fourier transform, we find the low wavenumber error, E_M, for the mixed scheme is

$$E_M \sim \left(\frac{1}{8} - \frac{47}{16}\lambda^2\right) h^2$$

so the ratio of the errors for the mixed scheme and for the basis time change scheme can be written as

$$\frac{E_M}{E} \sim \frac{-\frac{47}{16}\lambda^2 + \frac{1}{8}}{\frac{\lambda^2}{16} + \frac{1}{8}}$$

and a numerical comparison of the two schemes fits the observations very well up to the critical value of λ, apart of values of λ near 0.20, as can be seen in Figure 2.10.

The error in the mixed scheme changes sign there and higher order terms would need to be taken into account to describe the error ratio more accurately near to $\lambda = 0.20$.

Figure 2.10: Ratio of the Time Change and Mixed Scheme errors in the maximum norm (for up to 3200 timesteps)

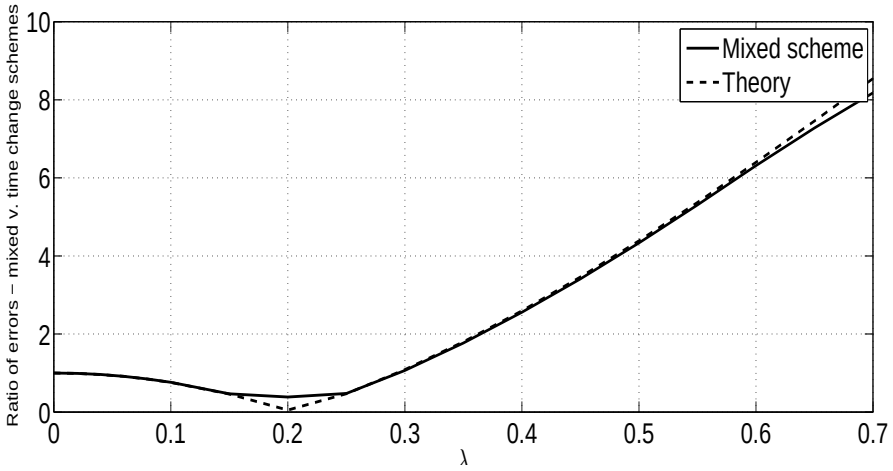

Turning to wavenumber regime IV, we again assume that $2\lambda^2 > 1$ so that $m^* = 1$. As before, we study the behaviour of the integral

$$I = \frac{F(h)}{h^{\frac{1}{\lambda^2}}} \;=\; \int_1^{2\lambda^2} \left(\frac{1}{(1-\xi)(1+3\xi)(1+4\xi)} \right) \frac{S(\xi,1)}{\sqrt{\xi}\sqrt{2\lambda^2-\xi}}\, h^{\frac{2}{\xi}-\frac{1}{2\lambda^2}}\, \mathrm{d}\xi.$$

Now we recall, from (2.9) and (2.12), that when $m^* = 1$, $S(\xi,1)$ now has a factor $\left(\frac{1-\xi}{1+\xi}\right)$ so that we can write

$$S(\xi,1) = \left(\frac{1-\xi}{1+\xi}\right) \tilde{S}(\xi,1)$$

where $\tilde{S}(\xi,1)$ is continuous and non-negative on $\xi =\in [1, 2\lambda^2]$, so we can write the integral as

$$I = \frac{F(h)}{h^{\frac{1}{\lambda^2}}} \;=\; \int_1^{2\lambda^2} \frac{S^*(\xi,1)}{\sqrt{\xi}\sqrt{2\lambda^2-\xi}}\, h^{\frac{2}{\xi}-\frac{1}{2\lambda^2}}\, \mathrm{d}\xi$$

where the the factors $(1+\xi)(1+3\xi)(1+4\xi)$ have been absorbed in $S^*(\xi,1)$ and where $S^*(\xi,1)$ is continuous and non-negative on $\xi \in [1, 2\lambda^2]$.

Now we have essentially the same behaviour as for the basic time change except that we will have a different multiplier inside the Gaussian integral

$$\int_0^\infty 2S^*(2\lambda^2, 1) \exp\left(-\frac{\eta^2}{\lambda^2}\right) \mathrm{d}\eta,$$

and so $h \to 0$ we have $I|\log h|^{\frac{1}{2}} = O(1)$, as before.

So for $2\lambda^2 > 1$, we expect to find that the modified scheme still has the same the asymptotic order of convergence, given by $\frac{1}{\lambda^2}$, and also has the same slowly varying logarithmic factor (although the size of the errors will be different).

It has proved difficult to demonstrate this result numerically as convergence to the expected slope of the log-log plot (analogous to Figure 2.3), is very slow.

In addition, Figure 2.11 compares the errors of the mixed scheme to those of the basic time change scheme. This plot shows that including the Rannacher steps for large λ results in smaller errors than for the basic time change scheme.

Figure 2.11: Comparison of errors of the basic Time Change scheme and the Mixed scheme

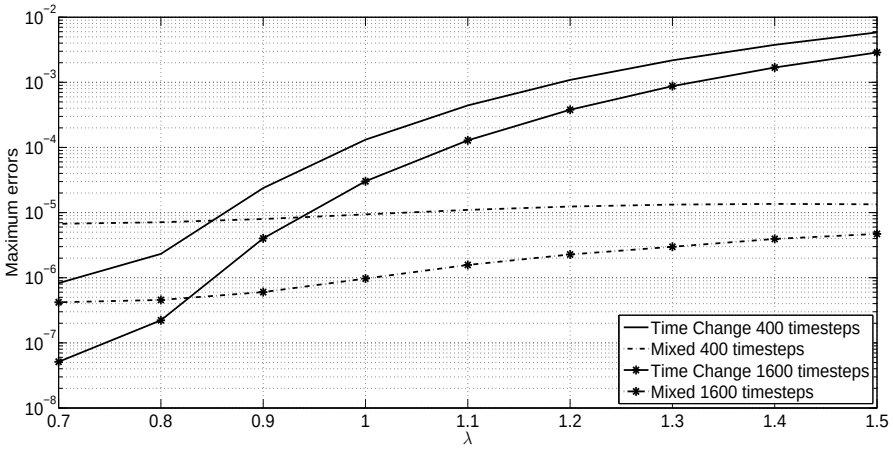

Overall, we see that combining the time change with the Rannacher scheme is only beneficial for small values of λ, i.e., where $\lambda < 0.30$ or for large values of λ, say, where $\lambda > 0.90$ (see Figure 2.10).

Note that for λ above the critical value, the original Rannacher scheme will have the best convergence behaviour as it displays quadratic convergence. However, taking into the account the computational complexity of the schemes suggests that the best results are obtained by taking λ below the critical value and using the time change (see 2.6).

Finally, Figure 2.12 shows a comparison of the convergence rates (for λ above the critical value) for the basic time change scheme, the 3-point scheme and the mixed scheme and with estimated errors for up to 800 time steps. The curves appear to converge to the theoretically predicted one as $h \to 0$, however convergence is slow especially for the mixed scheme.

Figure 2.12: Convergence rates for the three schemes for λ above the critical value

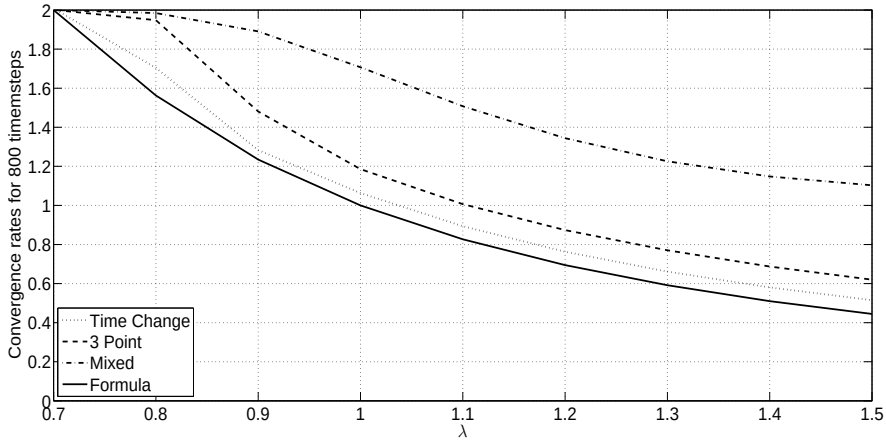

2.8 The time change applied to the Black-Scholes equation

In this section, we describe numerical results obtained by applying the time change to the Black-Scholes equation

$$\frac{\partial V}{\partial t} + \frac{1}{2}\sigma^2 S^2 \frac{\partial^2 V}{\partial S^2} + rS\frac{\partial V}{\partial S} - rV = 0, \quad S > 0,\ t \in (0, T]. \tag{2.16}$$

This is the equation that can be used to calculate, for example, the price, V, of a European option.

Here, S is the price of the underlying, σ is the volatility, r is the risk-free rate, and t is time.

For a call option, the terminal condition is given by the payoff, i.e., $V(S,T) = \max(S-K,0)$ for some $T > 0$, where K is the strike of the option.

Practically important sensitivities of the call price to the initial asset price, used in risk management, are given by the delta, Δ, and gamma, Γ, defined as

$$\Delta = \frac{\partial V}{\partial S}$$

and

$$\Gamma = \frac{\partial^2 V}{\partial S^2}$$

respectively.

Our investigation of convergence for the heat equation was based on Fourier analysis that relies on the PDE having constant coefficients whereas the Black-Scholes PDE used to price a European option does not have constant coefficients and so our analysis is not directly applicable in this case.

Nevertheless we have implemented the natural time change method to study the convergence behaviour of the gamma calculated with the modified numerical scheme. In this context the natural analogue to the solution of the heat equation with Dirac delta initial conditions would be the PDE satisfied by the gamma,

$$\frac{\partial \Gamma}{\partial t} + \frac{1}{2}\sigma^2 S^2 \frac{\partial^2 \Gamma}{\partial S^2} + (rS + 2\sigma^2)\frac{\partial \Gamma}{\partial S} + (r + \sigma^2)\Gamma = 0,$$

where the terminal condition for this equation is given by the second derivative of the payoff with respect to S, i.e., $\Gamma(S,T) = \delta(S-K)$. Here we have also assumed that

σ and r are constant.

This PDE could be used to test the performance of the time change approach but a more useful approach (as it reflects industry practice) is to apply the time change directly to the Black-Scholes equation and then use finite differences to derive approximate values for the gamma from the calculated option values. (Note that the scheme was also tested with the gamma PDE and gave identical results).

We first note that if we can write our PDE in the form

$$\frac{\partial V}{\partial \tau} - \mathcal{L}V = 0,$$

where $\tau = T - t$ is the time to maturity and where the spatial differential operator $\mathcal{L}$ has time-independent coefficients, then the transformed equation for $\tilde{t} = \sqrt{\tau}$ is simply

$$\frac{\partial V}{\partial \tilde{t}} - 2\,\tilde{t}\,\mathcal{L}V = 0.$$

If the coefficients in $\mathcal{L}$ are time-dependent, then these need to be rewritten in terms of $\tilde{t}$. This simple change to the equation results in very minimal changes to the solver code. The calculation done for a single time step in the original variables can be written as

$$(I - L)V^{n+1} = (I + L)V^n,$$

where L is a matrix dependent on k, h, S, σ and r while V^n is the solution vector at time step n. In the case of constant coefficients, and in the time-changed variables, this calculation simply becomes

$$(I - 2\,\tilde{t}_{n+1}L)\widetilde{V}^{n+1} = (I + 2\,\tilde{t}_n L)\widetilde{V}^n,$$

where $\widetilde{V}^n$ serves as numerical approximation to $\widetilde{V}(\cdot, \tilde{t}_n) = V(\cdot, T - \tilde{t}_n{}^2)$. In particular, the transformed Black-Scholes equation is

$$\frac{\partial \widetilde{V}}{\partial \tilde{t}} - 2\,\tilde{t}\,\left(\frac{1}{2}\sigma^2 S^2 \frac{\partial^2 \widetilde{V}}{\partial S^2} + rS\frac{\partial \widetilde{V}}{\partial S} - r\widetilde{V}\right) = 0$$

with the payoff function as the initial condition.

The transformed equation for $\widetilde{V}$ was solved using the Crank-Nicolson scheme and the gamma calculated by finite differences.

Although the scheme does not have the constant coefficients required for the direct application of Fourier analysis, the errors do behave in a very similar way to those for the heat equation.

The errors in gamma were computed from the analytic values and the convergence rate of the numerical error as a function of λ was analysed and is shown in Figure 2.13. The volatility, σ, was set to 20% and the strike, K, was set to 100. The risk-free

Figure 2.13: Convergence order for the gamma calculated from the time-changed Black-Scholes scheme as a function of λ

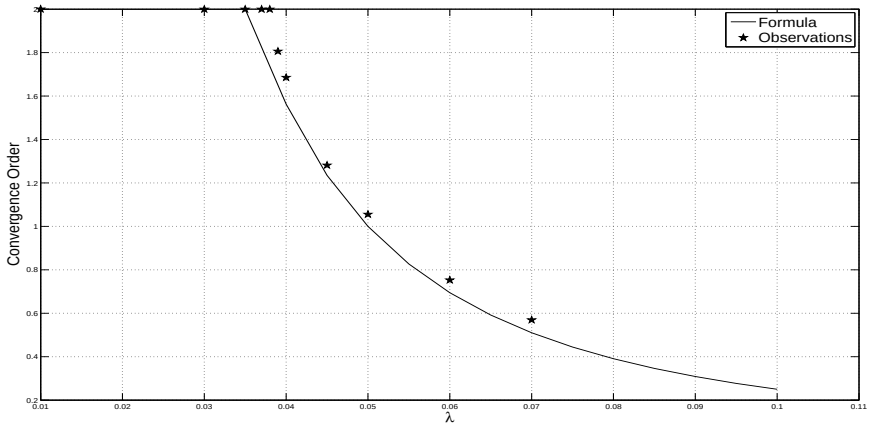

rate, r, was set to 5%.

The results of the analysis showed that there was a critical value of λ below which the error in the maximum norm was $O(h^2)$ and above which the h exponent declined in the same manner as for the heat equation (see Figure 2.2). Also shown in Figure 2.13 is the plot of $\min(2, 1/(\sigma^2 K^2 \lambda^2))$ and it is clear that this gives a reasonable description of the behaviour of the h exponent although it is not quite as good as with the heat equation itself.

We can justify the critical value of λ by noting that, in the Black-Scholes equation, the factor $\frac{1}{2}\sigma^2 S^2$ plays the same role as the factor $\frac{1}{2}$ in the heat equation and we also observe that if we had written the heat equation in the form $u_t = \frac{1}{2} D\, u_{xx}$, for some constant diffusivity D, we would have found the critical value of λ to be $1/\sqrt{2D}$.

Typically, the worst behaviour of a numerical scheme for the Black-Scholes equation with delta function initial conditions is seen at times close to maturity and in the

vicinity of the strike and so the strike is an appropriate parameter to use to represent the coefficient of $\frac{\partial^2 V}{\partial S^2}$ which then determines the critical value of λ.

Even without the precise results available from Fourier analysis, we can still attempt a partial explanation of how the time change improves the convergence of the Crank-Nicolson numerical scheme.

One consideration is that the truncation error of the numerical scheme has a leading order term proportional to the third derivative with respect to time of the European option price and the behaviour of this derivative is much improved by the time change.

The theta, Θ_C, of the call option is given by (see [17], p. 64)

$$\Theta_C = \frac{\partial C}{\partial t} = \frac{Sn(d_1)\sigma}{2\sqrt{T-t}} - rKe^{-r(T-t)}N(d_2),$$

where C is the solution to (2.16) with $C(S,T) = \max(S-K, 0)$, $N(x)$ is the cumulative Normal(0,1) distribution, $n(x)$ is its first derivative (the Gaussian function) and

$$d_{1,2} = \frac{(\log(S/K) + (r \pm \frac{1}{2}\sigma^2)(T-t))}{\sigma\sqrt{T-t}}.$$

Clearly Θ_C will become singular at the strike as $t \to T$ and any higher derivatives will also be singular there.

However, if we change the time variable to $\tilde{t} = \sqrt{T-t}$, we find that

$$\begin{aligned}\tilde{\Theta}_C = \frac{\partial C}{\partial \tilde{t}} = -2\tilde{t}\frac{\partial C}{\partial t} &= -2\tilde{t}\left(\frac{Sn(d_1)\sigma}{2\tilde{t}} - rKe^{-r\tilde{t}^2}N(d_2)\right) \\ &= -Sn(d_1)\sigma + 2\tilde{t}rKe^{-r\tilde{t}^2}N(d_2)\end{aligned}$$

and $\tilde{\Theta}_C$ is then not singular at $\tilde{t} = 0$.

Carrying on to the second 'time' derivative we see that

$$\frac{\partial^2 C}{\partial \tilde{t}^2} = -Sn'(d_1)\sigma\frac{\partial d_1}{\partial \tilde{t}} + 2rKe^{-r\tilde{t}^2}(1 - 2\,\tilde{t}\,r)N(d_2) - 2\,\tilde{t}\,rKe^{-r\tilde{t}^2}n(d_2)\frac{\partial d_2}{\partial \tilde{t}},$$

where we also have

$$\frac{\partial d_{1,2}}{\partial \tilde{t}} = -\frac{\log \frac{S}{K}}{\sigma\, \tilde{t}^2} + \frac{r \pm \frac{\sigma^2}{2}}{\sigma}$$

so there are potentially singular terms to consider, i.e., those featuring inverse powers of $\tilde{t}$.

However, if $S \neq K$ then both d_1 and $d_2 \to \pm\infty$ as $\tilde{t} \to 0$ so that the exponential factors in $n(d_i) = (1/\sqrt{2\pi}) \exp(-d_i^2/2)$ will eventually overwhelm the inverse powers of $\tilde{t}$.

Finally, if $S = K$ the term $\log(S/K)$ vanishes and the derivative is non-singular at the strike.

It is clear that this analysis will extend to the higher derivatives of C because the negative powers of $\tilde{t}$ will now only arise from differentiating N and will then only appear as multipliers of the Gaussian function.

These powers will only be present for $S \neq K$ where the Gaussian function will decay rapidly and overwhelm the inverse powers. So the higher derivatives will not become singular as $\tilde{t} \to 0$.

Although it is not entirely clear how to deduce convergence properties of the transformed numerical scheme directly from the above analysis, and particularly the convergence of derivatives of the solution, it seems plausible that the improved regularity of the truncation error is advantageous when using initial conditions that are not smooth.

2.9 American options

[12] investigate the convergence properties of Crank-Nicolson time-stepping when used to calculate the price of an American put by a penalty method. The penalised Black-Scholes equation is given by

$$\frac{\partial V}{\partial t} + \frac{1}{2}\sigma^2 S^2 \frac{\partial^2 V}{\partial S^2} + rS\frac{\partial V}{\partial S} - rV + \rho \max(\max(K - S, 0) - V, 0) = 0,$$

where $\rho > 0$ is a penalty parameter. This non-linear equation is solved with the terminal condition set equal to the option payoff. The penalty term comes into play when the solution violates the requirement that V should not fall below the payoff.

As the penalty parameter ρ increases, the solution of the equation converges to the value for the American option satisfying

$$\max\left(\frac{\partial V}{\partial t} + \frac{1}{2}\sigma^2 S^2 \frac{\partial^2 V}{\partial S^2} + rS\frac{\partial V}{\partial S} - rV, \max(K - S, 0) - V\right) = 0.$$

For the present purposes, we are interested solely in the convergence of the Crank-Nicolson scheme and choose ρ large enough to make the penalty solution numerically indistinguishable from its limit.

[12] implemented their solver using the Crank-Nicolson scheme with Rannacher start up and demonstrated that as the time step was reduced with the ratio of time step to space step held constant, the error in the calculated at-the-money (ATM) value of the American put tended to $O(h^{\frac{3}{2}})$ behaviour.

Their analysis of the problem suggests that non-uniform time-stepping might restore second order convergence so they went on to describe and implement an adaptive time-stepping procedure that did indeed yield second order convergence for the option value.

Their results suggest that the simple time change method described above might also be able to restore second order convergence.

The penalty code was modified to incorporate the time change and numerical results were generated.

Second order convergence was observed for the option value and delta for the ATM option and it was also observed that, for sufficiently small λ, the gamma showed second order convergence.

Table 2.2 shows the ratios of successive differences for mesh refinements with λ equal to 0.0125, 0.025 and 0.05. As with the European option discussed above, and with the strike, $K = 100$, and the volatility, $\sigma = 20\%$, the critical value of λ appears to be

Ratios of successive differences				
$\lambda = 0.0125$				
M	N	Value	Delta	Gamma
3200	640	3.98	3.92	3.91
6400	1280	3.97	3.97	3.94
12800	2560	3.97	3.97	3.96
25600	5120	3.99	3.97	3.99

Ratios of successive differences				
$\lambda = 0.0250$				
M	N	Value	Delta	Gamma
3200	320	3.84	4.01	3.80
6400	640	3.99	3.93	3.96
12800	1280	3.94	3.93	3.89
25600	2560	3.96	3.97	3.98

Ratios of successive differences				
$\lambda = 0.0500$				
M	N	Value	Delta	Gamma
3200	160	3.85	3.65	2.07
6400	320	3.78	3.87	2.08
12800	640	3.89	3.87	2.09
25600	1280	3.89	3.90	2.09

Table 2.2: Ratios of successive differences between numerical solutions for successive refinements for V, Δ and Γ; M the number of steps in S, N the number of steps in t; $\sigma = 0.20$, $r = 0.05$, $\rho = 10^6$

in the vicinity of $1/(\sigma K\sqrt{2}) = 0.035$.

We note, however, that the regularity of the value function for the American option close to expiry is fundamentally different from the European case. In particular, the second derivative in S – the Gamma – is bounded in the 'hold region' $S > S^*(t)$ and is seen to approach the bounded value $2rK/(\sigma S^*(t))^2$ as S approaches the exercise boundary $S^*(t)$ from the right (by using smooth pasting and the Black-Scholes PDE). The reduced convergence of the Crank-Nicolson scheme therefore has to be a consequence of the motion of the exercise boundary. It is shown in [6] that the asymptotic behaviour of the exercise boundary $S^*(t)$ close to expiry T is given by

$$S^*(t) - K \sim -K\sigma \sqrt{(T-t)\left|\log\left(\left(\frac{8\pi r^2}{\sigma^2}\right)(T-t)\right)\right|}.$$

Expressed as a function $\widetilde{S}$ of $\tilde{t} = \sqrt{T-t}$,

$$\widetilde{S}(\tilde{t}) - K \sim -\sqrt{2}K\sigma\tilde{t}\sqrt{\left|\log\left(\left(\frac{8\pi r^2}{\sigma^2}\right)^{\frac{1}{2}}\tilde{t}\right)\right|}.$$

Although the speed $\partial\widetilde{S}/\partial\tilde{t}$ of the boundary for the new time variable $\tilde{t}$ close to zero is still infinite, this is very barely noticeable numerically.

It was also observed that the plots of the calculated gamma revealed instability around the exercise boundary, behaviour which was also seen in [12], where the authors found that their adaptive time-stepping approach resulted in instability of the gamma at the exercise boundary unless fully-implicit time-stepping was used. This behaviour is a separate phenomenon independent of the short-time asymptotics addressed here.

In the previous section we suggested that the improved convergence properties of the Crank-Nicolson scheme might be related to improved regularity of the third time derivative of the value function of the European put in the vicinity of the strike and close to maturity.

We would like to be able to perform a similar analysis for the American put but, of course, no simple closed form expression for the value function is known. However, [28] do present an asymptotic expansion for the value function which can be decomposed into the value function of the European put plus the sum of an asymptotic series representing the early exercise premium.

In [28], some changes of variable are used to define the final form of the expansion. We write $S = Ke^x$ and $\xi = x/(2\sqrt{\tau_s})$, where τ_s is the rescaled time to maturity, equal to $2(T-t)/\sigma^2$. The transformed value function is then given by

$$v(x, \tau_s) = \frac{P(S,t) + S - K}{K}, \tag{2.17}$$

where $P(S,t)$ is the value of the American put as a function of the original variables. We can then write that

$$v(x, \tau_s) = v^E(x, \tau_s) + \sum_{n=2}^{\infty}\sum_{m=1}^{\infty}\tau_s^{n/2}(-\log\tau_s)^{-m}F_n^m(\xi), \tag{2.18}$$

where F_n^m are functions of the similarity variable ξ and $v^E(x, \tau_s)$ is the value of the European put expressed in the new variables.

In [28], only a few of the functions F_n^m are fully identified and discussion of those is restricted to $m = 1$. Those with $n \geq 2$ and $m = 1$ are, in principle, tractable but only partial results are known for the cases where $m > 1$. This limits our ability to draw conclusions from the behaviour of the derivatives of the early exercise premium.

Nevertheless, we will illustrate some aspects of the behaviour of the derivatives by describing a single term of the early exercise premium and its form and behaviour after the time change.

For example we find that the leading order coefficient of the early exercise premium is given by

$$F_2^1(\xi) = \mu(\xi \exp(-\xi^2/2)/\sqrt{\pi} + (2\xi^2 + 1)\text{erfc}(\xi))$$

for some constant μ.

After the time change this early exercise term in (2.18) is

$$G = \mu\tilde{t}^2(-2\log\tilde{t})^{-1}F_2^1(\eta),$$

where $\eta = x/(2\tilde{t})$. At the strike, we have

$$\begin{aligned}\frac{\partial G}{\partial \tilde{t}} &= \mu(2\tilde{t}(-2\log\tilde{t})^{-1} - 2\tilde{t}(-2\log\tilde{t})^{-2}),\\ \frac{\partial^2 G}{\partial \tilde{t}^2} &= \mu(2(-2\log\tilde{t})^{-1} + 4(-2\log\tilde{t})^{-2}) + 8(-2\log\tilde{t})^{-3})\end{aligned}$$

and

$$\frac{\partial^3 G}{\partial \tilde{t}^3} = \frac{\mu}{\tilde{t}}(4(-2\log\tilde{t})^{-2} + 16(-2\log\tilde{t})^{-3}) + 48(-2\log\tilde{t})^{-4}).$$

Acknowledging that this calculation only addresses a single term of the expansion of the early exercise premium we see that there is an improvement in the regularity of the derivatives of the put but unfortunately this does not obviously extend to the third derivative terms such as $\partial^3 G/\partial\tilde{t}^3$.

So, although we are encouraged by the empirical performance of the time change method applied to the American put, further analysis will be required to explain fully the improvement in convergence.

2.10 Conclusions

In this chapter we have presented the analysis of a simple and natural change of time variable that improves the convergence behaviour of the Crank-Nicolson scheme.

When applied to the solution of the heat equation with Dirac delta initial conditions, the numerical solution of the time changed PDE is always convergent with rate of convergence determined by the ratio, λ, of time step to space step (held constant during grid refinement).

This behaviour contrasts strongly to that of the Crank-Nicolson scheme when applied to the original PDE, which is always divergent and where λ controls how small the time step must be before the divergence appears. A proof of the behaviour of the time-changed scheme is given and numerical results presented to support the theoretical analysis.

Although the Fourier analysis used to prove this result cannot be applied directly to the Black-Scholes equation as it does not have constant coefficients, numerical experiments for the price and Greeks of a European call indicate that the time change method also leads to a convergent Crank-Nicolson scheme for this problem, without the need to introduce Rannacher steps, and quadratic convergence can be obtained if λ is chosen appropriately.

The change of convergence order at the value of λ which gives optimal complexity for given error tolerance is in line with the sensitivity of the error to λ observed in [14].

The present analysis does not support the conjecture made in [14], however, that the convergence of the Rannacher scheme with non-uniform (square-root) time-stepping is never of second order, the argument being that for small initial time-steps the smoothing effect diminishes. In fact, we see here that under square-root time smoothing is not necessary at all.

The experimentally observed second order convergence for the time-changed scheme extends to the computation of American option values which satisfy a linear complementarity problem with singular behaviour of the free boundary. These results are in line with, and extend, those of [41] and [12], for a Crank-Nicolson scheme with

Rannacher start-up on a locally refined time mesh.

It can be seen as an advantage of the time-changed scheme proposed here that it provides a remedy for both the reduced convergence order of the Crank-Nicolson scheme for European and American option values and for the divergence of their sensitivities by a single, simple modification.

Future work in this area will investigate other applications of the time variable change to option pricing and elsewhere. Specifically, it would be interesting to incorporate the square-root time change into a (semi-)Lagrangian approach to drift-dominated equations for standard European and American options (see [44]) or Asian options of either European or American type ([8] and [3]).

Chapter 3

Using the Kolmogorov forward equation to calculate hedging error distributions

3.1 The dynamics of hedging errors

Now we turn to a discussion of the mathematics of hedging errors.

We work in a framework where there is a $(d+1)$-dimensional vector, $\underline{X}_t$, of time-dependent underlying processes (e.g. asset prices, stochastic volatilities, etc.) and we are using a specified trading strategy to hedge the exposure of a European option, V, with payoff $F_V(\underline{X}_T)$, which is a function of values of the underlying processes at maturity, T.

We will assume that the trader does not know the true model of the underlying processes. He then uses a trading strategy based on an incorrect model. This leads to hedging errors due to model misspecification.

Model misspecification may be due to incorrect estimation of the parameters in the true model or may be due to the use of a different type of model or a combination of these effects. In some cases, very little structure might be assumed in the trader's model of the market.

Our analysis of the hedging problem uses the idea that in assessing the trader's hedging performance, we have more information than the trader has. The true model applies to a filtered probability space equipped with a filtration, $\mathcal{F}^{True}$, whereas the

model employed by the trader may use a different filtration, $\mathcal{F}^{Partial}$, reflecting the partial information available. This mismatch of information results in hedging errors.

In the simplest case, model misspecification may be due to misestimation of parameters in an otherwise correct model while, in other cases, the difference between the two filtrations might reflect, in part, different number of noise components in the two models.

For example, if the true model is a stochastic volatility model and the trader hedges by using a model with only one source of noise, the true filtration will be larger than the partial one and this will contribute to the hedging errors.

We will discuss these issues further in later sections of this chapter where we present specific examples of the hedging problem.

To start our analysis of hedging errors, we write the value of the hedging portfolio at time t as Π_t, where this represents the total value of the holdings in the tradeable underlyings, along with, where appropriate, any traded derivatives of the underlyings used for hedging. So, for example, the portfolio might contain cash, stocks, options on stocks, etc.

As we are trying to study the hedging errors that result from applying our hedging strategy to the option V, it might seem natural to compare the value of the hedging portfolio to the 'true' value of the option at time t. Indeed, we can do this, especially if we are interested in the behaviour of the hedging error before maturity. This might be desirable, for instance, if we wanted to analyse the consequences of liquidating the portfolio before maturity. In this thesis, however, we will instead compare the value of the hedging portfolio to a 'value function', $\widehat{V}_t$, which is only required to match the price of V_T at maturity, i.e. its value at time T equals the payoff F_V. We note that, as a special case, the value function given by the 'true' value of the option will have this property. This approach uses the ideas in [23] where a famous robustness result for the Black-Scholes model is demonstrated.

The motivation for our choice of value function $\widehat{V}_t$ is that we will generally take this to be the price of the option computed using a 'hedging model' which differs from the true model for $\underline{X}_t$, and will then analyse the hedging errors that result from the

trader using the mis-specified model.

We define our measure of the 'hedging error' to be the stochastic process Y_t given by

$$Y_t = \mathrm{e}^{-rt}(\Pi_t - \widehat{V}_t) \tag{3.1}$$

where $\widehat{V}_t$ is a process such that $\widehat{V}_T$ equals the payoff of V at time T.

Here r is the risk-free interest rate which we will always take as constant.

When the trader then hedges according to this 'incorrect' model, we will often find the dynamics of the 'hedging error' take on a particularly convenient form.

At maturity, we have $Y_T = \mathrm{e}^{-rT}(\Pi_T - \widehat{V}_T) = \mathrm{e}^{-rT}(\Pi_T - F_V)$, so the final value of Y_T is simply a constant times the 'true' hedging error at maturity. Analysis of the process Y_t will therefore provide information about the hedging error at maturity.

We investigate the dynamics of the 'hedging error', by writing it as

$$Y_t = \mathrm{e}^{-rt}(\Pi_t - \widehat{V}_t) = \mathrm{e}^{-rt}(\sum_{i=0}^{d} \phi_t^{(i)} X_t^{(i)} - \widehat{V}_t), \tag{3.2}$$

where the $X_t^{(i)}$ (the components of $\underline{X}_t$) are the traded instruments used in the hedging portfolio and the $\phi_t^{(i)}$ are the hedge ratios used by the trader to control the portfolio. Here $X_t^{(0)}$ is the value of a bond.

The portfolio is assumed to be self-financing, so we have

$$dY_t = -r\mathrm{e}^{-rt}(\sum_{i=0}^{d} \phi_t^{(i)} X_t^{(i)} - \widehat{V}_t)dt + \mathrm{e}^{-rt}(\sum_{i=0}^{d} \phi_t^{(i)} dX_t^{(i)} - d\widehat{V}_t). \tag{3.3}$$

Before we can make further progress with the analysis of the hedging error, we will need to specify the hedging strategy, the 'true' model for $\underline{X}_t$, and the definition of $\widehat{V}_t$. We can then apply Itô's lemma to find the dynamics of Y_t.

We observe that the terms $-r\mathrm{e}^{-rt}\phi_t^{(0)} X_t^{(0)}$ and $\mathrm{e}^{-rt}\phi_t^{(0)} dX_t^{(0)}$ will cancel. This is a consequence of working with the discounted form of the 'hedging error'.

3.2 The Kolmogorov equations

The Kolmogorov equations are a pair of partial differential equations (PDEs) satisfied by the transition density of moving from one state of a vector process to another state. We will assume that the process is Markovian so that we will be able to use the Kolmogorov equations shown below,

We let the vector process be $\underline{X}_t$ and write the transition density, $P(\underline{X}_0, t_0; \underline{X}_1, t_1)$, of the stochastic process as it moves from $\underline{X}_0$ at time t_0 to $\underline{X}_1$ at time t_1.

If the vector process $\underline{X}_t$ satisfies the following stochastic differential equation (SDE)

$$dX_t^{(i)} = b_i(\underline{X}_t, t)dt + \sum_{j=1}^{d} \sigma_{ij}(\underline{X}_t, t)dW_t^{(j)} \tag{3.4}$$

where W is a d-dimensional Brownian Motion, then we can associate with this process an operator A defined by

$$(Af)(\underline{x}, t) = \frac{1}{2}\sum_{i=1}^{d}\sum_{j=1}^{d} a_{ij}(\underline{x}, t)\frac{\partial^2 f(\underline{x}, t)}{\partial x_i \partial x_j} + \sum_{i=1}^{d} b_i(\underline{x}, t)\frac{\partial f(\underline{x}, t)}{\partial x_i}, \tag{3.5}$$

where the functions $a_{ij}(x)$ are defined to be

$$a_{ij}(\underline{x}, t) = \sum_{k=1}^{d} \sigma_{ik}(\underline{x}, t)\sigma_{jk}(\underline{x}, t). \tag{3.6}$$

We can also define the adjoint operator A^* by

$$(A^*f)(\underline{x}, t) = \frac{1}{2}\sum_{i=1}^{d}\sum_{j=1}^{d} \frac{\partial^2 (a_{ij}(\underline{x}, t)f(\underline{x}, t))}{\partial x_i \partial x_j} - \sum_{i=1}^{d} \frac{\partial (b_i(\underline{x}, t)f(\underline{x}, t))}{\partial x_i}. \tag{3.7}$$

Then the Kolmogorov equations are defined as follows.

The Kolmogorov forward equation (KFE) is

$$\frac{\partial P(\underline{x}_0, t_0; \underline{x}, t)}{\partial t} = A^* P(\underline{x}_0, t_0; \underline{x}, t) \text{ for } (\underline{x}, t) \in \mathbb{R}^d \times (0, \infty) \tag{3.8}$$

and the Kolmogorov backward equation (KBE) is

$$\frac{\partial P(\underline{x}, t; \underline{x}_1, t_1)}{\partial t} = A P(\underline{x}, t; \underline{x}_1, t_1) \text{ for } (\underline{x}, t) \in \mathbb{R}^d \times (0, \infty). \tag{3.9}$$

See [22] pp. 281-283. We note that the backward equation is often written so that the time variable, t, runs backwards (e.g. as in the Black-Scholes equation, where the variable is the time to maturity).

In this thesis we will only explicitly solve Kolmogorov forward equations. The backward equation will, however, be used in the derivation of the dynamics of the hedging error process we describe later and also in the calculation of the prices for the financial instruments we use in our examples.

The solution of the forward equation yields the probability distribution of the vector process at some future time given the initial state of the process. This distribution can then be used to evaluate statistics of functions of the future state (e.g. mean, variance, percentiles, etc.) given the fixed initial conditions. This form of the solution is useful when statistics of many terminal value functions need to be calculated with a given fixed initial condition.

On the other hand, the backward equation can be used to derive a PDE for the expectation of a given function of the terminal position and the solution of the PDE provides the expected value for a range of initial values and time periods. An example of this can be seen in European option pricing where the Black-Scholes formula for the option price is obtained by solving a KBE satisfied by the underlying process.

3.3 The extended Kolmogorov forward equation

The dynamics of the hedging error can be combined with those of $\underline{X}_t$ to give the dynamics of an 'extended state vector' from which we can derive an (extended) KFE.

In the examples we present in this chapter, the dynamics of the process Y_t will be found to consist only of a drift term, where the drift coefficient is independent of Y_t, so that we can write $dY_t = c(\underline{X}_t, t)dt$, where $c(\underline{X}_t, t)$ is the drift coefficient.

We now have an extended vector process, $(\underline{X}_t, Y_t)^T$, where

$$dX_t^{(i)} = b_i(\underline{X}_t, t)dt + \sum_{j=1}^{d} \sigma_{ij}(\underline{X}_t, t)dW_t^{(j)} \tag{3.10}$$

and

$$dY_t = c(\underline{X}_t, t)dt. \tag{3.11}$$

We can now derive a KFE for the joint probability, $P(\underline{x}, y, t)$, of the underlyings and the hedging error at time t, conditional on the values of $\underline{x}$ and y at the start of the time period, and we can then solve the KFE to obtain the joint density at the final time, i.e. at maturity.

Here we have written the probability density in the form of $P(\underline{x}, y, t)$, to highlight the role of the component y.

We will, in general, use lower case letters for the arguments of the probability density functions.

When we form the extended KFE we find the following:

- The enlarged matrix a does not have any new non-zero terms and no additional second derivative terms enter the KFE.
- The only additional term in the KFE is given by $\frac{\partial(c(\underline{x},t)P(\underline{x},y,t))}{\partial y} = c(\underline{x}, t)\frac{\partial P(\underline{x},y,t)}{\partial y}$.

So the extended KFE is just the original KFE for the joint density of $\underline{x}$ plus one additional drift term.

3.4 Examples of the extended Kolmogorov forward equation

3.4.1 Single asset — the El Karoui *et al.*, example

Our first example follows the analysis in El Karoui *et al.*, [23] where the true dynamics of a single underlying satisfy the SDE

$$\frac{dS_t}{S_t} = \mu_t dt + \sigma_t dW_t, \tag{3.12}$$

where σ_t is some volatility process. Here we have $X_t^{(1)} = S_t$. As we have not fully specified the volatiliy process σ_t, it may involve further noise processes apart from the Brownian motion, W_t.

We analyse the situation where the trader instead assumes that the underlying follows a different process, i.e. mis-specifies the model for S as

$$\frac{dS_t}{S_t} = \mu_t dt + \widehat{\sigma}(S_t, t) dW_t \tag{3.13}$$

for some local volatility process $\widehat{\sigma}(S_t, t)$.

We define $\widehat{V}$ to be the price of the European option with payoff $F(S_T)$ based on the process defined in (3.13) and we assume that the trader will then use hedge ratios based on $\widehat{V}$.

We have

$$dY_t = -r\mathrm{e}^{-rt}(\sum_{i=0}^{d} \phi_t^{(i)} X_t^{(i)} - \widehat{V}_t)dt + \mathrm{e}^{-rt}(\sum_{i=0}^{d} \phi_t^{(i)} dX_t^{(i)} - d\widehat{V}_t) \tag{3.14}$$

where $\phi_t^{(1)}$ is the holding in the asset, and use Itô's lemma to derive an SDE for $\widehat{V}_t$ as

$$d\widehat{V}_t = \left(\frac{\partial \widehat{V}}{\partial t} + \mu_t S_t \frac{\partial \widehat{V}}{\partial S} + \frac{1}{2}\sigma_t^2 S_t^2 \frac{\partial^2 \widehat{V}}{\partial S^2} \right) dt + \sigma_t S_t \frac{\partial \widehat{V}}{\partial S} dW_t \tag{3.15}$$

We note that this SDE depends on the true volatility process, σ.

Substituting this expression into dY_t we obtain

$$dY_t = \mathrm{e}^{-rt} \left(\phi_t^{(1)} - \frac{\partial \widehat{V}}{\partial S} \right) S_t((\mu_t - r)dt + \sigma_t dW_t)$$

$$-\mathrm{e}^{-rt}\mathcal{L}^{\widehat{\sigma}}\widehat{V}dt + \frac{1}{2}\mathrm{e}^{-rt}({\widehat{\sigma}_t}^2 - \sigma_t^2) S_t^2 \frac{\partial^2 \widehat{V}}{\partial S^2} dt.$$

Here $\mathcal{L}^{\widehat{\sigma}}\widehat{V}$ is defined to be

$$\mathcal{L}^{\widehat{\sigma}}\widehat{V} = \frac{\partial \widehat{V}}{\partial t} + \frac{1}{2}{\widehat{\sigma}_t}^2 S_t^2 \frac{\partial^2 \widehat{V}}{\partial S^2} + rS_t \frac{\partial \widehat{V}}{\partial S} - r\widehat{V},$$

and we observe that $\mathcal{L}^{\widehat{\sigma}}\widehat{V} = 0$ as $\widehat{V}$ is the value of the claim based on the erroneous volatility, $\widehat{\sigma}$.

If the trader then uses the hedge ratio $\frac{\partial \widehat{V}}{\partial S}$ from $\widehat{V}$ as the delta, we have $\phi_t^{(1)} = \frac{\partial \widehat{V}}{\partial S}$ and so

$$dY_t = \frac{1}{2}\mathrm{e}^{-rt}({\widehat{\sigma}_t}^2 - \sigma_t^2) S_t^2 \frac{\partial^2 \widehat{V}}{\partial S^2} dt \tag{3.16}$$

as in [23]. This is the famous 'robustness' result for the Black-Scholes model.

Here gamma, Γ, is defined by

$$\Gamma = \frac{\partial^2 \widehat{V}}{\partial S^2}$$

and this sensitivity ('Greek') comes from the mis-specified model.

We find that then the dynamics of Y_t, the 'hedging error', only consists of a drift term, i.e. there is no Brownian component.

In [23] the authors go on to argue that for a call (or put) option, where the gamma, Γ, is always positive, then if the volatility used for hedging dominates the true volatility, i.e. $\widehat{\sigma}_t \geq \sigma_t$ for all t, then the hedging errors (or hedging profit and loss (P&L)) can only increase with time and hedging losses at maturity will not occur if the option can be sold for at least $\widehat{V}_0$, where this is the initial price (premium) calculated, from the Black-Scholes formula, using the incorrect volatility, $\widehat{\sigma}$. This result relies on the 'convexity' of the option, as measured by its gamma, not changing sign.

Finally, based on the approach described in Section 3.3 above, we can write down the extended KFE for this situation.

To simplify the description, we assume that both σ and $\widehat{\sigma}$ are local volatilities, and μ is deterministic, so that $\sigma = \sigma(S,t)$ and $\widehat{\sigma} = \widehat{\sigma}(S,t)$ and so we can write (suppressing the arguments)

$$\frac{\partial P}{\partial t} = \frac{1}{2}\sigma^2 S^2 \frac{\partial^2 P}{\partial S^2} + (2\sigma^2 - \mu) S \frac{\partial P}{\partial S} + (\sigma^2 - \mu) P - c \frac{\partial P}{\partial y}, \tag{3.17}$$

where

$$c(S,t) = \frac{1}{2} \mathrm{e}^{-rt} (\widehat{\sigma}^2 - \sigma^2) S^2 \frac{\partial^2 \widehat{V}}{\partial S^2} \tag{3.18}$$

where $P(S,y,t)$ is the joint density of the asset and the hedging error at time t.

If we were to use an example where the true volatility, σ_t, incorporated additional noise components, we would have to include further terms in the KFE corresponding to these factors.

We give a numerical example of this in Chapter 6, Section 6.1.

3.4.2 Two assets — incorrect correlation

For our next example, we have a vector of two assets, where $(X_t^{(1)}, X_t^{(2)}) = (S_t^{(1)}, S_t^{(2)}) = \underline{S_t}$, where we assume that the vector process is driven by a two-dimensional correlated Brownian Motion with a true correlation coefficient ρ.

So we have

$$\begin{aligned} dS_t^{(1)} &= \mu_1(\underline{S_t}, t)dt + \sigma_1(\underline{S_t}, t)dW_t^{(1)} \\ dS_t^{(2)} &= \mu_2(\underline{S_t}, t)dt + \sigma_2(\underline{S_t}, t)dW_t^{(2)} \end{aligned} \tag{3.19}$$

where $d\langle W_t^{(1)}, W_t^{(2)}\rangle = \rho(\underline{S_t}, t)dt$.

We assume that the hedging strategy is based on an incorrect model which is of the same form, but where the correlation coefficient is taken to be $\widehat{\rho}$.

We take $\widehat{V}_t$ as the price of the option on $\underline{S_t}$ based on using the incorrect model and we 'double-delta-hedge' using this incorrect model where the hedge ratios are given by the first partial derivatives of the value function, $\widehat{V}$, with respect to $S^{(1)}$ and $S^{(2)}$.

The discounted hedging error is given by

$$Y_t = \mathrm{e}^{-rt}(\Pi_t - \widehat{V}_t) = e^{-rt}(\phi_t^{(1)} S_t^{(1)} + \phi_t^{(2)} S_t^{(2)} - \widehat{V}_t)$$

and we have

$$dY_t = -re^{-rt}(\phi_t^{(1)} S_t^{(1)} + \phi_t^{(2)} S_t^{(2)} - \widehat{V}_t)dt + e^{-rt}(\phi_t^{(1)} dS_t^{(1)} + \phi_t^{(2)} dS_t^{(2)} - d\widehat{V}_t)$$

and we need to obtain an expression for $d\widehat{V}_t$ by using Itô's lemma.

We get

$$d\widehat{V}_t = A_t dt + \sigma_1 \frac{\partial \widehat{V}}{\partial S^{(1)}} dW_t^{(1)} + \sigma_2 \frac{\partial \widehat{V}}{\partial S^{(2)}} dW_t^{(2)}$$

where

$$A_t = \frac{\partial \widehat{V}}{\partial t} + \mu_1 S_t^{(1)} \frac{\partial \widehat{V}}{\partial S^{(1)}}$$

$$+\mu_2 S_t^{(2)} \frac{\partial \widehat{V}}{\partial S^{(2)}} + \frac{1}{2}\sigma_1^2 (S_t^{(1)})^2 \frac{\partial^2 \widehat{V}}{\partial (S^{(1)})^2} + \rho\sigma_1\sigma_2 S_t^{(1)} S_t^{(2)} \frac{\partial^2 \widehat{V}}{\partial S^{(1)} S^{(2)}} + \frac{1}{2}\sigma_2^2 (S_t^{(2)})^2 \frac{\partial^2 \widehat{V}}{\partial (S^{(2)})^2}.$$

Substituting this expression into dY_t and making use of the PDE that is satisfied by $\widehat{V}$ where the incorrect correlation, $\widehat{\rho}$, is used, we arrive at the hedging error dynamics

$$dY_t = c(S_t^{(1)}, S_t^{(2)}, t)dt \tag{3.20}$$

where

$$c(S_t^{(1)}, S_t^{(2)}, t) = \mathrm{e}^{-rt}(\widehat{\rho} - \rho)\sigma_1\sigma_2 S_t^{(1)} S_t^{(2)} \frac{\partial^2 \widehat{V}}{\partial S^{(1)} \partial S^{(2)}} \tag{3.21}$$

and where the hedge ratios in the portfolio are taken as $\frac{\partial \widehat{V}}{\partial S^{(1)}}$ and $\frac{\partial \widehat{V}}{\partial S^{(2)}}$.

The extended KFE is then given by

$$\begin{aligned}\frac{\partial P}{\partial t} =& \frac{1}{2}\sigma_1^2 S^{(1)2}\frac{\partial^2 P}{\partial S^{(1)2}} + \rho\sigma_1\sigma_2 S^{(1)}S^{(2)}\frac{\partial^2 P}{\partial S^{(1)}\partial S^{(2)}} + \frac{1}{2}\sigma_2^2 S^{(2)2}\frac{\partial^2 P}{\partial S^{(2)2}} \\ &+ S^{(1)}(2\sigma_1^2 + \rho\sigma_1\sigma_2 - \mu_1)\frac{\partial P}{\partial S^{(1)}} + S^{(2)}(2\sigma_2^2 + \rho\sigma_1\sigma_2 - \mu_2)\frac{\partial P}{\partial S^{(2)}} \\ &+ (\sigma_1^2 + \rho\sigma_1\sigma_2 + \sigma_1^2 - \mu_1 - \mu_2)P - c(S^{(1)}, S^{(2)}, t)\frac{\partial P}{\partial y}.\end{aligned} \tag{3.22}$$

We give a numerical example of this in Chapter 6, Section 6.2.

More generally, other versions of this problem could be analysed where different elements of the correlation matrix could be mis-specified.

3.4.3 Stochastic volatility – implied volatility hedge

For our next example, we assume that the true model for the single asset, S_t, is given by a stochastic volatility model of the form

$$\begin{aligned}\frac{dS_t}{S_t} &= \mu_t dt + \sigma_t dW_t, \\ d\sigma_t &= m(\sigma_t)dt + \gamma(\sigma_t)dZ_t,\end{aligned} \tag{3.23}$$

where W and Z are correlated Brownian Motions with $d\langle W_t, Z_t\rangle = \rho\ dt$ and m and γ are functions of σ_t.

The trader would like to hedge a 'target' European option, V, which has payoff, $V_T = F(S_T, T)$, at maturity.

If the trader does not know the true model, he can employ a hedging strategy (described below) based on the use of 'implied volatilities' derived from observations of traded option prices.

We assume that a suitable traded option O_t (exposed to σ_t) exists, so that its price is available at all times.

The trader's strategy will lead to hedging errors which we seek to quantify.

We summarise the strategy used by the trader in this situation.

- The trader does not know the true model of the underlyings but can observe the price of the option, O, being traded in the market.
- He chooses a traded option to include in his hedging portfolio as he seeks to hedge the 'target' option, V.
- At each time, t, he observes the traded price of O_t and uses this price to calculate the instantaneous value of the implied volatility of O_t. This is done by using the Black-Scholes formula for the option O_t and finding constant volatility that corresponds to the observed price at the current stock price, S_t.
- He then uses the instantaneous implied volatility of O_t to calculate Greeks from a function, $\widehat{V}$, which satisfies the Black-Scholes formula using the instantaneous implied volatility as input and such that $\widehat{V}$ matches the payoff of V at maturity. These Greeks provide the hedge ratios the trader uses in his the hedging portfolio which is made up of bonds, the stock, S_t, and the traded option O_t.

In the analysis below we show that a suitable choice of hedge ratios will lead to a hedging error whose dynamics only involve a drift term and this is the basis of the trader's strategy.

The trader sets up a hedge portfolio

$$\Pi_t = \phi_t^{(0)} B_t + \phi_t^{(1)} S_t + \phi_t^{(2)} O_t$$

which includes the traded option O_t. We investigate a 'value function' $\widehat{V}$ which matches the payoff, V_T, at maturity and we consider the dynamics Y_t of the hedging error (as discussed in Section 3.1)

$$Y_t = \mathrm{e}^{-rt}(\phi_t^{(0)} B_t + \phi_t^{(1)} S_t + \phi_t^{(2)} O_t - \widehat{V}_t).$$

At this point we have not specified the hedge ratios $\phi^{(0)}$, $\phi^{(1)}$ and $\phi^{(2)}$ or $\widehat{V}$, and these will depend on the the choice of $\widehat{V}$ and on the hedging strategy employed.

The hedging strategy requires the calculation, at any time, t, the implied volatility derived from the observed price of O_t, which is defined implicitly by

$$O_t = O(t, S_t, \sigma_t) = O^{BS}(t, S_t, \widehat{\sigma}), \tag{3.24}$$

so that substituting the instantaneous value of the implied volatility in the Black-Scholes equation of the option, yields the instantaneous value of O_t.

So, for instance, if O_t is a call, with strike K, we have

$$O^{BS}(t, S_t, \widehat{\sigma}) = N(d_1)S - N(d_2)Ke^{-r(T-t)}$$

with

$$d_1 = \frac{1}{\widehat{\sigma}\sqrt{T-t}}\left[\log\left(\frac{S}{K}\right) + (r + \frac{\widehat{\sigma}^2}{2})(T-t)\right].$$

We note that O^{BS} depends on t, S and $\widehat{\sigma}$, and $\widehat{\sigma}$ itself is a stochastic process.

In the calculation of the dynamics of Y_t we can replace O_t by $O^{BS}(t, S_t, \widehat{\sigma}(t, S_t, \sigma))$, and then have to compute

$$dY_t = -re^{-rt}(\phi_t^{(1)}S_t + \phi_t^{(2)}O_t^{BS} - \widehat{V}_t)dt + e^{-rt}(\phi_t^{(1)}dS_t + \phi_t^{(2)}dO_t^{BS} - d\widehat{V}_t) \tag{3.25}$$

(we again note that the bond can be left out of this equation).

As O_t^{BS} and $\widehat{V}_t$ depend on t, S and $\widehat{\sigma}$ we have to take care when using Itô's rule.

We have

$$dO_t^{BS} = \left(\frac{\partial O^{BS}}{\partial t}dt + \frac{\partial O^{BS}}{\partial S}(\mu_t S_t + \sigma_t S_t dW_t) + \frac{\partial O^{BS}}{\partial \widehat{\sigma}}d\widehat{\sigma}_t + \frac{1}{2}\sigma^2 S^2\frac{\partial^2 O^{BS}}{\partial S^2}dt \right.$$
$$\left. + \frac{1}{2}\frac{\partial^2 O^{BS}}{\partial \widehat{\sigma}^2}d < \widehat{\sigma}, \widehat{\sigma} >_t + \frac{\partial^2 O^{BS}}{\partial S \partial \widehat{\sigma}}d < S, \widehat{\sigma} >_t \right)$$

and

$$d\widehat{V}_t = \left(\frac{\partial \widehat{V}}{\partial t} dt + \frac{\partial \widehat{V}}{\partial S}(\mu_t S_t + \sigma_t S_t dW_t) + \frac{\partial \widehat{V}}{\partial \widehat{\sigma}} d\widehat{\sigma}_t + \frac{1}{2}\sigma_t^2 S_t^2 \frac{\partial^2 \widehat{V}}{\partial S^2} dt \right.$$
$$\left. + \frac{1}{2}\frac{\partial^2 \widehat{V}}{\partial \widehat{\sigma}^2} d < \widehat{\sigma}, \widehat{\sigma} >_t + \frac{\partial^2 \widehat{V}}{\partial S \partial \widehat{\sigma}} d < S, \widehat{\sigma} >_t \right)..$$

We have

$$d\widehat{\sigma}_t = \frac{\partial \widehat{\sigma}}{\partial t} dt + \frac{\partial \widehat{\sigma}}{\partial S} dS_t + \frac{\partial \widehat{\sigma}}{\partial \sigma} d\sigma_t$$
$$+ \frac{1}{2}\sigma_t^2 S_t^2 \frac{\partial^2 \widehat{\sigma}}{\partial S^2} dt + \frac{1}{2}\gamma^2 \frac{\partial^2 \widehat{\sigma}}{\partial \sigma^2} dt + \rho\gamma\sigma_t S_t \frac{\partial^2 \widehat{\sigma}}{\partial \sigma \partial S} dt$$

or

$$d\widehat{\sigma}_t = \frac{\partial \widehat{\sigma}}{\partial t} dt + \frac{\partial \widehat{\sigma}}{\partial S}(\mu S_t dt + \sigma_t S_t dW_t^{(1)}) + \frac{\partial \widehat{\sigma}}{\partial \sigma}(m dt + \gamma dW_t^{(2)})$$
$$+ \frac{1}{2}\sigma_t^2 S_t^2 \frac{\partial^2 \widehat{\sigma}}{\partial S^2} dt + \frac{1}{2}\gamma^2 \frac{\partial^2 \widehat{\sigma}}{\partial \sigma^2} dt + \rho\gamma\sigma_t S_t \frac{\partial^2 \widehat{\sigma}}{\partial \sigma \partial S} dt$$

and so

$$d\widehat{\sigma}_t = A_t dt + \sigma_t S_t \frac{\partial \widehat{\sigma}}{\partial S} dW_t^{(1)} + \gamma \frac{\partial \widehat{\sigma}}{\partial \sigma} dW_t^{(2)}$$

where

$$A_t = \frac{\partial \widehat{\sigma}}{\partial t} + \mu S_t \frac{\partial \widehat{\sigma}}{\partial S} + m \frac{\partial \widehat{\sigma}}{\partial \sigma} + \frac{1}{2}\sigma_t^2 S_t^2 \frac{\partial^2 \widehat{\sigma}}{\partial S^2} + \frac{1}{2}\gamma^2 \frac{\partial^2 \widehat{\sigma}}{\partial \sigma^2} + \rho\gamma\sigma_t S_t \frac{\partial^2 \widehat{\sigma}}{\partial \sigma \partial S}.$$

We can then compute

$$d < \widehat{\sigma}, \widehat{\sigma} >_t = \left(\sigma_t^2 S_t^2 \left(\frac{\partial \widehat{\sigma}}{\partial S} \right)^2 + 2\rho\gamma\sigma_t S_t \frac{\partial \widehat{\sigma}}{\partial S} \frac{\partial \widehat{\sigma}}{\partial \sigma} + \gamma^2 \left(\frac{\partial \widehat{\sigma}}{\partial \sigma} \right)^2 \right) dt = D_t dt$$

and

$$d < \widehat{\sigma}, S >_t = \left(\sigma_t^2 S_t^2 \left(\frac{\partial \widehat{\sigma}}{\partial S} \right) + \rho\gamma\sigma_t S_t \left(\frac{\partial \widehat{\sigma}}{\partial \sigma} \right) \right) dt = E_t dt.$$

We can now calculate the dynamics of the hedging error as

$$e^{rt} dY_t = -r(\phi_t^{(1)} S_t + \phi_t^{(2)} O_t^{BS} - \widehat{V}_t) dt$$
$$+ \phi_t^{(1)}(\mu S_t dt + \sigma_t S_t dW_t^{(1)})$$

$$+\phi_t^{(2)}(\frac{\partial O^{BS}}{\partial t}dt+\frac{\partial O^{BS}}{\partial S}(\mu S_t dt+\sigma_t S_t dW_t^{(1)})+\frac{\partial O^{BS}}{\partial \widehat{\sigma}}(A_t dt+\sigma_t S_t\frac{\partial \widehat{\sigma}}{\partial S}dW_t^{(1)}+\gamma\frac{\partial \widehat{\sigma}}{\partial \sigma}dW_t^{(2)})\dots$$
$$\dots+\frac{1}{2}\sigma_t^2 S_t^2\frac{\partial^2 O^{BS}}{\partial S^2}dt+\frac{1}{2}\frac{\partial^2 O^{BS}}{\partial \widehat{\sigma}^2}D_t dt+\frac{\partial^2 O^{BS}}{\partial S\partial\widehat{\sigma}}E_t dt)$$
$$-(\frac{\partial \widehat{V}}{\partial t}dt+\frac{\partial \widehat{V}}{\partial S}(\mu S_t dt+\sigma_t S_t dW_t^{(1)})+\frac{\partial \widehat{V}}{\partial \widehat{\sigma}}(A_t dt+\sigma_t S_t\frac{\partial \widehat{\sigma}}{\partial S}dW_t^{(1)}+\gamma\frac{\partial \widehat{\sigma}}{\partial \sigma}dW_t^{(2)})\dots$$
$$\dots+\frac{1}{2}\sigma_t^2 S_t^2\frac{\partial^2 \widehat{V}}{\partial S^2}dt+\frac{1}{2}\frac{\partial^2 \widehat{V}}{\partial \widehat{\sigma}^2}D_t dt+\frac{\partial^2 \widehat{V}}{\partial S\partial\widehat{\sigma}}E_t dt)$$

using the formulae above. Next we collect terms in dt, $dW_t^{(1)}$ and $dW_t^{(2)}$ to find

$$e^{rt}dY_t = R_t dt+(\phi_t^{(1)}\sigma_t S_t-\sigma_t S_t\frac{\partial \widehat{V}}{\partial S}+\phi_t^{(2)}\sigma_t S_t\frac{\partial O^{BS}}{\partial S}+\sigma_t S_t\frac{\partial \widehat{\sigma}}{\partial S}(\phi_t^{(2)}\frac{\partial O^{BS}}{\partial \widehat{\sigma}}-\frac{\partial \widehat{V}}{\partial \widehat{\sigma}}))dW_t^{(1)}$$
$$+\gamma\frac{\partial \widehat{\sigma}}{\partial S}(\phi_t^{(2)}\frac{\partial O^{BS}}{\partial \widehat{\sigma}}-\frac{\partial \widehat{V}}{\partial \widehat{\sigma}})dW_t^{(2)}$$

where

$$R_t = \phi_t^{(1)}S_t(\mu-r)$$
$$+(r\widehat{V}-\frac{\partial \widehat{V}}{\partial t}-\frac{1}{2}\sigma_t^2 S_t^2\frac{\partial^2 \widehat{V}}{\partial S^2}-\mu S_t\frac{\partial \widehat{V}}{\partial S})$$
$$-\phi_t^{(2)}(rO^{BS}-\frac{\partial O^{BS}}{\partial t}-\frac{1}{2}\sigma_t^2 S_t^2\frac{\partial^2 O^{BS}}{\partial S^2}-\mu S_t\frac{\partial O^{BS}}{\partial S})$$
$$+A_t(\phi_t^{(2)}\frac{\partial O^{BS}}{\partial \widehat{\sigma}}-\frac{\partial \widehat{V}}{\partial \widehat{\sigma}})$$
$$+D_t(\phi_t^{(2)}\frac{\partial^2 O^{BS}}{\partial \widehat{\sigma}^2}-\frac{\partial^2 \widehat{V}}{\partial \widehat{\sigma}^2})$$
$$+E_t(\phi_t^{(2)}\frac{\partial^2 O^{BS}}{\partial S\partial\widehat{\sigma}}-\frac{\partial^2 \widehat{V}}{\partial S\partial\widehat{\sigma}}).$$

For the strategy we now want to describe, we choose the hedge ratios and $\widehat{V}$, so that the dynamics of Y_t consist only of a drift term.

So we set

$$\phi_t^{(2)}\frac{\partial O^{BS}}{\partial \widehat{\sigma}}-\frac{\partial \widehat{V}}{\partial \widehat{\sigma}}=0$$

and

$$\phi_t^{(1)}\sigma_t S_t-\sigma_t S_t\frac{\partial \widehat{V}}{\partial S}+\phi_t^{(2)}\sigma_t S_t\frac{\partial O^{BS}}{\partial S}+\sigma_t S_t\frac{\partial \widehat{\sigma}}{\partial S}(\phi_t^{(2)}\frac{\partial O^{BS}}{\partial \widehat{\sigma}}-\frac{\partial \widehat{V}}{\partial \widehat{\sigma}})=0$$

or

$$\phi_t^{(1)}\sigma_t S_t - \sigma_t S_t \frac{\partial \widehat{V}}{\partial S} + \phi_t^{(2)}\sigma_t S_t \frac{\partial O^{BS}}{\partial S} = 0$$

so that

$$\phi_t^{(2)} = \frac{\frac{\partial \widehat{V}}{\partial \widehat{\sigma}}}{\frac{\partial O^{BS}}{\partial \widehat{\sigma}}} \tag{3.26}$$

and

$$\phi_t^{(1)} = \frac{\partial \widehat{V}}{\partial S} - \frac{\partial O^{BS}}{\partial S}\frac{\frac{\partial \widehat{V}}{\partial \widehat{\sigma}}}{\frac{\partial O^{BS}}{\partial \widehat{\sigma}}}. \tag{3.27}$$

The expressions $\phi_t^{(1)}$ and $\phi_t^{(2)}$, are called (modified) delta-vega hedge ratios.

Finally, we substitute the hedge ratios into the formulae for the drift term to get

$$\begin{aligned}
R_t &= \phi_t^{(1)} S_t(\mu - r) \\
&+(r\widehat{V} - \frac{\partial \widehat{V}}{\partial t} - \frac{1}{2}\widehat{\sigma}_t^2 S_t^2 \frac{\partial^2 \widehat{V}}{\partial S^2} - rS_t \frac{\partial \widehat{V}}{\partial S}) - (\mu - r)S_t \frac{\partial \widehat{V}}{\partial S} - \frac{1}{2}(\sigma_t^2 - \widehat{\sigma}^2)S_t^2 \frac{\partial^2 \widehat{V}}{\partial S^2} \\
&-\phi_t^{(2)}(rO^{BS} - \frac{\partial O^{BS}}{\partial t} - \frac{1}{2}\widehat{\sigma}_t^2 S_t^2 \frac{\partial^2 O^{BS}}{\partial S^2} - rS_t \frac{\partial O^{BS}}{\partial S}) + \phi_t^{(2)}(\mu - r)S_t \frac{\partial O^{BS}}{\partial S} \\
&+\phi_t^{(2)} \frac{1}{2}(\sigma_t^2 - \widehat{\sigma}^2)S_t^2 \frac{\partial^2 O^{BS}}{\partial S^2} \\
&+D_t(\phi_t^{(2)} \frac{\partial^2 O^{BS}}{\partial \widehat{\sigma}^2} - \frac{\partial^2 \widehat{V}}{\partial \widehat{\sigma}^2}) \\
&+E_t(\phi_t^{(2)} \frac{\partial^2 O^{BS}}{\partial S \partial \widehat{\sigma}} - \frac{\partial^2 \widehat{V}}{\partial S \partial \widehat{\sigma}})
\end{aligned}$$

and

$$\begin{aligned}
R_t = (r\widehat{V} - \frac{\partial \widehat{V}}{\partial t} - \frac{1}{2}\widehat{\sigma}_t^2 S_t^2 \frac{\partial^2 \widehat{V}}{\partial S^2} - rS_t \frac{\partial \widehat{V}}{\partial S}) - \frac{1}{2}(\sigma_t^2 - \widehat{\sigma}^2)S_t^2 \frac{\partial^2 \widehat{V}}{\partial S^2} \\
+\phi_t^{(2)} \frac{1}{2}(\sigma_t^2 - \widehat{\sigma}^2)S_t^2 \frac{\partial^2 O^{BS}}{\partial S^2} \\
+D_t(\phi_t^{(2)} \frac{\partial^2 O^{BS}}{\partial \widehat{\sigma}^2} - \frac{\partial^2 \widehat{V}}{\partial \widehat{\sigma}^2}) \\
+E_t(\phi_t^{(2)} \frac{\partial^2 O^{BS}}{\partial S \partial \widehat{\sigma}} - \frac{\partial^2 \widehat{V}}{\partial S \partial \widehat{\sigma}}).
\end{aligned}$$

If we then choose $\widehat{V}$ so that

$$r\widehat{V} - \frac{\partial \widehat{V}}{\partial t} - \frac{1}{2}\widehat{\sigma}_t^2 S_t^2 \frac{\partial^2 \widehat{V}}{\partial S^2} - rS_t \frac{\partial \widehat{V}}{\partial S} = 0$$

so that, at any time, t, $\widehat{V}$ is defined so that it satisfies the Black-Scholes equation using the instantaneous implied volatility.

Finally, we have

$$\begin{aligned} R_t = \frac{1}{2}(\sigma_t^2 - \widehat{\sigma}^2) S_t^2 (\phi_t^{(2)} \frac{\partial^2 O^{BS}}{\partial S^2} - \frac{\partial^2 \widehat{V}}{\partial S^2}) \\ + D_t (\phi_t^{(2)} \frac{\partial^2 O^{BS}}{\partial \widehat{\sigma}^2} - \frac{\partial^2 \widehat{V}}{\partial \widehat{\sigma}^2}) \\ + E_t (\phi_t^{(2)} \frac{\partial^2 O^{BS}}{\partial S \partial \widehat{\sigma}} - \frac{\partial^2 \widehat{V}}{\partial S \partial \widehat{\sigma}}). \end{aligned}$$

so the hedging error dynamics are

$$\begin{aligned} dY_t = \mathrm{e}^{-rt} \frac{\partial V^{BS}}{\partial \widehat{\sigma}} \Bigg(\frac{1}{2}(\sigma_t^2 - \widehat{\sigma}_t^{\,2}) S_t^2 \left(\frac{\frac{\partial^2 O^{BS}}{\partial S^2}}{\frac{\partial O^{BS}}{\partial \widehat{\sigma}}} - \frac{\frac{\partial^2 V^{BS}}{\partial S^2}}{\frac{\partial V^{BS}}{\partial \widehat{\sigma}}} \right) \\ + D \left(\frac{\frac{\partial^2 O^{BS}}{\partial \widehat{\sigma} \partial S}}{\frac{\partial O^{BS}}{\partial \widehat{\sigma}}} - \frac{\frac{\partial^2 V^{BS}}{\partial \widehat{\sigma} \partial S}}{\frac{\partial V^{BS}}{\partial \widehat{\sigma}}} \right) + E \left(\frac{\frac{\partial^2 O^{BS}}{\partial \widehat{\sigma}^2}}{\frac{\partial O^{BS}}{\partial \widehat{\sigma}}} - \frac{\frac{\partial^2 V^{BS}}{\partial \widehat{\sigma}^2}}{\frac{\partial V^{BS}}{\partial \widehat{\sigma}}} \right) \Bigg) dt, \end{aligned} \tag{3.28}$$

where

$$D(t, S, \sigma) = \sigma_t^2 S_t^2 \frac{\partial \widehat{\sigma}}{\partial S} + \rho \gamma_t \sigma_t S_t \frac{\partial \widehat{\sigma}}{\partial \sigma}$$

and

$$E(t, S, \sigma) = \frac{1}{2} \left(\sigma_t^2 S_t^2 \left(\frac{\partial \widehat{\sigma}}{\partial S} \right)^2 + 2\rho \gamma_t \sigma_t S_t \frac{\partial \widehat{\sigma}}{\partial S} \frac{\partial \widehat{\sigma}}{\partial \sigma} + \gamma_t^2 \left(\frac{\partial \widehat{\sigma}}{\partial \sigma} \right)^2 \right).$$

The hedge ratios given above in (3.26) and (3.27) resemble those used in delta-vega hedging where the true form of the model is known and perfect hedging is possible.

Finally, we give an example of the case where the true model is the Heston stochastic volatility model, defined by the SDE

$$\begin{aligned} dS_t &= \mu S_t dt + \sqrt{v_t} S_t dW_t \\ dv_t &= \kappa(\eta - v_t) dt + \sigma \sqrt{v_t} dZ_t \end{aligned} \tag{3.29}$$

where W_t and Z_t are correlated Brownian motions with $d\langle W_t, Z_t \rangle = \rho dt$.

Here v_t acts as the variance of the asset price process and this follows a mean-reverting process, where κ controls the speed of mean-reversion of v_t towards the equilibrium level, η, and where σ is the 'volatility of volatility' or 'vol of vol'. ρ measures the correlation between the two Brownian motions.

We then get the extended KFE

$$\begin{aligned}\frac{\partial P}{\partial t} &= \frac{1}{2}S^2 v\frac{\partial^2 P}{\partial S^2} + \rho\sigma S v\frac{\partial^2 P}{\partial S \partial v} + \frac{1}{2}\sigma^2 v\frac{\partial^2 P}{\partial v^2} \\ &\quad + S(2v + \rho\sigma - \mu)\frac{\partial P}{\partial S} \\ &\quad + (\sigma^2 + \rho\sigma v - \kappa(\eta - v))\frac{\partial P}{\partial v} + (v + \rho\sigma + \kappa - \mu)P - c\frac{\partial P}{\partial y}, \end{aligned} \tag{3.30}$$

with

$$\begin{aligned} c(S,t) = \mathrm{e}^{-rt}\frac{\partial V^{BS}(\widehat{\sigma})}{\partial \widehat{\sigma}}\Bigg(\frac{1}{2}(v - \widehat{\sigma}^2)S^2\Bigg(\frac{\frac{\partial^2 O^{BS}}{\partial S^2}}{\frac{\partial O^{BS}}{\partial \widehat{\sigma}}} - \frac{\frac{\partial^2 V^{BS}}{\partial S^2}}{\frac{\partial V^{BS}}{\partial \widehat{\sigma}}}\Bigg) \\ + D\Bigg(\frac{\frac{\partial^2 O^{BS}}{\partial \widehat{\sigma}^2}}{\frac{\partial O^{BS}}{\partial \widehat{\sigma}}} - \frac{\frac{\partial^2 V^{BS}}{\partial \widehat{\sigma}^2}}{\frac{\partial V^{BS}}{\partial \widehat{\sigma}}}\Bigg) + E\Bigg(\frac{\frac{\partial^2 O^{BS}}{\partial \widehat{\sigma}\partial S}}{\frac{\partial O^{BS}}{\partial \widehat{\sigma}}} - \frac{\frac{\partial^2 V^{BS}}{\partial \widehat{\sigma}\partial S}}{\frac{\partial V^{BS}}{\partial \widehat{\sigma}}}\Bigg)\Bigg)dt, \end{aligned} \tag{3.31}$$

where

$$D(t,S,v) = vS^2\frac{\partial \widehat{\sigma}}{\partial S} + \rho\sigma v S\frac{\partial \widehat{\sigma}}{\partial v}$$

and

$$E(t,S,v) = vS^2\left(\frac{\partial \widehat{\sigma}}{\partial S}\right)^2 + 2\rho\sigma v S\left(\frac{\partial \widehat{\sigma}}{\partial S}\right)\left(\frac{\partial \widehat{\sigma}}{\partial v}\right) + v\sigma^2\left(\frac{\partial \widehat{\sigma}}{\partial v}\right)^2$$

We give a numerical example of this in Chapter 6, Section 6.3.

3.4.4 Stochastic volatility — uncertain volatility hedge

In our next example we consider a situation where the model for the volatility is not known. Instead we might only have beliefs about bounds on the volatility process. A hedging strategy can then be used that attempts to cope with this level of uncertainty.

The example is based on the well-known model due to Avellaneda *et al.*, [1] and Lyons [27] in which they assume that the asset price has dynamics given by

$$\frac{dS_t}{S_t} = \mu_t dt + \sigma_t dW_t$$

but where all that is known about the volatility process σ_t is that it lies within certain fixed bounds (σ_{min} and σ_{max}), i.e.

$$0 \leq \sigma_{min} \leq \sigma_t \leq \sigma_{max} \leq \infty \text{ for all } t.$$

Then, given a European option with payoff $F(S_T)$, it is possible to define a super-replication strategy (or super-hedge) so that if this strategy is followed and the process σ_t does remain within its bounds, the value of the portfolio at maturity will never fall below the payoff and no negative hedging errors will occur.

The required delta-hedge can be calculated by solving a non-linear PDE, the Black-Scholes-Barenblatt (BSB) equation, as referred to in [1], and defined as follows

$$\frac{\partial W(S,t)}{\partial t} + rS\frac{\partial W(S,t)}{\partial S} + \frac{1}{2}\widehat{\sigma}^2 S^2 \frac{\partial^2 W(S,t)}{\partial S^2} - rW(S,t) = 0. \tag{3.32}$$

In the BSB equation for W, $\widehat{\sigma}$ is defined by

$$\widehat{\sigma} = \begin{cases} \sigma_{max} \text{ if } \frac{\partial^2 W(S,t)}{\partial S^2} \geq 0 \\ \sigma_{min} \text{ if } \frac{\partial^2 W(S,t)}{\partial S^2} < 0 \end{cases} \tag{3.33}$$

so $\widehat{\sigma}$ is a function of $\frac{\partial^2 W(S,t)}{\partial S^2}$. The terminal condition is that W must equal the payoff of V at maturity.

Then $W(S_0, 0)$ is the minimum premium required to set up the super-hedge and $\frac{\partial W}{\partial S}$ is the dynamic hedge ratio required for the hedging portfolio.

We note, in passing, that if the option is convex or concave, the super-hedge can be carried out by just using a fixed volatility (one of the bounds). Only if the convexity can change sign might the volatility used in the calculation of the hedge ratios need to be changed during the hedging period. In the numerical example we give later, we will use an option of mixed convexity.

For our analysis, we will take for $\widehat{V}_t$ to be the price process obtained by solving the BSB equation. and we analyse the dynamics of the hedging as before.

Using Itô calculus which is very similar to the simple Black-Scholes case, we can write

$$\mathrm{e}^{rt} dY_t = \frac{1}{2}({\widehat{\sigma}_t}^2 - \sigma_t^2) S_t^2 \frac{\partial^2 \widehat{V}}{\partial S^2} - \left(\frac{\partial \widehat{V}}{\partial t} + rS_t \frac{\partial \widehat{V}}{\partial S} + \frac{1}{2}{\widehat{\sigma}_t}^2 S_t^2 \frac{\partial^2 \widehat{V}}{\partial S^2} - r\widehat{V} \right)$$

$$+\left(\phi_t^{(1)} - \frac{\partial \widehat{V}}{\partial S}\right)((\mu_t - r)S_t dt + \sigma_t S_t dW_t)$$

where $\widehat{\sigma}_t$ is the volatility process defined in the BS equation, that switches between σ_{min} and σ_{max} as the sign of $\frac{\partial^2 \widehat{V}}{\partial S^2}$ changes.

However, we know from the BSB equation that

$$\frac{\partial \widehat{V}}{\partial t} + rS\frac{\partial \widehat{V}}{\partial S} + \frac{1}{2}\widehat{\sigma}^2 S^2 \frac{\partial^2 \widehat{V}}{\partial S^2} - r\widehat{V} = 0$$

so if we set $\phi_t^{(1)} = \frac{\partial \widehat{V}}{\partial S}$ we arrive at

$$dY_t = \frac{1}{2}\mathrm{e}^{-rt}({\widehat{\sigma}_t}^2 - \sigma_t^2)S_t^2 \frac{\partial^2 \widehat{V}}{\partial S^2} dt \tag{3.34}$$

where the gamma now comes from the BSB equation.

In other words, if we hedge using the BSB delta and compare the hedging portfolio to the BSB super-replication price, the process Y_t will have dynamics consisting of only a drift term where the volatility $\widehat{\sigma}$ in the drift term is that specified in the BSB equation.

We will consider a case where the true model is given by the Heston model and we write the corresponding extended KFE as

$$\begin{aligned}\frac{\partial P}{\partial t} &= \frac{1}{2}S^2 v\frac{\partial^2 P}{\partial S^2} + \rho\sigma S v\frac{\partial^2 P}{\partial S \partial v} + \frac{1}{2}\sigma^2 v\frac{\partial^2 P}{\partial v^2} \\ &\quad + S(2v + \rho\sigma - \mu)\frac{\partial P}{\partial S} + (\sigma^2 + \rho\sigma v - \kappa(\eta - v))\frac{\partial P}{\partial v} \\ &\quad + (v + \rho\sigma + \kappa - \mu)P - c\frac{\partial P}{\partial y}\end{aligned} \tag{3.35}$$

where

$$c(S, v, t) = \frac{1}{2}\mathrm{e}^{-rt}(\widehat{\sigma}^2 - v)S^2 \frac{\partial^2 \widehat{V}}{\partial S^2} \tag{3.36}$$

and $\widehat{\sigma}$ is the volatility process defined by (3.33) and the BSB equation.

If we choose values for the volatility bounds, σ_{min} and σ_{max}, that do not capture the full volatility range for the true process, then the model mis-specification can lead to both positive and negative hedging errors, whereas without the mis-specification the hedging errors will never be negative as we have employed a superhedge. We give a numerical example of this in Chapter 6, Section 6.4.

3.4.5 Hedging a barrier option with incorrect volatility

We finally consider an up-and-out barrier option with initial asset price S and a barrier B and we assume that the true asset price follows the model

$$\frac{dS_t}{S_t} = \mu_t dt + \sigma_t dW_t.$$

where μ_t and σ_t can be stochastic processes.

We also assume that the trader hedges with the incorrect volatility, $\widehat{\sigma}$ and we obtain the same drift coefficient as in Section 3.4.1.

Clearly, if the initial value of S is far away from the barrier, there will be very little probability of S crossing the barrier and we expect that the KFE, modelling the presence of the barrier, would give results close to those based on the KFE in Section 3.4.1.

In the presence of the barrier, we must now take account of the non-zero probability of crossing the barrier, and will need to allow for different boundary conditions (i.e., at the barrier) when solving the KFE.

We note that for $S > B$, the option will have knocked out at some prior time and the option value will be zero thereafter. As the payoff will then be zero and is known, no further hedging is needed, and the portfolio will be converted into a bond which will then continue to grow at the risk-free rate.

There are two parts to the calculation of the hedging error distribution. Firstly, we consider what happens if the stock price never reaches the barrier for $t \in [0, T]$.

The KFE is defined on $S \leq B$ and if we assume that both σ_t and $\widehat{\sigma}_t$ (to simplify the situation) are local volatilities, and μ_t is deterministic, then the KFE is given by

$$\frac{\partial P}{\partial t} = \frac{1}{2}\sigma^2 S^2 \frac{\partial^2 P}{\partial S^2} + (2\sigma^2 - \mu) S \frac{\partial P}{\partial S} + (\sigma^2 - \mu) P - c\frac{\partial P}{\partial y} \tag{3.37}$$

where P is zero at $S = B$ and the drift coefficient c is given by

$$c(S, t) = \frac{1}{2}\mathrm{e}^{-rt}(\widehat{\sigma}^2 - \sigma^2) S^2 \frac{\partial^2 \widehat{V}}{\partial S^2} \tag{3.38}$$

where we use the gamma for the up-and-out option, calculated using the incorrect volatility, $\widehat{\sigma}$. We recall that $c(S,t)$ is independent of y.

We will show that the solution P, for $t > 0$, does not integrate to 1, as follows.

We define the marginal density, as function of y, where the barrier is not crossed, as

$$R(y,t) = \int_0^B P(\xi, y, t) d\xi$$

and so

$$\begin{aligned}
\frac{\partial R(y,t)}{\partial t} &= \int_0^B \frac{\partial P(\xi,y,t)}{\partial t} d\xi \\
&= \int_0^B \left(\frac{1}{2}\sigma^2 \xi^2 \frac{\partial^2 P}{\partial \xi^2} + (2\sigma^2 - \mu)\xi \frac{\partial P}{\partial \xi} + (\sigma^2 - \mu)P - c\frac{\partial P}{\partial y} \right) d\xi \\
&= \left[\frac{1}{2}\sigma^2 \xi^2 \frac{\partial P}{\partial \xi} \right]_0^B - \sigma^2 \int_0^B \xi \frac{\partial P}{\partial \xi} d\xi + (2\sigma^2 - \mu)\left([\xi P]_0^B - \int_0^B P d\xi \right) \\
&+ (\sigma^2 - \mu) \int_0^B P d\xi - \int_0^B c\frac{\partial P}{\partial y} d\xi \\
&= \left[\frac{1}{2}\sigma^2 \xi^2 \frac{\partial P}{\partial \xi} \right]_0^B - \sigma^2 \int_0^B \xi \frac{\partial P}{\partial \xi} d\xi + (2\sigma^2 - \mu)([\xi P]_0^B - R) \\
&+ (\sigma^2 - \mu)R - \int_0^B c\frac{\partial P}{\partial y} d\xi \\
&= \frac{1}{2}\sigma^2 B^2 \frac{\partial P}{\partial \xi}\bigg|_B - \sigma^2 \int_0^B \xi \frac{\partial P}{\partial \xi} d\xi - \sigma^2 R - \int_0^B c\frac{\partial P}{\partial y} d\xi \\
&= \frac{1}{2}\sigma^2 B^2 \frac{\partial P}{\partial \xi}\bigg|_B - \sigma^2 \left([\xi P]_0^B - \int_0^B P d\xi \right) - \sigma^2 R - \int_0^B c\frac{\partial P}{\partial y} d\xi \\
&= \frac{1}{2}\sigma^2 B^2 \frac{\partial P}{\partial \xi}\bigg|_B - \int_0^B c\frac{\partial P}{\partial y} d\xi
\end{aligned}$$

using the boundary conditions, $P(S = 0, y) = 0$ and $P(S = B, y) = 0$.

We see that the time rate of change of the marginal density has two components, one representing flow of probability across the barrier, and the other representing drift of probability in the y-direction.

If we now set

$$I(t) = \int_{-\infty}^{\infty} R(\eta, t) d\eta$$

this is the total probability where the barrier has not been crossed.

We have

$$\begin{aligned}
\frac{dI(t)}{dt} &= \int_{-\infty}^{\infty} \frac{\partial R(\eta,t)}{\partial t} d\eta \\
&= \int_{-\infty}^{\infty} \left(\frac{1}{2}\sigma^2 B^2 \frac{\partial P}{\partial \xi}\bigg|_B - \int_0^B c \frac{\partial P}{\partial y} d\xi \right) d\eta \\
&= \frac{1}{2}\sigma^2 B^2 \int_{-\infty}^{\infty} \frac{\partial P}{\partial \xi}\bigg|_B d\eta - \int_{-\infty}^{\infty} \left(\int_0^B c \frac{\partial P}{\partial y} d\xi \right) d\eta \\
&= \frac{1}{2}\sigma^2 B^2 \int_{-\infty}^{\infty} \frac{\partial P}{\partial \xi}\bigg|_B d\eta - \int_0^B c \left(\int_{-\infty}^{\infty} \frac{\partial P}{\partial y} d\eta \right) d\xi \\
&= \frac{1}{2}\sigma^2 B^2 \int_{-\infty}^{\infty} \frac{\partial P}{\partial \xi}\bigg|_B d\eta - \int_0^B c[P]_{-\infty}^{\infty} d\xi \\
&= \frac{1}{2}\sigma^2 B^2 \int_{-\infty}^{\infty} \frac{\partial P}{\partial \xi}\bigg|_B d\eta
\end{aligned}$$

using the boundary conditions, $P(S, y = \pm\infty)$=0.

The total probability from the KFE is not constant and, as $\frac{\partial P}{\partial \xi}|_B \leq 0$, probability is continually lost as more paths hit the barrier.

We still have to account for the probability associated with S having crossed the barrier. When the barrier is hit, the option is knocked out, the portfolio becomes risk-free and continues to grow at the risk-free of rate of interest, r.

However, as we are calculating the discounted hedging error, and the discounting exactly offsets the growth of the portfolio, this means that, for each value of y, the cumulative leakage, at time T, corresponding to paths which have hit the barrier, is given by

$$\frac{1}{2}\sigma^2 B^2 \int_0^T \frac{\partial P}{\partial \xi}\bigg|_B d\tau$$

and this accounts for the remainder of the probability distribution of the hedging error.

We give an example of this calculation in Chapter 6, Section 6.5.

Chapter 4

Numerical methods used to solve the extended Kolmogorov forward equation

In Chapter 3 we developed an extended Kolmogorov forward equation (KFE) which is satisfied by the joint density probability, $P(\underline{x}, y, t)$, of $\underline{x}$ and y at time t, in a situation where model mis-specification occurs. The KFE can then be solved to give the probability density of the hedging error at maturity. In this chapter we describe the numerical methods we have used to solve the KFE. We analyse the methods for a stylised 'toy' problem in Chapter 5 and apply them to hedging applications in Chapter 6.

We have based all our solutions on finite difference methods, where we use equally-spaced grids on, in principle, infinite domains. In practice, the grids will need to be truncated for numerical calculations.

We will write our approximate numerical solution as an array of values of $P(\underline{x}, y, t)$ defined at discrete grid points. For example, in the one-dimensional case for $\underline{X}$, we write (x_j, y_k, t_m) points of the form $(j\Delta x, k\Delta y, m\Delta t)$, for integers j, k and m, where $(j, k, m) \in \mathbb{Z} \times \mathbb{Z} \times [0, N]$.

Here Δx, Δy and Δt are the grid spacings in the corresponding directions and N is the largest index in the t-direction.

This can be easily extended to higher dimensions for $\underline{X}$.

The most straightforward approach to solving the KFE might be to simply discretise the problem in each direction and then solve the resulting system of linear equations. We will refer to this as using the 'basic finite difference method'. Unfortunately, this approach becomes more onerous in higher dimensions and it is helpful to achieve some reduction of dimension in these problems.

Due the special structure of the KFEs we have in the hedging problem, we are able to achieve a reduction of dimension because the drift term is independent of y and we have developed three solution methods that take advantage of this special situation.

First we will introduce the Fourier transforms that we will use in our numerical calculations and subsequent analysis of the convergence of our numerical schemes

4.1 Some preliminaries on the Fourier transform

In our solution methods and their analysis, we will make use of the Fourier transform which will be used in two forms, continuous and (semi-)discrete.

Given a function $f(x)$ defined on $[-\infty, \infty]$, we define the continuous Fourier transform as

$$\widehat{f}(s) = \int_{-\infty}^{\infty} f(x) e^{isx} dx$$

with the inverse

$$f(x) = \frac{1}{2\pi} \int_{-\infty}^{\infty} \widehat{f}(s) e^{-isx} ds$$

where s is the argument of the transformed function, $\widehat{f}(s)$.

Not all functions have Fourier transforms and/or inverse transforms. For a discussion on the applicability of the Fourier transform see [21]. We will assume that our solutions are square-integrable, i.e. are in L_2 so that the transforms exist.

As we are also dealing with δ-function initial conditions, we also need to be able to apply the necessary Fourier transforms to these initial conditions. A δ-function is a

generalised function (or a distribution) that is defined via its effect on any suitable 'test' function, $\phi(x)$, so that

$$\int_{-\infty}^{\infty} \delta(x)\phi(x)dx = \phi(x)|_{x=0} = \phi(0).$$

In fact, a δ-function is an example of 'tempered' distribution (see [21]), which guarantees that it has a Fourier transform and we have

$$\int_{-\infty}^{\infty} \delta(x)e^{ipx}dx = e^{ipx}|_{x=0} = 1.$$

Similarly, given a set of values f_j on a uniformly-spaced grid x_j we also define the (semi-)discrete Fourier transform

$$\widehat{f}(s) = \Delta x \sum_{j=-\infty}^{\infty} f_j e^{isx_j}$$

(where Δx is the grid spacing) and with the inverse

$$f_j = \frac{1}{2\pi} \int_{-\frac{\pi}{\Delta x}}^{\frac{\pi}{\Delta x}} \widehat{f}(s)e^{isx_j}ds.$$

We assume that the functions we use are in l_2.

We note that alternative definitions of these transforms exist with different possible scalings of the arguments and of the integrals and sums. However, what matters is that the transforms and their inverses be consistently defined.

In what follows, we will often refer to the Fourier transform as the 'z-FT' where z is the integration or summation argument in the transform, so as an example, we would write the continuous x-FT for $\int_{-\infty}^{\infty} f(x)e^{isx}dx$.

4.2 The solution methods for the KFE

Three numerical methods have to been used to solve the KFE, as follows:

- A semi-discrete 'Fourier' method where we first apply the continuous Fourier transform in the y-direction to the KFE, and then only discretise in the x direction, keeping t continuous.

- A discrete 'Fourier' method where we first apply the continuous Fourier transform in the y-direction to the KFE, and then discretise in both the x-direction and t-directions.
- The semi-Lagrangian method, applied to the original variables.

We will describe these solution methods in turn below but first we define some terms for later use.

In all the examples described in Chapter 3, the dynamics of the 'hedging error' were represented by a drift term alone, with drift coefficient only a function of $\underline{x}$ and t, i.e., independent of y.

The extended KFE can be written as

$$\frac{\partial P(\underline{x}, y, t)}{\partial t} - \mathcal{L}P(\underline{x}, y, t) + c(\underline{x}, t)\frac{\partial P(\underline{x}, y, t)}{\partial y} = 0 \tag{4.1}$$

where $\mathcal{L}P$ is an operator that does not depend on y.

For the examples we study, we will have

$$\mathcal{L}P(\underline{x}, y, t) = \sum_{j,l} A_{j,l}(\underline{x})\frac{\partial^2 P(\underline{x}, y, t)}{\partial x^{(j)}\partial x^{(l)}} + \sum_j B_j(\underline{x})\frac{\partial P(\underline{x}, y, t)}{\partial x^{(j)}} + C(\underline{x})P(\underline{x}, y, t)$$

where $A_{j,l}$, B_j and C are only functions of $\underline{x}$.

In passing, we note that we can sometimes make a logarithmic change of variables, so that the functions multiplying the derivatives become constants. This is not the case with the drift coefficient which remains a function of $\underline{x}$ and t. Generally, we have retained the original variables when applying our numerical methods.

4.3 Discretisation of the numerical schemes – Approximation of the derivatives

We will use numerical approximations to the derivatives in the KFE in our solutions.

The functions being approximated may be P, defined as a function of y, or the y-FT, $\widehat{P}$, defined as a function of p. In what follows below, z will refer to y or p as is appropriate. We will use the function F to represent either of these functions in this section.

We will only need to approximate first and second derivatives in our applications.

If we only discretise in the $\underline{x}$-direction, we approximate our function on a uniform grid with grid entries $\tilde{F}_{i_1,....,i_M}(z,t)$ which are functions of z and t.

To simplify the appearance of the formulae we give below, we first introduce shift operators applied to grid points, defined by

$$(S_k^+ F)_{i_1,.....,i_M} = S_{i_1,...,i_k+1...,i_M}$$

and

$$(S_k^- F)_{i_1,.....,i_M} = S_{i_1,...,i_k-1...,i_M}$$

.

For the space variables we write our approximation to a particular first derivative as the central difference

$$\frac{\partial F(x^{(1)},...,x^{(M)},z,t)}{\partial x^{(j)}}$$
$$\sim \frac{\tilde{F}(x^{(1)},...,x^{(j)}+\Delta x^{(j)},...,x^{(M)},z,t) - \tilde{F}(x^{(1)},,...,x^{(j)}-\Delta x^{(j)},...,x^{(M)},z,t)}{2\Delta x^{(j)}}$$

or

$$\frac{\partial F(\underline{x},z,t)}{\partial x^{(j)}} \sim \frac{(S_j^+ - S_j^-)\tilde{F}_{i_1,.....,i_M}(z,t)}{2\Delta x^{(j)}}$$

for all the allowable values of $i_1, i_2, ..., i_M$.

Similarly, we can define approximations to the second derivatives as

$$\left.\frac{\partial^2 F(\underline{x},z,t)}{\partial x^{(j)}\partial x^{(j)}}\right|_{\underline{x}=(x_{i_1},...,x_{i_M})} \sim \frac{(S_j^+ - 2 + S_j^-)\tilde{F}_{i_1,.....,i_M}(z,t)}{(\Delta x^{(j)})^2}$$

for the second derivative with respect to $x^{(j)}$, and

$$\left.\frac{\partial^2 F(\underline{x},z,t)}{\partial x^{(j)}\partial x^{(l)}}\right|_{\underline{x}=(x_{i_1},...,x_{i_M})}$$
$$\sim \frac{(S_j^+ S_l^+ - S_j^+ S_l^- - S_j^- S_l^+ + S_j^- S_l^-)\tilde{F}_{i_1,....,i_M}(z,t)}{\Delta x^{(j)}\Delta x^{(l)}}$$

the cross-derivative, (for $j \neq l$).

Here the indices i_j correspond to the values of $x^{(j)}$ on the grid.

If we also discretise in the t-direction we approximate the time derivatives by

$$\frac{\partial F(\underline{x}, z, t_n)}{\partial t} \sim \frac{\tilde{F}^{n+1}_{i_1,..,i_M}(z) - \tilde{F}^{n}_{i_1,....,i_M}(z)}{\Delta t}$$

for all allowable values of $i_1, i_2, ..., i_M$, and approximate the space derivatives as

$$\left.\frac{\partial F(\underline{x}, z, t)}{\partial x^{(j)}}\right|_{\underline{x}=(x_{i_1},...,x_{i_M})} \sim \frac{(S_j^+ - S_j^-)\tilde{F}^{n+1}_{i_1,.....,i_M}(z)}{2\Delta x^{(j)}}$$

$$\left.\frac{\partial^2 F(\underline{x}, z)}{\partial x^{(j)}\partial x^{(j)}}\right|_{\underline{x}=(x_{i_1},...,x_{i_M})} \sim \frac{(S_j^+ - 2 + S_j^-)\tilde{F}^{n+1}_{i_1,.....,i_M}(z)}{(\Delta x^{(j)})^2}$$

and

$$\left.\frac{\partial^2 F(\underline{x}, z, t)}{\partial x^{(j)}\partial x^{(l)}}\right|_{\underline{x}=(x_{i_1},...,x_{i_M})}$$

$$\sim \frac{(S_j^+ S_l^+ - S_j^+ S_l^- - S_j^- S_l^+ + S_j^- S_l^-)\tilde{F}^{n+1}_{i_1,....,i_M}(z)}{\Delta x^{(j)})\Delta x^{(l)}}$$

for $j \neq l$ and where we use the upper time level in the space derivatives.

For the basic finite difference method, we can approximate the y-derivative by using central differencing

$$\frac{\partial P(\underline{x}, y, t_n)}{\partial y} \sim \frac{\tilde{F}^{n'}_{i_1,..,i_M,j+1} - \tilde{F}^{n'}_{i_1,..,i_M,j-1}}{2\Delta y}$$

for each allowable value of $i_1, ..., i_M, j$ and where we may choose the time level, n', in various ways.

Alternatively, we may define a variable-direction upwinding method. We will only use the basic finite difference method for the toy model (see Chapter 5).

For the semi-Lagrangian method we only discretise in the $\underline{x}$ and t-directions but will use the Δy-spacing in calculations between time steps.

We are essentially dealing with a convection-diffusion equation set-up so we may have to consider the use of upwinding in the numerical scheme to improve its performance.

In our problems, the drift (convection) coefficients are variable (and functions of x) and so there may be particular issues with the upwinding definition, particularly if the convection coefficient changes sign.

However, in effect, the semi-Lagrangian method automatically incorporates a form of variable-direction upwinding for our problems and the numerical scheme can be defined to accommodate the necessary upwinding.

4.4 Inverting the y-FT

When we use either of the Fourier methods above to solve the KFE, the final step in the solution consists of applying the inverse y-FT.

We need to calculate the values of the approximate solution $U(x_j, y_k, t_m)$ at the grid points, as required, i.e.

$$U(x_j, y_k, t_m) = \frac{1}{2\pi} \int_{-\infty}^{\infty} V(x_j, p, t_m) e^{-ipy_k} dp$$

but the values of $V(x_j, p, t_m)$ will only be available for certain, discrete, values of p so we will need to approximate the inversion by some form of quadrature.

For the semi-discrete Fourier method, we have to find the values of $U(x_j, y_k, T)$, while for the discrete Fourier method we have to find the values of $U(x_j, y_k, t_n)$ where $T = m\Delta t$.

We will use the following simple quadrature rule to approximate the inversion formula by

$$U(x_j, y_k, t_m) \sim \frac{\Delta p}{2\pi} \sum_{l=l_{min}}^{l=l_{max}} V(x_j, p_k, t_m) e^{-ip_k y_k}. \tag{4.2}$$

and we have to calculate this for each grid point.

This is the simplest possible quadrature but we could, if necessary, use more sophisticated methods to improve the accuracy of the inversion.

We have to choose the set of values of l to use in the summation and this will influence the final result.

We could use a brute force approach to calculating (4.2) but there is an advantage to be gained from using the Fast Fourier Transform (FFT) which is provided within MATLAB, see [10]. This procedure greatly speeds up calculation of a Fourier transform but there are some subtleties to be aware of when using the FFT.

The MATLAB procedure (IFFT - Inverse Fast Fourier Transform) transforms a vector into its Fourier inverse. In the MATLAB documentation, [29], the IFFT is defined by the discrete inverse Fourier transform as

$$X_j = \frac{1}{N} \sum_{l=1}^{N} Y_l \omega_N^{-(j-1)(k-1)}$$

where

$$\omega_N = e^{-2i\pi/N}$$

and where both X and Y have length N.

This is not quite in the correct form for our inversion formula and we have to modify it somewhat.

Starting from our inversion formula, for a given i and m, we have

$$U_{j,k,m} \sim \frac{\Delta p}{2\pi} \sum_{l=l_{min}}^{l=l_{max}} V_{j,l,m} e^{-ip_l y_k}$$

for a suitable range of l-values, and we choose $l_{min} = -l_{max}$. We write $Y_k = U_{j,k,m}$ and $X_l = V_{j,l,m}$, so that

$$Y_k \sim \frac{\Delta p}{2\pi} \sum_{l=l_{min}}^{l=l_{max}} X_l e^{-ip_l y_k}$$

We then have

$$\begin{aligned}
\frac{\Delta p}{2\pi}\sum_{l=l_{min}}^{l=l_{max}} X_l e^{-ip_l y_k} &= \frac{\Delta p}{2\pi}\sum_{\tilde{l}=1}^{\tilde{l}=l_{max}-l_{min}+1} X_{\tilde{l}+l_{min}-1} e^{-i\Delta p(\tilde{l}+l_{min}-1)\Delta y k} \\
&= \frac{\Delta p}{2\pi}\sum_{\tilde{l}=1}^{\tilde{l}=l_{max}-l_{min}+1} X_{\tilde{l}+l_{min}-1} e^{-i\Delta p\Delta y(\tilde{l}+l_{min}-1)k} \\
&= \frac{\Delta p}{2\pi}\sum_{\tilde{l}=1}^{\tilde{l}=l_{max}-l_{min}+1} X_{\tilde{l}+l_{min}-1} e^{-\frac{2\pi i}{N}\frac{N\Delta p\Delta y}{2\pi}(\tilde{l}+l_{min}-1)k} \\
&= \frac{\Delta p}{2\pi}\sum_{\tilde{l}=1}^{\tilde{l}=l_{max}-l_{min}+1} X_{\tilde{l}+l_{min}-1} e^{-\frac{2\pi i}{N}(\tilde{l}+l_{min}-1)k}.
\end{aligned}$$

To make this fit in with the MATLAB procedure, we require

$$\frac{N\Delta p\Delta y}{2\pi} = 1$$

or

$$N = \frac{2\pi}{\Delta p\Delta y}$$

and $N = l_{max} - l_{min} + 1$.

Continuing, we then have

$$\begin{aligned}
\frac{\Delta p}{2\pi}\sum_{l=1}^{N} X_{l+l_{min}-1} e^{-\frac{2\pi i}{N}(l+l_{min}-1)k} &= \frac{\Delta p}{2\pi}\sum_{l=1}^{N} X_{l+l_{min}-1} e^{-\frac{2\pi i}{N}(l-1)k} e^{-\frac{2\pi i}{N}l_{min}k} \\
&= \frac{\Delta p}{2\pi}\sum_{l=1}^{N} X_{l+l_{min}-1} e^{-\frac{2\pi i}{N}(l-1)(\tilde{k}-1)} e^{-\frac{2\pi i}{N}l_{min}(\tilde{k}-1)} \\
&= \frac{1}{N}\sum_{l=1}^{N}\left(e^{-\frac{2\pi i}{N}l_{min}(\tilde{k}-1)}\frac{N\Delta p}{2\pi}\right) X_{l+l_{min}-1} e^{-\frac{2\pi i}{N}(l-1)(\tilde{k}-1)}
\end{aligned}$$

so that

$$Y_{\tilde{k}-1} \sim \frac{1}{N}\sum_{l=1}^{N} W_{l,\tilde{k}} e^{-\frac{2\pi i}{N}(l-1)(\tilde{k}-1)} = IFFT(W) \tag{4.3}$$

where, for each value of $\tilde{k}$,

$$W_{l,\tilde{k}} = \left(e^{-\frac{2\pi i}{N}l_{min}(\tilde{k}-1)}\frac{N\Delta p}{2\pi}\right) X_{l+l_{min}-1}.$$

So we have been able to write our inversion in terms of the MATLAB IFFT.

We now also have

$$\frac{(l_{max} - l_{min} + 1)\Delta p \Delta y}{2\pi} = 1.$$

If the p grid values are $(l_{min}\Delta p, ..., l_{max}\Delta p)$ then we have

$$p_{range} = p_{max} - p_{min} = \Delta p(l_{max} - l_{min})$$

and

$$\Delta y = \frac{2\pi}{N\Delta p} = \frac{2\pi}{(l_{max} - l_{min} + 1)\Delta p} = \frac{2\pi}{p_{range} + \Delta p} \sim \frac{2\pi}{p_{range}}.$$

Due to this definition, care has to be taken when applying these procedures to evaluate (4.2) above.

If we fix p_{range} and then refine the p-grid, the y-grid resolution will not change. If we want to provide values of the approximation at more closely-spaced y-values, we will have to increase the p-range.

Whether this refinement is needed will depend on the application.

Later in this chapter we will consider the interaction between the grid spacing in the x-direction and that in the p-direction.

4.5 The semi-discrete Fourier method

In this method we apply the continuous y-FT to the KFE in equation (4.1).

Applying the continuous y-FT to $P(x, y, t)$ gives

$$\widehat{P}(\underline{x}, p, t) = \int_{-\infty}^{\infty} P(\underline{x}, y, t) e^{ipy} dy$$

and we temporarily suppress the $\underline{x}$ and t arguments.

Applying the y-FT to the KFE gives

$$\widehat{\frac{\partial P(y)}{\partial t}} + c\widehat{\frac{\partial P(y)}{\partial y}} = \widehat{\mathcal{L}(P(y))}.$$

We use a standard property of the Fourier transform, i.e.

$$\widehat{\frac{\partial P(y)}{\partial y}} = -ip\widehat{P(p)},$$

and so we have

$$\widehat{\frac{\partial (cP(y))}{\partial y}} = -ipc\widehat{P(p)}$$

as the drift coefficient is independent of y, and we also have

$$\widehat{\mathcal{L}(P(y))} = \mathcal{L}(\widehat{P(p)})$$

as $\mathcal{L}$ is independent of y.

So we obtain the family of PDEs, indexed by p,

$$\frac{\partial \widehat{P}(\underline{x}, p, t)}{\partial t} - ipc(\underline{x}, t)\widehat{P}(\underline{x}, p, t) = \mathcal{L}(\widehat{P}(x, p, t)) \tag{4.4}$$

that are satisfied by $\widehat{P}(\underline{x}, p, t)$.

We can now use our approximations to the derivatives in the x-direction, from Section 4.3, while keeping t continuous. We illustrate the case where $\underline{x}$ is one-dimensional and obtain the family of ODEs

$$\begin{aligned}\frac{\partial \widehat{P}_j(p,t)}{\partial t} = A_{1,1}(x_j)\frac{\widehat{P}_{j+1}(p,t) - 2\widehat{P}_j(p,t) + \widehat{P}_{j-1}(p,t)}{\Delta x^2} + B_1(x_j)\frac{\widehat{P}_{j+1}(p,t) - \widehat{P}_{j-1}(p,t)}{2\Delta x} \\ +C(x_j)\widehat{P}_j(p,t) + ipc_j(t)\widehat{P}_j(p,t)\end{aligned}$$

or

$$\frac{\partial \widehat{P}(p,t)}{\partial t} = M\widehat{P}(p,t) \tag{4.5}$$

where $\widehat{P}(p,t)$ is a vector of functions of p and t and the matrix M satisfies

$$\begin{aligned} M_{j,j} =& \frac{-2A_{1,1}(x_j)}{\Delta x^2} + C(x_j) + ipc_j(t) \\ M_{j,j-1} =& \frac{A_{1,1}(x_j)}{\Delta x^2} - \frac{1}{2\Delta x}B_1(x_j), \text{and} \\ M_{j,j+1} =& \frac{A_{1,1}(x_j)}{\Delta x^2} + \frac{1}{2\Delta x}B_1(x_j). \end{aligned} \tag{4.6}$$

In principle, the matrix is infinite but, in practice, we will need to truncate the grid and the matrix.

If the drift is independent of t, then the matrix, M, is also independent of t and, in that case, the matrix ODE can be solved by using matrix exponentials to get

$$\widehat{P}(\underline{x}, p, t) = \widehat{P}(\underline{x}, p, 0)e^{At}$$

for each value of p.

An example of this will be described for the toy model discussed in Chapter 5, where the drift is independent of t.

To find the approximate numerical solution in the original variables x, y and t, we apply the inverse y-FT to $\widehat{P}(x_j, p, t)$. as discussed in Section 4.4.

4.6 The discrete Fourier method

In this method we again use the system of PDEs in (4.4),

$$\frac{\partial \widehat{P}(x,p,t)}{\partial t} - ipc(x,t)\widehat{P}(x,p,t) = \mathcal{L}(\widehat{P}(x,p,t))$$

which are indexed by p.

For this method, we discretise in the x-direction and also in the t-direction, using the discretisations given in Section 4.3, obtaining a set of linear equations to be solved for each value of p.

With this method we have

$$\frac{\widehat{P}_j^{n+1}(p) - \widehat{P}_j^n(p)}{\Delta t}$$
$$= A_{1,1}(x_j)\frac{\widehat{P}_{j+1}^{n+1}(p) - 2\widehat{P}_j^{n+1}(p) + \widehat{P}_{j-1}^{n+1}(p)}{\Delta x^2} + B_1(x_j)\frac{\widehat{P}_{j+1}^{n+1}(y) - \widehat{P}_{j-1}^{n+1}(p)}{2\Delta x}$$
$$+C(x_j)\widehat{P}_j^{n+1}(p) + ipc_j^{n+1}(t)\widehat{P}_j^{n+1}(p)$$

if the drift term is treated implicitly.

This gives the system of linear equations

$$M^{n+1}\widehat{P}^{n+1}(p) = \widehat{P}^{n}(p) \tag{4.7}$$

where the matrices, M^{n+1}, satisfy

$$\begin{aligned} M^{n+1}_{j,j} =& (1 + 2A_{1,1}(x_j)\lambda) - C(x_j)\Delta t - ipc^n_j\Delta t \\ M^{n+1}_{j,j-1} =& -A_{1,1}(x_j)\lambda + \frac{\mu}{2}B_1(x_j), \text{and} \\ M^{n+1}_{j,j+1} =& -A_{1,1}(x_j)\lambda - \frac{\mu}{2}B_1(x_j) \end{aligned} \tag{4.8}$$

with $\lambda = \frac{\Delta t}{\Delta x^2}$ and $\mu = \frac{\Delta t}{\Delta y}$ and we again note that, in general, the matrices, M^n, are time dependent.

As for the semi-discrete method, to find the approximate numerical solution in the original variables x, y and t, we apply the inverse y-FT to $\widehat{P}(x_j, p, t)$ and we use the Fast Fourier Transform (FFT) for this stage of the solution process.

4.7 The semi-Lagrangian method

The semi-Lagrangian method ([8], [31]) is suitable for problems which involve a drift (or convection) term in the PDE. It solves the KFE by reducing it to the solution of a system of lower-dimensional PDEs, one for each of the y-grid values.

The hedging problem KFEs have a convenient form in which the drift coefficient, $c(x, t)$, is independent of y, which offers a computational advantage with the semi-Lagrangian method.

The solution process is as follows

- Set up the initial conditions for the problem. These will consist of an approximation to a delta-function centred at the initial values in $\underline{x}$ and the initial value of y which is normally taken to be zero.

  We arrange the grids so that the numerical approximation to the delta-function is located at a grid point, and the initial value of the numerical approximation at that grid point is then given by

$$P(j_0, 0, 0) = \frac{1}{\Delta x \Delta y},$$

$$P(j,k,0) = 0 \text{ , for } (j,k) \neq (0.0)$$

(for the one-dimensional case), where x_{j_0} is the initial position of x. This ensures that the initial probability density has the correct mass.

- At each time step, m, we first calculate the array of 'shifts' in y using $y'_k = y_k - c(x_j, t_m)\Delta t$, where Δt is the time step. These shifts do not depend on y so can be calculated for all the y, simultaneously, at the current time step. In general, the shifted values of y will not be found at grid points.

- For each value of y, we calculate, by interpolation, the adjusted values for $P(x_j, y', t_m - \Delta t)$ at the start of the time step. This depends on the grid spacing in the y-direction. We use linear interpolation, although more complex interpolation schemes could be used.

- We then apply a PDE solver, based on discretisation in the $\underline{x}$ and t-directions, to the interpolated adjusted values at the start of the time step, for each value of y.

- We advance to the next time step.

Here we give further details of the discretisation method.

One-dimensional case

Interpolating between grid points at the start of the time step we define

$$RHS^{n+1}_{j,k} = P^{n+1}_{j,k} - A_{1,1}(x_j)\Delta t \frac{P^{n+1}_{j+1,k} - 2P^{n+1}_{j,k} + P^{n+1}_{j-1,k}}{\Delta x^2} - \Delta t B_1(x_j) \frac{P^{n+1}_{j+1,k} - P^{n+1}_{j-1,k}}{2\Delta x}$$

$$-\Delta t C(x_j) P^{n+1}_{j,k} = (1-\alpha) P^n_{j,\lfloor k - c_j \frac{\Delta t}{\Delta y} \rfloor} + \alpha P^n_{j,\lfloor k - c_j \frac{\Delta t}{\Delta y} \rfloor + 1}$$

for $c_j > 0$ and where $\alpha = (k - c_j \frac{\Delta t}{\Delta y}) - \left\lfloor k - c_j \frac{\Delta t}{\Delta y} \right\rfloor$, using the floor function. If we make $\alpha = c_j \frac{\Delta t}{\Delta y}$ small enough we have

$$RHS^n_{j,k} = (1-\alpha) P^n_{j,k-1} + \alpha P^n_{j,k}$$

i.e. using linear interpolation in the immediate grid cell with a y-grid spacing of Δy and we can derive have a similar expression for $c_j < 0$, except that the 'upwinding' reverses direction.

So for the case of small α, the method is identical to an upwind finite difference method which is described in Appendix A.

This leads to a system of equations similar to those used in the Fourier methods, except that the drift coefficient does not feature in the matrix, M, i.e.

$$MP_{j,k}^{n+1} = RHS_{j,k}^{n+1} \tag{4.9}$$

where the matrix, M, satisfies

$$\begin{aligned} M_{j,j}^{n+1} =& (1 + 2A_{1,1}(x_j)\lambda) - C(x_j)\Delta t \\ M_{j,j-1}^{n+1} =& A_{1,1}(x_j)\lambda - B_1(x_j)\frac{\mu}{2}, \text{and} \\ M_{j,j+1}^{n+1} =& A_{1,1}(x_j)\lambda + B_1(x_j)\frac{\mu}{2} \end{aligned} \tag{4.10}$$

where $\lambda = \frac{\Delta t}{\Delta x^2}$, $\mu = \frac{\Delta t}{\Delta x}$, and the right-hand side values are the interpolated values from the previous time step.

Two-dimensional case

The general form of the operator (with y fixed) in the KFE will then be

$$\mathcal{L}P(x,y,t) = A_{1,1}\frac{\partial^2 P(x^{(1)},x^{(2)},y,t)}{\partial x^{(1)}\partial x^{(1)}} + A_{1,2}\frac{\partial^2 P(x^{(1)},x^{(2)},y,t)}{\partial x^{(1)}\partial x^{(2)}} + A_{2,2}\frac{\partial^2 P(x^{(1)},x^{(2)},y,t)}{\partial x^{(2)}\partial x^{(2)}}$$
$$+ B_1\frac{\partial P(x^{(1)},x^{(2)},y,t)}{\partial x^{(1)}} + B_2\frac{\partial P(x^{(1)},x^{(2)},y,t)}{\partial x^{(2)}} + CP(x^{(1)},x^{(2)},y,t)$$

and we will discretise in the $x^{(1)}$, $x^{(2)}$ and t-directions.

For this case we need to include the approximation of the cross-derivatives.

We have some additional issues to consider.

Firstly, due to the increased dimensionality we have different choices for organising the solution into vector form. We have used the lexicographic ordering for the components of $\underline{x}$ in our calculations. Secondly, the presence of cross-derivatives complicates the structure of the matrix M, considerably increasing the bandwidth. Consequently, alternative solution methods might be sought to deal with the cross-derivatives.

A popular alternative is to use an alternating-direction implicit solution (ADI) method and this is what we have used for our KFE examples. These methods will be described

in more detail below. Without using ADI we would, for the fully implicit case, get a system of equations which we could write as

$$(I + \Delta t M_0 + \Delta t M_1 + \Delta t M_2) P^{n+1}(y) = RHS^n(y)$$

where we have written the left-hand side matrix as a sum of three separate matrices. Here M_1 contains the discretised terms arising from $\frac{\partial^2 P(x^{(1)},x^{(2)},y,t)}{\partial x^{(1)} \partial x^{(1)}}$, M_2 contains the discretised terms arising from $\frac{\partial^2 P(x^{(1)},x^{(2)},y,t)}{\partial x^{(2)} \partial x^{(2)}}$ and M_0 contains the discretised terms arising from the cross-derivative, $\frac{\partial^2 P(x^{(1)},x^{(2)},y,t)}{\partial x^{(1)} \partial x^{(2)}}$.

These separate matrices are then used in the ADI method, see the following section.

4.8 ADI splitting

In the simplest cases we have presented, the simple Black-Scholes case, and after order reduction using the semi-Lagrangian method, we need to solve a collection of one-dimensional PDEs which are straightforward to treat by standard finite difference methods.

However, in other examples given above, we will need to solve a collection of two-dimensional PDEs which are essentially the KFEs for the underlying processes, i.e. the PDEs that give the transition densities of the vector $\underline{x}$.

In particular, we have examples of a two-dimensional asset process and also a case where a stochastic volatility process is present.

So we see that calculation of the hedging error distributions is an extension of the method for calculating of these transition densities where the drift in the 'hedging error' results in the need to solve a collection of such problems.

For the two-dimensional problems, an alternating-direction implicit solution (ADI) method has been used to solve each of the resulting two-dimensional PDEs.

There are a number of ADI schemes available; in this work only the simplest, the Douglas-Rachford scheme, has been used. A brief description of the method follows.

The key numerical step in solving the two-dimensional PDE is the solution of a set of linear equations, obtained by discretising the PDE and using an approximation to the θ-scheme, that can be written as

$$(I - \theta\Delta tM_1 - \theta\Delta tM_2)u^{n+1} = (I + \Delta tM_0 + (1-\theta)\Delta tM_1 + (1-\theta)\Delta tM_2)u^n.$$

Here the solution at time step n is written as u^n, the time step is Δt, the matrix M_0 is made up of the finite difference terms corresponding to the mixed second derivative terms in the PDE.

The matrix M_1 is made up of the finite difference terms corresponding to the spatial derivatives with respect to the first independent variable and the matrix M_2 is made up of the finite difference terms corresponding to the spatial derivatives with respect to the second independent variable.

We see that the scheme is not quite the θ-scheme as the M_0 term is treated fully explicitly, appearing only on the right hand side of the equation. A consequence of this is that the error in this equation is only as good as $O(\Delta t^3)$ if $M_0 = 0$ and $\theta = 0.5$.

A more complex ADI method, the Craig-Sneyd scheme ([7]), can be used to achieve a higher order of accuracy but has not been used in this study. See [19] and [20] for papers on the relative performances of various ADI schemes.

The idea behind the ADI scheme (which is an example of a *splitting* scheme) is to replace the direct solution of this system of equations by the solution of related sub-problems where solutions are found in the separate directions of the first and second independent variables.

Dropping the error term, the original problem can be written as as

$$(I - \theta\Delta tM_1 - \theta\Delta tM_2 + \theta^2\Delta t^2 M_1M_2)u^{n+1}$$

$$= (I + \Delta tM_0 + (I-\theta)\Delta tM_1 + (I-\theta)\Delta tM_2 + \theta^2\Delta t^2 M_1M_2)u^n + \theta^2\Delta t^2 M_1M_2(u^{n+1} - u^n)$$

or to the same order of accuracy

$$(I - \theta\Delta tM_1 - \theta\Delta tM_2 + \theta^2\Delta t^2 M_1M_2)u^{n+1}$$

$$= ((I - \theta\Delta tM_1)(I - \theta\Delta tM_2) + \Delta tM_0 + \Delta tM_1 + \Delta tM_2)u^n$$

In the Douglas-Rachford scheme ([32],[9]) this can be written as

$$(I-\theta\Delta tM_1)(I-\theta\Delta tM_2)u^{n+1} = (I+\Delta tM_0+(I-\theta)\Delta tM_1)u^n - (I-\theta\Delta tM_1)\theta\Delta tM_2u^n$$

which allows the solution to be broken down into the following steps,

$$(I-\theta\Delta tM_1)Y = (I+\Delta tM_0+(I-\theta)\Delta tM_1+\Delta tM_2)u^n$$

$$(I-\theta\Delta tM_2)u^{n+1} = Y-\theta\Delta tM_2u^n$$

where Y is an intermediate solution. These two steps are, in effect solving first in the direction of the first independent variable and then in the direction of the second independent variable. Each step requires a matrix inversion and so has at least a partially implicit nature, hence the name, 'alternating direction implicit', for this scheme.

4.9 Properties of numerical solutions

Conservation of probability

At any time step we can calculate an estimate of the probability represented by the solution and we need to monitor this to ensure that we are neither gaining or losing significant amounts of probability due to the numerical approximations used.

Conservation of probability depends on the properties of the matrices used in the numerical solution. Essentially, we can expect probability to be conserved if the column sums of the matrices are all equal to one. Some analysis of the matrices used has been carried out and it is clear that these sums are not always exactly equal to one but the errors appear to be small enough to lead to only small errors in the total probability. It may be possible to improve the preservation of probability by using a discretisation scheme for the PDE that is specifically designed to be conservative.

The requirement for conservation of probability also has implications for the form of the boundary conditions to be applied to the solution. In the examples shown above, the simple Dirichlet boundary condition with the probability being zero at the 'underlying' boundaries has been used. This is not quite correct but appears to have little impact in the cases considered.

Note that the stochastic volatility (Heston) cases are such that the Feller condition applies. When the Feller condition is not satisfied, the variance process can reach zero, so we cannot set the probability of this event to zero. If an example of this type were to be studied, greater care would need to be taken with the definition of the boundary condition at zero variance.

Finally, conservation of probability relies on the grid being sufficiently extensive to capture the likely range of hedging errors that are reached as time passes. It has been found that if the grid is too restrictive, probability is not conserved.

Positivity of the solutions

Another issue which arises especially in the solution of two-dimensional problems is that of the positivity of the solutions.

We start with non-negative initial conditions and, because we are dealing with probability distributions, expect that the solution at any time step should be non-negative. However, when solving the linear systems arising from discretisation, the positivity of the solution is determined by the properties of the matrices involved.

The linear equations to be solved can typically be written in the following form, i.e.

$$K_1 u^{n+1} = K_2 u^n$$

where u^n is the solution vector at time step n and K_1 and K_2 are matrices. Attention needs to be paid to the matrices on both the left and right-hand sides of the equations to be solved. As we are dealing with vectors u^n that represent probability distributions, we will achieve positivity if we can ensure that all the elements of K_2 and K_1^{-1} are positive. The first condition can often be achieved by making the timestep sufficiently small and the second condition will be satisfied if K_1 is an M-matrix ([2]).

In this study, it appears that some of the left-hand side matrices encountered do not satisfy the conditions required for them to be M-matrices (this is most obvious in the case of the correlated two-asset example). In the solutions obtained above some negative values appear in certain ranges of hedging error but generally these are where the probability is very small.

Convergence of the numerical schemes

Apart from the issues of probability conservation and positivity, there is also a need to understand how the accuracy of the solution depends on the grid resolution.

The numerical solution may indeed be converging to the true solution but in order to gain confidence in this behaviour, it is desirable to have some supporting theoretical analysis of the convergence behaviour. For our general problem this analysis will be hard to achieve, so instead, in a later part of the thesis, we will study a 'toy' model which captures the key features of these problems and investigate the convergence of a simpler model.

4.10 Validation of the KFE approach by Monte Carlo simulation

We can assess the performance of our numerical schemes by comparing the numerical solution from the KFE against a Monte Carlo simulation of the (erroneous) hedging stratgey.

This is most convincingly achieved by running a Monte Carlo simulation of the hedging process in which the portfolio is dynamically rebalanced using the hedge ratios calculated from erroneous model at each time step (see the next section).

An alternative method of validating the KFE results would be to perform a Monte Carlo simulation based on the SDE representing the joint behaviour of $\underline{x}$ and y as in (3.10) and (3.11) of Chapter 3.

These two approaches will give the same results, up to a discretisation error, but the first approach more clearly illustrates the actual behaviour of the trader.

Monte Carlo simulation of hedging errors

We have estimated the hedging errors by Monte Carlo simulation. The calculation is illustrated by the following piece of pseudocode, Algorithm 1.

This example has been based on the KFE in Section 3.4.1.

Algorithm 1 Monte Carlo Simulation of Hedging Errors

procedure MONTE CARLO ▷
    -Set up the parameters for μ, σ, r and the time step, Δt
    -Set up the initial condition for S=S_0
    -Set up the number of paths to simulate (NPaths)
    -Set up the number of time steps in each path (NTimeSteps)
    for $i = 1$ to NPaths **do**
        -Initialise the path
        S_Old ← S_0
        -Calculate the premium and the initial hedge ratio from mis-specified model (function call)
        Premium←Initial_Price
        Asset_Holding_Old ← Initial_Hedge_Ratio_Old*S_Old
        Cash_Old←Premium-Asset_Holding_Old
        Portfolio_Old←Cash_Old+Asset_Holding_Old
        for $j = 1$ to NTimeSteps **do**
            -Sample the path for S using the correct model (function call)
            S_New←S_Old*(1+$\mu\Delta t$+$\sigma\sqrt{\Delta t}$*Normal_Variate_Sample)
            -Update hedge ratio from S_{New} using the mis-specified model
            -Recognise interest in the cash balance
            Cash_New←(1+$r\Delta t$)*Cash_Old
            Update the holding in S and rebalance portfolio
            Asset_Holding_New←Hedge_Ratio_New*S_New
            Cash_From_Rebalancing←Hedge_Ratio_Old*S_New-Asset_Holding_New
            Cash_New←Cash_New+Cash_From_Rebalancing
            Portfolio_New←Cash_New+Asset_Holding_New
            -Prepare for next time step
            Asset_Holding_Old←Asset_Holding_New
            Cash_Old←Cash_New
            S_Old←S_New
            Hedge_Ratio_Old←Hedge_Ratio_New
        end for
    end for
    -Calculate the payoff (function call)
    -Calculate the difference between the final portfolio and the payoff and apply the discounting
    Discounted_Hedging_Error ← e^{-rT}*(Portfolio_New-Payoff)
end procedure

The key points to observe are that

- we are using a very simple Euler method for simulation of the SDE for S,
- the premium (initial price) and hedge ratios are calculated using the misspecified model, and hence mimicking the behaviour of the trader, and
- the parameters used to update the path for S come from the correctly specified model.

Clearly, there is scope for a more sophisticated approach which might be more appropriate for, say, the barrier option example where the simulated paths might 'stray' over the barrier.

Accuracy of the Monte Carlo simulation results

We have generally obtained reasonable fits between the finite difference and Monte Carlo outputs but some comments are in order.

Firstly, the accuracy of the Monte Carlo simulation of the 'hedging error' will depend on the frequency of hedging, i.e. there will be a discretisation error. Of course, the KFE method also has a discretisation error so it is necessary to make both these errors small enough before trying to compare the distributions.

Secondly, when using Monte Carlo simulation, the finite sample size always results in uncertainty about the simulation results. When using Monte Carlo simulation to calculate an expectation, such as the value of an option, the standard error of the result can be estimated from the variance of the simulated values. However, in our application, we are trying to simulate the entire probability distribution and it is unclear how to assess the match. This clearly complicates the issue of comparing the Monte Carlo results against the KFE results, particularly for the tails of the distribution.

Chapter 5

Numerical analysis for a toy model of the Kolmogorov forward equation

In this chapter, we investigate the stability and accuracy of the numerical schemes used to solve our KFE problems.

We have seen in Chapter 2 and in [5], that Fourier transform methods are very useful in the analysis of stability for constant coefficient linear PDEs with δ-function initial conditions and we would like to apply these methods to the KFE.

The KFE for the joint probability density, $P(\underline{x}, y, t)$, of $\underline{x}$, y and t is in the form

$$\frac{\partial P(\underline{x}, y, t)}{\partial t} - \mathcal{L}P(\underline{x}, y, t) + c(\underline{x}, t)\frac{\partial P(\underline{x}, y, t)}{\partial y} = 0 \tag{5.1}$$

where $\mathcal{L}$ is an operator that does not depends on y or its derivatives. The initial condition is given by

$$P(\underline{x}, y, 0) = \delta(\underline{x})\delta(y).$$

For our KFE problems, T will be the time at maturity of the financial instrument studied.

We note the stylised features of the model:

- There is no diffusion term in the y-direction.
- The hedging error drift coefficient, $c(\underline{x}, t)$, is independent of y.

- The PDE has variable coefficients in $\underline{x}$ (and these may change sign).
- At time $t = 0$, we have a δ-function initial condition.

We cannot expect to analyse fully even the simplest KFE problem as the equation is complex. Instead we have studied a 'toy' model based on the stylised features of the KFE.

5.1 Introduction to the toy model

5.1.1 The toy model

The toy model we have selected for study is

$$\begin{aligned} u_t + xu_y &= u_{xx} \\ u(x, y, 0) &= \delta(x)\delta(y). \end{aligned} \tag{5.2}$$

For our theoretical analysis, we prefer to call the solution of the PDE $u(x, y, t)$, to avoid any confusion between the probability density, P, in the KFE and the argument, p, in the Fourier transform that we will use later.

For the toy model, the drift coefficient takes the simplest possible variable form, namely x, and the initial condition is taken to be a δ-function which represents the initial condition of the KFE.

5.1.2 Comments on the suitability of the toy model selection

We readily acknowledge that the toy model does not capture all the features of the KFE problems we have studied. In particular, in our real-life KFE problems the drift coefficient, $c(\underline{x}, t)$, may be a complicated function of time and of $\underline{x}$.

The toy model drift coefficient is independent of t. As we are mainly interested in the interplay of the Dirac initial data and the variable coefficient in the hyperbolic y-direction, we will ignore this limitation in this thesis. Put another way, we are mainly interested in the early time behaviour of the solution which is caused by the δ-function initial condition, so we will ignore the time dependence in the drift.

The KFE drift coefficient often has a strong dependence on $\underline{x}$ and so the toy model can only represent a first, linearising, step in our analysis. As we use δ-function initial conditions, we feel there is some justification for considering only first two terms of the Taylor expansion of c as the behaviour of the solution will initially be quite localised. The leading order term would then correspond to constant drift (a familiar convection-diffusion problem which can be analysed by standard Fourier techniques) whereas the linear term, proportional to $\underline{x}$ would, in the short term, represent the main variable element of the drift.

Consequently, we have investigated a toy model where the drift is simply proportional to the underlying. Even with this simpler problem formulation, involving a PDE with variable coefficients, the Fourier analysis is not straightforward and is incomplete, for some of the schemes we used, insofar as it relates to the analysis of stability and accuracy for the numerical methods.

5.1.3 Analytical solution of the toy model

The toy model PDE has a closed form solution which is as follows

$$u(x, y, t) = \frac{\sqrt{3}}{2\pi t^2} \exp\left(-\frac{1}{4t}x^2\right) \exp\left(-\frac{3}{t^3}\left(y - \frac{t}{2}x\right)^2\right).$$

To show that this is the solution we can simply substitute this expression into the PDE. We also need to check that the δ-function initial condition is satisfied by integrating out the solution for $t > 0$ in the x and y directions and showing that the integral remains equal to 1 for all $t > 0$. We also need to show that for any $(x, y) \neq (0, 0)$, $u(x, y, t) \to 0$ as $t \to 0$. Figure 5.1 shows the true solution at $t = 1$.

Figure 5.1: True solution for the toy model at $t = 1$

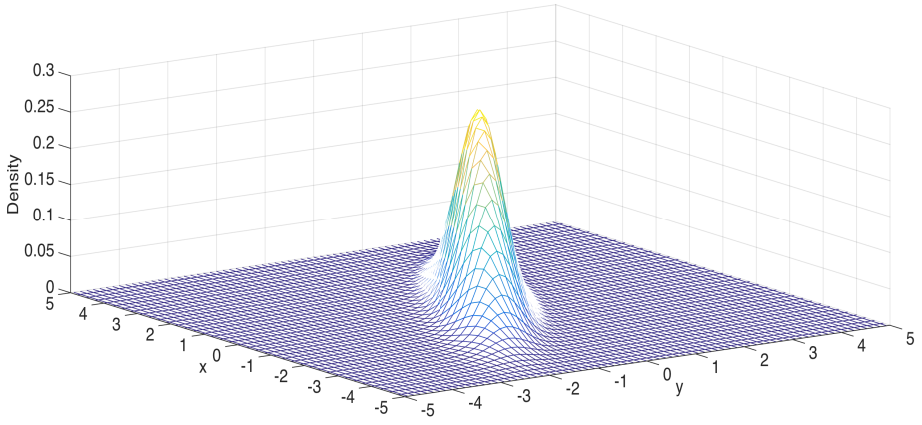

This PDE has a considerable history; one of its earliest appearances is in [25] and there are a number of recent papers that report on the long-time behaviour of the numerical solution of the equation, e.g. [34]. However, we stress that these references in the literature do not address the case of δ-function initial conditions.

The fundamental solution of the PDE (i.e., one for a δ-function initial condition) can be obtained by using Fourier methods as follows. We first apply the y-FT to the PDE and define $v(x, p, t)$ as the result of the transform. Using standard properties of the Fourier transform, we obtain

$$v_t(x, p, t) - ixpv(x, p, t) = v_{xx}(x, p, t). \tag{5.3}$$

We then apply the x-FT to this equation and define $w(x, p, t)$ as the result of performing the transform.

We note that

$$\frac{\partial}{\partial s} \int_{-\infty}^{\infty} v(x, p, t) e^{isx} dx = \int_{-\infty}^{\infty} ixv(x, p, t) e^{isx} dx$$

and so

$$\frac{\partial w(s, p, t)}{\partial t} - p \frac{\partial w(s, p, t)}{\partial s} = -s^2 w(s, p, t). \tag{5.4}$$

The initial condition is then $w(s, p, 0) \equiv 1$ and we solve the PDE for $w(s, p, t)$ to obtain

$$w(s, p, t) = \exp\left(-s^2 t - spt^2 - \frac{1}{3} p^2 t^3\right). \tag{5.5}$$

We will refer to w as the double Fourier transform (double-FT) in our later work where we have applied Fourier transforms in both directions.

Figure 5.2: The analytic double Fourier Transform at $t = 1$

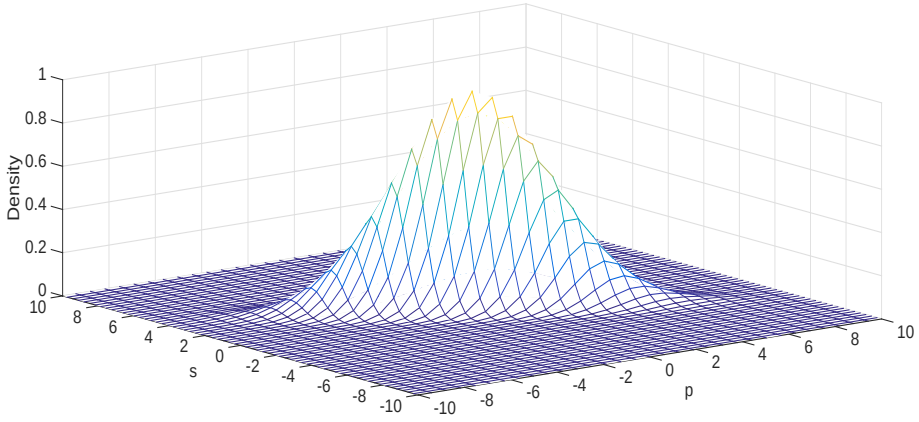

We note that after applying the two transforms, we have a function that is smooth for $t \geq 0$. Figure 5.2 shows the form of the double-FT at $t = 1$.

To obtain our solution for u, we invert the two Fourier transforms to obtain the solution given above.

Applying the inverse x-FT first gives

$$
\begin{aligned}
v(x,p,t) &= \frac{1}{2\pi}\int_{-\infty}^{\infty} w(s,p,t)e^{-isx}ds \\
&= \frac{1}{2\pi}\int_{-\infty}^{\infty} \exp\left(-s^2t - spt^2 - \frac{1}{3}p^2t^3\right)e^{-isx}ds \\
&= \frac{1}{2\pi}\exp\left(-\frac{1}{3}p^2t^3\right)\int_{-\infty}^{\infty}\exp\left(-s^2t - spt^2 - isx\right)ds \\
&= \frac{1}{2\pi}\exp\left(-\frac{1}{3}p^2t^3\right)\exp\left(t\left(\frac{pt+\frac{ix}{t}}{2}\right)^2\right)\int_{-\infty}^{\infty}\exp\left(-t\left(s-\frac{pt+\frac{ix}{t}}{2}\right)^2\right)ds \\
&= \frac{1}{2\pi\sqrt{t}}\exp\left(-\frac{1}{12}p^2t^3\right)\exp\left(\frac{ipxt}{2}-\frac{x^2}{4t}\right)\int_{-\infty}^{\infty}\exp\left(-\omega^2\right)d\omega
\end{aligned}
$$

where $\omega = \sqrt{t}\left(s - \frac{pt+\frac{ix}{t}}{2}\right)$, or

$$v(x,p,t) = \frac{1}{2\sqrt{t\pi}} \exp\left(-\frac{1}{12} p^2 t^3 \right) \exp\left(\frac{ipxt}{2} - \frac{x^2}{4t} \right).$$

A similar calculation using the inverse y-FT then leads to the solution for $u(x,y,t)$ given above. We note that v is complex while u and w are real as a result of the choice of the initial conditions.

We will use the analytical solution to assess the behaviour of the numerical schemes we use to solve the toy model PDE.

5.2 The analysis of stability and accuracy for the toy model numerical schemes

We have considered the following solution methods for the toy model PDE

- the semi-discrete Fourier method,
- the discrete Fourier method,
- the semi-Lagrangian method,

as described in Chapter 4.

In this section we discuss the general features of the analysis we will carry out for each of our numerical schemes. For each of the schemes we will discuss

- the discretisation of the scheme,
- the numerical results from the scheme,
- the time-evolution of the double-FT, and
- progress made towards analysing the error between the true and numerical double-FT and what this tells us about the performance of the numerical scheme in the original variables.

The finite difference approximations to the functions u, v and w will be written using upper case letters, U, V and W.

5.2.1 Discretisation

When solving the toy model numerically, we will restrict attention to finite difference methods and will discretise the problem by defining the numerical approximation, U, to u on an unbounded uniform grid with spacings, Δx, Δy and Δt, where appropriate.

That is, we will define a numerical approximation to the solution of the PDE by finding the values, $U(j,k,m)$, of the approximation at the grid points (x_j, y_k, t_m), where $j \in \mathbb{Z}$, $k \in \mathbb{Z}$ and m is a integer in $[0, N]$, where $T = N\Delta t$ is the largest time value for the PDE.

For numerical calculations, we will have to truncate the grids in the x and y directions, as appropriate, although, in our Fourier analysis, we will ignore the truncation.

Depending on the scheme under consideration, we will not need to discretise in all directions although our final numerical implementations will inherently involve a discretisation process.

The discretisations for the various methods we use have been described in Chapter 4, Section 4.3 and for the toy model, correspond to the choices, $A_{1,1} \equiv 1$, $B_1 \equiv 0$, $C \equiv 0$. We also have $c(x,t) \equiv x$.

5.2.2 The time evolution of the double-FT

Our approach is to start with an analysis of the error between the numerical and true double transforms and understand the behaviour of the error as $\Delta t \to 0$ in Fourier space. To do this we apply Fourier transforms in the appropriate directions to derive an expression for the time evolution of the numerical double-FT.

In some cases, this time evolution is in the form of a PDE depending on t while in other cases it is in the form of recursion for the double-FT at consecutive time steps. This latter recursive behaviour is familiar from the case of a constant-coefficient PDE where a closed form solution for the numerical transform at time t (see [5]) can be found.

In the constant-coefficient case we can study the time evolution of the double-FT, analyse the error between the numerical and true transforms and also analyse the error, expressed in the original variables, as the grid is refined in an appropriate way and demonstrate the convergence, or otherwise, of the numerical scheme. See, for example, [5] and [36]. For the toy model, which has variable coefficients, the time evolution we observe is more complicated and closed form solutions for the numerical double-FT are not generally available.

In the case of the semi-discrete Fourier method, however, we have been able to complete the analysis and have solved the accuracy problem. We have been less successful with the discrete Fourier method, where we lack a full understanding of the wavenumber analysis and still need to complete the stability analysis.

For the semi-Lagrangian method, it is not possible to apply the Fourier transform techniques used for the two Fourier methods. If we assume that the grid step sizes are chosen suitably, however, then the semi-Lagrangian scheme can be considered as a variable-direction upwinding version of the basic finite difference scheme. In Appendix A we give some analysis of the recursion and convergence analysis for the latter scheme. Unfortunately, it has been too difficult to complete this analysis but, nevertheless, the progress made has been reported in Appendix A.

5.3 The semi-discrete Fourier method

With this method, we apply the y-FT to the original problem, taking advantage of the fact that the drift coefficient, x, is independent of y. We then discretise in the x-direction keeping the problem continuous in time.

5.3.1 The numerical scheme for the semi-discrete Fourier method

Applying the Fourier transform in y-direction to the toy model PDE we get

$$v_t - ipxv = v_{xx},$$

where

$$v(x,p,t) = \int_{y=-\infty}^{y=\infty} u(x,y,t)e^{ipy}dy$$

and then discretise only in the x-direction, using central differencing, to obtain

$$\frac{\partial V_j(p,t)}{\partial t} - ipx_jV_j(p,t) = \frac{V_{j+1}(p,t) - 2V_j(p,t) + V_{j-1}(p,t)}{\Delta x^2} \tag{5.6}$$

so that the functions $V_j(p,t)$ satisfy this equation for each j and, as a result, and we have a family of ODEs parametrised by p.

The initial condition for this system is $V_j(p,0) = 0$ for $j \neq 0$ and $V_0(p,0) = \frac{1}{\Delta x}$, for all p.

5.3.2 Solving the numerical scheme

The system of equations above can be written as

$$\frac{\partial \underline{V}(p,t)}{\partial t} = M\underline{V}(p,t) \tag{5.7}$$

where $M = M_1 + ipM_2$, with

$$M_1 = \frac{1}{\Delta x^2}\begin{pmatrix} \dots & \dots & \dots & \dots & \dots & \dots & \dots \\ \dots & -2 & 1 & 0 & 0 & 0 & \dots \\ \dots & 1 & -2 & 1 & 0 & 0 & \dots \\ \dots & 0 & 1 & -2 & 1 & 0 & \dots \\ \dots & 0 & 0 & 1 & -2 & 1 & \dots \\ \dots & 0 & 0 & 0 & 1 & -2 & \dots \\ \dots & \dots & \dots & \dots & \dots & \dots & \dots \end{pmatrix}$$

and

$$M_2 = \Delta x\begin{pmatrix} \dots & \dots & \dots & \dots & \dots & \dots & \dots \\ \dots & -2 & 0 & 0 & 0 & 0 & \dots \\ \dots & 0 & -1 & 0 & 0 & 0 & \dots \\ \dots & 0 & 0 & 0 & 0 & 0 & \dots \\ \dots & 0 & 0 & 0 & 1 & 0 & \dots \\ \dots & 0 & 0 & 0 & 0 & 2 & \dots \\ \dots & \dots & \dots & \dots & \dots & \dots & \dots \end{pmatrix}.$$

As the matrix, M, is independent of t, (5.7) has the obvious solution

$$\underline{V}(p,t) = \underline{V}(p,0)e^{Mt}. \tag{5.8}$$

After solving the ODE problem, we can invert the y-FT, obtaining an approximation to the values $u(x_j, y, t)$.

5.3.3 Numerical output for the semi-discrete method

In this section we give the results of applying this solution method to the toy model.

We have used MATLAB to compute the solution of (5.7), as it provides an implementation of the matrix exponential function. MATLAB uses the 'the scaling and squaring method', see [18].

The solution for (5.7) can, in principle, be found for any value of p but, in practice we will only be able to calculate a discrete set of values for $V_j(p_k, T)$. To complete the solution in the original variables, we need to numerically invert the y-FT, using the grid values, $V_j(p_k, T)$. In order to perform the inversion efficiently, it is advisable to use the Fast Fourier Transform (FFT), which is also available as a function in MATLAB. By using this method, we appear to have avoided the discretisation in the y-direction but, in effect, this is replaced by a discretisation in the p-direction.

The numerical solution, U, at time T, is calculated at grid points (x_j, y_k) and is then numerically integrated over x to give the marginal probability distribution for y and its features are then plotted.

Figure 5.3 shows a 2-dimensional plot of the error between the two solutions.

Figure 5.4 plots the true and numerical marginal densities while Figure 5.5 shows the difference between the marginal densities of the true and numerical solutions.

We took $x \in [-20, 20]$ and $p \in [-20, 20]$ with 80 grid points in the p-direction and up to 2560 grid points in the x-direction.

Figure 5.3: Toy Model - Semi-discrete Fourier method using the matrix exponential - Difference between the solutions. x ∈[-20,20], p ∈[-20,20], np=80, nx=1800.

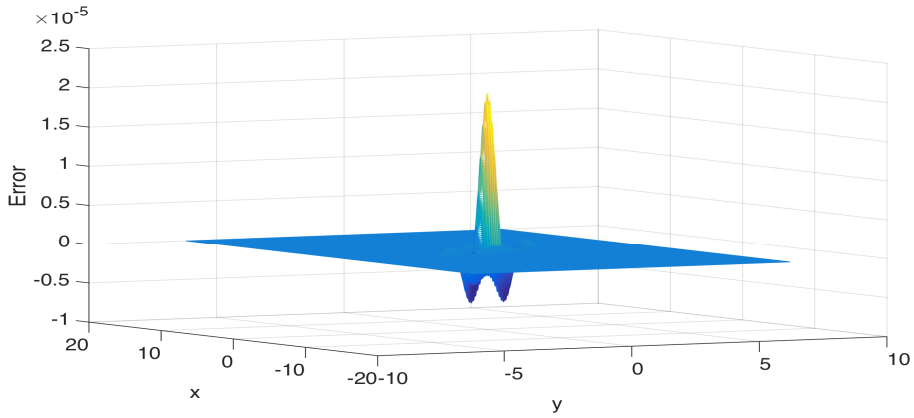

Figure 5.4: Toy Model - Semi-discrete Fourier method using the matrix exponential – Marginal Density – Comparison of solutions. x ∈[-20,20], p ∈[-20,20], np=80, nx=1800.

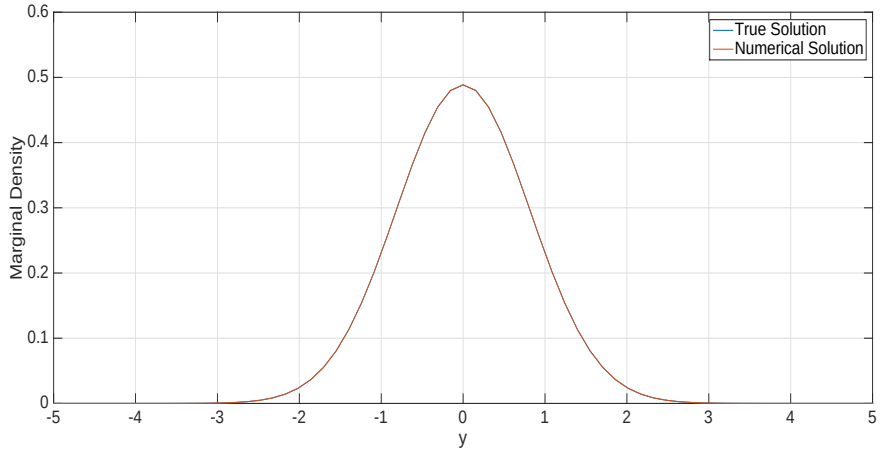

Figure 5.5: Toy Model - Semi-discrete Fourier method using the matrix exponential - Difference between solutions. x ∈[-20,20], p ∈[-20,20], np=80, nx=1800.

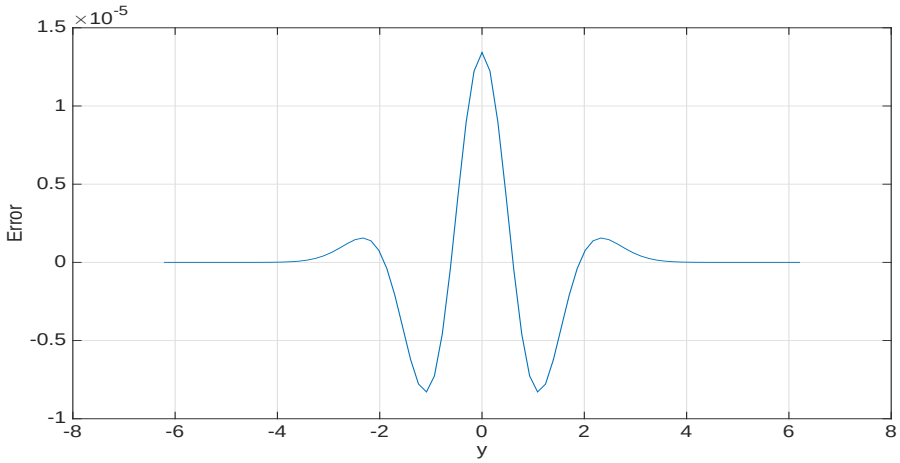

Finally, Figure 5.6 shows the convergence rate for the solution as $\Delta x \to 0$. We observe second order convergence in Δx, in the maximum norm.

Figure 5.6: Toy Model - Semi-discrete Fourier method using the matrix exponential - Convergence Plot. x ∈[-20,20], p ∈[-20,20], np=80.

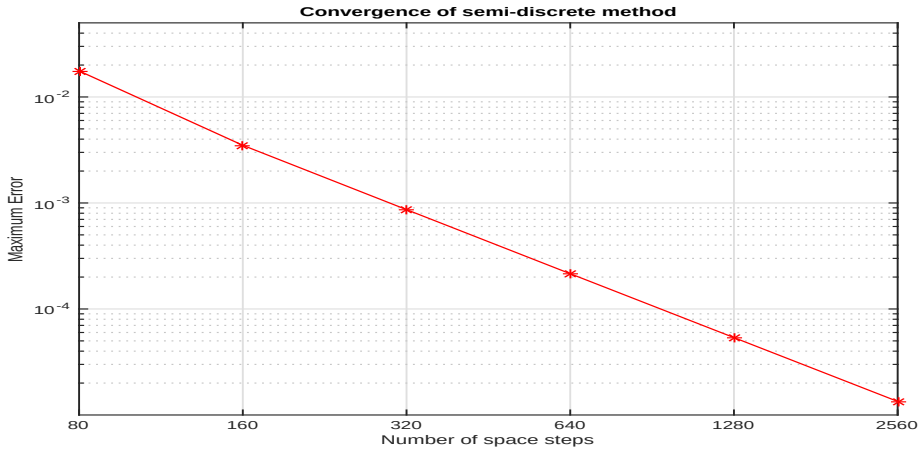

5.3.4 The time evolution of the numerical double transform for the semi-discrete Fourier scheme

At after applying the y-FT and discretising in the x-direction we have, as in (5.6),

$$\frac{\partial V_j(p,t)}{\partial t} - ipx_jV_j(p,t) = \frac{V_{j+1}(p,t) - 2V_j(p,t) + V_{j-1}(p,t)}{\Delta x^2}$$

for each value of p and for each j.

The initial condition is $V_j(p,0) = 0$ for $j \neq 0$ and $V_0(p,0) = \frac{1}{\Delta x}$, for all p.

We apply the discrete x-FT by writing

$$\begin{aligned}
&\Delta x\Big(\sum_{j=-\infty}^{j=\infty} \frac{\partial V_j(p,t)}{\partial t} e^{isx_j} - ip \sum_{j=-\infty}^{j=\infty} x_j V_j(p,t) e^{isx_j}\Big) \\
&= \Delta x \sum_{j=-\infty}^{j=\infty} \frac{V_{j+1}(p,t)e^{isx_j} - 2V_j(p,t)e^{isx_j} + V_{j-1}(p,t)e^{isx_j}}{\Delta x^2} \\
&= \Delta x \sum_{j=-\infty}^{j=\infty} \frac{e^{-is\Delta x}V_j(p,t)e^{isx_j} - 2V_j(p,t)e^{isx_j} + e^{is\Delta x}V_j(p,t)e^{isx_j}}{\Delta x^2} \\
&= W(s,p,t)\frac{e^{-is\Delta x} - 2 + e^{is\Delta x}}{\Delta x^2} \\
&= W(s,p,t)\frac{2(\cos(s\Delta x) - 1)}{\Delta x^2}
\end{aligned}$$

so that we have the following PDE for the numerical double transform, $W(s,p,t)$,

$$\frac{\partial W(s,p,t)}{\partial t} - p\frac{\partial W(s,p,t)}{\partial s} = -W(s,p,t)\frac{4\sin^2\left(\frac{s\Delta x}{2}\right)}{\Delta x^2} \tag{5.9}$$

or

$$\frac{\partial W(s,p,t)}{\partial t} - p\frac{\partial W(s,p,t)}{\partial s} = -W(s,p,t)(s^2 - g(s)) \tag{5.10}$$

where

$$g(s) = s^2 - \frac{4\sin^2\left(\frac{s\Delta x}{2}\right)}{\Delta x^2}. \tag{5.11}$$

We can now use the analysis above to investigate the relationship between the numerical and true double transforms, as follows.

From (5.4) we have that the true double transform satisfies the PDE

$$\frac{\partial w}{\partial t}(s,p,t) - p\frac{\partial w}{\partial s}(s,p,t) = -s^2 w(s,p,t). \tag{5.12}$$

The two PDEs above, (5.10) and (5.12), can be written as

$$\frac{\partial \log\left(W(s,p,t)\right)}{\partial t} - p\frac{\partial \log\left(W(s,p,t)\right)}{\partial s} = -(s^2 - g(s))$$

and

$$\frac{\partial \log\left(w(s,p,t)\right)}{\partial t} - p\frac{\partial \log\left(w(s,p,t)\right)}{\partial s} = -s^2.$$

So by defining

$$Z(s,p,t) = \log\left(\frac{W(s,p,t)}{w(s,p,t)}\right)$$

we have

$$\frac{\partial Z(s,p,t)}{\partial t} - p\frac{\partial Z(s,p,t)}{\partial s} = g(s),$$

which we can solve to obtain

$$Z(s,p,t) = \frac{1}{p}\int_s^{s+pt} g(\sigma)d\sigma.$$

by using the initial conditions for W and w, so that $Z(s,p,0) = \log\left(\frac{W(s,p,0)}{w(s,p,0)}\right) = 0$.

Hence we have

$$W(s,p,t) = w(s,p,t)\exp\left(\frac{1}{p}\int_s^{s+pt} g(\sigma)d\sigma\right) \tag{5.13}$$

an expression for the numerical double transform (reflecting the x-discretisation) in terms of the true double transform, w.

We can also write this as

$$\begin{aligned} W(s,p,t) &= w(s,p,t)\exp\left(\frac{1}{p}\int_s^{s+pt} g(\sigma)d\sigma\right) \\ &= w(s,p,t)\exp\left(\frac{1}{p}\int_s^{s+pt}\sigma^2 d\sigma\right)\exp\left(-\frac{1}{p}\int_s^{s+pt}\frac{4}{\Delta x^2}\sin^2\left(\frac{\sigma\Delta x}{2}\right)d\sigma\right) \\ &= w(s,p,t)w(s,p,t)^{-1}\exp\left(-\frac{2}{p\Delta x^2}\int_s^{s+pt}(1-\cos\left(\sigma\Delta x\right))d\sigma\right) \\ &= \exp\left(-\frac{2}{p\Delta x^2}[\sigma-\sin\left(\sigma\Delta x\right)]_s^{s+pt}\right) \\ &= \exp\left(-\frac{2t}{\Delta x^2}(1-\operatorname{sinc}\left(\xi\Delta x\right)\cos\left(\eta\Delta x\right))\right) \end{aligned} \tag{5.14}$$

where $\eta = s + \frac{pt}{2}$, $\xi = \frac{pt}{2}$, and sinc is the unnormalised sinc function, defined to be

$$\operatorname{sinc}(x) = \frac{\sin(x)}{x}$$

for $x \neq 0$ (see [30]).

We also have

$$w(\eta,\xi,t) = \exp\left(-\eta^2 t - \frac{1}{3}\xi^2 t\right)$$

in the new variables, η and ξ.

These expressions will be used below in the convergence analysis.

5.3.5 Convergence analysis for the semi-discrete Fourier method

We will analyse the behaviour of the difference (error) between the numerical and true solutions for the PDE, using the semi-discrete method. It should be noted that this analysis only relates to the exact solution of (5.7) and its subsequent exact y-FT inversion. In particular we want to see how rapidly the error reduces as $\Delta x \to 0$.

We approach this task by applying inverse Fourier transforms to the error between W and w, and then performing wavenumber analysis of the resulting integrals to establish convergence. This method is based on the same kind of ideas used in [5] and [36].

Applying the inverse transforms to the error term we obtain an equation for the error in (x, y)-space, i.e.

$$(2\pi)^2(U(x,t,y) - u(x,y,t)) = \int_{-\infty}^{\infty}\int_{-\frac{\pi}{\Delta x}}^{\frac{\pi}{\Delta x}}(W(s,p,t) - w(s,p,t))e^{-isx}e^{-ipy}dsdp$$

and by changing the variables we get

$$2\pi^2 t(U(x,t,y) - u(x,y,t)) = \int_{-\infty}^{\infty}\int_{-\frac{\pi}{\Delta x}+\xi}^{\frac{\pi}{\Delta x}+\xi}(W(\eta,\xi,t) - w(\eta,\xi,t))e^{-i(\eta-\xi)x}e^{-i\frac{2y}{\xi}}d\eta d\xi$$

We will replace the infinite integration limits by $\pm\Delta x^{-r}$ for some suitable $r > 0$, chosen so that the integral converges (see below), and we consider

$$I = \int_{-\Delta x^{-r}}^{\Delta x^{-r}}\int_{-\frac{\pi}{\Delta x}+\xi}^{\frac{\pi}{\Delta x}+\xi}(W(\eta,\xi,t) - w(\eta,\xi,t))e^{-i(\eta-\xi)x}e^{-i\frac{2y}{\xi}}d\eta d\xi$$

Breaking this into suitable wavenumber regimes, we write I as

$$I = \sum_{k=1}^{k=5}\int_{\Omega_k}(W(\eta,\xi,t) - w(\eta,\xi,t))e^{-i(\eta-\xi)x}e^{-i\frac{2y}{\xi}}d\eta d\xi$$

where

$$\begin{aligned}
\Omega_1 &= [-\Delta x^{p-1}, \Delta x^{p-1}]\mathsf{x}[-\Delta x^{q-1}, \Delta x^{q-1}]\\
\Omega_2 &= [-\Delta x^{p-1}, \Delta x^{p-1}]\mathsf{x}[-\frac{\pi}{\Delta x}+\xi, -\Delta x^{q-1}]\\
\Omega_3 &= [-\Delta x^{p-1}, \Delta x^{p-1}]\mathsf{x}[\Delta x^{q-1}, \frac{\pi}{\Delta x}+\xi]\\
\Omega_4 &= [\Delta x^{p-1}, \Delta x^{-r}]\mathsf{x}[-\frac{\pi}{\Delta x}+\xi, \frac{\pi}{\Delta x}+\xi]\\
\Omega_5 &= [-\Delta x^{-r}, -\Delta x^{p-1}]\mathsf{x}[-\frac{\pi}{\Delta x}+\xi, \frac{\pi}{\Delta x}+\xi].
\end{aligned}$$

The first integral, I_1, relates to the joint low wavenumber regime, and is given by

$$I_1 = \int_{-\Delta x^{p-1}}^{\Delta x^{p-1}}\int_{-\Delta x^{q-1}}^{\Delta x^{q-1}}((W(\eta,\xi,t) - w(\eta,\xi,t))e^{-i(\eta-\xi)x}e^{-i\frac{2y}{\xi}}d\eta d\xi$$

where we need to determine suitable exponents p and q to define the wavenumber regime.

We can also write

$$I = I_1 + \sum_{k=2}^{k=5} \int_{\Omega_k} W(\eta, \xi, t) e^{-i(\eta-\xi)x} e^{-i\frac{2y}{\xi}} d\eta d\xi$$
$$- \sum_{k=2}^{k=5} \int_{\Omega_k} w(\eta, \xi, t) e^{-i(\eta-\xi)x} e^{-i\frac{2y}{\xi}} d\eta d\xi$$

and apart from the joint low wavenumber regime, we will perform separate calculations on W and w. We will find that all but the first term can be made exponentially small, while the first term is $O(\Delta x^2)$.

We start with the joint low wavenumber analysis.

Joint low wavenumbers

We have to determine exponents p and q, for $0 < p, q < 1$, such that in Ω_1

$$|\eta \Delta x| < \Delta x^q \to 0$$

and

$$|\xi \Delta x| < \Delta x^p \to 0$$

and certain Taylor expansions can be usefully truncated.

We can write expansions

$$\cos(\eta \Delta x) = 1 - \frac{1}{2!}(\eta \Delta x)^2 + \frac{1}{4!}(\eta \Delta x)^4 + O((\eta \Delta x)^6)$$

then

$$\text{sinc}(\xi \Delta x) = 1 - \frac{1}{3!}(\xi \Delta x)^2 + \frac{1}{5!}(\xi \Delta x)^4 + O((\xi \Delta x)^6)$$

so then

$$-\frac{2t}{\Delta x^2}(1 - \text{sinc}(\xi \Delta x)\cos(\eta \Delta x))$$

$$= -\eta^2 t - \frac{1}{3}\xi^2 t + \frac{2t}{4!}\eta^4 \Delta x^2 + \frac{2t}{5!}\xi^4 \Delta x^2 + O(\eta^6 \Delta x^4) + O(\xi^6 \Delta x^4).$$

So then if we write I_1 as

$$\int_{\Omega_1} \exp\left(-\eta^2 t - \frac{1}{3}\xi^2 t\right)\left(\exp\left(\frac{2t}{4!}\eta^4\Delta x^2 + \frac{2t}{5!}\xi^4\Delta x^2 + o(\Delta x^2)\right) - 1\right) e^{-i(\eta-\xi)x} e^{-i\frac{2y}{\xi}} d\eta d\xi$$

$$= \int_{\Omega_1} \exp\left(-\eta^2 t - i(\eta-\xi)x - \frac{1}{3}\xi^2 t - i\frac{2y}{\xi}\right)\left(\exp\left(\frac{2t}{4!}\eta^4 + \frac{2t}{5!}\xi^4 + o(\Delta x^2)\right) - 1\right) d\eta d\xi$$

$$= \Delta x^2 \int_{\Omega_1} \exp\left(-\eta^2 t - i(\eta-\xi)x - \frac{1}{3}\xi^2 t - i\frac{2y}{\xi}\right)\left(\frac{2t}{4!}\eta^4\Delta x^2 + \frac{2t}{5!}\xi^4\Delta x^2\right) d\eta d\xi + o(\Delta x^2)$$

$$= \Delta x^2 F(x,y,t) + o(\Delta x^2)$$

where

$$F(x,y,t) = \int_{\Omega_1} \exp\left(-\eta^2 t - i(\eta-\xi)x - \frac{1}{3}\xi^2 t - i\frac{2y}{\xi}\right)\left(\frac{2t}{4!}\eta^4 + \frac{2t}{5!}\xi^4\right) d\eta d\xi$$

and

$$|F(x,y,t)| \leq \int_{-\infty}^{\infty}\int_{-\infty}^{\infty} \exp\left(-\eta^2 t - \frac{1}{3}\xi^2 t\right)\left(\frac{2t}{4!}\eta^4 + \frac{2t}{5!}\xi^4\right) d\eta d\xi$$

or

$$|F(x,y,t)| \leq \int_{-\infty}^{\infty} \frac{2t}{4!}\eta^4 \exp\left(-\eta^2 t\right) d\eta \int_{-\infty}^{\infty} \frac{2t}{5!}\xi^4 \exp\left(-\frac{1}{3}\xi^2 t\right) d\xi$$

so that $|F(x,y,t)|$ is bounded by a product of fourth moments of the Gaussian function.

We require

$$\Delta x^2(\eta^8 + \xi^8) \to 0$$

for the remainders to be valid. So we can take $p, q > \frac{3}{4}$ to define the joint low wavenumber regime because we have, for example,

$$\eta\Delta x < \Delta x^q$$

so that

$$\eta^4\Delta x^4 < \Delta x^{4q}$$

and

$$\eta^4 \Delta x < \Delta x^{4q-3} \to 0$$

for $q > \frac{3}{4}$.

Next we look at the remaining terms involving W. There are two cases to consider.

Low ξ-wavenumbers and high η-wavenumbers.

We consider the terms

$$I_2 = \int_{\Omega_2} W(\eta, \xi, t) e^{-i(\eta-\xi)x} e^{-i\frac{2y}{\xi}} d\eta d\xi + \int_{\Omega_3} W(\eta, \xi, t) e^{-i(\eta-\xi)x} e^{-i\frac{2y}{\xi}} d\eta d\xi$$

so that

$$|I_2| \leq \int_{\Omega_2} W(\eta, \xi, t) d\eta d\xi + \int_{\Omega_3} W(\eta, \xi, t) d\eta d\xi$$

For these wavenumbers we have $\eta \in [-\frac{\pi}{\Delta x} + \xi, \frac{\pi}{\Delta x} + \xi]$ and so $\eta \Delta x \in [-\pi + \xi \Delta x, \pi + \xi \Delta x]$ and for small ξ this interval only contains the single point $\eta = 0$ where $\cos(\eta \Delta x) = 1$.

We have

$$\sin^2\left(\frac{\theta}{2}\right) \geq \left(\frac{\theta}{\pi}\right)^2$$

for $\theta \in [-\pi, \pi]$, so then

$$\cos(\eta \Delta x) = 1 - 2\sin^2\left(\frac{\eta \Delta x}{2}\right) \leq 1 - 2\left(\frac{\eta \Delta x}{\pi}\right)^2 = 1 - \frac{2}{\pi^2}(\eta \Delta x)^2$$

with equality at $\eta = \frac{\pi}{\Delta x}$. So we can then chose $\alpha < \frac{2}{\pi^2}$ such that we will have

$$\cos(\eta \Delta x) < 1 - \alpha(\eta \Delta x)^2$$

for $\eta \Delta x$ on $[-\pi + \epsilon, \pi + \epsilon]$, and ϵ small enough, so this will hold for $\eta \in [-\frac{\pi}{\Delta x} + \xi, \frac{\pi}{\Delta x} + \xi]$ as $\xi \Delta x < \Delta x^{3/4} \to 0$ as $\Delta x \to 0$.

Also, for $\xi \Delta x$ small enough, and hence for low ξ-wavenumbers, we can ensure that

$$\frac{1}{2} < \operatorname{sinc}(\xi \Delta x) \leq 1.$$

So then

$$\operatorname{sinc}(\xi\Delta x)\cos(\eta\Delta x) \leq 1 - \alpha(\eta\Delta x)^2$$

and

$$\alpha(\eta\Delta x)^2 \leq 1 - \operatorname{sinc}(\xi\Delta x)\cos(\eta\Delta x),$$

so that

$$\begin{aligned}\exp\left(-\frac{2t}{\Delta x^2}(1-\operatorname{sinc}(\xi\Delta x)\cos(\eta\Delta x))\right) &\leq \exp\left(-\frac{2t}{\Delta x^2}\alpha(\eta\Delta x)^2\right)\\ &= \exp\left(-2\alpha t\eta^2\right)\\ &\leq \exp\left(-2\alpha t\Delta x^{-\frac{1}{2}}\right)\end{aligned}$$

as $\eta\Delta x > \Delta x^{3/4}$ we have $\eta > \Delta x^{-1/4}$ and $\eta^2 > \Delta x^{-1/2}$, so the contribution to the integral satisfies

$$\begin{aligned}|I_2| \leq& \int_\Omega W(\eta,\xi,t)d\eta d\xi\\ =& \int_\Omega \exp\left(-\frac{2t}{\Delta x^2}(1-\operatorname{sinc}(\xi\Delta x)\cos(\eta\Delta x))\right)d\eta d\xi\\ \leq& \int_\Omega \exp\left(-2\alpha t\Delta x^{-\frac{1}{2}}\right)d\eta d\xi\\ \leq& (2\Delta x^{p-1})(2\pi\Delta x^{-1})\exp\left(-2\alpha t\Delta x^{-\frac{1}{2}}\right)\\ \leq& 4\pi\Delta x^{p-2}\exp\left(-2\alpha t\Delta x^{-\frac{1}{2}}\right)\\ =& o(\Delta x^m)\end{aligned}$$

for all $m > 0$, where $\Omega = \Omega_2 \cup \Omega_3$.

So this contribution to the integral is exponentially small as $\Delta x \to 0$.

High ξ-wavenumbers.

Next we consider the terms

$$I_3 = \int_{\Omega_4} W(\eta,\xi,t)e^{-i(\eta-\xi)x}e^{-i\frac{2y}{\xi}}d\eta d\xi + \int_{\Omega_5} W(\eta,\xi,t)e^{-i(\eta-\xi)x}e^{-i\frac{2y}{\xi}}d\eta d\xi$$

so that

$$|I_3| \leq \int_{\Omega_4} W(\eta, \xi, t) d\eta d\xi + \int_{\Omega_5} W(\eta, \xi, t) d\eta d\xi$$

and

$$|I_3| \leq \int_{\Omega_4} \exp\left(\frac{-2t}{\Delta x^2}(1 - \operatorname{sinc}(\xi\Delta x)\cos(\eta\Delta x))\right) d\eta d\xi$$
$$+ \int_{\Omega_5} \exp\left(\frac{-2t}{\Delta x^2}(1 - \operatorname{sinc}(\xi\Delta x)\cos(\eta\Delta x))\right) d\eta d\xi$$

and we will show that each of these integrals is exponentially small, as $\Delta x \to 0$.

We observe that $\operatorname{sinc}(\xi\Delta x)$ is decreasing from $\xi = \Delta x^{-1/4}$ to some $\xi = \xi_0$, if we make Δx small enough. The first local minimum of the sinc function satisfies

$$\frac{d \operatorname{sinc}(\xi\Delta x)}{d\xi} = \frac{d\frac{\sin(\xi\Delta x)}{\xi\Delta x}}{d\xi}$$

$$= \frac{\xi\Delta x^2 \cos(\xi\Delta x) - \sin(\xi\Delta x)\Delta x}{(\xi\Delta x)^2} = \frac{\xi\Delta x \cos(\xi\Delta x) - \sin(\xi\Delta x)}{\xi^2\Delta x} = 0$$

and hence define ξ_0 as the smallest positive solution to $\tan(\xi_0\Delta x) = \xi_0\Delta x$ and then $|\operatorname{sinc}(\xi_0\Delta x)| = \alpha$ and where $\alpha < 0.3$, say, and for values of $\xi > \xi_0$, we have $|\operatorname{sinc}(\xi\Delta x)| < \alpha$.

This is illustrated in Figure 5.7, where we see that for values of $x = \xi\Delta x$ less than $\xi_0\Delta x$ we also have

$$\operatorname{sinc}(\xi\Delta x) < 1 - \frac{1}{100}(\xi\Delta x)^2.$$

Figure 5.7: Plot of the $\text{sinc}(x) = \frac{\sin(x)}{x}$ function

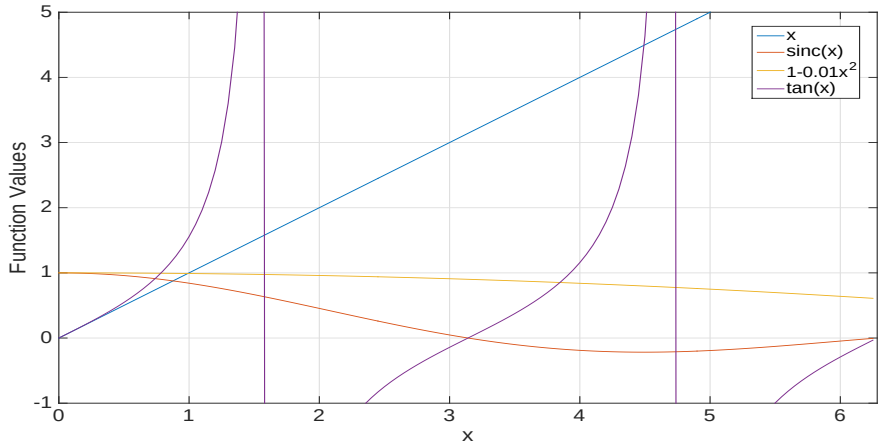

For $\xi_0 \Delta x < \xi \Delta x$ we have

$$|\operatorname{sinc}(\xi \Delta x)| \leq \alpha$$

and, for $\beta = 1 - \alpha$,

$$-(1-\beta) = -\alpha < \operatorname{sinc}(\xi \Delta x) \leq \alpha = 1 - \beta.$$

So for $\Delta x^{\frac{3}{4}} < \xi \Delta x < \xi_0 \Delta x$ we have

$$\operatorname{sinc}(\xi \Delta x) \leq 1 - \frac{1}{100} \min\left(\Delta x^{\frac{3}{2}}, 100\beta\right)$$

and

$$\operatorname{sinc}(\xi \Delta x) \geq -\left(1 - \frac{1}{100} \min\left(\Delta x^{\frac{3}{2}}, 100\beta\right)\right)$$

for small enough $\xi \Delta x$.

We have $-1 < \cos(\eta \Delta x) < 1$ so we now have two cases to consider.

The first case is where $0 < \cos(\eta \Delta x) < 1$ so that

$$\operatorname{sinc}(\xi \Delta x) \cos(\eta \Delta x) < 1 - \frac{1}{100} \min\left(\Delta x^{\frac{3}{2}}, 100\beta\right)$$

so that

$$\frac{1}{100} \min\left(\Delta x^{\frac{3}{2}}, 100\beta\right) < 1 - \operatorname{sinc}(\xi \Delta x) \cos(\eta \Delta x)$$

and

$$\frac{1}{100}\min\left(\Delta x^{\frac{3}{2}}, 100\beta\right) < 1 - \operatorname{sinc}\left(\xi\Delta x\right)\cos\left(\eta\Delta x\right)$$

or

$$\frac{-2t}{\Delta x^2}\frac{1}{100}\min\left(\Delta x^{\frac{3}{2}}, 100\beta\right) > \frac{-2t}{\Delta x^2}(1 - \operatorname{sinc}\left(\xi\Delta x\right)\cos\left(\eta\Delta x\right))$$

so that

$$\exp\left(\frac{-2t}{\Delta x^2}(1 - \operatorname{sinc}\left(\xi\Delta x\right)\cos\left(\eta\Delta x\right))\right) \leq \exp\left(-\frac{t}{50\Delta x^2}\min\left(\Delta x^{\frac{3}{2}}, 100\beta\right)\right)$$

$$\leq \exp\left(-\frac{t}{50\Delta x^{\frac{1}{2}}}\min\left(1, 100\beta\Delta x^{-\frac{3}{2}}\right)\right) \leq \exp\left(-\frac{t}{50\Delta x^{\frac{1}{2}}}\right)$$

for small enough Δx.

The last string of inequalities also holds for the case where $-1 < \cos\left(\eta\Delta x\right) < 0$ using

$$\operatorname{sinc}\left(\xi\Delta x\right) \geq -\left(1 - \frac{1}{100}\min\left(\Delta x^{\frac{3}{2}}, 100\beta\right)\right).$$

Then we have

$$|I_3| \leq \int_{\Omega'} \exp\left(\frac{-2t}{\Delta x^2}(1 - \operatorname{sinc}\left(\xi\Delta x\right)\cos\left(\eta\Delta x\right))\right) d\eta d\xi$$

$$\leq (2\Delta x^{-r})(2\pi\Delta x^{-1})\exp\left(-\frac{t\Delta x^{-\frac{1}{2}}}{50}\right) = o(\Delta x^m)$$

for all $m > 0$, where Ω' is the set of values of (η, ξ) such that $\xi \in [-\Delta x^{-r}, \Delta x^{-r}]$, $\eta \in [-\frac{\pi}{\Delta x} + \xi, \frac{\pi}{\Delta x} + \xi]$ and $|\xi\Delta x| > \Delta x^{\frac{3}{4}}$.

So this contribution to the integral is exponentially small as $\Delta x \to 0$.

We note that for the high ξ-wavenumber integration range to exist, we need

$$\Delta x^{-1/4} < \xi < \Delta x^{-r}$$

or

$$\Delta x^{r-\frac{1}{4}} < 1$$

with $\Delta x^{r-\frac{1}{4}} \to 0$ as $\Delta x \to 0$. So we require $r > \frac{1}{4}$.

If $r < \frac{1}{4}$, there is only a low ξ-wavenumber regime, but this is irrelevant for the computations, and the derivations show that quadratic convergence is guaranteed for any $r \in (0, 1)$.

Finally, we need to estimate the value of the error contribution for the remaining terms which involve w. We write

$$I_4 = -\sum_{k=2}^{k=5} \int_{\Omega_k} w(\eta, \xi, t) e^{-i(\eta-\xi)x} e^{-i\frac{2y}{\xi}} d\eta d\xi$$

so that

$$|I_4| \leq \sum_{k=2}^{k=5} \int_{\Omega_k} w(\eta, \xi, t) d\eta d\xi$$

so that

$$\begin{aligned} |I_4| \leq & \int_{-\infty}^{\infty} \int_{-\infty}^{-\Delta x^{q-1}} w(\eta, \xi, t) d\eta d\xi + \int_{-\infty}^{\infty} \int_{\Delta x^{q-1}}^{\infty} w(\eta, \xi, t) d\eta d\xi \\ & + \int_{\Delta x^{p-1}}^{\Delta x^{-r}} \int_{-\infty}^{\infty} w(\eta, \xi, t) d\eta d\xi + \int_{-\Delta x^{-r}}^{-\Delta x^{p-1}} \int_{-\infty}^{\infty} w(\eta, \xi, t) d\eta d\xi \end{aligned}$$

and hence

$$\begin{aligned} |I_4| \leq & \int_{-\infty}^{\infty} \int_{-\infty}^{-\Delta x^{q-1}} w(\eta, \xi, t) d\eta d\xi + \int_{-\infty}^{\infty} \int_{\Delta x^{q-1}}^{\infty} w(\eta, \xi, t) d\eta d\xi \\ & + \int_{\Delta x^{p-1}}^{\infty} \int_{-\infty}^{\infty} w(\eta, \xi, t) d\eta d\xi + \int_{-\infty}^{-\Delta x^{p-1}} \int_{-\infty}^{\infty} w(\eta, \xi, t) d\eta d\xi. \end{aligned}$$

As we have

$$\int_{-\infty}^{\infty} w(\eta, \xi, t) d\eta = \exp\left(-\frac{1}{3}\xi^2\right) \int_{-\infty}^{\infty} \exp(-\eta^2) d\eta = \sqrt{\pi} \exp\left(-\frac{1}{3}\xi^2\right)$$

and

$$\int_{-\infty}^{\infty} w(\eta, \xi, t) d\xi = \exp(-\eta^2) \int_{-\infty}^{\infty} \exp\left(-\frac{1}{3}\xi^2\right) d\xi = \sqrt{3\pi} \exp(-\eta^2)$$

so

$$\begin{aligned} |I_4| \leq & \sqrt{3\pi} \int_{-\infty}^{-\Delta x^{q-1}} \exp(-\eta^2) d\eta + \sqrt{3\pi} \int_{\Delta x^{q-1}}^{\infty} \exp(-\eta^2) d\eta \\ & + \sqrt{\pi} \int_{\Delta x^{p-1}}^{\infty} \exp\left(-\frac{1}{3}\xi^2\right) d\xi + \sqrt{\pi} \int_{-\infty}^{-\Delta x^{p-1}} \exp\left(-\frac{1}{3}\xi^2\right) d\xi. \end{aligned}$$

Lemma 3 in the Appendix of [13] proves that each of these integrals are $O(\Delta x^m)$, for any $m > 0$, and so $|I_4|$ is exponentially small as $\Delta x \to 0$.

Collecting the above results together we find that

$$|I| \leq |I_1| + |I_2| + |I_3| + |I_4|$$

and we find that for small enough Δx we have

$$|I| \leq O(\Delta x^2) + o(\Delta x^m)$$

for all $m > 0$ and so long as the integration range for high ξ-wavenumbers is restricted to $\xi \in [-\Delta x^{-r}, \Delta x^{-r}]$ and where $r > \frac{1}{4}$.

Consequently, and in practice, the numerical inversion in the solution method leads to quadratic convergence for the semi-discrete method.

5.3.6 The interaction between the $x-$ and p-discretisations

When we solve the KFE using the semi-discrete method, we need to consider the effect of the numerical inversion of the y-FT in the final step of the solution. As the inversion is only approximate, we have to decide how to set the parameters for the inversion, i.e. the range of p-wavenumbers to use and the p-step to choose. See Chapter 4, Section 4.4.

Figure 5.8: Toy Model - Semi-discrete Fourier method. Effect of np on the y-FT and the resulting convergence in Δx.

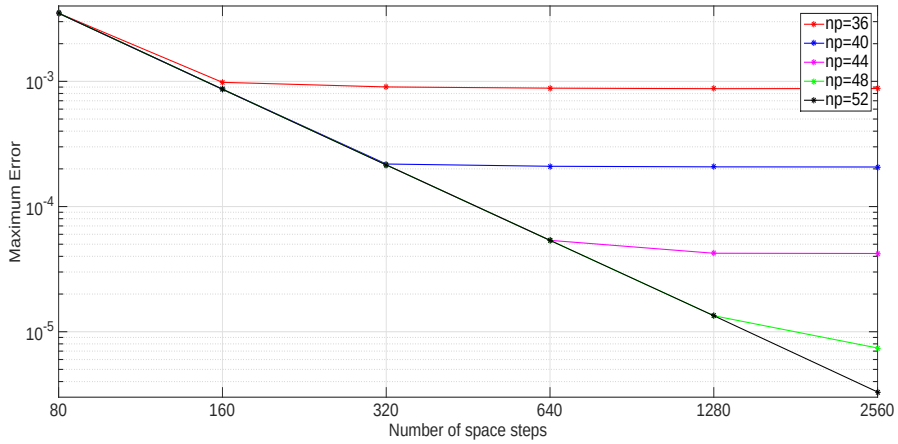

As Δx is reduced we will find that we need to also reduce Δp to maintain the quadratic convergence. This behaviour is demonstrated in Figure 5.8. Here we define the x-range as $[-10, 10]$ and the p-range as $[-20, 20]$ and then monitor the convergence as $\Delta x \to 0$ for a range of values of Δp, which correspond to $np = 36, 40, 44, 48, 52$.

We see that, for a given value of Δp, quadratic convergence only continues to hold, as $\Delta x \to 0$, up to a critical value of Δx, beyond which convergence stops. It follows that in order to use this method we need to reduce Δp appropriately in order to achieve a satisfactory degree of accuracy.

We can also see that as np increases towards the value where the error approaches the log-log line of quadratic convergence in x, the convergence in p is very fast. This behaviour is a feature of quadrature using the trapezoidal rule which converges exponentially for smooth, periodic integrands.

For a real function on a finite interval periodicity refers to the periodic extension, so what matters is whether the derivatives on the left and right boundaries match up to make the periodic extension analytic.

In our case the solution and its derivatives vanish so rapidly for large p, and the function truncated to, say, p between +/-20 is very close to the analytic/periodic case and for reasonable accuracy levels we observe exponential convergence of the p-quadrature. See [42] for further discussion of this behaviour.

5.4 The discrete Fourier method

5.4.1 The numerical scheme for the discrete Fourier method

Applying the y-FT to the toy model PDE (5.2), as before, we have

$$v_t - ipxv = v_{xx}. \tag{5.15}$$

We then discretise in the $x-$ and t-direction. We will always use implicit central differencing for the diffusion term but have considered two alternative treatments of the drift term.

5.4.1.1 Explicit drift case

Here we treat the drift term explicitly so that after discretisation, we have the scheme

$$\frac{V_j^{n+1}(p) - V_j^n(p)}{\Delta t} - ipj\Delta x V_j^n(p) = \frac{V_{j+1}^{n+1}(p) - 2V_j^{n+1}(p) + V_{j-1}^{n+1}(p)}{\Delta x^2}. \tag{5.16}$$

We define a shape factor, $\lambda = \frac{\Delta t}{\Delta x^2}$, and rearrange the scheme to get

$$-\lambda V_{j-1}^{n+1}(p) + (1+2\lambda)V_j^{n+1}(p) - \lambda V_{j+1}^{n+1}(p) = (1 + ipj\Delta t\Delta x)V_j^n(p). \tag{5.17}$$

We solve this system of linear equations, as a function of the parameter, p, noting that $V_j^n(p)$ is complex and we will only determine the values of $V_j^n(p)$ for selected values of p.

We note that the truncation error of the scheme is $O(\Delta x^2) + O(\Delta t)$, so it is computationally efficient to keep the shape factor, λ, fixed as the grid is refined. We do this in our numerical calculations using the scheme.

5.4.1.2 Implicit drift case

For the second case, we treat the drift term implicitly and write

$$\frac{V_j^{n+1}(p) - V_j^n(p)}{\Delta t} - ipj\Delta x V_j^{n+1}(p) = \frac{V_{j+1}^{n+1}(p) - 2V_j^{n+1}(p) + V_{j-1}^{n+1}(p)}{\Delta x^2} \tag{5.18}$$

and we obtain the numerical scheme

$$-\lambda V_{j-1}^{n+1}(p) + (1 + 2\lambda - ipj\Delta t\Delta x)V_j^{n+1}(p) - \lambda V_{j+1}^{n+1}(p) = V_j^n(p). \tag{5.19}$$

5.4.2 Numerical results from the Fourier method

We now solve the system of linear equations (either (5.17) or (5.19)) and apply the inverse y-FT as described in Chapter 4, Section 4.4.

We present the results found by applying the two methods above to the toy model PDE.

As with the semi-discrete Fourier method, the solution for U is first integrated over x, before being plotted against y.

We took $x \in [-20, 20]$ and $p \in [-20, 20]$ with 1800 grid points in the x-direction, 80 grid points in the p-direction and up to 1800 grid points in the x-direction and 10240

grid points in the t-direction.

We first present the results obtained by treating the drift explicitly.

5.4.2.1 Explicit drift case

Figure 5.9 shows the difference between the true and numerical solutions. The numerical solution itself closely resembles the result in Figure 5.4.

Figure 5.9: Toy Model - Discrete Fourier method : Difference between solutions - Explicit Drift. $x \in$[-20,20], $p \in$[-20,20], np=80, nx=1800, nt=10240.

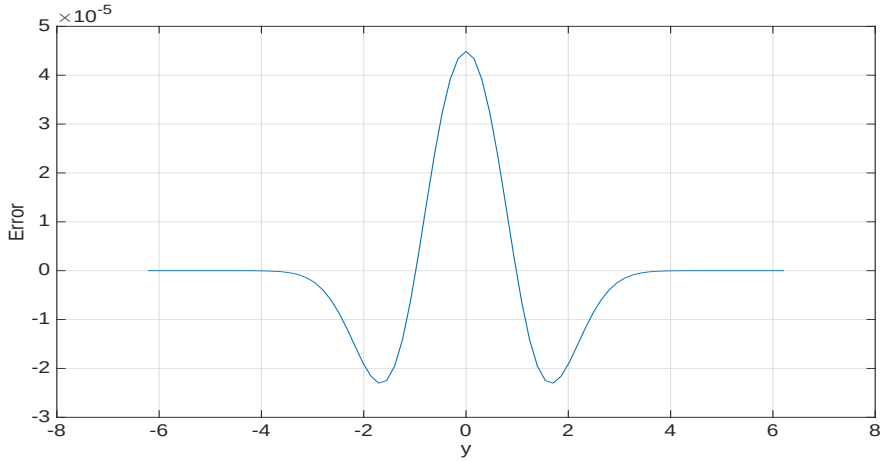

Finally, Figure 5.10 shows the convergence rate for the solution as the grid is refined with $\lambda = \frac{\Delta t}{\Delta x^2}$ held constant.

We observe first order convergence in time where the error is evaluated in the maximum norm. The slope of the last two points of the log-log plot is 1.00.

Figure 5.10: Toy Model - Discrete Fourier method : Convergence plot of the discrete Fourier scheme - Explicit Drift. $x \in$[-20,20], $p \in$[-20,20], np=80.

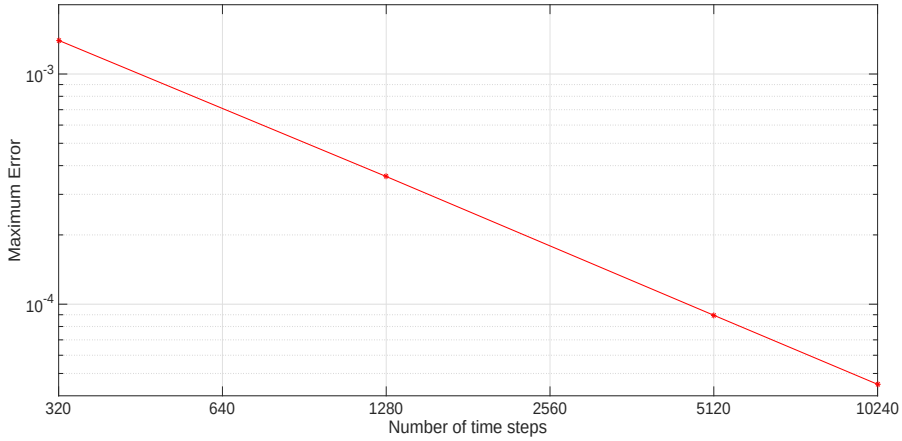

For this method, it is interesting to note that the maximum error in this case is approximately four times the corresponding error of the semi-discrete method (see Figures 5.5 and 5.9) and we observe upwards 'bumps' at around ± 2 in the latter case.

5.4.2.2 Implicit drift case

Next we present the results based on treating the drift implicitly.

Figure 5.11 shows the difference between the true and numerical solutions. Once again, the numerical solution itself closely resembles the result in Figure 5.4.

Figure 5.11: Toy Model - Discrete Fourier method : Difference between solutions - Implicit Drift. $x \in$[-20,20], $p \in$[-20,20], np=80, nx=1800, nt=10240.

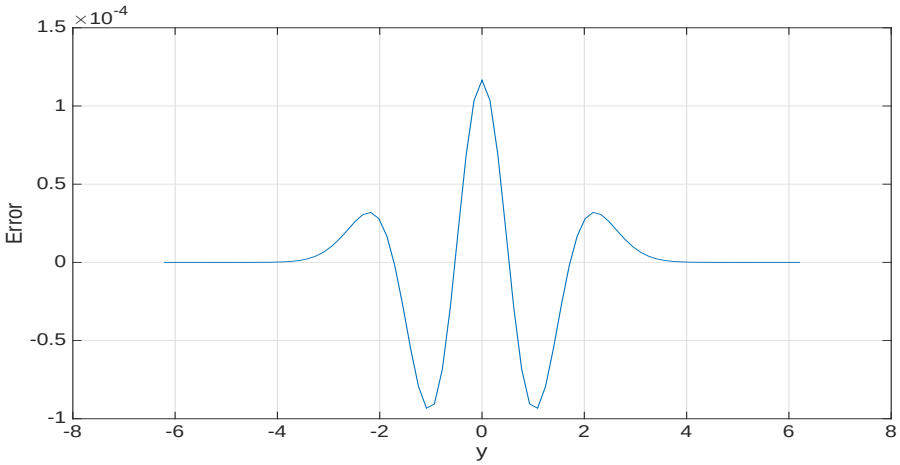

Finally, Figure 5.12 shows the convergence rate for the solution as the grid is refined. We observe first order convergence in time where the error is evaluated in the maximum norm. The slope of the last two points of the log-log plot is 1.00.

Figure 5.12: Toy Model - Discrete Fourier method : Convergence plot of the discrete Fourier scheme - Implicit Drift. $x \in$[-20,20], $p \in$[-20,20], np=80.

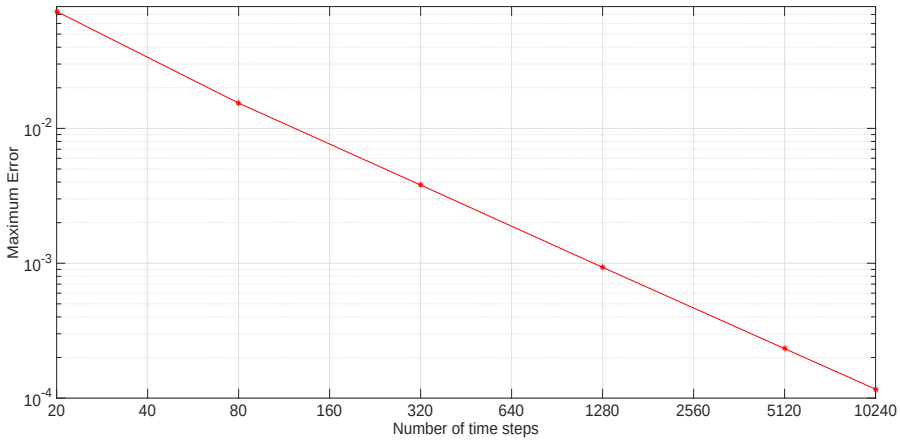

We observe that the maximum error in this case is approximately twice the corresponding error of the explicit drift case (see Figures 5.11 and 5.9).

5.4.3 The time evolution of the numerical double transform for the discrete Fourier schemes

We now define recursions for the numerical double-FT, showing the time evolution of the transform. The objective is to use these results to investigate convergence of these numerical schemes.

5.4.3.1 Explicit drift case

First we analyse the case where the drift is treated explicitly. From (5.17) above, we have

$$-\lambda V_{j-1}^{n+1}(p) + (1+2\lambda)V_j^{n+1}(p) - \lambda V_{j+1}^{n+1}(p) = V_j^n(p) + ip\Delta t x_j V_j^n(p)$$

and we apply the discrete x-FT to this system of equations.

We use the fact that

$$\Delta x \sum_{j=-\infty}^{j=\infty} ip\Delta t x_j V_j^n(p) e^{isx_j} = p\Delta t \frac{\partial W^n(s,p)}{\partial s}$$

and obtain the recursion

$$f(s)W^{n+1}(s,p) = W^n(s,p) + p\Delta t \frac{\partial W^n(s,p)}{\partial s} \tag{5.20}$$

where

$$f(s) = (1+2\lambda) - 2\lambda\cos(s\Delta x) = 1 + 4\lambda\sin^2\left(\frac{s\Delta x}{2}\right).$$

This is a 'differential recursion', i.e. one where recursion involves a differential operator, $\mathcal{L}$, defined by

$$\mathcal{L}F(s,p) = \frac{1}{f(s)}\left(F(s,p) + p\Delta t \frac{\partial F(s,p)}{\partial s}\right).$$

so that

$$W^{n+1}(s,p) = \mathcal{L}W^n(s,p)$$

and to 'solve' to the recursion, i.e. find the form of W at time $T = n\Delta t$, we need to understand the iterated form of the operator, $\mathcal{L}$.

We can also write the recursion in another form by first introducing an integrating factor

$$I(s,p) = \exp\left(\frac{s}{p\Delta t}\right)$$

so that we have

$$f(s)(I(s,p)W^{n+1}(s,p)) = p\Delta t\frac{\partial(I(s,p)W^{n}(s,p))}{\partial s}.$$

Defining

$$Z^n(s,p) = I(s,p)W^{(n)}(s,p)$$

we have

$$f(s)Z^{n+1}(s,p) = p\Delta t\frac{\partial Z^{n}(s,p)}{\partial s}.$$

If we set

$$\psi = s\Delta x,\ \frac{1}{\eta} = p\Delta x\Delta t\ \text{, and } r(s) = \frac{1}{f(s)} = \frac{1}{(1+2\lambda) - 2\lambda\cos(\psi)}$$

then we have

$$Z^{n+1}(\psi,\eta) = r(\psi)\frac{1}{\eta}\frac{\partial Z^{n}(\psi,\eta)}{\partial \psi}.$$

We also note that

$$Z^0(s,p) = I(s,p)W^{(0)}(s,p) = \exp\left(\frac{s}{p\Delta t}\right) = \exp(\psi\eta).$$

So we write the recursion in the form

$$\eta^n Z^n(\psi,\eta) = r(\psi)\frac{\partial}{\partial\psi}\left(\ldots r(\psi)\frac{\partial}{\partial\psi}\left(r(\psi)\frac{\partial Z^0(\psi,\eta)}{\partial\psi}\right)\ldots\right).$$

5.4.3.2 Implicit drift case

We next analyse the case where the drift is treated implicitly. The calculation steps are very similar to the explicit drift case and we obtain the recursion

$$f(s)W^{n+1}(s,p) + p\Delta t\frac{\partial W^{n+1}(s,p)}{\partial s} = W^n(s,p). \tag{5.21}$$

The recursion again involves a differential operator but, this time, it acts on the upper time level.

In this case we would have to 'solve' the recursion by solving a sequence of first-order linear ODEs, to find the form of $W^n(s,p)$ at time $T = n\Delta t$. At each time step, we would need to find a 'constant of integration', to determine $W^n(s,p)$.

5.4.4 Convergence analysis for the discrete Fourier method.

Ideally, we would have 'closed-form' solutions for the recursions above (in (5.20) and (5.21)) which might allow to us to analyse the behaviour of the solution in particular wavenumber regimes (as found with the semi-discrete Fourier method).

Then we would hope to be able to use Fourier inversion to transfer this analysis to the original domain and study the convergence of the scheme in the original variables.

For the discrete Fourier method, however, we have not been able to completely solve the recursions or complete the convergence analysis, but will describe what can be said about the two cases above.

5.4.4.1 Explicit drift

Then, as above in (5.20), the recursion is given by

$$W^{n+1}(s,p) = r(s)\left(W^n(s,p) + p\Delta t\frac{\partial W^n(s,p)}{\partial s}\right)$$

where

$$r(s) = \frac{1}{f(s)}.$$

The recursion starts with $W^0(s,p) = 1$, because of the δ-function initial condition.

So we get

$$W^1(s,p) = r(s)\left(W^0(s,p) + p\Delta t\frac{\partial W^0(s,p)}{\partial s}\right) = r(s)$$

and

$$W^2(s,p) = r(s)\left(W^1(s,p) + p\Delta t\frac{\partial W^1(s,p)}{\partial s}\right) = r(s)^2 + (p\Delta t)r(s)\frac{\partial r(s)}{\partial s}.$$

Then we have

$$\begin{aligned}
W^3(s,p) &= r(s)\left(W^2(s,p) + p\Delta t\frac{\partial W^2(s,p)}{\partial s}\right)\\
&= r(s)(r(s)^2 + (p\Delta t)r(s)\frac{\partial r(s)}{\partial s} + (p\Delta t)\frac{\partial (r(s)^2 + (p\Delta t)r(s)\frac{\partial r(s)}{\partial s})}{\partial s}\\
&= r(s)^3 + (p\Delta t)\left(r(s)^2\frac{\partial r(s)}{\partial s} + r(s)\frac{\partial (r(s)^2)}{\partial s}\right) + (p\Delta t)^2 r(s)\frac{\partial (r(s)\frac{\partial r(s)}{\partial s})}{\partial s}\\
&= r(s)^3 + (p\Delta t)\left(r(s)^2\frac{\partial r(s)}{\partial s} + 2r(s)^2\frac{\partial (r(s))}{\partial s}\right) + (p\Delta t)^2 r(s)\frac{\partial (r(s)\frac{\partial r(s)}{\partial s})}{\partial s}\\
&= r(s)^3 + 3(p\Delta t)r(s)^2\frac{\partial r(s)}{\partial s} + (p\Delta t)^2 r(s)\left(\left(\frac{\partial r(s)}{\partial s}\right)^2 + r(s)\frac{\partial^2 r(s)}{\partial s^2}\right).
\end{aligned}$$

Clearly, there are some patterns developing here but it difficult to see how to deal with the case for general n.

The calculations involve the derivatives of $r(s) = \frac{1}{(1+2\lambda)-2\lambda\cos(s\Delta x)}$ and, for low wavenumbers, we would need to expand these derivatives in s.

To analyse the error between W^n and the true solution,

$$w^n = \exp\left(-s^2T - spT^2 - \frac{1}{3}p^2T^3\right),$$

where $T = n\Delta t$, we would like to find a relationship between these two functions (as was achieved with the semi-discrete method). To some extent, the above expansion can help with this, giving the leading terms of this relationship although not much more progress can then be made with the formulation above.

Instead of using the iterated derivative method above, we can use another approach to developing an expansion for W^n, which tries to apply logarithms to the problem, as suggested by the analysis of constant-coefficient problems in [5] as in [36].

Here we will only focus on the low wavenumber analysis.

5.4.4.2 Low wavenumbers

We define Y^n by $W^n = \exp(Y^n)$, to obtain, from (5.20)

$$f(s)\exp(Y^{n+1}) = \exp(Y^n) + p\Delta t\frac{\partial \exp(Y^n)}{\partial s} = \left(1 + p\Delta t\frac{\partial Y^n}{\partial s}\right)\exp(Y^n).$$

Taking logs we get

$$Y^{n+1} = Y^n - \log f(s) + \log\left(1 + p\Delta t\frac{\partial Y^n}{\partial s}\right)$$

or the expansion

$$Y^{n+1} = Y^n - \log f(s) + p\Delta t\frac{\partial Y^n}{\partial s} - \frac{1}{2}(p\Delta t)^2\left(\frac{\partial Y^n}{\partial s}\right)^2 \dots \tag{5.22}$$

which we hope will apply for, as yet undefined, low p-wavenumbers. We also define $g(s) = \log f(s)$.

For $n = 0$, we have $W^0 = 1$, so $Y^0 = 0$ and we can calculate, in succession,

$$Y^1 = g(s),$$

$$Y^2 = -2g - p\Delta t\frac{\partial g}{\partial s} - \frac{1}{2}(p\Delta t)^2\left(\frac{\partial g}{\partial s}\right)^2 - \frac{1}{3}(p\Delta t)^3\left(\frac{\partial g}{\partial s}\right)^3 \dots$$

and

$$Y^3 = -3g - 3p\Delta t\frac{\partial g}{\partial s} - (p\Delta t)^2\left(-\frac{5}{2}\left(\frac{\partial g}{\partial s}\right)^2 - \frac{\partial^2 g}{\partial s^2}\right) - (p\Delta t)^3\left(-3\left(\frac{\partial g}{\partial s}\right)^3 - 2\frac{\partial g}{\partial s}\frac{\partial^2 g}{\partial s^2}\right)\dots$$

From this we can develop an ansatz of the form

$$\begin{aligned} Y^n = &- ng - p\Delta t A^n\frac{\partial g}{\partial s} \\ &- (p\Delta t)^2\left(B^n\left(\frac{\partial g}{\partial s}\right)^2 + C^n\frac{\partial^2 g}{\partial s^2}\right) \\ &- (p\Delta t)^3\left(D^n\left(\frac{\partial g}{\partial s}\right)^3 + E^n\left(\frac{\partial g}{\partial s}\right)\left(\frac{\partial^2 g}{\partial s^2}\right) + F^n\frac{\partial^3 g}{\partial s^3}\right) \\ &- (p\Delta t)^4\left(G^n\left(\frac{\partial g}{\partial s}\right)^4 + H^n\left(\frac{\partial g}{\partial s}\right)^2\left(\frac{\partial^2 g}{\partial s^2}\right) + I^n\left(\frac{\partial g}{\partial s}\right)\left(\frac{\partial^3 g}{\partial s^3}\right) + J^n\frac{\partial^4 g}{\partial s^4}\right)\dots \end{aligned} \tag{5.23}$$

where the term in $(p\Delta t)^m$ is a linear combination of products of derivatives of g, where the sequences A^n, B^n, have to be determined.

For each m, the allowed products of derivatives of g are 'homogeneous', in the sense that in each term exactly m derivatives have been applied.

If we substitute this expression in (5.22) and equate powers of $p\Delta t$, we will obtain recursions for the sequences above.

We substitute the formula for Y^{n+1} and Y^n into the recursion to get

$$\begin{aligned}
Y^{n+1} &= -(n+1)g - p\Delta t A^{n+1}\frac{\partial g}{\partial s} - (p\Delta t)^2\left(B^{n+1}\left(\frac{\partial g}{\partial s}\right)^2 + C^{n+1}\frac{\partial^2 g}{\partial s^2}\right)\dots \\
&= -ng - p\Delta t A^n\frac{\partial g}{\partial s} - (p\Delta t)^2\left(B^n\left(\frac{\partial g}{\partial s}\right)^2 + C^n\frac{\partial^2 g}{\partial s^2}\right)\dots - g \\
&+ (p\Delta t)\left(\frac{\partial}{\partial s}\left(-ng - p\Delta t A^n\frac{\partial g}{\partial s} - (p\Delta t)^2\left(B^n\left(\frac{\partial g}{\partial s}\right)^2 + C^n\frac{\partial^2 g}{\partial s^2}\right)\dots\right)\right) \\
&- \frac{1}{2}(p\Delta t)^2\left(\frac{\partial}{\partial s}\left(-ng - p\Delta t A^n\frac{\partial g}{\partial s} - (p\Delta t)^2\left(B^n\left(\frac{\partial g}{\partial s}\right)^2 + C^n\frac{\partial^2 g}{\partial s^2}\right)\dots\right)\right)^2\dots
\end{aligned}$$

so that

$$\begin{aligned}
Y^{n+1} &= -(n+1)g - p\Delta t A^{n+1}\frac{\partial g}{\partial s} - (p\Delta t)^2\left(B^{n+1}\left(\frac{\partial g}{\partial s}\right)^2 + C^{n+1}\frac{\partial^2 g}{\partial s^2}\right)\dots \\
&= -(n+1)g - p\Delta t A^n\frac{\partial g}{\partial s} - (p\Delta t)^2\left(B^n\left(\frac{\partial g}{\partial s}\right)^2 + C^n\frac{\partial^2 g}{\partial s^2}\right)\dots \\
&+ (p\Delta t)(\frac{\partial}{\partial s}\left(-ng - p\Delta t A^n\frac{\partial g}{\partial s} - (p\Delta t)^2\left(B^n\left(\frac{\partial g}{\partial s}\right)^2 + C^n\frac{\partial^2 g}{\partial s^2}\right)\dots\right)\right) \\
&- \frac{1}{2}(p\Delta t)^2\left(\frac{\partial}{\partial s}\left(-ng - p\Delta t A^n\frac{\partial g}{\partial s} - (p\Delta t)^2\left(B^n\left(\frac{\partial g}{\partial s}\right)^2 + C^n\frac{\partial^2 g}{\partial s^2}\right)\dots\right)\right)^2\dots
\end{aligned}$$

We then equate coefficients to find

$$A^{n+1} = A^n + n,\ B^{n+1} = B^n + \frac{1}{2}n^2\ \text{, and } C^{n+1} = C^n + A^n.$$

From the starting values $A^0 = 0$, $B^0 = 0$ and $C^0 = 0$ we find

$$A^n = \frac{1}{2}(n-1)n,\ B^n = \frac{1}{12}(n-1)n(2n-1), \text{ and } C^n = \frac{1}{6}(n-2)(n-1)n.$$

So the leading terms of Y^n are

$$Y^n = -ng - p\Delta t\frac{1}{2}(n-1)n\frac{\partial g}{\partial s}$$

$$-(p\Delta t)^2\left(\frac{1}{12}(n-1)n(2n-1)\left(\frac{\partial g}{\partial s}\right)^2 + \frac{1}{6}(n-2)(n-1)n\frac{\partial^2 g}{\partial s^2}\right)\ldots$$

Clearly, further terms could be derived but the calculations become quite involved and a general formula is hard to find.

To complete the calculation we need to develop an expansion of $g(s)$, i.e.

$$g(s) = \log f(s) = \log\left((1+2\lambda) - 2\lambda\cos(s\Delta x)\right) = \log\left(1 + 2\lambda(1-\cos(s\Delta x))\right)$$

which can be expanded to give

$$g(s) = s^2\Delta t - \left(\frac{1}{2} + \frac{1}{12\lambda}\right)s^4\Delta t^2 + O(\Delta t^3)$$

Then we have, symbolically, i.e. assuming the derivatives of the $O(\Delta t^3)$ terms are also $O(\Delta t^3)$,

$$\frac{\partial g}{\partial s} = 2s\Delta t - \left(2 + \frac{1}{3\lambda}\right)s^3\Delta t^2 + O(\Delta t^3)$$

and

$$\frac{\partial^2 g}{\partial s^2} = 2\Delta t - \left(6 + \frac{1}{\lambda}\right)s^2\Delta t^2 + O(\Delta t^3)$$

Using these expressions above we get

$$\begin{aligned}
Y^n =& -ng - p\Delta t\frac{1}{2}(n-1)n\frac{\partial g}{\partial s} \\
&- (p\Delta t)^2\left(\frac{1}{12}(n-1)n(2n-1)\left(\frac{\partial g}{\partial s}\right)^2 + \frac{1}{6}(n-2)(n-1)n\frac{\partial^2 g}{\partial s^2}\right)\ldots \\
=& -n\left(s^2\Delta t - \left(\frac{1}{2} + \frac{1}{12\lambda}\right)s^4\Delta t^2 + O(\Delta t^3)\right) \\
&- p\Delta t\frac{1}{2}(n-1)n\left(2s\Delta t - \left(2 + \frac{1}{3\lambda}\right)s^3\Delta t^2 + O(\Delta t^3)\right) \\
&- (p\Delta t)^2\frac{1}{12}(n-1)n(2n-1)\left(2s\Delta t - \left(2 + \frac{1}{3\lambda}\right)s^3\Delta t^2 + O(\Delta t^3)\right)^2\ldots \\
&+ \frac{1}{6}(n-2)(n-1)n\left(2\Delta t - \left(6 + \frac{1}{\lambda}\right)s^2\Delta t^2 + O(\Delta t^3)\right) + \ldots
\end{aligned}$$

or, using $T = n\Delta t$,

$$\begin{aligned}
Y^n = &- \left(s^2 T - \left(\frac{1}{2} + \frac{1}{12\lambda} \right) s^4 T \Delta t + O(\Delta t^2) \right) \\
&- p\Delta t \frac{1}{2}(n-1) \left(2sT - \left(2 + \frac{1}{3\lambda} \right) s^3 T \Delta t + O(\Delta t^2) \right) \\
&- (p\Delta t)^2 \frac{1}{12}(n-1)n\Delta t^2(2n-1) \left(2s - \left(2 + \frac{1}{3\lambda} \right) s^3 \Delta t + O(\Delta t^2) \right)^2 \dots \\
&+ \frac{1}{6}(n-2)(n-1) \left(2T - \left(6 + \frac{1}{\lambda} \right) s^2 T \Delta t + O(\Delta t^2) \right) + \dots
\end{aligned}$$

so that

$$\begin{aligned}
Y^n = &- s^2 T + \left(\frac{1}{2} + \frac{1}{12\lambda} \right) s^4 T \Delta t + O(\Delta t^2) \\
&- pT \left(sT - \left(1 + \frac{1}{6\lambda} \right) s^3 T \Delta t + O(\Delta t^2) \right) \\
&+ p\Delta t \left(sT - \left(1 + \frac{1}{6\lambda} \right) s^3 T \Delta t + O(\Delta t^2) \right) \\
&- (p\Delta t)^2 \frac{1}{12}(n-1)n\Delta t^2(2n-1) \left(4s^4 - 4s \left(2 + \frac{1}{3\lambda} \right) s^3 \Delta t + O(\Delta t^2) \right) \dots \\
&+ \frac{1}{3}(n-2)(n-1) \left(T - \left(3 + \frac{1}{2\lambda} \right) s^2 T \Delta t + O(\Delta t^2) \right) + \dots
\end{aligned}$$

and then

$$\begin{aligned}
Y^n = &\left(- s^2 T - spT^2 - \frac{1}{3} p^2 T^3 \right) + \left(\frac{1}{2} + \frac{1}{12\lambda} \right) s^4 T \Delta t \\
&- \left(1 + \frac{1}{6\lambda} \right) ps^3 T^2 \Delta t + O(\Delta t^2) + psT\Delta t + O(\Delta t^2) \\
&- p^2 T^3 \Delta t \frac{1}{12} \left(1 - \frac{\Delta t}{T} \right) \left(2 - \frac{\Delta t}{T} \right) \left(4s^4 - 4s \left(2 + \frac{1}{3\lambda} \right) s^3 \Delta t + O(\Delta t^2) \right) \dots \\
&+ (pT)^2 \frac{1}{3} \left(1 - \left(1 - \frac{2\Delta t}{T} \right) \left(1 - \frac{\Delta t}{T} \right) \right) T \dots \\
&- (pT)^2 \frac{1}{3} \left(1 - \frac{2\Delta t}{T} \right) \left(1 - \frac{\Delta t}{T} \right) \left(- \left(3 + \frac{1}{2\lambda} \right) s^2 T \Delta t + O(\Delta t^2) \right) + \dots
\end{aligned}$$

and finally

$$Y^n = \left(- s^2 T - spT^2 - \frac{1}{3} p^2 T^3 \right) + F(s, p, T, \lambda)\Delta t + O(\Delta t^2) \tag{5.24}$$

where

$$\begin{aligned}
&F(s, p, T, \lambda) \\
&\quad = \left(\frac{1}{2} + \frac{1}{12\lambda} \right) s^4 T - \left(1 + \frac{1}{6\lambda} \right) ps^3 T^2 + psT - \frac{2}{3} p^2 s^4 T^3 - p^2 T + p^2 s^2 T^3 \left(1 + \frac{1}{6\lambda} \right)
\end{aligned} \tag{5.25}$$

so long as this expansion converges, i.e. for sufficiently low wavenumbers.

We recall that

$$\log(w^n) = -s^2T - spT^3 - \frac{1}{3}p^2T^3$$

so

$$\log(W^n) - \log(w^n) = F(s,p,T,\lambda)\Delta t + O(\Delta t^2)\ldots$$

and hence

$$W^n = w^n(1 + F(s,p,T,\lambda)\Delta t + O(\Delta t^2)) \tag{5.26}$$

The error between the solutions, in Fourier space, is then given by

$$E^n = W^n - w^n = w^n(F(s,p,T,\lambda)\Delta t + O(\Delta t^2)). \tag{5.27}$$

The relationship in (5.26) between the true and numerical solutions, in Fourier space, can then be used to analyse the difference between the schemes in the original variables. This is done by inverting the two Fourier transforms and using the fact that the product $w^nF(s,p,T,\lambda)$ is easy to invert (cf. the techniques in [5]).

However, this analysis remains incomplete because we still need to

- show that there are no other terms of $O(1)$ in F; this requires further analysis of the expansion in equation 5.23 above,
- identify and bound the remainder in the 'low' wavenumber expansion, i.e., the term of the form $w^nO(\Delta t^2)$, and
- properly define 'low' $s-$ and p-wavenumber regimes.

5.4.4.3 High wavenumbers

At present, we do not know how to analyse the high wavenumber regime. We note that, for the heat equation, and for the semi-discrete method above, the high wavenumber analysis does not involve an expansion in high wavenumbers but, rather, seeks to determine a bound on the solution (see [5] and Section 5.3.5 above).

5.4.4.4 Error analysis for the explicit drift case

In order to finish the analysis of the error in the original variables (as in, say, [5]) we would need to

- complete the expansion of the numerical double-FT in low (s,p)-wavenumbers;
- determine the behaviour of the double numerical transform for high (s,p)-wavenumbers.

5.4.4.5 Implicit drift

Next, we analyse the recursion (5.21) where the drift is treated implicitly

$$f(s)W^{n+1}(s,p) - p\Delta t\frac{\partial}{\partial s}W^{n+1}(s,p) = W^n(s,p)$$

and we write the integrating factor

$$I(s,p) = \exp\left(-\frac{\rho(s)}{p\Delta t}\right)$$

where

$$f(s) = 1 + 4\lambda\sin^2\left(\frac{s\Delta x}{2}\right) = (1+2\lambda) - 2\lambda\cos\left(s\Delta x\right)$$

and

$$\rho(s) = (1+2\lambda)s - \frac{2\lambda}{\Delta x}\sin\left(s\Delta x\right).$$

We have

$$\frac{\partial}{\partial s}(I(s,p)W^{n+1}(s,p)) = -\frac{f(s)}{p\Delta t}I(s,p)W^{n+1}(s,p) + I(s,p)\frac{\partial}{\partial s}W^{n+1}(s,p)$$

so that

$$\begin{aligned} p\Delta t\frac{\partial}{\partial s}(I(s,p)W^{n+1}(s,p)) &= -f(s)I(s,p)W^{n+1}(s,p) + p\Delta t I(s,p)\frac{\partial}{\partial s}W^{n+1}(s,p) \\ &= -I(s,p)(f(s)W^{n+1}(s,p) - p\Delta t\frac{\partial}{\partial s}W^{n+1}(s,p)) \\ &= -I(s,p)W^n(s,p) \end{aligned}$$

and so

$$\frac{\partial}{\partial s}(I(s,p)W^{n+1}(s,p)) = -\frac{1}{p\Delta t}I(s,p)W^n(s,p).$$

We now solve the single-step ODE to get

$$[I(s,p)W^{n+1}(\sigma,p)]_{s_0}^{s} = -\int_{s_0}^{s} \frac{1}{p\Delta t} I(\sigma,p)W^{n}(\sigma,p)d\sigma.$$

for an arbitrary s_0 where we need to determine the constant of integration. We do this by using the boundary conditions, which we obtain from the periodicity of the double transform.

We can write

$$[I(s,p)W^{n+1}(\sigma,p)]_{-\frac{\pi}{\Delta x}}^{s} = -\int_{-\frac{\pi}{\Delta x}}^{s} \frac{1}{p\Delta t} I(\sigma,p)W^{n}(\sigma,p)d\sigma$$

to get

$$I(s,p)W^{n+1}(s,p) - I(-\frac{\pi}{\Delta x},p)W^{n+1}(-\frac{\pi}{\Delta x},p) = -\int_{-\frac{\pi}{\Delta x}}^{s} \frac{1}{p\Delta t} I(\sigma,p)W^{n}(\sigma,p)d\sigma$$

and

$$\begin{aligned} &I(-\frac{\pi}{\Delta x},p)^{-1}I(s,p)W^{n+1}(s,p) - W^{n+1}(-\frac{\pi}{\Delta x},p) \\ &= -I(-\frac{\pi}{\Delta x},p)^{-1}\int_{-\frac{\pi}{\Delta x}}^{s} \frac{1}{p\Delta t} I(\sigma,p)W^{n}(\sigma,p)d\sigma. \end{aligned}$$

Similarly we get

$$\begin{aligned} &I(\frac{\pi}{\Delta x},p)^{-1}I(s,p)W^{n+1}(s,p) - W^{n+1}(\frac{\pi}{\Delta x},p) \\ &= -I(\frac{\pi}{\Delta x},p)^{-1}\int_{\frac{\pi}{\Delta x}}^{s} \frac{1}{p\Delta t} I(\sigma,p)W^{n}(\sigma,p)d\sigma. \end{aligned}$$

By periodicity we have

$$W^{n+1}(\frac{\pi}{\Delta x},p) = W^{n+1}(-\frac{\pi}{\Delta x},p)$$

and using this equality obtain

$$\begin{aligned} &I(\frac{\pi}{\Delta x},p)^{-1}I(s,p)W^{n+1}(s,p) - I(-\frac{\pi}{\Delta x},p)^{-1}I(s,p)W^{n+1}(s,p) \\ &= -I(\frac{\pi}{\Delta x},p)^{-1}\int_{\frac{\pi}{\Delta x}}^{s} \frac{1}{p\Delta t} I(\sigma,p)W^{n}(\sigma,p)d\sigma + I(-\frac{\pi}{\Delta x},p)^{-1}\int_{-\frac{\pi}{\Delta x}}^{s} \frac{1}{p\Delta t} I(\sigma,p)W^{n}(\sigma,p)d\sigma \end{aligned}$$

so that

$$W^{n+1}(s,p)$$
$$= \frac{-I(\frac{\pi}{\Delta x},p)^{-1}\int_{\frac{\pi}{\Delta x}}^{s} I(\sigma,p)W^n(\sigma,p)d\sigma + I(-\frac{\pi}{\Delta x},p)^{-1}\int_{-\frac{\pi}{\Delta x}}^{s} I(\sigma,p)W^n(\sigma,p)d\sigma}{p\Delta t(I(\frac{\pi}{\Delta x},p)^{-1}I(s,p) - I(-\frac{\pi}{\Delta x},p)^{-1}I(s,p))}$$

so we have a formula for $W^{n+1}(s,p)$ in terms of $W^n(s,p)$.

In principle, we can obtain $W^{n+2}(s,p)$ from $W^n(s,p)$ by substituting the formula for $W^{n+1}(s,p)$ into the formula for $W^{n+2}(s,p)$. This, however, would result in an expression consisting of four double integrals. Clearly, extending this approach to give a formula $W^n(s,p)$ in terms of $W^0(s,p)$ would result in a formula for $W^n(s,p)$ made up of many multiple integrals and would become extremely cumbersome.

By rearranging the order of integration in these multiple integrals, it is possible to replace the formula for $W^n(s,p)$ by one just using two single integrals plus additional terms determined by a recursive algorithm. The analysis is cumbersome so only the final result will be given here. It can be obtained by checking that the solution satisfies the recursion, using mathematical induction.

We find that the solution for $W^{(n)}(s,p)$, takes the form

$$I\left(\frac{\gamma}{\eta},\eta\right)W^{(n)}(s,p) = \alpha\int_0^{\gamma+\eta\pi}\frac{1}{(n-1)!}(\omega-\gamma-\eta\pi)^{n-1}G(\omega)d\omega$$
$$+\alpha(-1)^{n-1}\int_0^{-\gamma+\eta\pi}\frac{1}{(n-1)!}(\omega+\gamma-\eta\pi)^{n-1}G(-\omega)d\omega$$
$$+\sum_{m=0}^{n-1}\frac{1}{m!}\gamma^m A_n^m(\eta)$$

where

$$\gamma = \frac{s}{p\Delta t},$$

$$\eta = \frac{1}{p\Delta t\Delta x},$$

$$\alpha = \frac{1}{2\sinh\left(\eta(1+2\lambda)\pi\right)},$$

$$\rho(s) = (1+2\lambda)s - \frac{2\lambda}{\Delta x}\sin(s\Delta x),$$

$$I\left(\frac{\gamma}{\eta},\eta\right) = \exp\left(-\frac{\rho(s)}{p\Delta t}\right),$$

and

$$G(\omega) = \exp\left(-((1+2\lambda)\omega + 2\lambda\eta\sin(\frac{\omega}{\eta}))\right).$$

Here the functions $A_n^m(\eta)$ of η can be calculated recursively using the relationships

$$-A_{n+1}^1(\eta) = A_n^0(\eta)$$
$$-A_{n+1}^2(\eta) = A_n^1(\eta)$$
$$\ldots$$

and

$$A_n^0 = \alpha(-I(-\pi,\eta)\alpha\eta^n\int_0^{2\pi}\frac{1}{(n-1)!}(\xi-2\pi)^{n-1}G(\eta\xi)d\xi$$
$$+I(\pi,\eta)\alpha(-1)^{n-1}\eta^n\int_0^{2\pi}\frac{1}{(n-1)!}(\xi-2\pi)^{n-1}G(-\eta\xi)d\xi$$
$$-(I(-\pi,\eta)+I(\pi,\eta))\eta\pi A_n^1 - (I(-\pi,\eta)-I(\pi,\eta))\frac{1}{2}(\eta\pi)^2A_n^2\ldots))$$

so we can find A_{n+1}^0, as the functions A_{n+1}^k for $k > 0$ are known from the previous value of n. We also find that $A_1^0 = 0$.

Although this formula for $W^{(n)}(s,p)$ avoids the multiple integrals mentioned above, it is still very difficult to get much further with the wavenumber analysis needed to demonstrate convergence of the numerical scheme.

It does seem likely that the wavenumber regimes will be more easily described in terms of the variables γ and ζ given above. This analysis has similarities with the analysis of the semi-discrete method where the wavenumbers are best described in terms of the variables $s + \frac{pt}{2}$ and $\frac{pt}{2}$.

5.4.4.6 Error analysis for the implicit drift case

Although we now have a 'solution' for the recursion, it is an open question how to carry out wavenumber analysis of this result.

5.5 The semi-Lagrangian method

5.5.1 The numerical scheme for the semi-Lagrangian method

When we apply this method to the toy model, we obtain a system of PDEs in x and t which we discretise in the x and t directions. The drift coefficient is just x.

The initial condition for the scheme is given by

$$U(0,0,0) = \frac{1}{\Delta x \Delta y}$$

and

$$U(j,k,0) = 0 \text{ for } (j,k) \neq (0,0).$$

This ensures that the initial probability density has the correct mass.

At the current time step we calculate an array of 'shifts' as

$$y'_k = y_k - x_j \Delta t$$

and we note that the shifts are independent of k. In general, k' will not be an integer.

We interpolate the solution values from the previous time step, using the y-grid values y'_k. The interpolation makes use of the grid spacing in the y-direction. We use linear interpolation but other methods are possible.

Finally, we use the interpolated values of the solution $U(j,k,t,m-1)$ at the previous time step, as the right-hand side for the discretisation scheme based on the x grid and then solve the resulting linear system to find the values for $U(j,k,m)$.

We discretise the problem using an equally spaced grid of points, $(j\Delta x, k\Delta y)$ and interpolate between grid points at the start of the time step and then define

$$RHS^{n+1}_{j,k} = U^{n+1}_{j,k} - \Delta t \frac{U^{n+1}_{j+1,k} - 2U^{n+1}_{j,k} + U^{n+1}_{j-1,k}}{\Delta x^2} = (1-\alpha)U^n_{j,\lfloor k - x_j \frac{\Delta t}{\Delta y} \rfloor} + \alpha U^n_{j,\lfloor k - x_j \frac{\Delta t}{\Delta y} \rfloor + 1}$$

for $x_j > 0$ and where $\alpha = (k - x_j \frac{\Delta t}{\Delta y}) - \left\lfloor k - x_j \frac{\Delta t}{\Delta y} \right\rfloor$, using the floor function. If we make $\alpha = x_j \frac{\Delta t}{\Delta y}$ small enough and we have

$$RHS^n_{j,k} = (1 - \alpha) U^n_{j,k-1} + \alpha U^n_{j,k}.$$

We can derive a similar expression for $x_j < 0$, except that the 'upwinding' reverses direction.

Then the numerical scheme can then be written as

$$-\lambda U^{n+1}_{j+1,k} + (1 + 2\lambda) U^{n+1}_{j,k} - \lambda U^{n+1}_{j-1,k} = (1 - x_j \nu) U^n_{j,k} + x_j \nu U^n_{j,k+l_j}$$

reflecting the interpolation, so that

$$-\lambda U^{n+1}_{j+1,k} + (1 + 2\lambda) U^{n+1}_{j,k} - \lambda U^{n+1}_{j-1,k} = U^n_{j,k} - x_j \nu U^n_{j,k} + x_j \nu U^n_{j,k-l_j}$$

for $j > 0$ and

$$-\lambda U^{n+1}_{j+1,k} + (1 + 2\lambda) U^{n+1}_{j,k} - \lambda U^{n+1}_{j-1,k} = U^n_{j,k} + x_j \nu U^n_{j,k} - x_j \nu U^n_{j,k+l_j}$$

for $j < 0$ where l_j determines how far the interpolation moves from $U^n_{j,k}$, and where $\lambda = \frac{\Delta t}{\Delta x^2}$ and $\nu = \frac{\Delta t}{\Delta y}$.

5.5.2 Numerical output for the semi-Lagrangian method

We have solved the toy model problem using the semi-Lagrangian method and show a plot of the numerical solution at $T = 1.0$.

We have also studied the rate of convergence (in the maximum norm) of the scheme when the grid is refined with $\lambda = \frac{\Delta t}{\Delta x^2}$ and $\nu = \frac{\Delta t}{\Delta y}$ are held constant.

Figure 5.13 shows a convergence rate of slightly less than 'first order'; the time and space variables (y) are tied together, as ν is held constant . The slope between the last two points of the log-log plot is 0.98.

Figure 5.13: Semi-Lagrangian method: Convergence Plot

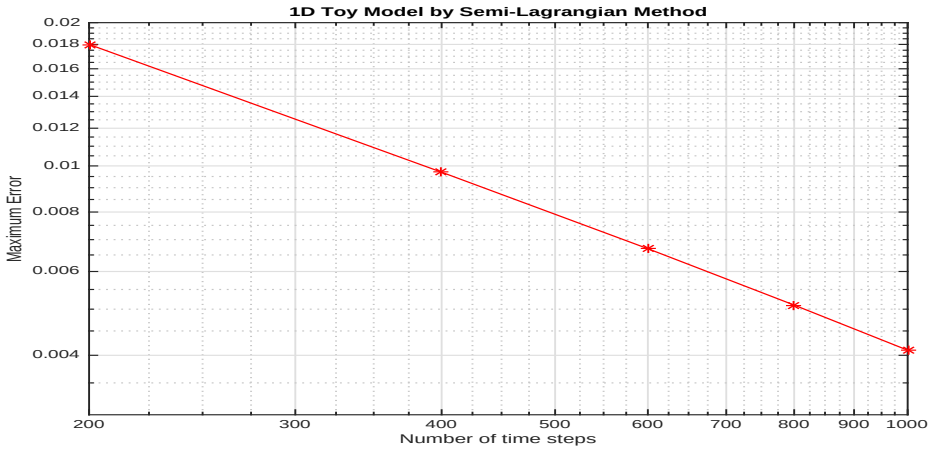

5.5.3 The time evolution of the numerical double transform for the semi-Lagrangian scheme

We would like to derive a recursion for the semi-Lagrangian method but the complexities of the interpolation make this difficult. This is because, for large values of the drift, the extrapolation might skip a number of grid cells. For the toy model, the drift increases with x. We will, in any case, need to truncate the grid and, for a sufficiently small time step (relative to Δy), we could arrange that the interpolation is limited to the immediate grid cell.

To investigate the analysis of the numerical scheme, we will assume linear interpolation and only consider the situation where the interpolation shift is limited to the immediate grid cell.

We then assume $|\frac{x_j \Delta t}{\Delta y}|$ small enough so that

$$-\lambda U^{n+1}_{j+1,k} + (1+2\lambda)U^{n+1}_{j,k} - \lambda U^{n+1}_{j-1,k} = U^n_{j,k} - x_j \nu (U^n_{j,k} - U^n_{j,k-1})$$

for $j > 0$ and

$$-\lambda U^{n+1}_{j+1,k} + (1+2\lambda)U^{n+1}_{j,k} - \lambda U^{n+1}_{j-1,k} = U^n_{j,k} + x_j \nu (U^n_{j,k} - U^n_{j,k+1})$$

for $j < 0$.

In this case we see that the scheme coincides with the variable-direction upwinding basic finite difference scheme with explicit drift.

In Appendix A we present some analysis of the latter case, leading to a recursion for the double-FT.

5.6 Conclusions from the analysis of the solution methods

Our objective in studying the toy model was to investigate the stability and accuracy of the numerical schemes we employed for our KFE problems. As these problems incorporated δ-function initial conditions, we hoped to use the Fourier transform techniques as seen in [5] and [36], in the absence of other ways of demonstrating stability.

This plan has only been partially successful.

For the semi-discrete method, and subject to using the inverse Fourier transform to complete the solution, we have been able to use the techniques from [5] to demonstrate convergence of the method.

For the Fourier method we have been able to derive some results about the behaviour of the recursion but we lack a full wavenumber analysis and, what is more, do not have a clear demarcation between the possible wavenumber regimes.

For the semi-Lagrangian method, when the grid step sizes are chosen appropriately, the scheme can be viewed as a variable-direction upwinding version of the basic finite difference scheme. As explained in Appendix A it very difficult to find stability results for that scheme using Fourier techniques. The alternative of using energy techniques, or appealing to a maximum principle does not appear to give any insight for the Dirac data case.

5.7 Further toy models – multi-dimensional problems – the use of the Fourier method

It is straightforward to extend the toy model by introducing diffusive terms and/or adding multiple drift terms.

5.7.1 Multiple diffusive terms

We consider the case where the (single) drift coefficient is a linear combination of the components of $\underline{x}$. Hence we investigate the PDE

$$u_t + (\gamma_1 x_1 + \gamma_2 x_2) u_y = a_{11} u_{x_1 x_1} + 2a_{12} u_{x_1 x_2} + a_{22} u_{x_2 x_2}$$

which extends the toy model to one containing two independent variables, x_1 and x_2.

The semi-discrete model for this example is given in Appendix B.1 along with a numerical example.

For the semi-discrete case, we expect that the stability analysis will follow along the same lines as in the one-dimensional case.

5.7.2 Multiple drift terms

Another extension of the models would be a model of the form

$$u_t + x u_{y_1} + x u_{y_2} = u_{xx}$$

where we have two drift terms and neither of the drift coefficients depend on x.

An example of this situation is also given in Appendix B.2.

Chapter 6

Examples of numerical solution of the extended KFE

In this chapter we present some examples of the numerical solution of the extended KFE and compare the output from our finite difference methods with output from the corresponding Monte Carlo simulations.

6.1 A simple Black-Scholes case

In this first example we work in a simple Black-Scholes set-up where the true volatility is a constant, σ, but we delta-hedge using a different constant volatility $\widehat{\sigma}$. See (3.4.1).

The KFE is given by (see (3.17))

$$\frac{\partial P}{\partial t} - \frac{1}{2}\sigma^2 S^2 \frac{\partial^2 P}{\partial S^2} - (2\sigma^2 - \mu) S \frac{\partial P}{\partial S} - (\sigma^2 - \mu) P + c(S,t) \frac{\partial P}{\partial y} = 0, \tag{6.1}$$

with

$$c(S,t) = \frac{1}{2} \mathrm{e}^{-rt} (\widehat{\sigma}^2 - \sigma^2) S^2 \frac{\partial^2 \widehat{V}}{\partial S^2} \tag{6.2}$$

where the gamma is calculated using the erroneous volatility.

The KFE has been solved using the following parameters, $\sigma = 0.1$, $\widehat{\sigma} = 0.2$, $\mu = 0.05$, and $r = 0.05$.

Referring to the general form of the KFE (see 4.1) we have

$$A_{1,1} = \frac{1}{2}\sigma^2 S^2$$
$$B_1 = (2\sigma^2 - \mu)$$
$$C = \sigma^2 - \mu.$$

We have $T = 1.0$, $S_0 = 125$, and the option being hedged is a spread with payoff defined as

$$F_V(T) = (S_T - 100)^+ - (S_T - 150)^+,$$

and we note the convexity of this option payoff changes sign as S varies.

To find the univariate density of the discounted terminal hedging error, the joint density was integrated over the S direction.

Two univariate distributions have been calculated by finite differences, one using the semi-Lagrangian method, and a second by the Fourier method. A Monte Carlo hedging simulation was also performed where the asset price was simulated according to the true asset model (which used the true volatility) while the hedged portfolio was controlled by delta-hedging using the Black-Scholes equation with the erroneous volatility.

Figure 6.1 shows how the three distributions compare. The fit is good. The two finite difference solutions compare very well except near the left-hand tail. The shape of the hedging error distribution can be rationalised by noting that the positive drift, μ, implies that the stock price is more likely to move into a regime where the option gamma is negative, resulting in a preponderance of negative hedging errors. Note that in these calculations, we assume that the option is sold for a price consistent with $\widehat{\sigma}$ so that Y starts from zero. If some other price were initially realised, it would result in the densities being shifted by this amount.

For the semi-Lagrangian method, we used $S \in [5, 300]$, $y \in [-30, 30]$ with $nS = 2000$, $ny = 8000$ and $nt = 200$.

For the discrete Fourier method (developed later), we used $S \in [5, 245]$, $y \in [-20, 20]$ and $p \in [-20, 20]$ with $nS = 400$, $ny = 150$, $np = ny$ and $nt = 100$.

Figure 6.1: Black-Scholes model with mis-specified volatility. Comparison of the KFE and Monte Carlo results.

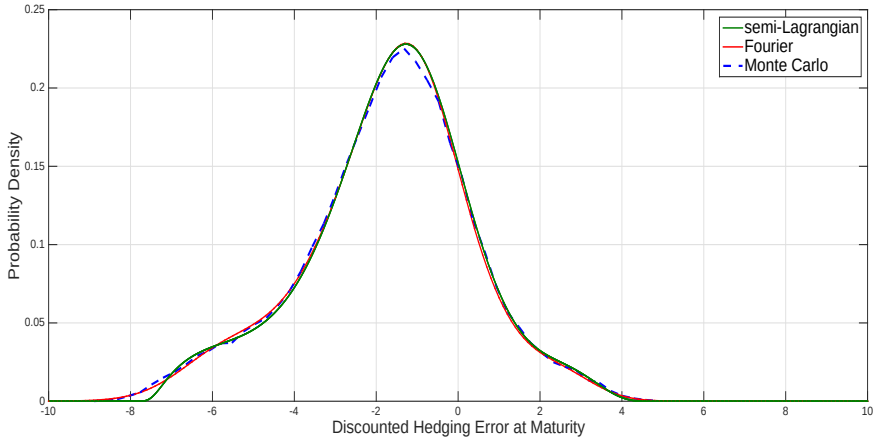

6.2 Two correlated assets

In our next example, we have a vector of two assets, where $(X_t^{(1)}, X_t^{(2)}) = (S_t^{(1)}, S_t^{(2)}) = \underline{S_t}$, and we assume that the asset process is driven by a two-dimensional correlated Brownian Motion with a true correlation coefficient ρ. See (3.4.2).

The KFE in this case is given by

$$\begin{aligned}\frac{\partial P}{\partial t} - \frac{1}{2}\sigma_1^2 S^{(1)2}\frac{\partial^2 P}{\partial S^{(1)2}} - \rho\sigma_1\sigma_2 S^{(1)}S^{(2)}\frac{\partial^2 P}{\partial S^{(1)}\partial S^{(2)}} - \frac{1}{2}\sigma_2^2 S^{(2)2}\frac{\partial^2 P}{\partial S^{(2)2}} \\ - S^{(1)}(2\sigma_1^2 + \rho\sigma_1\sigma_2 - \mu_1)\frac{\partial P}{\partial S^{(1)}} - S^{(2)}(2\sigma_2^2 + \rho\sigma_1\sigma_2 - \mu_2)\frac{\partial P}{\partial S^{(2)}} \\ - (\sigma_1^2 + \rho\sigma_1\sigma_2 + \sigma_1^2 - \mu_1 - \mu_2)P + c(S^{(1)}, S^{(2)}, t)\frac{\partial P}{\partial y} = 0. \qquad (6.3)\end{aligned}$$

with

$$c(S^{(1)}, S^{(2)}, t) = \mathrm{e}^{-rt}(\widehat{\rho} - \rho)\sigma_1\sigma_2 S_t^{(1)} S_t^{(2)}\frac{\partial^2 \widehat{V}}{\partial S^{(1)}\partial S^{(2)}}.$$

We apply this to hedging a quotient call option V, i.e. one that has payoff at maturity T given by

$$F_V(S_T^{(1)}, S_T^{(2)}) = (S_T^{(1)}/S_T^{(2)} - X)^+.$$

A pricing formula for this option is given in Haug [17] who in turn refers to [47] as the original source of the formula. The call price is given by

$$C_t = \mathrm{e}^{-r(T-t)}[F_t N(d_1) - XN(d_2)]$$

where the 'adjusted forward' F_t is given (in the case where neither stock pays dividends) by

$$F_t = \frac{S_t^{(1)}}{S_t^{(2)}} \exp[(\sigma_2^2 - \rho\sigma_1\sigma_2)(T-t)],$$

where

$$\begin{aligned} d_1 &= \frac{\ln(F_t/X) + \frac{1}{2}(T-t)\widehat{\sigma}^2}{\widehat{\sigma}\sqrt{T-t}} \\ d_2 &= d_1 - \widehat{\sigma}\sqrt{T-t}, \end{aligned}$$

and

$$\widehat{\sigma}^2 = \sigma_1^2 + \sigma_2^2 - 2\rho\sigma_1\sigma_2.$$

Then the delta-hedge ratios for the two assets are given by

$$\frac{\partial C}{\partial S^{(1)}} = \mathrm{e}^{-r(T-t)} N(d_1) \frac{\partial F}{\partial S^{(1)}}$$

and

$$\frac{\partial C}{\partial S^{(2)}} = \mathrm{e}^{-r(T-t)} N(d_1) \frac{\partial F}{\partial S^{(2)}},$$

so that

$$\frac{\partial^2 C}{\partial S^{(1)} \partial S^{(2)}} = \mathrm{e}^{-r(T-t)} \left(N(d_1) \frac{\partial^2 F}{\partial S^{(1)} \partial S^{(2)}} + n(d_1) \frac{\partial F}{\partial S^{(2)}} \frac{\partial d_1}{\partial S^{(1)}} \right),$$

which after some further manipulation leads to

$$\frac{\partial^2 C}{\partial S^{(1)} \partial S^{(2)}} = -\exp\left(-r(T-t) + (\sigma_2^2 - \rho\sigma_1\sigma_2)(T-t)\right) \frac{\left(N(d_1) + \frac{n(d_1)}{\hat{\sigma}\sqrt{T-t}}\right)}{S^{(2)2}},$$

so we see that

$$\frac{\partial^2 C}{\partial S^{(1)} \partial S^{(2)}} \leq 0.$$

In these formulae, $N(x)$ is the standard cumulative Normal distribution and $n(x)$ is

the density of the standard Gaussian distribution.

We apply this to the case where $\widehat{V}$ is a quotient call hedged with incorrect correlation $\widehat{\rho}$. If $\widehat{\rho} < \rho$, we will always have $dY_t \geq 0$, so no negative hedging errors will occur.

We use the parameters $S_0^{(1)} = 130$, $S_0^{(2)} = 100$, $\sigma_1 = 0.1$, $\sigma_2 = 0.4$, $\rho = 0.5$, $\mu_1 = \mu_2 = 0.05$, $r = 0.03$, $T = 0.25$ and $X = 1.3$, while the hedging is done using the mis-specified $\widehat{\rho} = -0.5$. As $\widehat{\rho} < \rho$, we expect to find that the hedging errors at maturity are positive.

Referring to the general form of the KFE (see 4.1) we have

$$\begin{aligned}
A_{1,1}(S^{(1)}, S^{(2)}) &= \frac{1}{2}\sigma_1^2 S^{(1)2} \\
A_{1,2}(S^{(1)}, S^{(2)}) &= \rho\sigma_1\sigma_2 S^{(1)} S^{(2)} \\
A_{2,2}(S^{(1)}, S^{(2)}) &= \frac{1}{2}\sigma_2^2 S^{(2)2} \\
B_1(S^{(1)}, S^{(2)}) &= S^{(1)}(2\sigma_1^2 + \rho\sigma_1\sigma_2 - \mu_1) \\
B_2(S^{(1)}, S^{(2)}) &= S^{(2)}(2\sigma_2^2 + \rho\sigma_1\sigma_2 - \mu_2) \\
C(S^{(1)}, S^{(2)}) &= (\sigma_1^2 + \rho\sigma_1\sigma_2 + \sigma_1^2 - \mu_1 - \mu_2).
\end{aligned}$$

We found the KFE solution by the semi-Lagrangian method and also performed a Monte Carlo simulation to check the results.

In the simulation, we allowed the process $(S_t^{(1)}, S_t^{(2)})$ to evolve according to the (true) model (with $\rho = 0.5$), while we hedged the portfolio using the two deltas from the incorrect model, which has $\rho = -0.5$. We note that the mis-specification of the correlation parameter is quite severe in this case.

Figure 6.2 compares the KFE solution to the Monte Carlo results. We see that no negative errors occur.

6.3 Stochastic volatility – The implied volatility hedge

In this example we show the numerical results from solving the extended KFE for the case where

Figure 6.2: Mis-specified correlation between two assets - Distribution of discounted terminal hedging error – MC and KFE (semi-Lagrangian) solutions; 100000 simulation and 2500 time steps for Monte Carlo simulation. 150 time steps for the KFE, S^1_{max}=400, S^2_{max}=400, 100 space steps in each direction, y ∈[-0.1,0.1], 200 steps in y-direction.

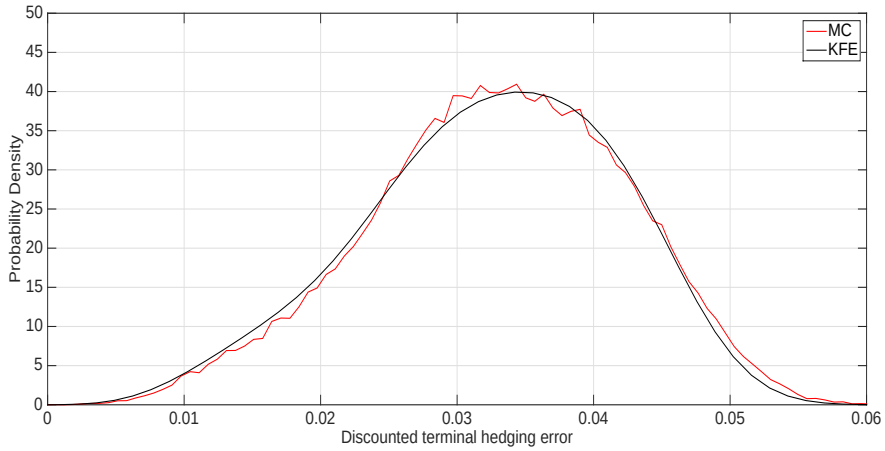

- the true model is the Heston stochastic volatility model (see (3.29)),
- a traded option O_t exists in the market from which an instantaneous implied volatility process is deduced,
- and hedging is carried out using Black-Scholes Greeks for V and O based on this implied volatility process.

The KFE is

$$\begin{aligned}\frac{\partial P}{\partial t} &= \frac{1}{2}S^2 v\frac{\partial^2 P}{\partial S^2} + \rho\sigma S v\frac{\partial^2 P}{\partial S\partial v} + \frac{1}{2}\sigma^2 v\frac{\partial^2 P}{\partial v^2} \\ &\quad + S(2v + \rho\sigma - \mu)\frac{\partial P}{\partial S} \\ &\quad + (\sigma^2 + \rho\sigma v - \kappa(\eta - v))\frac{\partial P}{\partial v} + (v + \rho\sigma + \kappa - \mu)P - c\frac{\partial P}{\partial y}, \end{aligned} \tag{6.4}$$

with

$$\begin{aligned}c(S,t) = \mathrm{e}^{-rt}\frac{\partial V^{BS}(\widehat{\sigma})}{\partial\widehat{\sigma}}\Bigg(&\frac{1}{2}(v-\widehat{\sigma}^2)S^2\left(\frac{\frac{\partial^2 O^{BS}}{\partial S^2}}{\frac{\partial O^{BS}}{\partial\widehat{\sigma}}} - \frac{\frac{\partial^2 V^{BS}}{\partial S^2}}{\frac{\partial V^{BS}}{\partial\widehat{\sigma}}}\right) \\ &+ D\left(\frac{\frac{\partial^2 O^{BS}}{\partial\widehat{\sigma}^2}}{\frac{\partial O^{BS}}{\partial\widehat{\sigma}}} - \frac{\frac{\partial^2 V^{BS}}{\partial\widehat{\sigma}^2}}{\frac{\partial V^{BS}}{\partial\widehat{\sigma}}}\right) + E\left(\frac{\frac{\partial^2 O^{BS}}{\partial\widehat{\sigma}\partial S}}{\frac{\partial O^{BS}}{\partial\widehat{\sigma}}} - \frac{\frac{\partial^2 V^{BS}}{\partial\widehat{\sigma}\partial S}}{\frac{\partial V^{BS}}{\partial\widehat{\sigma}}}\right)\Bigg)dt, \end{aligned} \tag{6.5}$$

where

$$D(t,S,v) = vS^2\frac{\partial\widehat{\sigma}}{\partial S} + \rho\sigma vS\frac{\partial\widehat{\sigma}}{\partial v}$$

and

$$E(t,S,v) = vS^2\left(\frac{\partial\widehat{\sigma}}{\partial S}\right)^2 + 2\rho\sigma vS\left(\frac{\partial\widehat{\sigma}}{\partial S}\right)\left(\frac{\partial\widehat{\sigma}}{\partial v}\right) + v\sigma^2\left(\frac{\partial\widehat{\sigma}}{\partial v}\right)^2$$

where the Greeks used in the calculation of the drift coefficient, and used in hedging, are calculated using the implied volatility process, $\widehat{\sigma}$ (see Chapter 3).

The parameters used the Heston model were $\mu = 0.05$, $\kappa = 2.0$, $\eta = 0.2$ and $\sigma = 0.3$.

Referring to the general form of the KFE (see 4.1) we have we have

$$\begin{aligned}
A_{1,1}(S,v) &= \frac{1}{2}S^2v \\
A_{1,2}(S,v) &= \rho\sigma Sv \\
A_{2,2}(S,v) &= \frac{1}{2}\sigma^2 v \\
B_1(S,v) &= S(2v + \rho\sigma - \mu) \\
B_2(S,v) &= (\sigma^2 + \rho\sigma v - \kappa(\eta - v)) \\
C(S,v) &= (v + \rho\sigma + \kappa - \mu).
\end{aligned}$$

The traded option O was a call with maturity $T = 1.5$ years, struck at $K = 125$ and the option V was again taken to be the spread with payoff at maturity ($T = 1.0$ year) given by

$$F_V(T) = (S_T - 100)^+ - (S_T - 150)^+.$$

We that note the convexity of this option can change sign.

In this example we have used the semi-Lagrangian method for the KFE and also ran a Monte Carlo simulation of the erroneous hedging strategy. The Monte Carlo simulation calculated the evolution of S_t and v_t and then performed dynamic hedging of the portfolio, using the Greeks computed with the implied volatility, to find the distribution of the hedging errors.

Figure 6.3 shows the result obtained by solving the KFE for the joint density of S, v and Y and then integrating out in the S and v directions to get the density of the discounted terminal hedging error and was based on the following settings; $S \in [0, 800]$,

Figure 6.3: Implied Volatility Hedging with Heston model - Distribution of discounted terminal hedging error – MC and KFE (semi-Lagrangian) solutions.

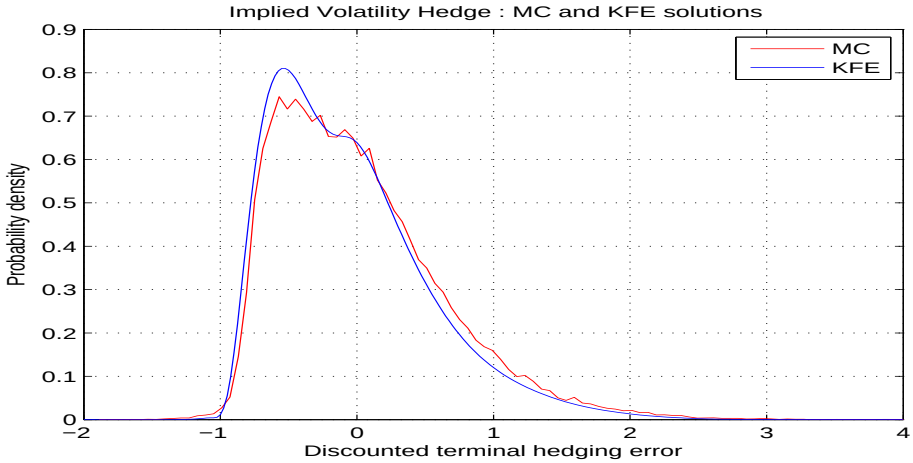

$v \in [0, 5]$ with $S_0 = 100$ and $v_0 = 0.2$. We used $nS = 100$, $nv = 200$ and $nt = 60$.

For this kind of model mis-specification, where the trader might not have a view on the underlying model, he may be still prepared to price and hedge the option, by using the implied volatilities derived from the traded option to provide the hedge ratios. As a result of this lack of knowledge of the true model, hedging errors will occur.

We assume that the trader will calculate the initial premium for V by using the implied volatility, derived from the traded option at time $t = 0$, in the Black-Scholes model.

We also note that, in this case, although we know the initial value of the underlying, we do not know the initial value of the hidden volatility process, v, and we assumed that $v_0 = 0.2$. So this introduces an additional element of uncertainty into the evaluation. We could evaluate a range of starting values of v to assess the impact of this additional uncertainty.

6.4 The uncertain volatility model

In this example we suppose that the true model of the process is the Heston model as used in the previous section.

We will consider what happens if we hedge an option V assuming only the existence of volatility limits, σ_{min} and σ_{max}, such that the unknown volatility process, σ_t, satisfies

$$0 < \sigma_{min} \leq \sigma_t \leq \sigma_{max} < \infty$$

for all t, as per the set-up from Section 3.4.4.

If this assumption holds, a superhedge can be constructed, using the BSB PDE (see (3.32) above) and we would not expect negative hedging errors to occur. If the condition $\sigma_{min} \leq \sigma_t \leq \sigma_{max}$, is not satisfied by the underlying volatility process, negative hedging errors may arise from this hedging strategy.

The KFE is

$$\begin{aligned}\frac{\partial P}{\partial t} &= \frac{1}{2}S^2 v\frac{\partial^2 P}{\partial S^2} + \rho\sigma S v\frac{\partial^2 P}{\partial S \partial v} + \frac{1}{2}\sigma^2 v\frac{\partial^2 P}{\partial v^2} \\ &\quad + S(2v + \rho\sigma - \mu)\frac{\partial P}{\partial S} + (\sigma^2 + \rho\sigma v - \kappa(\eta - v))\frac{\partial P}{\partial v} \\ &\quad + (v + \rho\sigma + \kappa - \mu)P - c\frac{\partial P}{\partial y} \end{aligned} \tag{6.6}$$

where

$$c(S, v, t) = \frac{1}{2}\mathrm{e}^{-rt}(\widehat{\sigma}^2 - v)S^2\frac{\partial^2 \widehat{V}}{\partial S^2} \tag{6.7}$$

$\widehat{\sigma}$ is the volatility process defined by the BSB equation.

Referring to the general form of the KFE (see 4.1) we again have

$$\begin{aligned} A_{1,1}(S, v) &= \frac{1}{2}S^2 v \\ A_{1,2}(S, v) &= \rho\sigma S v \\ A_{2,2}(S, v) &= \frac{1}{2}\sigma^2 v \\ B_1(S, v) &= S(2v + \rho\sigma - \mu) \\ B_2(S, v) &= (\sigma^2 + \rho\sigma v - \kappa(\eta - v)) \\ C(S, v) &= (v + \rho\sigma + \kappa - \mu). \end{aligned}$$

This is illustrated by Figure 6.4 which shows the distribution of discounted terminal hedging errors for a butterfly spread option with payoff defined as

$$(S - 100)^+ - 2(S - 150)^+ + (S - 200)^+$$

Figure 6.4: Uncertain Volatility Hedging with Heston model. Distribution of discounted terminal Hedging Error for KFE and MC solutions. σ between 0.1 and 0.3.

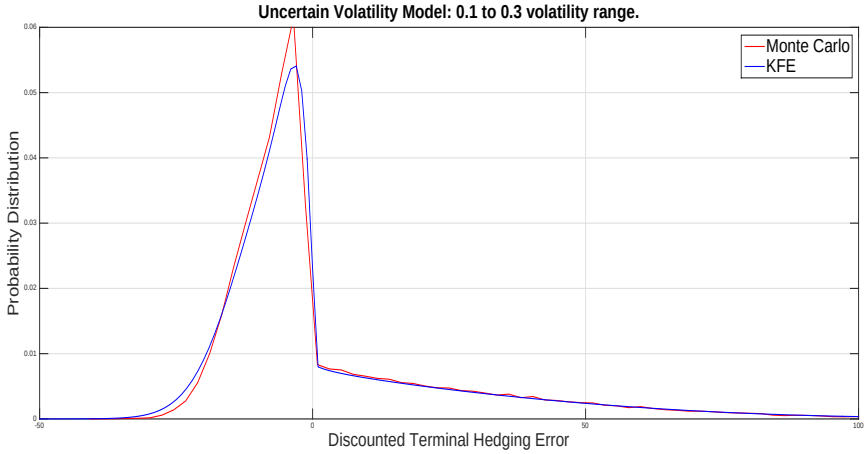

with maturity at $T = 1.0$. Using the parameters $\sigma_{min} = 0.1$ and $\sigma_{max} = 0.3$, we have calculated the distribution of discounted terminal hedging errors using the KFE and by a Monte Carlo simulation. As expected, we find that both positive and negative hedging errors can occur. There is a reasonable match between the two distributions.

The stationary distribution, $P(\sigma_H)$, for the square root of the variance process $\sigma_H = \sqrt{v}$, is given by

$$P(\sigma_H) = \frac{2\alpha^\alpha}{\Gamma(\alpha)} \frac{\sigma^{2\alpha-1}}{\eta^\alpha} e^{-\alpha\sigma_H^2/\alpha}$$

where

$$\alpha = \frac{2\eta\kappa}{\sigma^2}.$$

This can be derived from the Kolmogorov forward equation for the Heston process by setting the time term $\frac{\partial P}{\partial t}$ to zero and solving the resultant PDE.

In Figure 6.5 we show the stationary distribution for the volatility process used in the Heston model.

For this choice of parameters, we have $\alpha = 8.89$. In this case we see that very little of the density relates to the uncertainty range $[0.1, 0.3]$. As a consequence, we expect to see a high proportion of negative hedging errors, as observed in Figure 6.4.

Figure 6.5: Heston Stationary Distribution. κ=2.0, η=0.2 and σ=0.3.

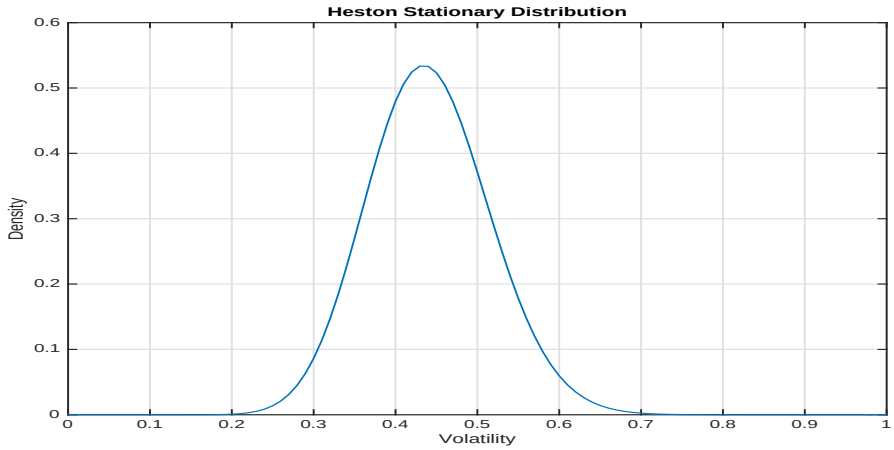

This rather extreme example was chosen to show that very significant hedging errors could arise if the assumed volatility range was badly chosen.

6.5 Hedging a barrier option with incorrect volatility

Finally, we consider an up-and-out barrier option with initial asset price S and a barrier B where we assume that the true asset price follows the simple Black-Scholes model and we assume that the trader hedges with the incorrect volatility, $\widehat{\sigma}$.

The KFE is defined on $S \leq B$ and is given by

$$\frac{\partial P}{\partial t} = \frac{1}{2}\sigma^2 S^2 \frac{\partial^2 P}{\partial S^2} + (2\sigma^2 - \mu) S \frac{\partial P}{\partial S} + (\sigma^2 - \mu) P - c \frac{\partial P}{\partial y}$$

where P is zero at $S = B$ (see Section 3.4.5) and the drift coefficient c is given by

$$c(S,t) = \frac{1}{2} \mathrm{e}^{-rt} (\widehat{\sigma}(S,t)^2 - \sigma^2(S,t)) S_t^2 \frac{\partial^2 \widehat{V}}{\partial S^2}.$$

where we use the gamma for the up-and-out option, calculated using the incorrect volatility, $\widehat{\sigma}$.

The required option price calculations for the erroneous model (i.e. price, delta and gamma) were derived from formulae in [17].

We still have to account for the probability associated with S having crossed the barrier (as discussed in 3.4.5). When the barrier is hit, the option is knocked out, the portfolio becomes risk-free but then continues to grow at the risk-free of rate of interest, r.

However, as we are calculating the discounted hedging error, this means that the probability of the hedging error of the liquidated portfolio only changes over time by the rate of 'leakage' of probability defined by

$$\frac{1}{2}B^2\sigma^2\frac{\partial P}{\partial \xi}\bigg|_B.$$

So to calculate the hedging error distribution, at time t, we need to

- solve the KFE for (S, y, t), applying the boundary condition at $S = B$, and integrate the solution over $S \in [0, B]$,
- calculate the cumulative 'leakage' of probability

$$\frac{1}{2}\sigma^2 B^2 \int_0^T \frac{\partial P}{\partial \xi}\bigg|_B d\tau$$

  corresponding to those paths that reach the barrier, and then
- add the two probability contributions to give the overall hedging error distribution.

An example of these calculations is given for the case when the true value of σ is 0.1 while the hedging is done with $\sigma = 0.2$. We have $\mu = 0.05$ and $r = 0.03$.

Referring to the general form of the KFE (see 4.1) we again have we have

$$\begin{aligned} A_{1,1} &= \frac{1}{2}\sigma^2 S^2 \\ B_1 &= (2\sigma^2 - \mu)S \\ C &= \sigma^2 - \mu. \end{aligned}$$

The option is a call with strike $K = 95$ and the initial value of $S = 90$. The barrier is set at $B = 100$.

Figure 6.6 shows the joint density for S and y at maturity for the paths that have not hit the barrier. As the strike is set at $K = 95$, more significant hedging errors can start to occur once the option is in the money.

Figure 6.6: Barrier Option - Mis-specfied volatility - Joint Density of S and the discounted terminal hedging error (barrier not crossed). $\sigma = 0.1$ and $\widehat{\sigma} = 0.2$

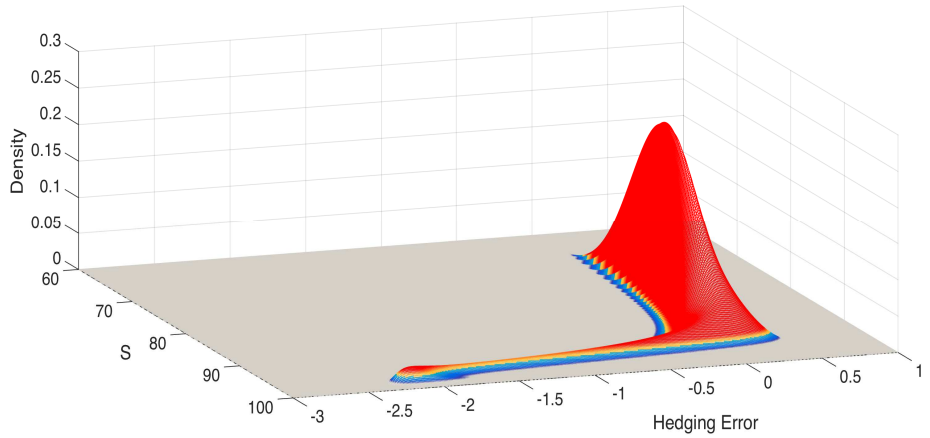

A Monte Carlo simulation was been performed to verify these results, i.e. a simulation has been done to model the asset price paths, delta-hedge the position and observe the resultant hedging errors.

Separate plots are shown for the two components of the hedging error distribution at $t = T$ (Figures 6.7 and 6.8). Figure 6.9 shows the total hedging error distribution.

Figure 6.7: Barrier Option - Mis-specfied volatility - Distribution of discounted terminal hedging error (barrier not crossed) - KFE and MC solutions. $\sigma = 0.1$ and $\widehat{\sigma} = 0.2$

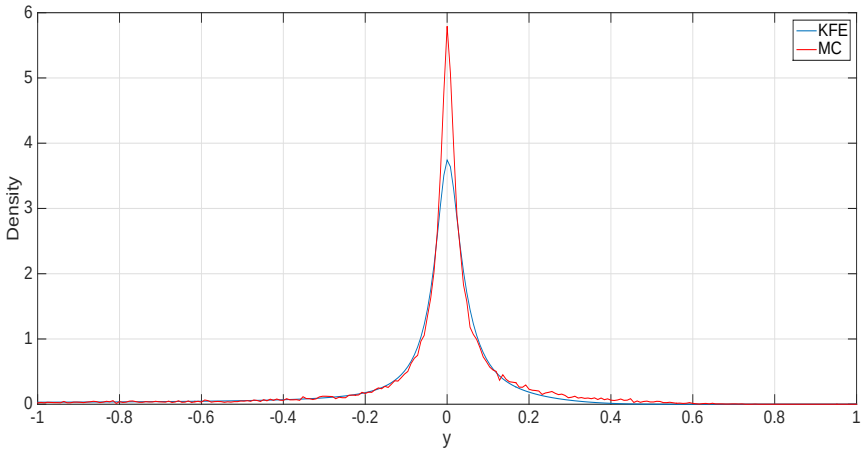

Figure 6.8: Barrier Option - Mis-specfied volatility - Distribution of discounted terminal hedging error (barrier crossed) - KFE and MC solutions. $\sigma = 0.1$ and $\widehat{\sigma} = 0.2$

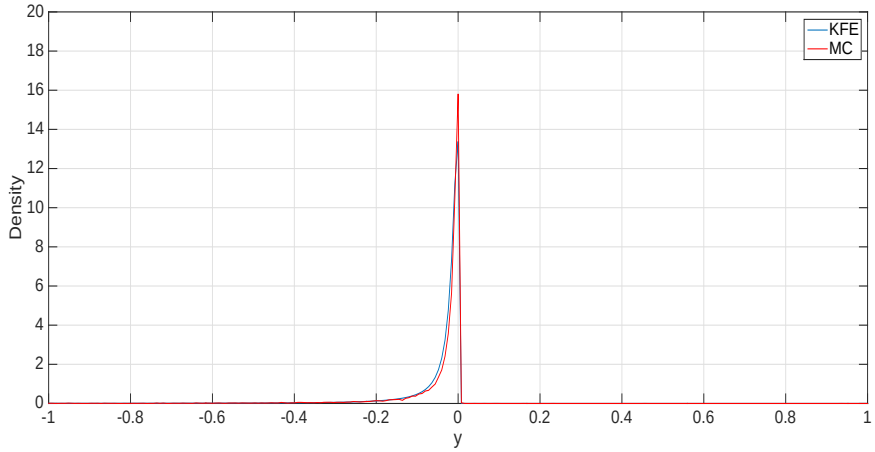

Figure 6.9: Barrier Option - Mis-specfied volatility - Distribution of Total discounted terminal hedging error - KFE and MC solutions. $\sigma = 0.1$ and $\widehat{\sigma} = 0.2$. 1000 S steps, 1000 y steps, 200 t steps.

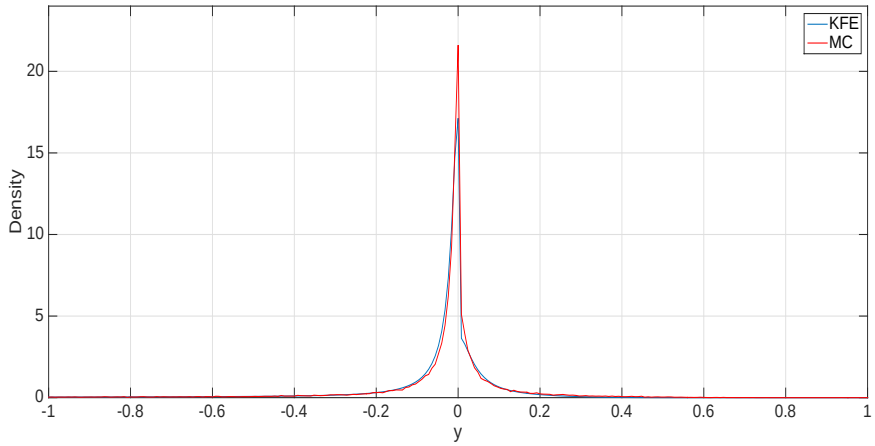

There are some discrepancies between the KFE and Monte Carlo results which would warrant further investigation.

We note that if the the initial value of S were to be far below the barrier, the first component of P would be very close to the results from Section 6.1.

6.6 Interpretation of the hedging error distributions

Our analysis using the KFE yields a hedging error distribution (at maturity) that results from model mis-specification.

For example, applying this to the simple Black-Scholes case, given above in Section 6.1, we obtain the hedging error distribution shown in Figure 6.10. However, we need to put the overall range of errors into some context. Is the range large or small? If the range is 'small' then perhaps the model mis-specification is not of much concern.

One approach to 'normalising' the distribution could be to compare the 'width' of the distribution (perhaps measured by its the standard deviation) to a reference value for the option. Alternatively, some other measure of 'risk' could be used, e.g. 'value at risk', VaR.

Figure 6.10: Black-Scholes model with mis-specified volatility. Comparison of the KFE and Monte Carlo results

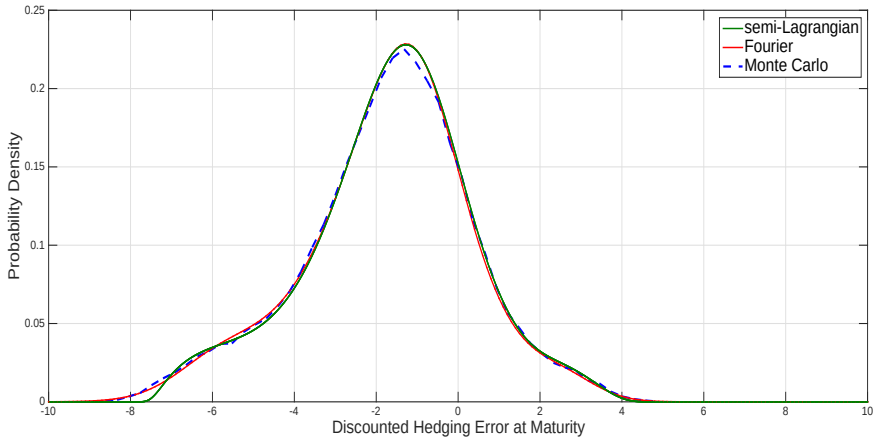

In the example shown, the 'true' price of the option is 26.7 (per unit of the underlying) as estimated by the trader. If he had the correct model, he would then expect the hedging errors to be small. Our analysis shows that the standard deviation of the hedging error is 2.02 (also per unit), which gives an indication of the relative hedging risk.

Figure 6.11: Sensitivity of Standard Deviation of Hedging Error Distribution to Parameter Uncertainty.

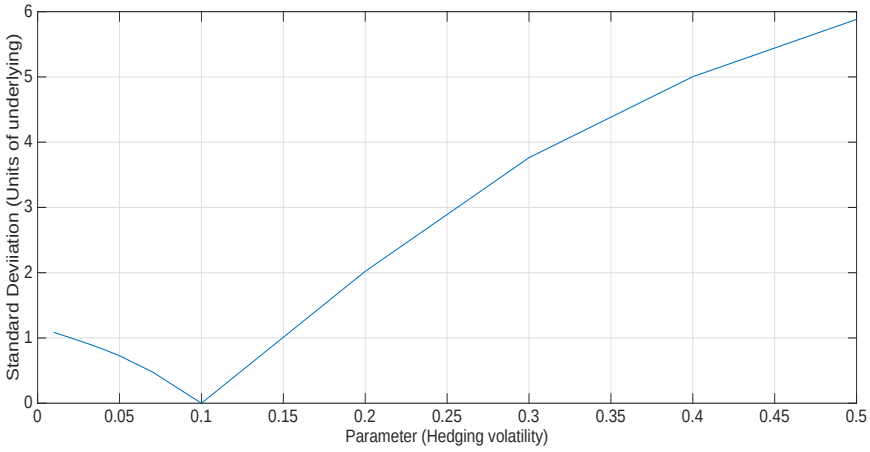

Another approach to this issue would be to consider the sensitivity of the 'width' of the distribution to the amount of parameter uncertainty. In Figure 6.11 we plot the standard deviation of the hedging error distribution against the difference between the hedging volatility and the true volatility. This could indicate how much effort

might be invested in firming up the volatility estimates. If the risk measure is small, there would not be much to be gained from such efforts.

Chapter 7

Future work on the extended KFE and the toy model

We have established a PDE-based method for generating hedging error distributions. As we have only presented a limited number of applications of the method there is scope for further investigations into the method.

The thesis has also presented our attempts to analyse the convergence of the numerical schemes used to solve the KFE. Our focus has been on the use of Fourier transform techniques which are particularly suitable for PDE problems with non-smooth initial conditions.

As we have been dealing with a PDE which has variable-coefficients, the Fourier analysis we have performed has not been completely successful, but some good progress has been made, particularly with the semi-discrete Fourier method.

Further studies on these convergence analyses would be worthwhile.

We list some of these possible areas of further study below.

7.1 Extensions to other option types

The examples given in this thesis are all for options of European type and, with the exception of the the barrier option example, with path-independent payoffs.

We might also want to investigate whether KFEs can be derived and solved for further option types, such as other exotic and American options.

In the case of an American option, an interesting feature arises. Suppose we are considering a simple American put under the Black-Scholes model with constant volatility. If we are hedging using an incorrect value of the volatility we have an incorrect expectation of when the option will be exercised by the holder (the exercise boundary can be computed in advance). If we assume that the option holder has the same erroneous estimate of the volatility (this perhaps being confirmed by the price at which we can sell the option) then until the asset price hits the exercise boundary, it is likely that the 'hedging error' process follows the El Karoui formula (as with the knock-out call). Once it hits the boundary, we can assume that the option is exercised and thereafter we have $dY_t = 0$ so this scenario is similar to the knock-out call but with a more complex (but pre-computable) exercise boundary. So we would hope that the study of the knock-out call would guide us with this example.

This approach assumes that the option holder never changes his mind about the location of the exercise boundary. However, in practice, observation of the actual volatility of the asset could provide information on the volatility to the option holder so that this assumption may no longer be valid.

7.2 Extensions to other underlying dynamics

Many popular models of asset dynamics incorporate jump processes and we want to investigate how hedging error dynamics behave under these conditions. We will first have to consider the hedging strategies that are available when the market exhibits this form of incompleteness.

Some investigations of hedging errors in this kind of environment have been made by Elder [11] who uses the Kolmogorov backward equation in his researches. We can expect that the KFE, if it can be defined, will take the form of a partial-integro-differential equation (PIDE).

7.3 Extensions to other hedging strategies

We might also want to investigate how the KFE approach can be applied to a variety of other hedging strategies, e.g. vanna-volga hedging, quantile hedging and mean-

variance hedging.

For example, in the case of quantile hedging where the premium has been set to achieve a specified target probability of avoiding a hedging error, we would expect that the KFE method would generate a probability distribution for the 'hedging error' that is consistent with the target. At the same time, the availability of the entire probability distribution should provide additional information about the characteristics of this hedging method.

We could also investigate how this probability distribution changes if, say, the volatility were to be mis-specified.

7.4 Hedging errors from model calibration

The models used for hedging are often derived from a calibration process. In this case the derived model is not expected to precisely fit the data used for calibration (e.g. observed option prices). So one line of research is to consider how the KFE might be applied when this imperfect fit is present.

Another possible approach is to look at the Bayesian method for model calibration. In this approach, a family of possible models is identified each with a probability weighting (discrete or continuous). We can imagine applying the KFE approach to each candidate model and then combining the hedging error distributions using the probability weights of the model family members. This is likely to be very computationally intensive and so would benefit from improvements in the basic KFE algorithms.

7.5 Further work on the toy model

The purpose of the toy model was to investigate the stability of the numerical schemes we used for the KFE problems.

The main difficulty was originally thought to be the complication arising from the non-smooth initial conditions and we had hoped to use the techniques from [5] to make progress with the analysis.

However, the approach via Fourier analysis has only been partially successful. This is because the time evolution of the double-FT used in our analysis is more complex than expected and has not yielded to complete analysis.

For the case of the semi-discrete Fourier method, a satisfactory solution was found but in the case of the discrete Fourier method, we obtained a 'differential recursion' recursion that looked quite simple and yet proved to be to difficult to analyse.

We found ourselves dealing with the behaviour of an iterated differential operator (which depended on the timestep Δt) and where the number of iterations, n, tends to infinity while Δt tends to zero with the product $T = n\Delta t$ held constant.

It is surprising that the solution of this kind of problem does not seem to be readily found in the literature.

It would be pleasing to get further with understanding the behaviour of this kind of problem and perhaps finish the analysis of the toy model, at least for one of its time-stepping variants.

Chapter 8

Conclusions

The work described in this thesis was primarily motivated by the problem of analysing hedging errors under model mis-specification.

We developed an extended Kolmogorov forward equation (KFE), a partial differential equation (PDE) which can be solved to obtain the joint probability distribution for the underlying and the hedging error at maturity.

Notable features of the KFE we have used are that, typically, the hedging error only features as a convection/drift term (in the hedging error direction) in the PDE whereas the underlying appears in an 'orthogonal' diffusion term and the drift coefficient of the hedging error derivative only appears as a function of the underlying and of time.

These special features of the KFE made it easier to implement certain types of numerical solutions for the hedging problems and we implemented various numerical schemes for a selection of model mis-specification types.

In the KFE problems we studied, the initial conditions took the form of a δ-function, which can make it difficult to analyse the stability of numerical schemes used to solve the PDE and we sought a theoretical explanation for the behaviour of the numerical schemes we used.

The literature includes examples of the analysis of the stability of numerical schemes for PDEs with δ-function initial conditions and, indeed, as a part of the thesis we include a chapter which makes a further contribution to this literature ([36]).

Motivated by these examples in the literature, we attempted to apply similar methods of analysis to the KFE problem and, to simplify the analysis, we have done this by investigating a toy model that aims to capture the main features of the KFE model.

The main difficulty stems from the fact that the PDE has variable coefficients and so Fourier analysis would not normally be very useful in this case. In the case of the toy model, however, we have employed Fourier transform techniques to investigate stability and have made some good progress.

Appendices

Appendix A

The basic finite difference method

For the basic finite difference method we discretise in all directions. As mentioned above we have alternative, more efficient, solution methods that can take advantage of the special structure of the KFE so we would not expect to use this method for 'real-life' problems. However, we will provide some analysis of this method to allow some comparison with the the semi-Lagrangian method. We define two versions of the scheme, one with and one without variable-direction upwinding. The basic finite difference scheme without variable-direction upwinding does not perform well and this will be explained in the section on solving the recursions.

A.0.1 The numerical scheme for the basic finite difference method with variable-direction upwinding

The variable-direction unwinding scheme is defined as

$$\frac{U^{n+1}(j,k) - U^n(j,k)}{\Delta t}$$
$$+x_j \left(\left(\frac{1+\text{sgn}(x_j)}{2} \right) \frac{U^n(j,k) - U^n(j,k-1)}{\Delta y} + \left(\frac{1-\text{sgn}(x_j)}{2} \right) \frac{U^n(j,k+1) - U^n(j,k)}{\Delta y} \right)$$
$$= \frac{U^{n+1}(j+1,k) - 2U^{n+1}(j,k) + U^{n+1}(j-1,k)}{\Delta x^2}$$

where we have treated the drift term explicitly. This is written in a compact form

that applies for all values of j by using the signum function (sgn), where

$$\begin{aligned}
&\text{sgn}(x) = x, \text{ for } x > 0, \\
&\text{sgn}(x) = -x, \text{ for } x < 0, \text{and} \\
&\text{sgn}(x) = 0, \text{ for } x = 0.
\end{aligned}$$

In this form we see that we have an overall upwinding term that changes sign with x.

Alternatively, we can write the scheme in two parts, i.e.

$$\begin{aligned}
&\frac{U^{n+1}(j,k) - U^n(j,k)}{\Delta t} + x_j \left(\frac{U^n(j,k) - U^n(j,k-1)}{\Delta y} \right) \\
&= \frac{(U^{n+1}(j+1,k) - 2U^{n+1}(j,k) + U^{n+1}(j-1,k))}{\Delta x^2}
\end{aligned}$$

for $j \geq 0$, and there is a similar expression for $j < 0$.

We define the two 'shape' factors, $\lambda = \frac{\Delta t}{\Delta x^2}$ and $\nu = \frac{\Delta t}{\Delta y}$ and can write the scheme as

$$\begin{aligned}
-\lambda U^{n+1}(j+1,k) + (1+2\lambda)U^{n+1}(j,k) - \lambda U^{n+1}(j-1,k) \\
= U^n(j,k) - x_j \nu (U^n(j,k) - U^n(j,k-1))
\end{aligned} \tag{A.1}$$

for $j \geq 0$ and where we have a similar expression for $j < 0$.

A.0.2 The numerical scheme for the basic finite difference method without variable-direction upwinding

For this scheme we replace the separate upwinding terms and use central differencing instead, so the numerical scheme is somewhat simpler.

We have

$$\begin{aligned}
&\frac{U^{n+1}(j,k) - U^n(j,k)}{\Delta t} + x_j \left(\frac{U^n(j,k+1) - U^n(j,k-1)}{2\Delta y} \right) \\
&= \frac{U^{n+1}(j+1,k) - 2U^{n+1}(j,k) + U^{n+1}(j-1,k)}{\Delta x^2}
\end{aligned}$$

and this now applies for all j.

We can write the scheme as

$$-\lambda U^{n+1}(j+1,k) + (1+2\lambda)U^{n+1}(j,k) - \lambda U^{n+1}(j-1,k) \qquad \text{(A.2)}$$
$$= U^n(j,k) - \frac{1}{2}x_j\nu(U^n(j,k+1) - U^n(j,k-1))$$

for all j.

A.0.3 Numerical output for the basic finite difference method

A.0.3.1 With variable-direction upwinding

Figure A.1 shows the solution with variable-direction upwinding.

Figure A.1: Basic finite difference method - Variable-direction upwinding solution

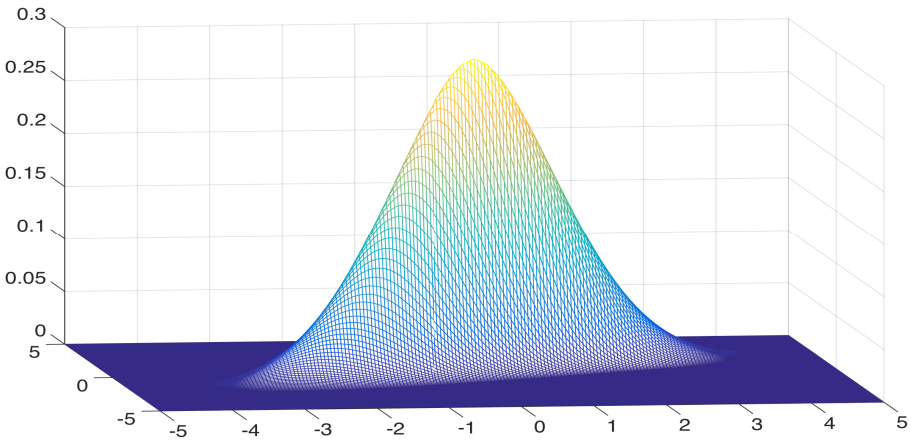

A.0.3.2 Without variable-direction upwinding

Figure A.2 shows the solution without variable-direction upwinding. Noticeable instabilities are apparent in this case. The reasons for this will be explained in Section A.0.4.2.

Figure A.2: Basic finite difference method - No upwinding solution showing instability

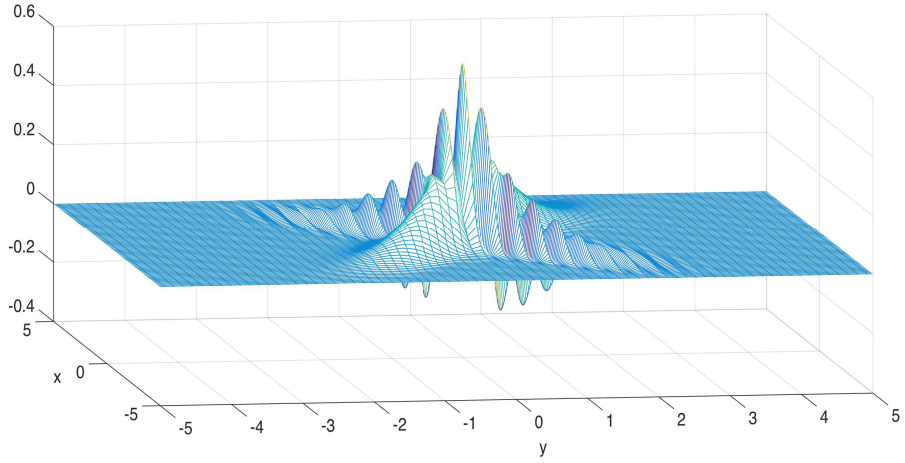

A.0.4 The recursions for the basic finite difference scheme

A.0.4.1 The recursion with variable-direction upwinding

For the scheme with variable-direction upwinding we have

$$-\lambda U_{j+1,k}^{n+1} + (1+2\lambda)U_{j,k}^{n+1} - \lambda U_{j-1,k}^{n+1} = U_{j,k}^{n} - x_j\nu(U_{j,k}^{n} - U_{j,k-1}^{n})$$

for $j > 0$ and

$$-\lambda U_{j+1,k}^{n+1} + (1+2\lambda)U_{j,k}^{n+1} - \lambda U_{j-1,k}^{n+1} = U_{j,k}^{n} - x_j\nu(U_{j,k}^{n} - U_{j,k+1}^{n})$$

for $j < 0$.

We first apply the discrete FT in the y-direction and write

$$\Delta y \sum_{k=-\infty}^{k=\infty} (-\lambda U_{j+1,k}^{n+1} + (1+2\lambda)U_{j,k}^{n+1} - \lambda U_{j-1,k}^{n+1})e^{ipy_k}$$
$$= \Delta y \sum_{k=-\infty}^{k=\infty} (U_{j,k}^{n} - x_j\nu U_{j,k}^{n} + x_j\nu U_{j,k-1}^{n})e^{ipy_k}$$

for $j > 0$, which gives

$$\begin{aligned}-\lambda V_{j+1}^{n+1}(p) + (1+2\lambda)V_j^{n+1}(p) - \lambda V_{j-1}^{n+1}(p) =& V_j^n(p) - x_j\nu V_j^n(p) + e^{ip\Delta y}x_j\nu V_j^n(p)\\ =& V_j^n(p) - x_j\nu(1-e^{ip\Delta y})V_j^n(p)\end{aligned}$$

and there is a similar expression for $j < 0$. Here we have defined $V_j^n(p)$ to be the y-FT of U.

We next define two half-transforms

$$W_1^n(s,p) = \Delta x\left(\frac{1}{2}V_0^n(p) + \sum_{j=1}^{j=\infty} V_j^n(p)e^{isx_k}\right)$$

and

$$W_2^n(s,p) = \Delta x\left(\frac{1}{2}V_0^n(p) + \sum_{j=-\infty}^{j=-1} V_j^n(p)e^{isx_k}\right)$$

so that the numerical double-FT is given by

$$W^n(s,p) = W_1^n(s,p) + W_2^n(s,p).$$

Due to the change in direction of the upwinding terms, we have to derive separate recursions for $W_1^n(s,p)$ and $W_2^n(s,p)$. However we will find, below, that they are complex conjugates.

Firstly, we develop a recursion for $W_1^n(s,p)$ by summing over $j > 0$, to get

$$\begin{aligned}&\Delta x\sum_{j=1}^{j=\infty}(-\lambda V_{j+1}^{n+1}(p) + (1+2\lambda)V_j^{n+1}(p) - \lambda V_{j-1}^{n+1}(p))e^{isx_j}\\ =&\Delta x\sum_{j=1}^{j=\infty} V_j^n(p)e^{isx_j} - \Delta x\nu(1-e^{ip\Delta y})\sum_{j=1}^{j=\infty} x_jV_j^n(p)e^{isx_j}\\ =&\Delta x\sum_{j=1}^{j=\infty} V_j^n(p)e^{isx_j} + i\nu(1-e^{ip\Delta y})\frac{\partial}{\partial s}\left(\Delta x\sum_{j=1}^{j=\infty} V_j^n(p)e^{isx_j}\right)\end{aligned}$$

The first term on the left-hand side is

$$\begin{aligned}-\lambda\Delta x\sum_{j=1}^{j=\infty}V_{j+1}^{n+1}(p)e^{isx_j} &= -\lambda e^{-is\Delta x}\Delta x\sum_{j=1}^{j=\infty}V_{j+1}^{n+1}(p)e^{isx_{j+1}}\\ &= -\lambda e^{-is\Delta x}\Delta x\sum_{j=2}^{j=\infty}V_{j}^{n+1}(p)e^{isx_j}\\ &= -\lambda e^{-is\Delta x}\bigg(W_1^{n+1}(s,p)-\frac{1}{2}\Delta xV_0^{n+1}(p)-\Delta xV_1^{n+1}(p)e^{is\Delta x}\bigg).\end{aligned}$$

Similarly, we find the second term is

$$(1+2\lambda)\Delta x\sum_{j=1}^{j=\infty}V_{j}^{n+1}(p)e^{isx_j}=(1+2\lambda)\bigg(W_1^{n+1}(s,p)-\frac{1}{2}\Delta xV_0^{n+1}(p)\bigg).$$

Finally, we find the third term is

$$\begin{aligned}-\lambda\Delta x\sum_{j=1}^{j=\infty}V_{j-1}^{n+1}(p)e^{isx_j} &= -\lambda e^{is\Delta x}\Delta x\sum_{j=1}^{j=\infty}V_{j-1}^{n+1}(p)e^{isx_{j-1}}\\ &= -\lambda e^{is\Delta x}\Delta x\sum_{j=0}^{j=\infty}V_{j}^{n+1}(p)e^{isx_j}\\ &= -\lambda e^{is\Delta x}\bigg(W_1^{n+1}(s,p)+\frac{1}{2}\Delta xV_0^{n+1}(p)\bigg).\end{aligned}$$

Also, in the right-hand side the first term is

$$\Delta x\sum_{j=1}^{j=\infty}V_{j}^{n}(p)e^{isx_j}=W_1^{n}(s,p)-\frac{1}{2}\Delta xV_0^{n}(p).$$

So we have

$$\begin{aligned}&-\lambda e^{-is\Delta x}\bigg(W_1^{n+1}(s,p)-\frac{1}{2}\Delta xV_0^{n+1}(p)-\Delta xV_1^{n+1}(p)e^{is\Delta x}\bigg)\\ &+(1+2\lambda)\bigg(W_1^{n+1}(s,p)-\frac{1}{2}\Delta xV_0^{n+1}(p)\bigg)-\lambda e^{is\Delta x}\bigg(W_1^{n+1}(s,p)+\frac{1}{2}\Delta xV_0^{n+1}(p)\bigg)\\ &=W_1^{n}(s,p)-\frac{1}{2}\Delta xV_0^{n}(p)+i\nu(1-e^{ip\Delta y})\frac{\partial W_1^n(s,p)}{\partial s}.\end{aligned}$$

After defining $f(s)=(1+2\lambda)-2\lambda\cos(s\Delta x)=1+4\lambda\sin^2(\frac{s\Delta x}{2})$ we get

$$f(s)W_1^{n+1}(s,p)+\lambda\Delta xV_1^{n+1}(p)-\Delta xV_0^{n+1}(p)\bigg(\frac{1}{2}(1+2\lambda)+i\lambda\sin(s\Delta x)\bigg)$$

$$= i\nu(1 - e^{ip\Delta y})\frac{\partial W_1^n(s,p)}{\partial s} + W_1^n(s,p) - \frac{1}{2}\Delta x V_0^n(p)$$

We can also make use of the scheme definition at $x = 0$ by writing

$$\frac{V_0^{n+1}(p) - V_0^n(p)}{\Delta t} = \frac{V_1^{n+1}(p) - 2V_0^{n+1}(p) + V_{-1}^{n+1}(p)}{\Delta x^2}$$

to express $V_0^n(p)$ as

$$V_0^n(p) = -\lambda V_1^{n+1}(p) + (1 + 2\lambda)V_0^{n+1}(p) - \lambda V_{-1}^{n+1}(p)$$

and use this to obtain

$$f(s)W_1^{n+1}(s,p) + \lambda\Delta x V_1^{n+1}(p) - \Delta x V_0^{n+1}(p)\left(\frac{1}{2}(1+2\lambda) + i\lambda\sin(s\Delta x)\right)$$

$$= i\nu(1-e^{ip\Delta y})\frac{\partial W_1^n(s,p)}{\partial s} + W_1^n(s,p) - \frac{1}{2}\Delta x(-\lambda V_1^{n+1}(p) + (1+2\lambda)V_0^{n+1}(p) - \lambda V_{-1}^{n+1}(p))$$

which leads to

$$f(s)W_1^{n+1}(s,p) - i\Delta x V_0^{n+1}(p)\lambda\sin(s\Delta x) + \frac{1}{2}\lambda\Delta x(V_1^{n+1}(p) - V_{-1}^{n+1}(p)) \qquad \text{(A.3)}$$
$$= W_1^n(s,p) + i\nu(1 - e^{ip\Delta y})\frac{\partial W_1^n(s,p)}{\partial s}$$

which is the recursion for $W_1^n(s,p)$.

Similarly, we develop a recursion for $W_2^n(s,p)$ by instead summing over $j < 0$ and proceeding as above.

So, for general p the recursions are

$$f(s)W_2^{n+1}(s,p) + C^{n+1}(p) = W_1^n(s,p) + i\nu(1 - e^{ip\Delta y})\frac{\partial W_1^n(s,p)}{\partial s}$$

and

$$f(s)W_2^{n+1}(s,p) + \overline{C^{n+1}(p)} = W_2^n(s,p) - i\nu(1 - e^{-ip\Delta y})\frac{\partial W_2^n(s,p)}{\partial s} \qquad \text{(A.4)}$$

where

$$C^{n+1}(p) = -\frac{1}{2}\lambda\Delta x(V_1^{n+1}(p) - V_{-1}^{n+1}(p)) + i\Delta x V_0^{n+1}(p)\lambda\sin(s\Delta x).$$

We observe that

$$\overline{V_j^n(p)} = \overline{\Delta x \sum_{-\infty}^{\infty} U_{j,k}^n e^{ipk\Delta y}} = \Delta x \sum_{-\infty}^{\infty} U_{j,k}^n e^{-ipk\Delta y} = \Delta x \sum_{-\infty}^{\infty} U_{-j,-k}^n e^{-ipk\Delta y} = V_{-j}^n(p)$$

where we have the reality and the symmetry of the solution U and so

$$\overline{V_0^n(p)} = V_0^n(p)$$

and hence $V_0^n(p)$ is real and $V_j^n(p)$ and $V_{-j}^n(p)$ are complex conjugates.

It follows that $\overline{W_2^{n+1}(s,p)} = W_1^{n+1}(s,p)$ and, finally, $W^{n+1}(s,p) = W_1^{n+1}(s,p) + W_2^{n+1}(s,p)$ is real, as expected.

For the special case where $p_0 = \frac{\pi}{\Delta y}$ we have can use symmetry to show that $V_1^{n+1}(p_0) - V_{-1}^{n+1}(p_0) = 0$, so that we have

$$\begin{aligned} f(s)W_1^{n+1}(s,p_0) + i\Delta x V_0^{n+1}(p_0)\lambda \sin(s\Delta x) \\ = W_1^n(s,p_0) + 2i\nu \frac{\partial W_1^n(s,p_0)}{\partial s} \end{aligned}$$

so the recursion is a little simpler for this value of p. Here, p_0, is the highest wavenumber for p.

A.0.4.2 The recursion without variable-direction upwinding

.

For the scheme without variable-direction upwinding we have

$$\begin{aligned} -\lambda U^{n+1}(j+1,k) + (1+2\lambda)U^{n+1}(j,k) - \lambda U^{n+1}(j-1,k) \\ = U^n(j,k) - \frac{1}{2}x_j\nu(U^n(j,k+1) - U^n(j,k-1)) \end{aligned}$$

and this now applies for all j.

We now apply the discrete y-FT to get

$$\begin{aligned} -\lambda V^{n+1}(j+1,p) + (1+2\lambda)V^{n+1}(j,p) - \lambda V^{n+1}(j-1,p) \\ = V^n(j,p) - \frac{1}{2}x_j\nu(\exp(-ip\Delta y)V^n(j,p) - \exp(ip\Delta y)V^n(j,p)) \\ = V^n(j,p) + ix_j\nu \sin(p\Delta y)V^n(j,p). \end{aligned}$$

Then we apply the x-FT to get

$$\begin{aligned}
&-\lambda \exp(-is\Delta x)W^{n+1}(s,p) + (1+2\lambda)W^{n+1}(s,p) - \lambda \exp(-is\Delta x)W^{n+1}(s,p) \\
&= ((1+2\lambda) - 2\lambda\cos(s\Delta x))W^{n+1}(s,p) \\
&= W^n(s,p) + \nu \sin(p\Delta y)\frac{\partial W^n(s,p)}{\partial s}.
\end{aligned}$$

We can write the recursion as

$$f(s)W^{n+1}(s,p) = W^n(s,p) + \nu \sin(p\Delta y)\frac{\partial W^n(s,p)}{\partial s}. \tag{A.5}$$

If we consider the particular high p-wavenumber case where $p = \frac{\pi}{\Delta y}$, we find

$$f(s)W^{n+1}(s,\frac{\pi}{\Delta y}) = W^n(s,\frac{\pi}{\Delta y})$$

and if we choose $s = 0$, so that $f(s) = 0$, we get

$$W^{n+1}(0,\frac{\pi}{\Delta y}) \equiv W^n(0,\frac{\pi}{\Delta y}) = 1$$

and so the numerical transform cannot converge to the true solution for high p-wavenumbers. This behaviour is illustrated in Figure A.3.

Figure A.3: Basic finite difference method – Fourier space – Solution without upwinding

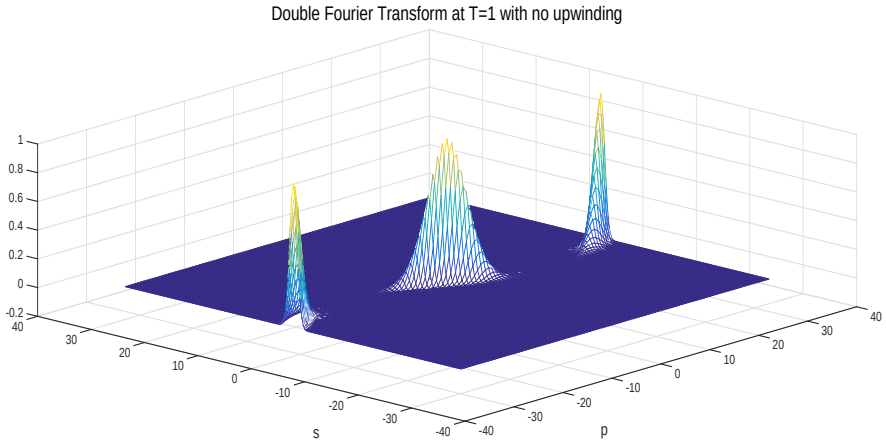

As a result, the no-upwinding scheme will behave poorly and induce oscillations in the numerical solution due to the lack of damping of the high wavenumbers, as seen in Figure A.2 above.

A.0.5 Convergence analysis for the basic finite difference method

In this section we will only consider the variable-direction upwinding version of this method as the method without upwinding clearly causes instability, as indicated above.

For general p we have written the recursions as

$$f(s)W_1^{n+1}(s,p) + C^{n+1}(p) = W_1^n(s,p) + i\nu(1 - e^{ip\Delta y})\frac{\partial W_1^n(s,p)}{\partial s}$$

and

$$f(s)W_2^{n+1}(s,p) + \overline{C^{n+1}(p)} = W_2^n(s,p) - i\nu(1 - e^{-ip\Delta y})\frac{\partial W_2^n(s,p)}{\partial s}$$

where

$$C^{n+1}(p) = -\frac{1}{2}\lambda\Delta x(V_1^{n+1}(p) - V_{-1}^{n+1}(p)) + i\Delta x V_0^{n+1}(p)\lambda\sin(s\Delta x).$$

We note that

$$\begin{aligned}\overline{C^{n+1}(p)} &= -\frac{1}{2}\lambda\Delta x(\overline{V_1^{n+1}(p)} - \overline{V_{-1}^{n+1}(p)}) - i\Delta x\overline{V_0^{n+1}(p)}\lambda\sin(s\Delta x)\\ &= -\frac{1}{2}\lambda\Delta x(V_{-1}^{n+1}(p) - V_1^{n+1}(p)) - i\Delta x V_0^{n+1}(p)\lambda\sin(s\Delta x)\end{aligned}$$

by the symmetry properties of the solution.

So we find that $C^{n+1}(p) + \overline{C^{n+1}(p)} = 0$.

Clearly, solution of this recursion is rather daunting with a particular complication arising from the 'matching condition' at $s = 0$, i.e. the presence of the term $C^{n+1}(p)$ which is like an internal 'boundary condition'.

If we were able to ignore the matching conditions we would be seeking to solve a recursion of the form

$$f(s)W_1^{n+1}(s,p) = W_1^n(s,p) + i\nu(1-e^{ip\Delta y})\frac{\partial W_1^n}{\partial s}(s,p)$$

and observe that our solution would arise from a repeated process of differentiation and we would make use of the initial condition $W_1^0(s,p) = \frac{1}{2}$.

We need to identify the additional terms in the recursion to make progress. We can start by adding the two recursions to get

$$f(s)W_1^{n+1}(s,p) + C^{n+1}(p) + f(s)W_2^{n+1}(s,p) + \overline{C^{n+1}(p)}$$

$$= W_1^n(s,p) + i\nu(1-e^{ip\Delta y})\frac{\partial W_1^n(s,p)}{\partial s} + W_2^n(s,p) - i\nu(1-e^{-ip\Delta y})\frac{\partial W_2^n(s,p)}{\partial s}$$

or

$$f(s)W^{n+1}(s,p) = W^n(s,p) + i\nu(1-e^{ip\Delta y})\frac{\partial W_1^n(s,p)}{\partial s} - i\nu(1-e^{-ip\Delta y})\frac{\partial W_2^n(s,p)}{\partial s}$$

and

$$W^{n+1}(s,p) = \frac{W^n(s,p)}{f(s)} + \frac{i\nu(1-e^{ip\Delta y})}{f(s)}\frac{\partial W_1^n(s,p)}{\partial s} - \frac{i\nu(1-e^{-ip\Delta y})}{f(s)}\frac{\partial W_2^n(s,p)}{\partial s}.$$

Multiplying by $e^{-isj\Delta x}$ and integrating from $-\frac{\pi}{\Delta x}$ to $\frac{\pi}{\Delta x}$ we get

$$\frac{1}{2\pi}\int_{-\frac{\pi}{\Delta x}}^{\frac{\pi}{\Delta x}} W^{n+1}(s,p)e^{-isj\Delta x}ds$$

$$= \frac{1}{2\pi}\int_{-\frac{\pi}{\Delta x}}^{\frac{\pi}{\Delta x}} \frac{W^n(s,p)}{f(s)}e^{-isj\Delta x}ds + \frac{1}{2\pi}\int_{-\frac{\pi}{\Delta x}}^{\frac{\pi}{\Delta x}} \frac{i\nu(1-e^{ip\Delta y})}{f(s)}\frac{\partial W_1^n(s,p)}{\partial s}e^{-isj\Delta x}ds$$

$$-\frac{1}{2\pi}\int_{-\frac{\pi}{\Delta x}}^{\frac{\pi}{\Delta x}} \frac{i\nu(1-e^{-ip\Delta y})}{f(s)}\frac{\partial W_2^n(s,p)}{\partial s}e^{-isj\Delta x}ds.$$

We recognise the first term as $V_j^{n+1}(p)$ so we have

$$V_j^{n+1}(p) = \frac{1}{2\pi}\int_{-\frac{\pi}{\Delta x}}^{\frac{\pi}{\Delta x}} \frac{W^n(s,p)}{f(s)}e^{-isj\Delta x}ds + \frac{1}{2\pi}i\nu(1-e^{ip\Delta y})\int_{-\frac{\pi}{\Delta x}}^{\frac{\pi}{\Delta x}} \frac{1}{f(s)}\frac{\partial W_1^n(s,p)}{\partial s}e^{-isj\Delta x}ds$$

$$-\frac{1}{2\pi}i\nu(1-e^{-ip\Delta y})\int_{-\frac{\pi}{\Delta x}}^{\frac{\pi}{\Delta x}} \frac{1}{f(s)}\frac{\partial W_2^n(s,p)}{\partial s}e^{-isj\Delta x}ds.$$

In principle, we could now calculate $V_j^{n+1}(p)$ from the solution values at time step n.

So, for example, we can take $j = 0$ and write

$$V_0^{n+1}(p) = \frac{1}{2\pi}\int_{-\frac{\pi}{\Delta x}}^{\frac{\pi}{\Delta x}} \frac{W^n(s,p)}{f(s)}ds + \frac{1}{2\pi}i\nu(1-e^{ip\Delta y})\int_{-\frac{\pi}{\Delta x}}^{\frac{\pi}{\Delta x}} \frac{1}{f(s)}\frac{\partial W_1^n(s,p)}{\partial s}ds$$
$$-\frac{1}{2\pi}i\nu(1-e^{-ip\Delta y})\int_{-\frac{\pi}{\Delta x}}^{\frac{\pi}{\Delta x}} \frac{1}{f(s)}\frac{\partial W_2^n(s,p)}{\partial s}ds.$$

For the first time step we can write

$$V_0^1(p) = \frac{1}{2\pi}\int_{-\frac{\pi}{\Delta x}}^{\frac{\pi}{\Delta x}} \frac{1}{f(s)}ds$$
$$V_1^1(p) = \frac{1}{2\pi}\int_{-\frac{\pi}{\Delta x}}^{\frac{\pi}{\Delta x}} \frac{1}{f(s)}e^{-is\Delta x}ds$$
$$V_{-1}^1(p) = \frac{1}{2\pi}\int_{-\frac{\pi}{\Delta x}}^{\frac{\pi}{\Delta x}} \frac{1}{f(s)}e^{is\Delta x}ds.$$

In passing, we see that $V_0^1(p)$ is real and $V_1^1(p)$ and $V_{-1}^1(p)$ are complex conjugates.

Also at the first time step, there is no dependence on p.

At the next time step we can calculate, for example,

$$V_0^2(p) = \frac{1}{2\pi}\int_{-\frac{\pi}{\Delta x}}^{\frac{\pi}{\Delta x}} \frac{W^1(s,p)}{f(s)}ds + \frac{1}{2\pi}i\nu(1-e^{ip\Delta y})\int_{-\frac{\pi}{\Delta x}}^{\frac{\pi}{\Delta x}} \frac{1}{f(s)}\frac{\partial W_1^1(s,p)}{\partial s}ds$$
$$-\frac{1}{2\pi}i\nu(1-e^{-ip\Delta y})\int_{-\frac{\pi}{\Delta x}}^{\frac{\pi}{\Delta x}} \frac{1}{f(s)}\frac{\partial W_2^1(s,p)}{\partial s}ds$$

and use integration by parts to write

$$V_0^2(p) = \frac{1}{2\pi}\int_{-\frac{\pi}{\Delta x}}^{\frac{\pi}{\Delta x}} \frac{W^1(s,p)}{f(s)}ds - \frac{1}{2\pi}i\nu(1-e^{ip\Delta y})\int_{-\frac{\pi}{\Delta x}}^{\frac{\pi}{\Delta x}} (\frac{1}{f(s)})'W_1^1(s,p)ds$$
$$+\frac{1}{2\pi}i\nu(1-e^{-ip\Delta y})\int_{-\frac{\pi}{\Delta x}}^{\frac{\pi}{\Delta x}} (\frac{1}{f(s)})W_2^1(s,p)ds$$

which uses periodicity of W.

The overall scope of the calculation would consequently lead to a requirement to perform repeated integration and differentiation to find an expression for W^n.

It has not been possible to obtain a closed-form solution, but it may be worth revisiting the problem in the future.

A.0.5.1 Convergence of the scheme

We have not been able the complete the solution of the recursion or analyse the wavenumber behaviour for this scheme. So we have not been able to establish convergence of the scheme.

Appendix B

The use of the Fourier method for multi-dimensional problems – further toy models

It is straightforward to extend the toy model to more higher dimensions by introducing multiple diffusive terms and/or multiple drift terms.

For the semi-discrete case, we expect that the stability analysis will be similar to that carried out for the one-dimensional case.

B.1 Multiple diffusive terms

B.1.1 An example with a single drift coefficient which is a linear combination of the components of $\underline{\mathbf{x}}$

We consider the case of a PDE with a single drift coefficient which is a linear combination of the components of $\underline{x}$.

$$u_t + (\gamma_1 x_1 + \gamma_2 x_2) u_y = a_{11} u_{x_1 x_1} + 2a_{12} u_{x_1 x_2} + a_{22} u_{x_2 x_2}$$

which extends the toy model to one containing two independent variables x_1 and x_2.

We apply the y-FT to get

$$v_t - ip(\gamma_1 x_1 + \gamma_2 x_2) v = a_{11} v_{x_1 x_1} + 2a_{12} v_{x_1 x_2} + a_{22} v_{x_2 x_2}.$$

Now for the true solution we next apply the x_1-FT and the x_2-FT in turn to get

$$w_t - p\left(\gamma_1 \frac{\partial w}{\partial s_1} + \gamma_2 \frac{\partial w}{\partial s_2}\right) v = -(a_{11}s_1^2 + 2a_{12}s_1 s_2 + a_{22}s_2^2)w.$$

Now we can solve this directly but we can also use an ansatz by writing

$$w(s_1, s_2, p, t) = \exp\left(-b_{11}s_1^2 t - 2b_{12}s_1 s_2 t - b_{22}s_2^2 t - B_1 s_1 p t^2 - B_2 s_2 p t^2 - C p^2 t^3\right)$$

and then finding the coefficients that fit the PDE. We have already used the assumption that

$$w(s_1, s_2, p, 0) = 1.$$

So we have

$$w_t = (-b_{11}s_1^2 - 2b_{12}s_1 s_2 - b_{22}s_2^2 - 2B_1 s_1 p t - 2B_2 s_2 p t - 3C p^2 t^2)w$$

$$\frac{\partial w}{\partial s_1} = (-2b_{11}s_1 t - 2b_{12}s_2 t - B_1 p t^2)w$$

$$\frac{\partial w}{\partial s_2} = (-2b_{12}s_2 t - 2b_{22}s_2 t - B_2 p t^2)w$$

So then

$$(-b_{11}s_1^2 - 2b_{12}s_1 s_2 - b_{22}s_2^2 - 2B_1 s_1 p t - 2B_2 s_2 p t - 3C p^2 t^2)$$

$$-p(\gamma_1(-2b_{11}s_1 t - 2b_{12}s_2 t - B_1 p t^2) + \gamma_2(-2b_{12}s_1 t - 2b_{22}s_2 t - B_2 p t^2)) = -(a_{11}s_1^2 + 2a_{12}s_1 s_2 + a_{22}s_2^2)$$

and by comparing coefficients we have

$$b_{11} = a_{11}$$

$$b_{12} = a_{12}$$

$$b_{22} = a_{22}$$

$$B_1 - \gamma_1 b_{11} - \gamma_2 b_{12} = 0$$

$$B_2 - \gamma_1 b_{12} - \gamma_2 b_{22} = 0$$

and

$$3C + B_1 + B_2 = 0.$$

So we get

$$B_1 = \gamma_1 b_{11} + \gamma_2 b_{12} = \gamma_1 a_{11} + \gamma_2 a_{12}$$

$$B_2 = \gamma_1 b_{12} + \gamma_2 b_{22} = \gamma_1 a_{12} + \gamma_2 a_{22}$$

and

$$C = -\frac{1}{3}(\gamma_1 a_{11} + \gamma_2 a_{12} + \gamma_1 a_{12} + \gamma_2 a_{22})$$
$$= -\frac{1}{3}(\gamma_1(a_{11} + a_{12}) + \gamma_2(a_{12} + a_{22}))$$

so we have the true solution in Fourier space. We could, if necessary, invert all these transforms but we will instead concentrate on the effect of discretisation in the x_1 and x_2 directions.

So we now start with the PDE

$$v_t - ip(\gamma_1 x_1 + \gamma_2 x_2)v = a_{11} v_{x_1 x_1} + 2a_{12} v_{x_1 x_2} + a_{22} v_{x_2 x_2}$$

and discretise this as follows by writing

$$V_t(x_{1,j}, x_{2,k}) - ip(\gamma_1 x_{1,j} + \gamma_2 x_{2,k})V(x_{1,j}, x_{2,k})$$
$$= a_{11}\frac{V(x_{1,j+1}, x_{2,k}) - 2V(x_{1,j}, x_{2,k}) + V(x_{1,j-1}, x_{2,k})}{\Delta x_1^2}$$
$$+2a_{12}\frac{V(x_{1,j+1}, x_{2,k+1}) - V(x_{1,j+1}, x_{2,k-1} - V(x_{1,j-1}, x_{2,k+1}) + V(x_{1,j-1}, x_{2,k-1})}{4\Delta x_1 \Delta x_2}$$
$$+a_{22}\frac{V(x_{1,j}, x_{2,k+1}) - 2V(x_{1,j}, x_{2,k}) + V(x_{1,j}, x_{2,k-1})}{\Delta x_2^2}$$

and we can then apply the Fourier transforms to get

$$W_t - p(\gamma_1 \frac{\partial W}{\partial s_1} + \gamma_2 \frac{\partial W}{\partial s_2})$$
$$= (a_{11}\frac{4}{\Delta x_1^2}\sin^2\left(\frac{s_1 \Delta x_1}{2}\right) + \frac{2a_{12}}{4}\frac{2}{\Delta x_1}\frac{2}{\Delta x_2}\sin(s_1\Delta x_1)\sin(s_2\Delta x_2) + a_{22}\frac{4}{\Delta x_2^2}\sin^2\left(\frac{s_2\Delta x_2}{2}\right))W$$
$$= (a_{11}\frac{4}{\Delta x_1^2}\sin^2\left(\frac{s_1 \Delta x_1}{2}\right) + \frac{2a_{12}}{\Delta x_1 \Delta x_2}\sin(s_1\Delta x_1)\sin(s_2\Delta x_2) + a_{22}\frac{4}{\Delta x_2^2}\sin^2\left(\frac{s_2\Delta x_2}{2}\right))W.$$

Now we have

$$\frac{1}{W}W_t - p\left(\gamma_1\frac{1}{W}\frac{\partial W}{\partial s_1} + \gamma_2\frac{1}{W}\frac{\partial W}{\partial s_2}\right)$$

$$= (a_{11}\frac{4}{\Delta x_1^2}\sin^2\left(\frac{s_1\Delta x_1}{2}\right) + \frac{2a_{12}}{\Delta x_1\Delta x_2}\sin\left(s_1\Delta x_1\right)\sin\left(s_2\Delta x_2\right) + a_{22}\frac{4}{\Delta x_2^2}\sin^2\left(\frac{s_2\Delta x_2}{2}\right))$$

or, with $Z = \log(W)$

$$\frac{\partial Z}{\partial t} - p(\gamma_1\frac{\partial Z}{\partial s_1} + \gamma_2\frac{\partial Z}{\partial s_2}).$$

$$= (a_{11}\frac{4}{\Delta x_1^2}\sin^2\left(\frac{s_1\Delta x_1}{2}\right) + \frac{2a_{12}}{\Delta x_1\Delta x_2}\sin\left(s_1\Delta x_1\right)\sin\left(s_2\Delta x_2\right) + a_{22}\frac{4}{\Delta x_2^2}\sin^2\left(\frac{s_2\Delta x_2}{2}\right)).$$

For the true solution we have

$$w_t - p\left(\gamma_1\frac{\partial w}{\partial s_1} + \gamma_2\frac{\partial w}{\partial s_2}\right) = -(a_{11}s_1^2 + 2a_{12}s_1s_2 + a_{22}s_2^2)w$$

and with $z = \log(w)$ we get

$$\frac{\partial z}{\partial t} - p\left(\gamma_1\frac{\partial z}{\partial s_1} + \gamma_2\frac{\partial z}{\partial s_2}\right) = -a_{11}s_1^2 - 2a_{12}s_1s_2 + a_{22}s_2^2$$

so if we write $F = Z - z = \log(\frac{W}{w})$ we have

$$\frac{\partial F}{\partial t} - p\left(\gamma_1\frac{\partial F}{\partial s_1} + \gamma_2\frac{\partial F}{\partial s_2}\right)$$
$$= a_{11}s_1^2 + 2a_{12}s_1s_2 + a_{22}s_2^2$$
$$-a_{11}\frac{4}{\Delta x_1^2}\sin^2\left(\frac{s_1\Delta x_1}{2}\right) - \frac{2a_{12}}{\Delta x_1\Delta x_2}\sin\left(s_1\Delta x_1\right)\sin\left(s_2\Delta x_2\right) - a_{22}\frac{4}{\Delta x_2^2}\sin^2\left(\frac{s_2\Delta x_2}{2}\right)$$

$$= a_{11}g_{11}(s_1) + 2a_{12}g_{12}(s_1, s_2) + a_{22}g_{22}(s_2)$$

where

$$g_{11}(s_1) = s_1^2 - \frac{4}{\Delta x_1^2}\sin^2\left(\frac{s_1\Delta x_1}{2}\right)$$

$$g_{12}(s_1, s_2) = s_1s_2 - \frac{1}{\Delta x_1\Delta x_2}\sin\left(s_1\Delta x_1\right)\sin\left(s_2\Delta x_2\right)$$

and

$$g_{22}(s_2) = s_2^2 - \frac{4}{\Delta x_2^2}\sin^2\left(\frac{s_2\Delta x_2}{2}\right).$$

To solve this equation we change variables by writing

$$\eta_1 = \lambda_{11} s_1 + \lambda_{12} s_2$$

and

$$\eta_2 = \lambda_{21} s_1 + \lambda_{22} s_2$$

where we have to determine the λ_{ij}.

We have

$$\frac{\partial F}{\partial S_1} = \frac{\partial F}{\partial \eta_1}\frac{\partial \eta_1}{\partial S_1} + \frac{\partial F}{\partial \eta_2}\frac{\partial \eta_2}{\partial S_1}$$

and

$$\frac{\partial F}{\partial S_2} = \frac{\partial F}{\partial \eta_1}\frac{\partial \eta_1}{\partial S_2} + \frac{\partial F}{\partial \eta_2}\frac{\partial \eta_2}{\partial S_2}$$

so that

$$\frac{\partial F}{\partial S_1} = \lambda_{11}\frac{\partial F}{\partial \eta_1} + \lambda_{21}\frac{\partial F}{\partial \eta_2}$$

and

$$\frac{\partial F}{\partial S_2} = \lambda_{12}\frac{\partial F}{\partial \eta_1} + \lambda_{22}\frac{\partial F}{\partial \eta_2}.$$

The equation

$$\frac{\partial F}{\partial t} - p\left(\gamma_1\frac{\partial F}{\partial s_1} + \gamma_2\frac{\partial F}{\partial s_2}\right) = a_{11}g_{11}(s_1) + 2a_{12}g_{12}(s_1, s_2) + a_{22}g_{22}(s_2)$$

becomes

$$\frac{\partial F}{\partial t} - p\left(\gamma_1\left(\lambda_{11}\frac{\partial F}{\partial \eta_1} + \lambda_{21}\frac{\partial F}{\partial \eta_2}\right) + \gamma_2\left(\lambda_{12}\frac{\partial F}{\partial \eta_1} + \lambda_{22}\frac{\partial F}{\partial \eta_2}\right)\right)$$
$$= a_{11}g_{11}(\eta_1, \eta_2) + 2a_{12}g_{12}(\eta_1, \eta_2) + a_{22}g_{22}(\eta_1, \eta_2)$$

or

$$\frac{\partial F}{\partial t} - p\left((\gamma_1\lambda_{11} + \gamma_2\lambda_{12})\frac{\partial F}{\partial \eta_1} + (\gamma_1\lambda_{21} + \gamma_2\lambda_{22})\frac{\partial F}{\partial \eta_2}\right)$$
$$= a_{11}g_{11}(\eta_1, \eta_2) + 2a_{12}g_{12}(\eta_1, \eta_2) + a_{22}g_{22}(\eta_1, \eta_2).$$

We now chose λ_{21} and λ_{22} such that we have

$$\gamma_1\lambda_{21} + \gamma_2\lambda_{22} = 0$$

and then we have

$$\frac{\partial F}{\partial t} - p(\gamma_1\lambda_{11} + \gamma_2\lambda_{12})\frac{\partial F}{\partial \eta_1} = a_{11}g_{11}(\eta_1, \eta_2) + 2a_{12}g_{12}(\eta_1, \eta_2) + a_{22}g_{22}(\eta_1, \eta_2).$$

Then we have the solution

$$F = \frac{1}{p(\gamma_1\lambda_{11} + \gamma_2\lambda_{12})}\int_{\eta_1}^{\eta_1 + p(\gamma_1\lambda_{11}+\gamma_2\lambda_{12})t} (a_{11}g_{11}(\sigma, \eta_2)+2a_{12}g_{12}(\sigma, \eta_2)+a_{22}g_{22}(\sigma, \eta_2))d\sigma$$

which we can check by calculating $\frac{\partial F}{\partial t}$ and $\frac{\partial F}{\partial \eta_1}$.

We note that we can choose λ_{12} and λ_{11} such that $\gamma_1\lambda_{11} + \gamma_2\lambda_{12} = 1$ so we have

$$F(\eta_1, \eta_2) = \frac{1}{p}\int_{\eta_1}^{\eta_1 + pt} (a_{11}g_{11}(\sigma, \eta_2) + 2a_{12}g_{12}(\sigma, \eta_2) + a_{22}g_{22}(\sigma, \eta_2))d\sigma$$

and hence we have the solution for the double transform

$$W(\eta_1, \eta_2) = w(\eta_1, \eta_2)\exp\left(\frac{1}{p}\int_{\eta_1}^{\eta_1 + pt} (a_{11}g_{11}(\sigma, \eta_2) + 2a_{12}g_{12}(\sigma, \eta_2) + a_{22}g_{22}(\sigma, \eta_2))d\sigma\right). \tag{B.1}$$

We can then investigate the low and high wavenumber behaviour in terms of the new variables.

The analysis would match that for the one-dimensional semi-discrete method. All we have really done is to make an appropriate change of variables to get the solution into a familiar form.

To sum up, for the semi-discrete case, stability can be investigated by a simple change of variables and is a straightforward extension of the one-dimensional problem.

B.1.2 A numerical example of a 2D toy model

We used the Fourier solution technique to solve the 2D toy model

$$u_t + (x_1 + x_2)u_y = u_{x_1^2} + u_{x_2^2}$$

with a δ-function initial condition

$$u(x_1, x_2, y, 0) = \delta(x_1 = 0)\delta(x_2 = 0)\delta(y = 0).$$

The true solution of this problem is given by

$$u(x_1, x_2, y, t) = \frac{\sqrt{6}}{8\pi^{3/2}t^{5/2}} \exp\left(-\frac{(x_1^2 + x_2^2)}{4t} \right) \exp\left(-\frac{3}{2t^3}\left(\frac{(x_1 + x_2)t}{2} - y \right)^2 \right).$$

After applying the y-FT to the problem, we have discretised the problem in the x_1, x_2 and t-directions and obtained the approximate solution for $v(x_1, x_2, p, t)$, where p is a Fourier argument.

We then applied the inverse FFT to obtain the approximate solution for $u(x_1, x_2, y, T)$ and compared it with the true solution above.

To simplify the comparison we integrated u over x_1 and x_2 to obtain a plot of this integral against y.

Figure B.1: 2D Toy Model by Fourier Method - KFE and True solutions

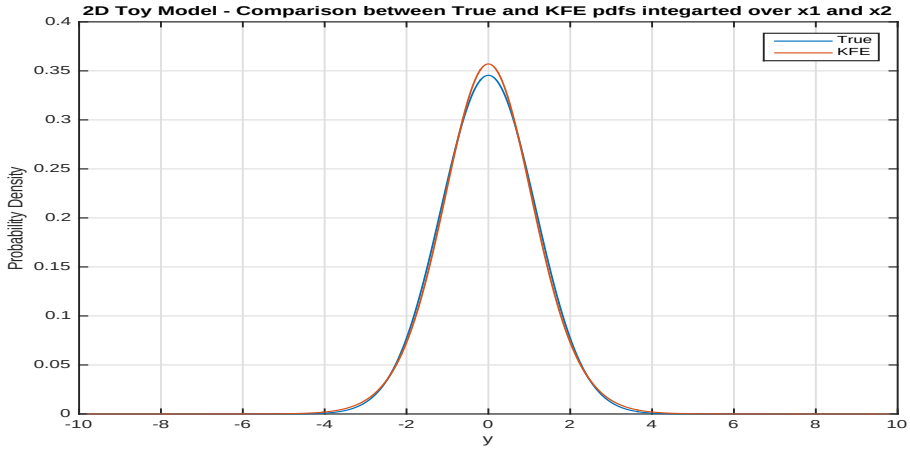

B.2 Multiple drift terms

Another extension of the models would be a model of the form

$$u_t + xu_{y_1} + xu_{y_2} = u_{xx}$$

where we have two drift terms and neither of the drift coefficients depend on y.

An example of a model with two drift terms is where we have a stochastic volatility model such as the Heston model

$$dS_t = \mu S_t dt + \sqrt{v_t} dW_t$$
$$dv_t = \kappa(v_t - \eta)dt + \sigma\sqrt{v_t} dZ_t.$$

If we then define the realised variance

$$R_t = \int_0^t v_t dt$$

so that we have

$$dR_t = v_t dt.$$

We then have an extended state vector which includes the underlyings, the realised volatility and the hedging error

$$d\begin{pmatrix} S_t \\ \tilde{v}_t \\ \tilde{R}_t \\ y \end{pmatrix} = \begin{pmatrix} \mu S_t \\ \kappa(v_t - \eta) \\ v_t \\ C_t \end{pmatrix} dt + \begin{pmatrix} dW_t \\ dZ_t \\ 0 \\ 0 \end{pmatrix}.$$

In this example, we have two 'x' coordinates as well, but for simplicity we focus here on the effect of the two 'y's.

If we then set up and solve the extended KFE and integrate over the underlyings, we will then have a two-dimensional representation of the relationship between the hedging error and the realised volatility at time T.

For a toy model representing the type of set-up in B.2, we can apply the y_1-FT and the y_2-FT to get

$$v_t - ip_1 xv - ip_2 xv = v_{xx}$$

where p_1 and p_2 are wavenumbers. Here the y-variables would be appropriately scaled to represent the linearisation about starting point.

To find the true solution we apply the x-FT to get

$$w_t - p_1 \frac{\partial w}{\partial s} - p_2 \frac{\partial w}{\partial s} = -s^2 w$$

or

$$w_t - (p_1 + p_2) \frac{\partial w}{\partial s} = -s^2 w.$$

The analysis would then continue as before but with $p_1 + p_2$ as a joint wavenumber but in this situation, the wavenumbers have to be handled differently. For example, we can have separately large values of p_1 and p_2 but the value of $p_1 + p_2$ can be small.

Bibliography

[1] M. Avellaneda, A. Levy, and A. Paras. 'Pricing and Hedging Derivative Securities in Markets with Uncertain Volatilities'. *Applied Mathematical Finance, Vol.2, Issue 2*, pages 73–88, 1995.

[2] A. Berman and R. Plemmons. *'Nonnegative matrices in the mathematical sciences'*. Academic Press, 1979.

[3] A. Bermúdez, M.R. Nogueiras, and C. Vázquez. 'Numerical solution of variational inequalities for pricing Asian options by higher order Lagrange-Galerkin methods'. *Applied Numerical Mathematics*, pages 1256–1270, 2006.

[4] N. Branger, E. Krautheim, C. Schlag, and N. Seeger. 'Hedging Under Model Mis-Specification: All risk factors are equal, but some are more equal than others.....'. *The Journal of Futures Markets, Vol. 32, No.5*, pages 397–430, 2008.

[5] R. Carter and M. Giles. 'Sharp error estimates for discretizations of the 1D convection-diffusion equation with Dirac initial data'. *IMA Journal of Numerical Analysis*, pages 406–425, 2007.

[6] X. Chen, J. Chadam, Jiang L., and W. Zheng. 'Convexity of the Exercise Boundary of the American Put Option on a Zero Dividend Asset'. *Mathematical Finance*, pages 185–197, 2008.

[7] I. Craig and A. Sneyd. 'An alternating-direction implicit scheme for parabolic equations with mixed derivatives'. *Computers and Mathematics with Applications, Vol.20, Issue 3*, pages 52–63, 1988.

[8] Y. D'Halluin, P.A. Forsyth, and G. Labahn. 'A semi-Lagrangian approach for American Asian options under jump-diffusion.'. *SIAM Journal on Scientific Computing*, pages 315–345, 2005.

[9] J. Douglas and H. Rachford. 'On the numerical solution of heat conduction problems in two and three space variables'. *Transactions of the American Mathematical Society*, pages 421–439, 1956.

[10] P. Duhamel and M. Vetterli. 'Fast Fourier transforms: A tutorial review and a state of the art, 19'. *Signal Processing*, pages 259–299, 1990.

[11] J. Elder. 'Hedging Strategies for Financial Derivatives'. DPhil Thesis - Oxford University, 2012.

[12] P.A. Forsyth and K.R. Vetzal. 'Quadratic convergence of a penalty method for valuing American options'. *SIAM Journal of Scientific Computing*, pages 2096–2123, 2002.

[13] M. Giles. 'Sharp error estimates for a discretisation of the 1D convection-diffusion equation with Dirac initial data. Report no. 04-17'. *Oxford University Computing Laboratory*, 2004.

[14] M. Giles and R. Carter. 'Convergence analysis of Crank-Nicolson and Rannacher time-marching'. *Journal of Computational Finance, 9(4)*, pages 89–112, 2006.

[15] M.B. Giles and E. Süli. 'Adjoint methods for PDEs: a posteriori error analysis and postprocessing by duality. *Acta Numerica (A. Iserles ed.)*, pages 145–236, 2002.

[16] A. Gupta, C. Reisinger, and A.Whitley. 'Model Uncertainty and its Impact on Derivative Pricing'. In 'K. Bocker', editor, *'Rethinking Risk Measurement and Reporting, Volume 2'*, pages 137–175. RISK Books, 2010.

[17] E. Haug. *'The Complete Guide to Option Pricing Formulas'*. McGraw-Hill, 2007.

[18] N. Higham. 'The Scaling and Squaring Method for the Matrix Exponential Revisited'. *SIAM Journal on Matrix Analysis and Applications, 26, No. 4*, pages 1179–1193, 2005.

[19] K.J. in 't Hout and C. Mishra. 'Stability of ADI schemes for multidimensional diffusion equations with mixed derivative terms'. *Applied Numerical Mathematics, 74*, pages 83–94, 2013.

[20] K.J. in 't Hout and B.D. Welfert. 'Stability of ADI schemes applied to convectiondiffusion equations with mixed derivative terms'. *Applied Numerical Mathematics, 57*, pages 19–35, 2007.

[21] M. Joshi and F. Friedlander. *'Introduction to the theory of distributions'*. Cambridge University Press, 2008.

[22] I. Karatzas and S. Shreve. *'Brownian Motion and Stochastic Calculus'*. Springer, 1991.

[23] N. El Karoui, M. Jeanblanc-Picqué, and S. Shreve. 'Robustness of the Black and Scholes formula'. *Mathematical Finance*, pages 93–126, 1998.

[24] A.Q.M. Khaliq, D.A. Voss, and M. Yousuf. 'Pricing exotic options with L-stable Padé schemes'. *Journal of Banking Finance*, pages 3438–3461, 2007.

[25] Von A. Kolmogoroff. 'Zufällige Bewegungen (Zur Theorie der Brownschen Bewegung'. *Annals of Mathematics, Vol. 35, No. 1*, pages 116–117, 1934.

[26] M. Luskin and R. Rannacher. 'On the smoothing property of the Crank-Nicolson scheme'. *Applied Analysis, 14*, pages 117–135, 1982.

[27] T. Lyons. 'Uncertain volatility and the risk-free synthesis of derivatives'. *Applied Mathematical Finance*, pages 117–133, 1995.

[28] R. Mallier and G. Alobaidi. 'The American put option close to maturity'. *Acta Mathematica Universitatis Comenianae*, pages 161–174, 2004.

[29] Mathworks. 'Matlab Documentation'. uk.mathworks.com/help/matlab/ref/fft.html.

[30] F.W.J. Olver, D.M. Lozier, R.F. Boisvert, and C.W. Clark. *"'Numerical methods", NIST Handbook of Mathematical Functions'*. Cambridge University Press, 2010.

[31] K. Parrott and N. Clarke. 'A parallel solution of early exercise Asian options with stochastic volatility'. *Proceedings of the 11th Domain Decomposition Conference, Greenwich*, 1998.

[32] D. Peaceman and H. Rachford. 'The numerical solution of parabolic and elliptic differential equations'. *Journal of the Society for the Industrial Applications of Mathematics*, pages 28–41, 1955.

[33] D.M. Pooley, Vetzal, K.R., and P.A. Forsyth. 'Convergence remedies for non-smooth payoffs in option pricing'. *Journal of Computational Finance, 6*, pages 25–40, 2003.

[34] A Porretta and E. Zuazua. 'Numerical hypocoercivity for the Kolmogorov equation'. *Submitted*, 2015.

[35] R. Rannacher. 'Finite element solution of diffusion problems with irregular data'. *Numerische Mathematik*, pages 309–327, 1984.

[36] C. Reisinger and A. Whitley. 'The Impact of a Natural Time Change on the Convergence of the Crank-Nicolson Scheme'. *IMA Journal of Numerical Analysis*, pages 1156–1192, 2013.

[37] W.T. Shaw. *'Modelling Financial Derivatives with MATHEMATICA'*. Cambridge University Press, 1999.

[38] G.D. Smith. *'Numerical Solution of Partial Differential Equations – Finite Difference Methods'*. Oxford University Press, 1985.

[39] G. Strang. *'Introduction to Applied Mathematics'*. Wellesley-Cambridge Press, 1986.

[40] V. Timofte. 'Integral estimates for convergent positive series'. *Journal of Mathematical Analysis and Applications*, pages 90–102, 2005.

[41] J. Toivanen. *'Finite Difference Methods for Early Exercise Options'*. Encyclopedia of Quantitative Finance, Wiley, 2010.

[42] L.N. Trefethen and J.A.C. Weideman. 'The Exponentially Convergent Trapezoidal Rule'. *SIAM Review, Vol. 56, No. 3*, pages 385–458, 2014.

[43] T. Trif. 'On certain sequences derived from generalised Euler-Mascheroni constants'. *Journal of Mathematical Inequalities*, pages 107–116, 2011.

[44] C. Vázquez. 'An upwind numerical approach for an American an European option pricing model'. *Applied Mathematics and Computation, 97*, pages 273–286, 1998.

[45] B.A. Wade, A.Q.M. Khaliq, M. Yousuf, J. Vigo-Aguiar, and R. Deininger. 'On smoothing of the Crank-Nicolson scheme and higher order schemes for pricing barrier options'. *Journal of Computational and Applied Mathematics, 204(1)*, pages 144–158, 2007.

[46] P. Wilmott, S.D. Howison, and J. Dewynne. *'The Mathematics of Financial Derivatives: A Student Introduction"'*. Cambridge University Press, 1995.

[47] P. Zhang. *'Exotic Options: A Guide to the Second Generation Options'*. World Scientific, 1998.